AD-A136 085 COMPUTER-BASED METHODS FOR THERMODYNAMIC ANALYSIS OF MATERIALS PROCESSING(U) MANLABS INC CAMBRIDGE MASS L KAUFMAN 30 NOV 83 AFOSR-TR-83-1099 F49620-80-C-0020 1/2

UNCLASSIFIED F/G 9/2 NL

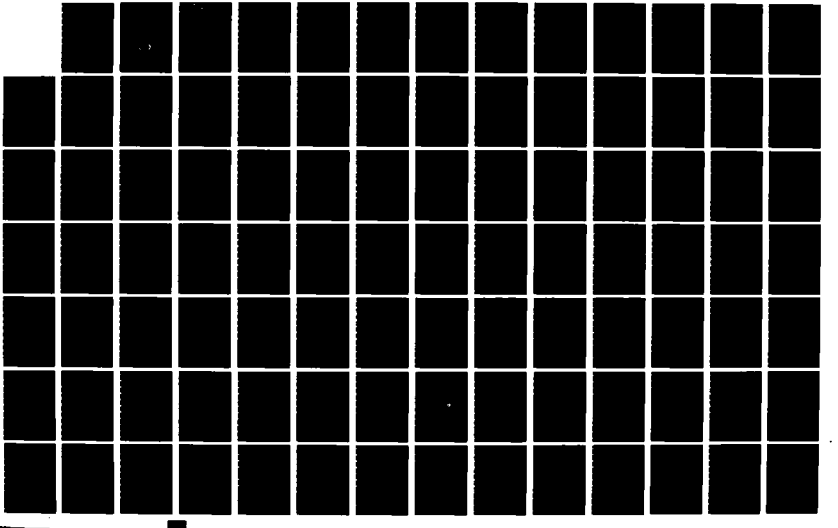

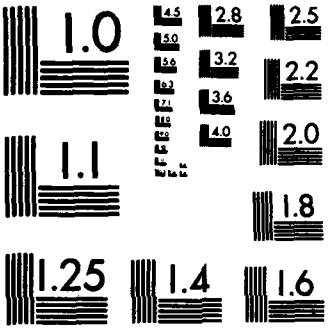

(2)

AFOSR-TR- 83-1099

FINAL REPORT

ON

Contract F 49620-80-C-0020

Computer Based Methods for Thermodynamic Analysis of Materials Processing

1 October 1979 to 30 September 1983

Submitted to

Air Force Office of Scientific Research (AFSC)
Bolling Air Force Base, D.C. 20332

30 November 1983

by

Larry Kaufman

ManLabs, Inc.
21 Erie Street
Cambridge, Massachusetts 02139

AD-A136 085

83 12 20 039

UNCLASSIFIED

SECURITY CLASSIFICATION OF THIS PAGE (When Data Entered)

REPORT DOCUMENTATION PAGE	READ INSTRUCTIONS BEFORE COMPLETING FORM
1. REPORT NUMBER AFOSR-TR-83-1098	2. GOVT ACCESSION NO / 3. RECIPIENT'S CATALOG NUMBER
4. TITLE (and Subtitle) Computer Based Methods for Thermodynamic Analysis of Materials Processing	5. TYPE OF REPORT & PERIOD COVERED Final Report, Oct. 1979 to September 1983
	6. PERFORMING ORG. REPORT NUMBER
7. AUTHOR(s) Larry Kaufman	8. CONTRACT OR GRANT NUMBER(s) F 49620-80-C-0020
9. PERFORMING ORGANIZATION NAME AND ADDRESS ManLabs, Inc. 21 Erie Street Cambridge, Mass. 02139	10. PROGRAM ELEMENT, PROJECT, TASK AREA & WORK UNIT NUMBERS 61102F 2306A2
11. CONTROLLING OFFICE NAME AND ADDRESS Air Force Office of Scientific Research/NE Bolling Air Force Base Washington, D.C. 20332	12. REPORT DATE 30 November 1983
	13. NUMBER OF PAGES 157
14. MONITORING AGENCY NAME & ADDRESS(if different from Controlling Office)	15. SECURITY CLASS. (of this report) Unclassified
	15a. DECLASSIFICATION/DOWNGRADING SCHEDULE

16. DISTRIBUTION STATEMENT (of this Report)

Approved for public release; distribution unlimited.

17. DISTRIBUTION STATEMENT (of the abstract entered in Block 20, if different from Report)

18. SUPPLEMENTARY NOTES

Accession For	
NTIS GRA&I	☐
DTIC TAB	☑
Unannounced	☐
Justification	
By	
Distribution/	
Availability Codes	
Dist	Avail and/or Special
A-1	

DTIC COPY INSPECTED

19. KEY WORDS (Continue on reverse side if necessary and identify by block number)

Data Base	Quasibinary	Zirconia Ceramics
Phase Diagrams	Quasiternary	Iron Base Alloys
Ceramic Systems	Alloy SemiConductors	Titanium Carbide
Sialons	Halide Glasses	Titanium Nitride
Thermochemistry	Order-Disorder Reactions	Titanium Carbonitride

20. ABSTRACT (Continue on reverse side if necessary and identify by block number)

The data base previously developed for multicomponent Sialon Ceramic phase diagrams has been expanded to cover Ce_2O_3, BeO and Y_2O_3 additions. Isothermal sections in the MgO-Si_3N_4-SiO_2, Y_2O_3-SiO_2-Si_3N_4 and Ce_2O_3-SiO_2-Si_3N_4 system near 2000°K were computed and compared with limited experimental data. The trajectory of ordering temperatures for A2/B2 and B2/DO_3 reactions has been computed along the Fe_3Si-Fe_3Al composition path in the BCC of the Fe-Al-Si system and compared with experiment. The two phase (fcc &

DD FORM 1 JAN 73 1473 EDITION OF 1 NOV 65 IS OBSOLETE

Unclassified

SECURITY CLASSIFICATION OF THIS PAGE (When Data Entered)

bcc) fields for ordered phases in the iron-aluminum-nickel, iron-aluminum-manganese, and the iron-nickel-manganese systen between 700°C and 1200°C. Construction of a data base for fluoride systems consisting of systems containing ZrF_4 which are employed tp synthesize fluoride glasses has been initiated and used to calculate the composition of maximum liquid stability in the ZrF_4-LaF_3-BaF_2 and the ZrF_4-BaF_2-NaF systems where glass formation has been observed. The calculations have been extended to consider the effects of AlF_3 additions on the glass compositions with good results. An analysis of the titanium-carbon-nitrogen system coupling the thermochemical and phase diagram data was performed to caculate the ternary phase diagram and thermochemical properties over a range of temperature. This information should be useful in vapor deposition of coatings based on this system which are used in metal cutting and wear resistance applications. The addition of ZrO_2 to the data base has been initiated and applied to calculation of the ZrO_2-Al_2O_3 and ZrO_2-Y_2O_3 binary systems and well as isothermal sections in the Al_2O_3-ZrO_2-Y_2O_3 ternary system between 1427°C and 2427°C.

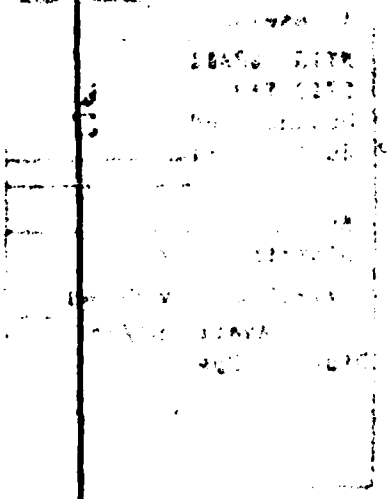

DISTRIBUTION LIST

AFOSR/NE
Dr. A.H. Rosenstein
Bolling AFB Washington DC 20332

16 Annual Tech Reports
16 Final Tech Report (1 Draft)
6 Reprints of Each Publication

1 Copy Each:

AFWAL/MLLM
Attn: H. Graham
Wright-Patterson AFB OH 45433

AFWAL/MLLS
Attn: Branch Chief
Wright-Patterson AFB OH 45433

AFWAL/MLLM
Attn: N. Geyer
Wright-Patterson AFB OH 45433

AFWAL/MLLM
Attn: B. Ruh
Wright-Patterson AFB OH 45433

AFWAL/MLLN
Attn: Branch Chief
Wright-Patterson AFB OH 45433

AFWAL/MLBP
Attn: Branch Chief
Wright-Patterson AFB OH 45433

AFWAL/MLBM
Attn: Branch Chief
Wright-Patterson AFB OH 45433

AFWAL/MLLP
Attn: Branch Chief
Wright-Patterson AFB OH 45433

AFWAL/MLPJ
Attn: Branch Chief
Wright-Patterson AFB OH 45433

AFWAL/MLPO
Attn: Branch Chief
Wright-Patterson AFB OH 45433

DARPA
Attn: Lt Col Jacobson
1400 Wilson Blvd
Arlington VA 20339

D.O.E(Material Sciences)
Attn: R.J. Gottschall
Office of Energy Research
Washington DC 20545

Office of Naval Research
Attn: Dr R. Pohanka
800 N. Quincy St.
Arlington VA 22203

U.S. Army Research Office
Metallurgy and Materials Sciences
P.O. Box 12211
Research Triangle Park NC 27709

U.S. Naval Air Systems Command
Attn: Mr. I Machlin (AIR 52031B)
Washington DC 20360

U.S. Naval Research Laboratory
Attn: Dr. R.W. Rice, Chem Div (6360)
Washington DC 20375

NASA-Lewis
Attn: H.B. Probst (Stop 49-3)
21000 Brookpark Rd.
Cleveland OH 44135

J.A. Carpenter Jr
Oak Ridge National Lab
Oak Ridge TN 37830

National Bureau of Standards
Attn: S.M. Wiederhorn
Washington DC 20234

N.S.F. (Materials Research)
Attn: B.A. Wilcox
1800 G Street, N.W.
Washington DC 20550

Materials Research Lab (AMMRC)
Attn: Dr R.N. Katz
Watertown MA 02172

DOE Fossil Energy Div
Dr S.R. Skaggs
FE-3/C-156 Germantown
Washington DC 20544

Dr F.F. Lange
Rockwell International Science Center
Thousand Oaks CA 91360r)

Dr A.H. Heuer
Dept of Material Science
Case Western Reserve University
Cleveland Oll 43201

Dr G.H. Meier
Dr F.S. Pettit
Metallurigical and Materials Engineering
University of Pittsburgh
Pittsburgh PA 15261

Dr. L. Kaufman
ManLabs, Inc.
21 Erie St.
Cambridge, MA 02139

Dr I. Allam
SRI Internationl
333 Ravenswood Ave
Menlo Park CA 94025

Dr D. Rowcliff
SRI International
333 Ravenswood Ave.
Menlo Park, CA 94025

Dr Roger R. Wills
Section Manager, Ceramics and
Materials Processing Section
Battelle Columbus Labs
Columbus OH 43201

ABSTRACT The data base previously developed for multicomponent SIALON Ceramic phase diagrams has been expanded to cover Ce_2O_3, BeO and Y_2O_3 additions. Isothermal sections in the $MgO-Si_3N_4-SiO_2$, $Y_2O_3-SiO_2-Si_3N_4$ and $Ce_2O_3-SiO_2-Si_3N_4$ systems near 2000°K have been computed and compared with limited experimental data. The trajectory of ordering temperatures for A2/B2 and $B2/DO_3$ reactions has been computed along the Fe_3Si-Fe_3Al composition path in the BCC phase of the Fe-Al-Si system and compared with experiment. The two phase (fcc + bcc) fields for ordered phases in the iron-aluminum-nickel, iron-aluminum-manganese, and the iron-nickel-manganese system between 700°C and 1200°C were calculated. Construction of a data base covering fluoride systems consisting of systems containing ZrF_4 which are employed to synthesize fluoride glasses has been initiated and used to calculate the composition of maximum liquid stability in the $ZrF_4-LaF_3-BaF_2$ and the ZrF_4-BaF_2-NaF ternary systems where glass formation has been observed. The calculations have been extended to consider the effects of AlF_3 additions on the glass compositions with good results. An analysis of the titanium-carbon-nitrogen system coupling the thermochemical and phase diagram data has been performed to permit calculation of the ternary phase diagram and thermochemical properties over a range of temperatures. This information should be useful in vapor deposition of coatings based on this system which are used in metal cutting and wear resistance applications. The addition of ZrO_2 to the data base has been initiated and applied to calculation of the ZrO_2-AlO_3 and $ZrO_2-Y_2O_3$ binary system as well as isothermal sections in the $Al_2O_3-ZrO_2-Y_2O_3$ ternary system between 1427°C and 2427°C.

I. INTRODUCTION AND SUMMARY

U.S. Air Force requirements for an expanding variety of materials and energy sources with the constraints imposed by ever increasing costs and budget restrictions has magnified the need for evaluating current methods of materials processing and performance. The most rational basis from which to perform such an evaluation is an extensive thermodynamic frame work for describing and predicting the behavior of materials systems over a broad range of environmental conditions. Development of such a frame work would permit interrelation of phase diagram and thermochemical data yielding a more complete description of a given system. The utility of computer based methods for developing and utilizing coupled phase diagram and thermochemical data on metallic systems has been well documented, the present work is directed toward achieving a similar facility in dealing with ceranic, glass and compound based systems used in electronic, metal cutting and high temperature structural applications.

Section II, pages 5-15, published CALPHAD (1981) 5 163-84) extends the present data base to BeO, Y_2O_3 and Ce_2O_3 ceramics. Previous segments of this base cover combinations of Cr_2O_3, MgO, Al_2O_3, Fe_2O_3, Fe_3O_4, "FeO", SiO_2, CaO, Si_2N_4 and AlN. Lattice Stability, Solution and Compound Phase Parameters were derived covering the liquid, spinel, corundum, periclase, crystobalite, tridymite, quartz, hexagonal and beta prime phases which appear in the binary systems composed of pairs of these compounds. Compound phases formed from specific binary combinations of these compounds (i.e. $MgO \cdot Cr_2O_3$) were also characterized. This description is based on observed thermochemistry and phase diagrams for the binary systens of interest. Selected ternary systems have been computed based on the foregoing data base for comparison with experimental sections in order to illustrate the usefulness of the data base.

Section III, pages 16-28, (published in High Temperatures-High Pressures (1982) 14 619-31) illustrates application of the data base to the processing and performance of SIALON Ceramics by calculation of quasiternary sections in the SiO_2-MgO-Si_3N_4,

SiO_2-Ce_2O_3-Si_3N_4 and SiO_2-Y_2O_3- Si_3N_4 between 1900 and 2100K which agree well with experimental findings.

In order to illustrate application of these techinques to alloy semiconductors, Section IV,, pages 29-58, deals with development of a data base covering the binary systems composed of Aluminum, Gallium, Indium, Phosphous , Arsenic and Antimony has been constructed by analyzing the fifteen combinations of these elements in terms of lattice stability, solution phase and compound parameters. These compound semi-conductors are important for a wide range of electro-optical applications because then properties can be tailored by controlling the composition of the solid, which is grown from the liquid or deposited from the vapor. Although crystal growers have become very adept at controlling the temperature (and pressure) of the parent phase in order to obtain the desired characteristics of alloy semiconductors, phase diagram data is indispensible in order to deal with increasingly complex systems.. Partial isothermal sections in the P-In-As, As-In-Sb, P-Ga-As, Ga-Sb-In and Al-Sb-Ga systems were then calculated using the foregoing data base for comparison with experimental isothermal sections and quasi-binary III-V phase diagrams. It was found that ternary liquid and III-V compound interaction parameters were required to attain good agreement in some cases. Similar calculations were performed for the Te-Cd, Hg-Cd, and Te-Hg binary systems and the Cd-Te-Hg ternary systems at pressures up to 74 atmospheres. Comparison of the calculated results with experimental data on tie-line compositions between Cd-Te-Hg liquid and quasi-binary CdTe-HgTe alloys is important in the liquid phase epitaxial growth of controlled band gap electro-optical materials. Pages 29-58 comprise a paper published in CALPHAD 5 (1981) 217 covering this work.

The recent discovery of a new family of non-oxide glasses based on mixtures of ZrF_4 or HfF_4 with other metallic fluorides by M. Poulain and coworkers offers great potential in optical fiber, window and source/detector applications. Due to the limited phase diagram data available for the binary, ternary and multicomponent fluoride systems currently employed to synthesize these glasses most of the progress in identifying new compositions has proceeded along empirical

lines. In order to remedy this situation, the development of a data base covering fluoride glasses has been undertaken. Coupled thermochemical analysis of the ZrF_4-BaF_2, ZrF_4-LaF_3, ZrF_4-PbF_2, ZrF_4-NaF, ZrF_4-KF, ZrF_4-RbF and ZrF_4-CsF, LaF_3-BaF_2 and BaF_2-NaF systems was completed. The results were employed to calculate the composition of maximum liquid stability in the ZrF_4-LaF_3-BaF_2 and the ZrF_4-BaF_2-NaF ternary systems where glass formation has been observed. Section V, pages 59-69 (published in CALPHAD (1983) 7 71-82) illustrates these results.

Requirements for engine components in advanced air craft engine designs have stimulated interest in iron base alloys exhibiting ordered phases which are stable at temperatures between 900 and 1500K. Section VI, pages 71-84, presents a calculation of ordering temperatures in the quasi-binary section between Fe_2Al and Fe_3Si. Section VII, pages 85-103, examines ordering reactions in the iron-aluminum system and the effects of ordering on the fcc/bcc equilibria in iron rich alloys containing aluminum, manganese and nickel between 973K and 1473K.

The use of titanium carbide, titanium nitride and titanium carbo nitride as cutting tool materials or as coatings for cutting tools and wear parts has expanded substantially during the past decade. Section VIII, pages 104-129, provides a thermodynamic evaluation of the Ti-C, Ti-N and Ti-C-N systems covering the range of processing and performance. Ternary isothermal sections are presented between 1600K and 2500K and isoactivity lines for the elemental components are presented at 1800K.

Ceramic composites based on ZrO_2 or in which ZrO_2 is present as a second pahse have wide applications in high temperature technology. Recently it has been found that composites which contain ZrO_2 dispersions can exhibit enhanced fracture toughness due to a mechanism which is based on the titrogonal-monoclinic transformation in ZrO_2. Such enhancement has been reported for Al_2O_3, Si_3N_4 and SiC-Al_2O_3-SiO_2 composites. Accordingly Section IX, pages 130-136, describes the initial step in adding ZrO_2 to the data base covering the ZrO_2-Y_2O_3 and ZrO_2-Al_2O_3 binary systems and the Al_2O_3-ZrO_2-Y_2O_3 ternary systems.

Section X, pages 137-38, provides a calculation of the heat of fusion of eutectic glasses in the ZrF_4-BaF_2

and ZrF_4-LaF_3 systems while Section XI, pages 139-160, provides a calculation of the effect of AlF_3 additions on glass compositions of ternary ZrF_4-LaF_3-BaF_2 fluorides which agree with observations. Additions of AlF_3 are found to facilitate fabrication of large fluoride glass windows.

1A. PROGRAM PERSONNEL

Technical Activities on this program have been performed by L. Kaufman, D. Birnie, K. Taylor, J. Nell, F. Hayes, J. Agren, E.P. Warekois, C. Thielen, J. Kozaczka, R. Garcia, J. Davis, C. Bidell, J. Smith, A. Rabinkin, S. Drake, G. Inden, S. Sprung, and D. Hay.

1B. INTERACTION WITH OTHER TECHNICAL ACTIVITIES

Technical lectures covering the work of this program were presented at the following meetings: CALPHAD IX, Montreal, Canada; May 1980: American Ceramics Society, Washington, D.C.; May 1981: CALPHAD X, Vienna, Austria; July 1981: Conference on Chemistry at High Temperatures, AERE, Harwell, England; Sept. 1981: First International Symposium on Halide Glasses, Cambridge, England; March 1982: CALPHAD XI, Argonne national Laboratory; May 1983: Alloy Workshop, Los Alamos National Laboratory; September 1982: Institute for Defense Analysis Conference, Alexandria, Virginia; June 1983: Second International Symposium on Halide Glasses Rensselaer Polytechnic Institute, Troy, New York; August 1983: Materials Research Society Conference, Boston, Massachusetts; November 1983: and Joint Meeting of the Boston Section AIME and Worcester Section of ASM, Framingham, Ma.; February 1983.

II. CALCULATION OF QUASI-BINARY CERAMIC SYSTEMS

L. Kaufman, F. Hayes and D. Birnie, CALPHAD (1981) 5 163-184

(This paper was presented at CALPHAD X, Vienna, Austria, July 1981)

ABSTRACT. A data base is being developed for calculation of quasi-binary and quasi-ternary phase diagrams of ceramic systems (1-3). Previous segments of this base cover combinations of Cr_2O_3, MgO, Al_2O_3, Fe_2O_3, Fe_3O_4, "FeO", SiO_2, CaO, Si_3N_4 and AlN. Lattice Stability, Solution and Compound Phase Parameters were derived covering the liquid, spinel, corundum, periclase, crystobalite, tridymite, quartz, hexagonal and beta prime phases which appear in the binary systems composed of pairs of these compounds. Compound phases formed from specific binary combinations of these compounds (i.e. $MgO{\cdot}Cr_2O_3$) were also characterized. This description is based on observed thermochemistry and phase diagrams for the binary systems of interest. Selected ternary systems have been computed based on the foregoing data base for comparison with experimental sections in order to illustrate the usefulness of the data base. The present paper extends the data base to cover BeO, Y_2O_3 and Ce_2O_3 additions. Moreover, ternary sections in the SiO_2-MgO-Si_3N_4, SiO_2-Y_2O_3-Si_3N_4 and SiO_2-Ce_2O_3-Si_3N_4 were calculated between 1900K and 2100K for comparison with experiment.

1. Introduction

The utility of computer based methods for coupling phase diagrams and thermochemical data for metallic systems has been well documented in many papers published in this journal. A considerable effort is being applied toward developing an extensive base for metallic systems. Recently similar efforts have begun in order to provide a similar facility with ceramic systems. The expanded studies of SIALON composites, combining silicon and aluminum nitrides with oxides of silicon, aluminum, magnesium, beryllium, cerium and yttrium and other metals has provided additional motivation for predicting multicomponent phase diagrams of ceramic systems.

2. Description of the Thermochemical System Employed to Characterize Solution and Compound Phases

The method utilized for describing solution and compound phases is the same as that employed earlier (1-3) comprising some symbolic usage which facilitates data handling as indicated below. The free energy, G^L, of a liquid (solution) phase, L, in the binary system Y_2O_3-BeO is given by Equation (1) where T is in Kelvins, R=8.314 J/g. at°K, while x is the atomic fraction of BO(i.e. BO=½BeO) and(1-x)is the fraction of YO(i.e. 1/5Y_2O_3). The mass basis is thus one mole of atoms (i.e. a gram-atom)

$$G^L=(1-x)\,{}^\circ G^L_{YO}+x\,{}^\circ G^L_{BO}+RT(x\ell nx+(1-x)\ell n(1-x))+x(1-x)[LYOBO(1-x)+xLBOYO]\ J/g.at \qquad (1)$$

where ${}^\circ G^L_{YO}$ and ${}^\circ G^L_{BO}$ are the free energies of one gram atom of pure liquid YO and BO. Table 1 defines the lattice stabilities of the liquid and solid forms of YO, BO and the other components of current interest. These data derived from earlier studies and compilations of thermochemical and phase diagram data, (1-8), when combined with the solution and compound phase parameters shown in Tables 2 and 3 permit calculation of the binary phase diagrams shown in Figures 1-12. The solution parameters LYOBO and LBOYO, which describe the liquid Y_2O_3-BeO solution are listed in Table 2 (LYOBO=LBOYO=-2092 Joules/g.at). Similar parameters for the liquid and solid phases are listed in Table 2. The free energy of the solid phases are described in a manner similar to equation (1). Thus, for example, the free energy of the body centered cubic (Mn_2O_3)Y phase in the YO-BO system is given by

$$G^Y=(1-x)\,{}^\circ G^Y_{YO}+x\,{}^\circ G^Y_{BO}+RT(x\ell nx+(1-x)\ell n(1-x))+x(1-x)[YYOBO(1-x)+xYBOYO]\ J/g.at. \qquad (2)$$

TABLE 1

SUMMARY OF LATTICE STABILITY PARAMETERS
(All units in Joules per gram atom (mole of atoms), T in Kelvins)

AO = (1/5)Al_2O_3, SO = (1/3)SiO_2, MO = (1/2)MgO, AN = (1/2)AlN, SN = (1/7)Si_3N_4

BO = (1/2)BeO, YO = (1/5)Y_2O_3, CE = (1/5)Ce_2O_3

P = Periclase, C = Corundum, X = Crystobalite, T = Tridymite, H = α quartz

R = β quartz, B = beta Si_3N_4, N = hexagonal AlN and BeO, Y = body centered cubic $(Mn_2O_3)Y_2O_3$ and Ce_2O_3 structure

BOBOLN* = (1/2)BeO(Liquid)-(1/2)BeO(hexagonal)

YOYOLY = (1/5)Y_2O_3(Liquid)-(1/5)Y_2O_3 (body centered cubic)

YOYOLY =	22694 - 8.368T	CECELY =	20334 - 8.368T
YOYOLN =	0 - 14.142T	CECELN =	0 - 14.142T
YOYOLX =	0 - 2.092T	CECELX =	0 - 2.092T
YOYOLB =	0 - 12.510T	CECELB =	0 - 12.510T
YOYOLC =	0 - 10.209T	CECELC =	0 - 10.209T
BOBOLN =	40376 - 14.142T	AOAOLY =	0 - 8.368T
BOBOLX =	0 - 1.674T	ANANLY =	0 - 8.368T
BOBOLC =	0 - 10.209T	SNSNLB =	33949 - 12.510T
BOBOLB =	0 - 12.510T	SNSNLY =	0 - 8.368T
BOBOLY =	0 - 8.368T	SOSOLY =	0 - 2.092T
		SOSOLN =	0 - 2.092T
		SOSOLX =	3347 - 1.674T
		SOSOLR =	5042 - 3.096T

* These differences specify the free energy of one phase (i.e. liquid) minus the free energy of the second phase (i.e. hexagonal) for a given compound.

TABLE 2

SUMMARY OF SOLUTION PHASE PARAMETERS
(All units in Joules per gram atom (mole of atoms), T in Kelvins)

L = Liquid, N = hexagonal, X = Crystobalite, T = Tridymite, Y = body centered cubic

B = beta Si_3N_4, AO = (1/5)Al_2O_3, SO = (1/3)SiO_2, AN = (1/2)AlN, SN = (1/7)Si_3N_4, BO = (1/2)BeO

YO = (1/5)Y_2O_3, CE = (1/5)Ce_2O_3

LSOBO = LBOSO = 41840
NSOBO = NBOSO = 83680
XSOBO = XBOSO = 83680
TSOBO = TBOSO = 83680

LYOBO = LBOYO = -2092
YYOBO = YBOYO = -2092
NYOBO = NBOYO = 83680

LAOBO = LBOAO = 8368
CAOBO = CBOAO = 83680
NAOBO = NBOAO = 83680

LBOAN = LANBO = 20920
NBOAN = NANBO = 83680

LCESN = LSNCE = 4180
BCESN = BSNCE = 62760
YCESN = YSNCE = 62760

LBOSN = LSNBO = 20920
BBOSN = BSNBO = 83680
NBOSN = NSNBO = 83680

LYOAO = LAOYO = 12552
YYOAO = YAOYO = 83680
CYOAO = CAOYA = 83680

LYOAN = LANYO = 20920
YYOAN = YANYO = 83680
NYOAN = NANYO = 83680

LSNSO = LSOSN = 29288
XSNSO = XSOSN = 125520
TSNSO = TSOSN = 125520

LYOSN = LSNYO = 4180
BYOSN = BSNYO = 83680
YYOSN = YSNYO = 83680

$0 \leq x_{SO} \leq 0.60$*

LYOSO = LSOYO = -92048+36.82T

$0.6 \leq x_{SO} \leq 1.0$

LYOSO = -216,000+66.94T
LSOYO = -9414+16.74T
YYOSO = YSOYO = 83680
XYOSO = XSOYO = 83680
TYOSO = TSOYO = 83680

$0 \leq x_{SO} \leq 0.60$

LCESO = LSOCE = -92048 + 36.82T

$0.6 \leq x_{SO} \leq 1.0$

LCESO = -216,000+66.94T
LSOCE = -9414+16.74T
YCESO = YSOCE = 83680
XCESO = XSOCE = 83680
TCESO = TSOCE = 83680

*x_{SO} = atomic fraction SO in YO-SO or CE-SO

TABLE 3

SUMMARY OF COMPOUND PARAMETERS FOR BINARY SYSTEMS
(All units in Joules per gram atom (mole of atoms) T in Kelvins)

Compound	Name	Stoichiometry	Stability	Base	Compound Parameter (Joules/g.at.)
$(1/7)(SiO_2 \cdot 2BeO)$	G	$SO_{0.429}BO_{0.571}$	stable	N	62132-7.406T
$(1/17)(3Al_2O_3 \cdot BeO)$	Q	$AO_{0.882}BO_{0.118}$	stable	C	75312
$(1/7)(Al_2O_3 \cdot BeO)$	I	$AO_{0.714}BO_{0.286}$	stable	C	76567
$(1/11)(Al_2O_3 \cdot 3BeO)$	J	$AO_{0.455}BO_{0.545}$	stable	N	61923+9.916T
$(1/15)(2Y_2O_3 \cdot Al_2O_3)$	U	$YO_{0.667}AO_{0.333}$	stable	Y	70291
$(1/10)(Y_2O_3 \cdot Al_2O_3)$	V	$YO_{0.500}AO_{0.500}$	stable	C	48534+20.083T
$(1/40)(3Y_2O_3 \cdot 5Al_2O_3)$	WA	$YO_{0.375}AO_{0.625}$	stable	C	82425
$(1/5)(Si_2N_2O)$	R	$SN_{0.7}SO_{0.3}$	stable	B	62760-1.255T
$(1/12)(Y_2O_3 \cdot Si_3N_4)$	S	$YO_{0.417}SN_{0.583}$	stable	B	44769+14.644T
$(1/8)(Y_2O_3 \cdot SiO_2)$	M	$YO_{0.625}SO_{0.375}$	stable	Y	-15900+29.288T
$(1/19)(2Y_2O_3 \cdot 3SiO_2)$	K	$YO_{0.527}SO_{0.473}$	stable	Y	-30334+36.819T
$(1/11)(Y_2O_3 \cdot 2SiO_2)$	O	$YO_{0.455}SO_{0.545}$	stable	Y	-2218+23.849T
$(1/12)(Ce_2O_3 \cdot Si_3N_4)$	S	$CE_{0.417}SN_{0.583}$	stable	B	44769+14.644T
$(1/8)(Ce_2O_3 \cdot SiO_2)$	M	$CE_{0.625}SO_{0.375}$	stable	Y	418+24.058T
$(1/62)(7Ce_2O_3 \cdot 9SiO_2)$	Z	$CE_{0.565}SO_{0.435}$	stable	Y	6276+24.434T
$(1/11)(Ce_2O_3 \cdot 2SiO_2)$	O	$CE_{0.455}SO_{0.545}$	stable	Y	7531+25.230T
$0.01(14Si_3N_4 \cdot BeO)$	BP	$SN_{0.98}BO_{0.02}$	stable	B	83680+4.184T
$(1/150)(21Si_3N_4 \cdot SiO_2)$	BP	$SN_{0.98}SO_{0.02}$	stable	B	71128+4.184T
$0.0040(35Si_3N_4 \cdot Y_2O_3)$	BP	$SN_{0.98}YO_{0.02}$	stable	B	83680+4.184T
$0.0040(35Si_3N_4 \cdot Ce_2O_3)$	BP	$SN_{0.98}CE_{0.02}$	stable	B	83680+4.180T

The solution parameters for the Y phase (YYOBO=YBOYO=-2092 J/g.at) are listed in Table 2. The free energy difference between the L and Y forms of YO and BO, i.e. YOYOLY=${}^{\circ}G^{L}_{YO}-{}^{\circ}G^{Y}_{YO}$ and ${}^{\circ}G^{L}_{BO}-{}^{\circ}G^{Y}_{BO}$=BOBOLY are listed in Table 1. The free energy of a compound phase such as $G=(1/7)(SiO_2 \cdot 2BeO)=SO_{0.429}BO_{0.571}$ is defined on the basis of Table 3 in terms of the base phase, the compound parameter, C, and the stoichiometry by equation (3)

$$G^{G}=0.429G^{N}_{SO}+0.571G^{N}_{BO}+(0.429)(0.571)[0.429LSOBO+0.571LBOSO -C] \text{ J/g.at.} \quad (3)$$

Reference to Table 2 shows that LSOBO=LBOSO=41840 J/g.at while Table 3 shows that C=62132-7.406T. Thus

$$G^{G}=0.429G^{N}_{SO}+0.571G^{N}_{BO}-4971+1.813T \text{ J/g.at.} \quad (4)$$

At 298K reference to Figure 1 shows that the stable form of quartz is the beta form (designated R). Table 1 shows that

$$G^{N}_{SO}-G^{R}_{SO}=SOSOLR-SOSOLN=5042-1.004T \text{ J/g.at.} \quad (5)$$

Substitution of equation (5) into eq ation (4) yields an expression for the free energy of formation of $(1/7)(SiO_2 \cdot BeO)$ at 298K from the stable forms of it s compound components as,

$$\Delta G_f[298K]=G^{G}-0.429G^{R}_{SO}-0.571G^{N}_{BO}=-2808+1.382T \text{ J/g.at.} \quad (6)$$

TABLE 4

CALCULATED FREE ENERGY OF FORMATION OF COMPOUND PHASES
(All Units in Joules per gram atom (mole of atoms), T in Kelvins)

Compound	Name	Stoichiometry	Free Energy of Formation, ΔG_f[298K] from Component Compounds
$(1/7)(SiO_2 \cdot 2BeO)$	G	$SO_{0.429}BO_{0.571}$	-2808 + 1.382T/-2809+0.777T(8)
$(1/17)(3Al_2O_3 \cdot BeO)$	Q	$AO_{0.882}BO_{0.118}$	-2203 - 0.464T
$(1/7)(Al_2O_3 \cdot BeO)$	I	$AO_{0.714}BO_{0.286}$	-2381 - 1.125T
$(1/11)(Al_2O_3 \cdot 3BeO)$	J	$AO_{0.455}BO_{0.545}$	-2524 - 1.049T
$(1/15)(2Y_2O_3 \cdot Al_2O_3)$	U	$YO_{0.667}AO_{0.333}$	-4950 - 0.615T
$(1/10)(Y_2O_3 \cdot Al_2O_3)$	V	$YO_{0.500}AO_{0.500}$	-2351 - 4.100T
$(1/40)(3Y_2O_3 \cdot 5Al_2O_3)$	WA	$YO_{0.375}AO_{0.625}$	-7866 + 0.690T
$(1/5)(Si_2N_2O)$	R	$SN_{0.700}SO_{0.300}$	-5514 - 0.038T/-5781 + 0.40T(5)
$(1/12)(Y_2O_3 \cdot Si_3N_4)$	S	$YO_{0.417}SN_{0.583}$	-404 - 1.833T
$(1/8)(Y_2O_3 \cdot SiO_2)$	M	$YO_{0.625}SO_{0.375}$	-15958 + 1.389T
$(1/19)(2Y_2O_3 \cdot 3SiO_2)$	K	$YO_{0.527}SO_{0.473}$	-13000 - 0.475T
$(1/11)(Y_2O_3 \cdot 2SiO_2)$	O	$YO_{0.455}SO_{0.545}$	-19527 - 2.669T
$(1/12)(Ce_2O_3 \cdot Si_3N_4)$	S	$CE_{0.417}SN_{0.583}$	-1389 - 1.828T
$(1/8)(Ce_2O_3 \cdot SiO_2)$	M	$CE_{0.625}SO_{0.375}$	-19787 + 2.615T
$(1/62)(7Ce_2O_3 \cdot 9SiO_2)$	Z	$CE_{0.565}SO_{0.435}$	-21974 + 2.606T
$(1/11)(Ce_2O_3 \cdot 2SiO_2)$	O	$CE_{0.455}SO_{0.545}$	-21945 + 2.326T
$0.01(14Si_3N_4 \cdot BeO)$	BP	$SN_{0.980}BO_{0.020}$	-423 - 0.113T
$(1/150)(21Si_3N_4 \cdot SiO_2)$	BP	$SN_{0.980}SO_{0.020}$	-720 - 0.102T
$0.004(35Si_3N_4 \cdot Y_2O_3)$	BP	$SN_{0.980}YO_{0.020}$	-1104
$0.004(35Si_3N_4 \cdot Ce_2O_3$	BP	$SN_{0.980}CE_{0.020}$	-1158

Reference to Table 4 shows that this result is in keeping with the experimental (8) thermochemical data on the free energy of formation of $2BeO \cdot SiO_2$. Table 4 also displays the calculated free energy of formation for the remaining compounds listed in Table 3 and shown in Figures 1-12. It should be noted that this compound parameter for $SN_{0.7}SO_{0.3}$ currently shown as G=62760-1.255T J/g.at. has been revised from the previously stated value G=115060-25.10T J/g.at.(5) The current value is based on the assessment of Doerner et al (5) and leads to slight revisions in the previously calculated SN-SO and SO-AO-SN phase diagrams presented earlier (3). The revised versions, which differ slightly from the earlier results are shown in Figures 8

References

1. L. Kaufman and H. Nesor, CALPHAD 2 35 (1978)
2. L. Kaufman, CALPHAD 3 27 (1979)
3. L. Kaufman, CALPHAD 3 279 (1979)
4. L.J. Gaukler, H.L. Lukas, E.Th. Henig and G. Petzow, CALPHAD 2 349 (1979).
5. P. Doerner, L.J. Gaukler, H. Krieg, H.L. Lukas, G. Petzow and J. Weiss, CALPHAD 3 239 (1979).
6. J. Weiss, H.L. Lukas, J. Lorenz, G. Petzow ans H. Krieg, CALPHAD 5 123 (1981).
7. E.M. Levin, C.R. Robbins and H.F. McMurdie, Phase Diagrams for Ceramists, American Ceramics Society, Columbus, Ohio (1964), First Supplement (Ibid) (1969) Second Supplement, Ibid (1975)
8. O. Kubaschewski and C.B. Alcock, Metallurgical Thermochemistry Fifth Edition (1979) Pergamon Press, Oxford.
9. R. Mueller, Thesis University of Stuttgart (1981) To be Published in CALPHAD by J. Weiss, R. Mueller, H.L. Lukas, H. Krieg, G. Petzow and T.Y. Tien.
10. L.J. Gaukler, H. Hohnke and T.Y. Tien, J. American Ceramic Society 63 35 (1980)
11. F.F. Lange, Ceramic Bulletin 59 239 (1980).

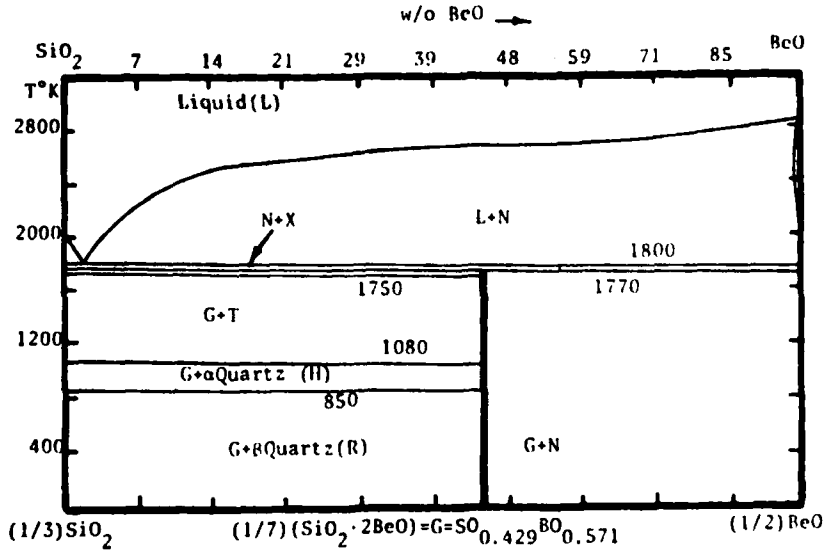

Figure 1. Calculated $(1/3)SiO_2$-(1/2)BeO Phase Diagram.

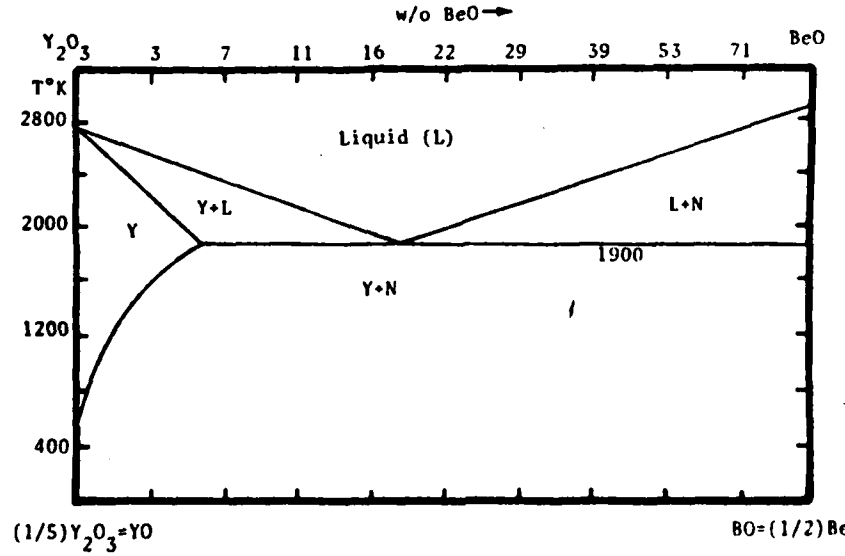

Figure 2. Calculated $(1/5)Y_2O_3$-(1/2)BeO Phase Diagram.

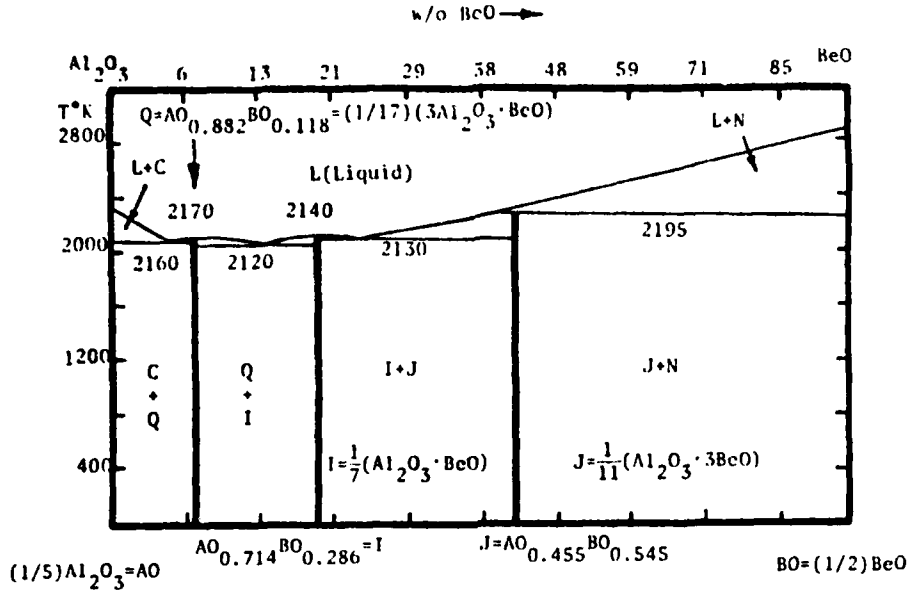

Figure 3. Calculated $(1/5)Al_2O_3$-(1/2)BeO Phase Diagram.

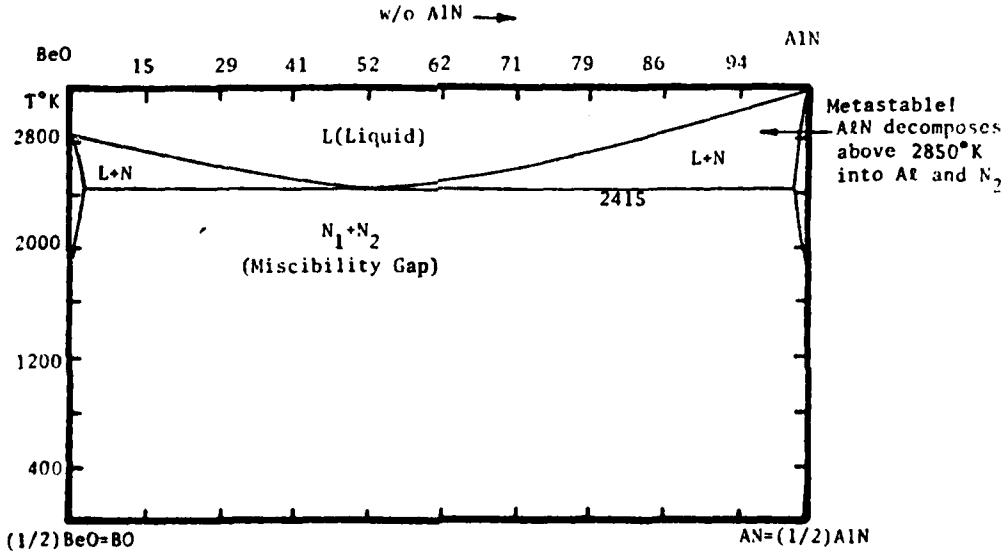

Figure 4. Calculated (1/2)BeO-(1/2)AlN Phase Diagram.

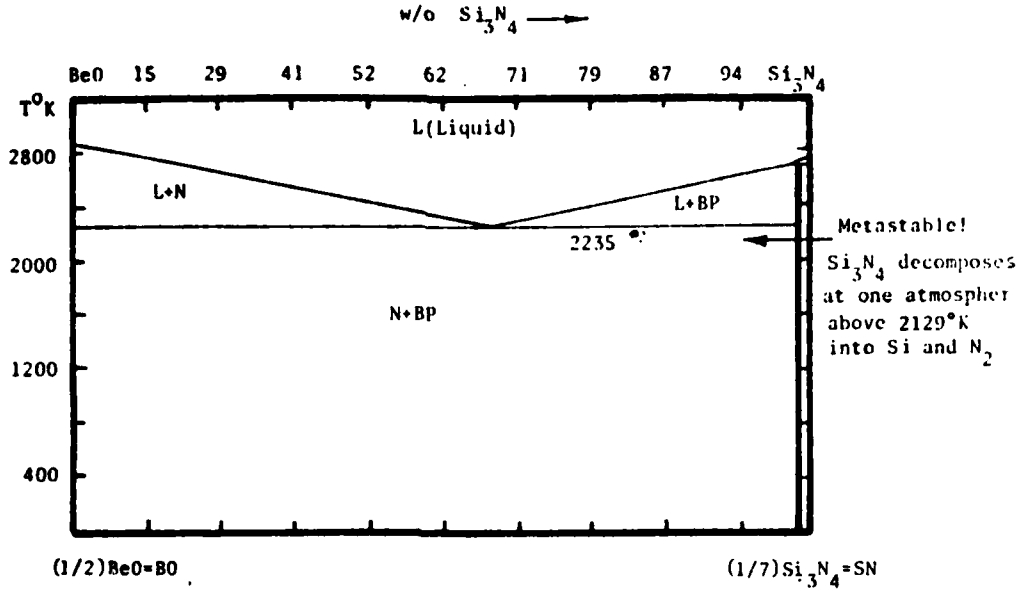

Figure 5. Calculated 1/2BeO - 1/7 Si_3N_4 Phase Diagram

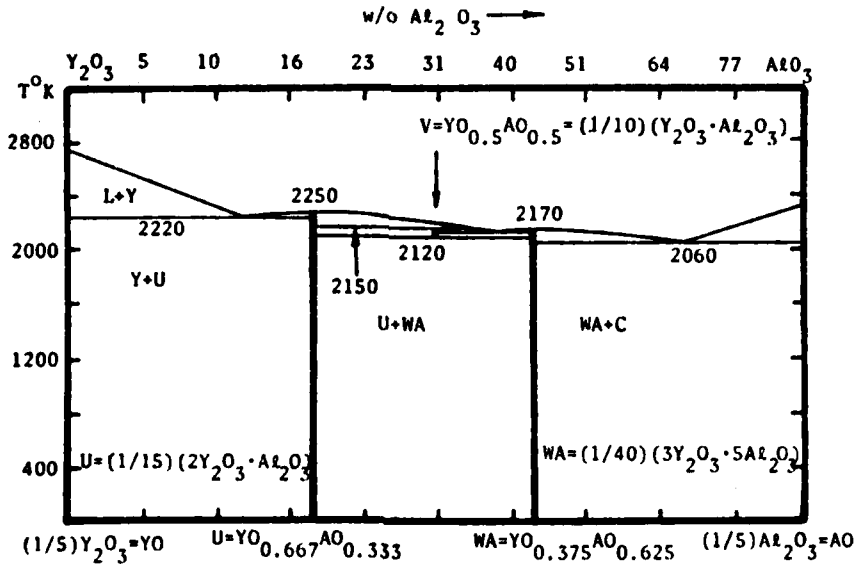

Figure 6. Calculated 1/5Y_2O_3 - 1/5Al_2O_3 Phase Diagram

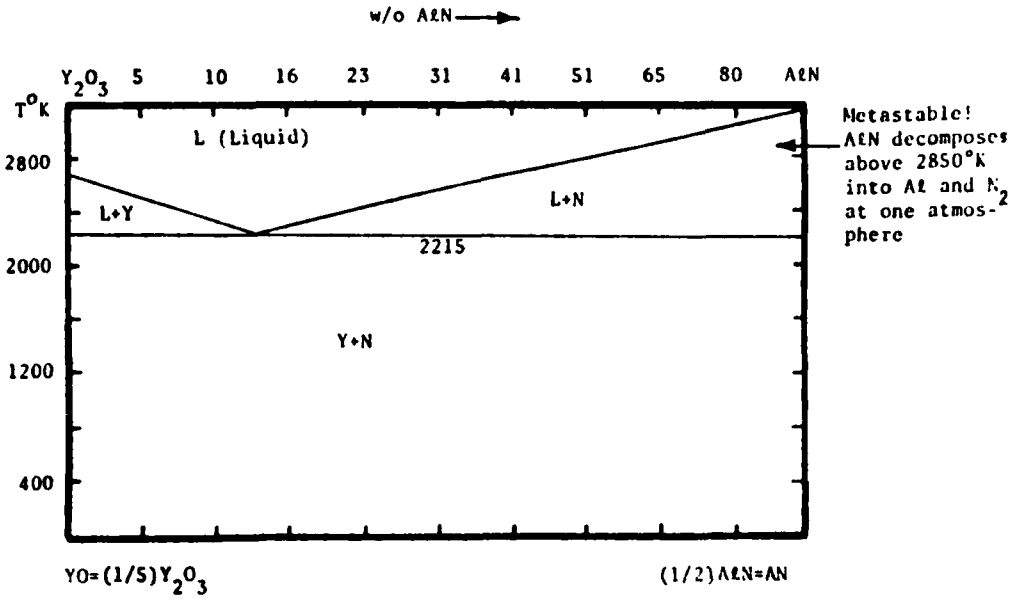

Figure 7. Calculated 1/5Y_2O_3 - 1/2AℓN Phase Diagram

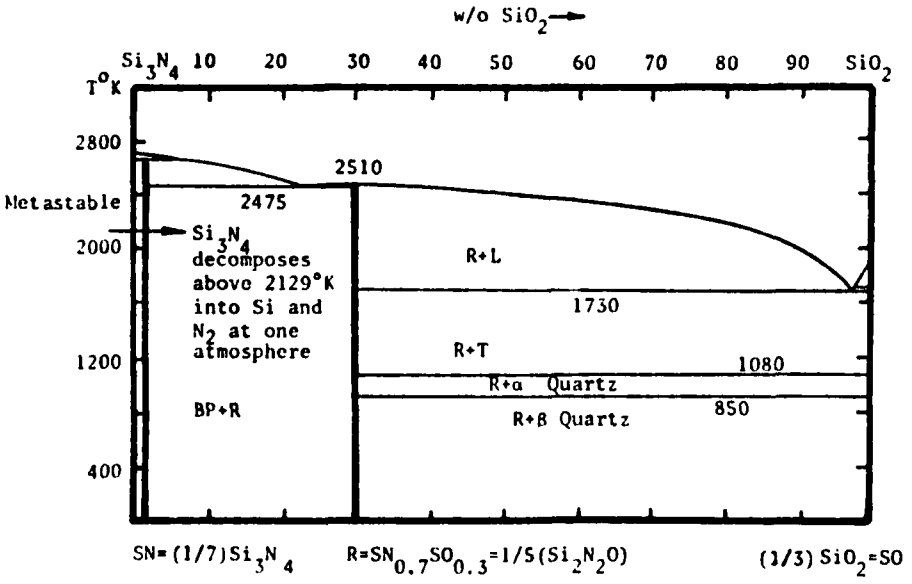

Figure 8. Calculated 1/7Si_3N_4 - 1/3SiO_2 Phase Diagram

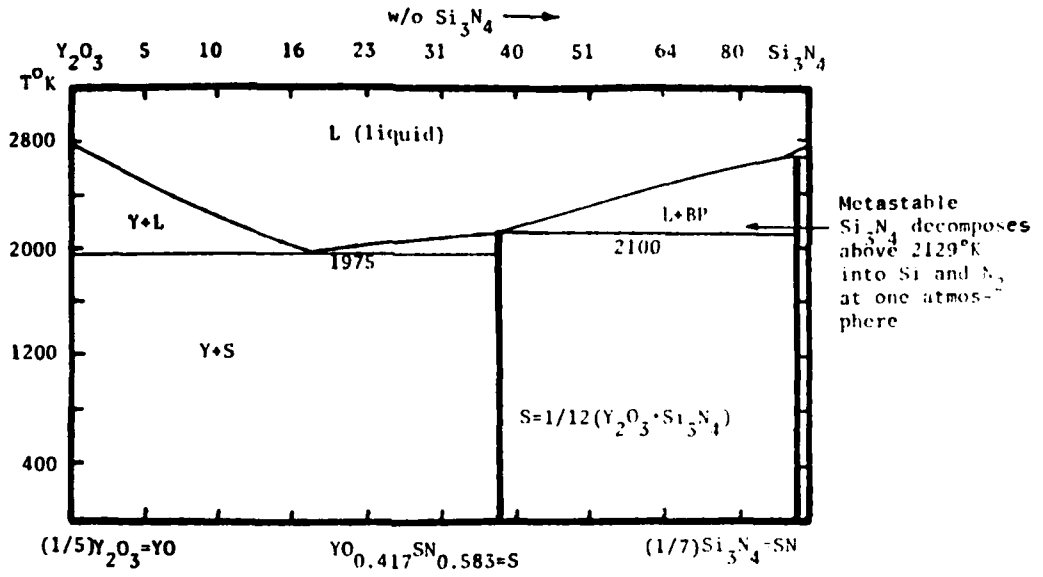

Figure 9. Calculated $1/5Y_2O_3$ - $1/7Si_3N_4$ Phase Diagram

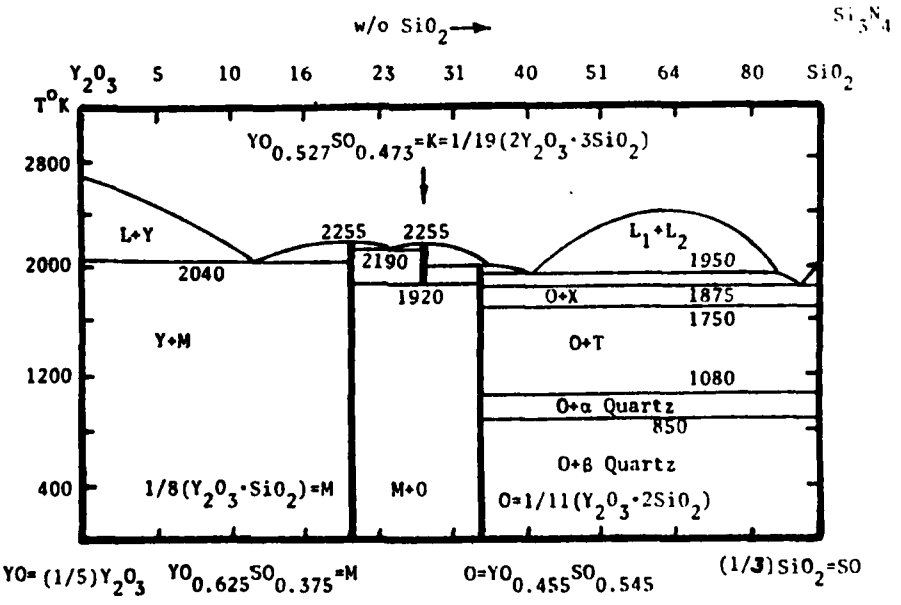

Figure 10. Calculated $1/5Y_2O_3$ - $1/3SiO_2$ Phase Diagram

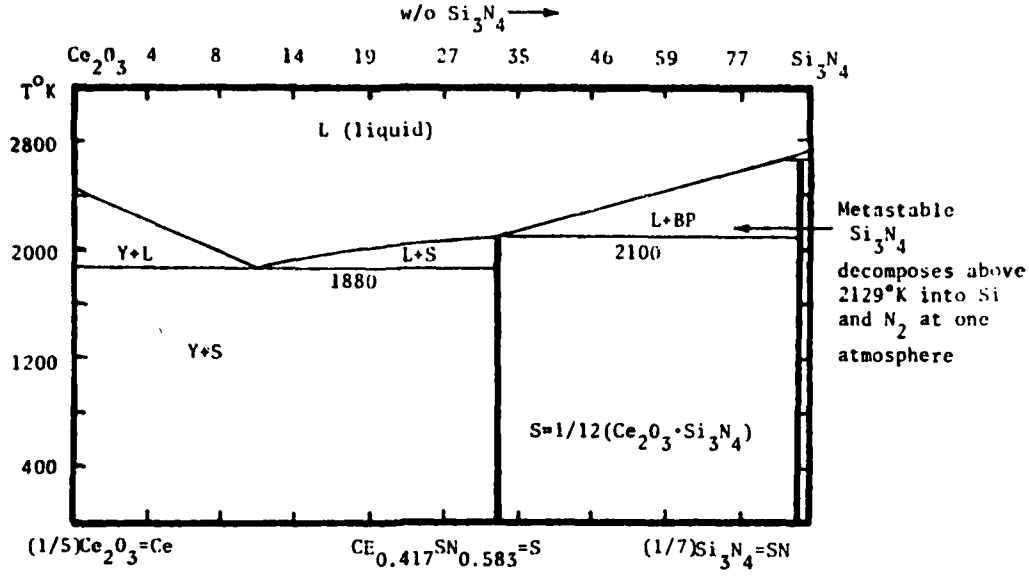

Figure 11. Calculated 1/5 Ce_2O_3 - 1/7Si_3N_4 Phase Diagram

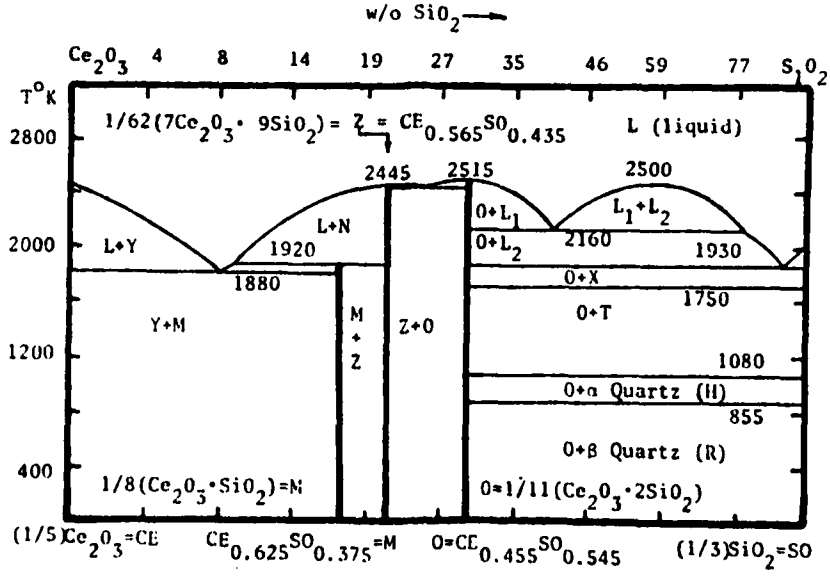

Figure 12. Calculated 1/5Ce_2O_3 - 1/3SiO_2 Phase Diagram

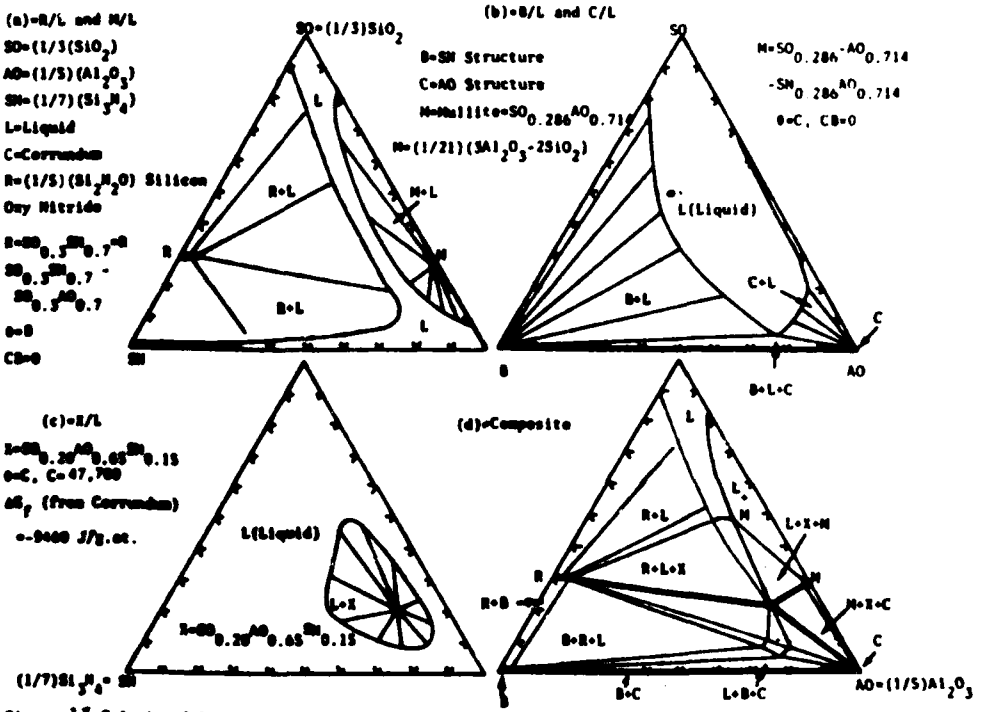

Figure 13 Calculated Pairwise (a-c) and Composite Equilibrium (d) in the $(1/3)(SiO_2)$ - $(1/7)(Si_3N_4)$-$(1/5)Al_2O_3$ System at 2000K and one atmosphere

III. CALCULATION OF QUASI-TERNARY CERAMIC SYSTEMS

L. Kaufman, F. Hayes, and D. Birnie, High Temperatures-High Pressures (1982) 14 619-31

Abstract. Phase diagrams for the quasibinary systems Si_3N_4-SiO_2, Y_2O_3-Si_3N_4, Y_2O_3-SiO_2, Ce_2O_3-Si_3N_4, and Ce_2O_3-SiO_2 are recalculated to illustrate a method by which these and more complex equilibria can be elucidated from thermodynamic data. New results for the quasiternary systems SiO_2-MgO-Si_3N_4, SiO_2-Y_2O_3-Si_3N_4, and SiO_2-Ce_2O_3-Si_3N_4 are derived from these phase diagrams and presented as component pairwise equilibria and complete isothermal sections of the appropriate ternary phase diagrams. These sections are compared with experimental data from the literature, and good agreement was obtained in the cases of SiO_2-MgO-Si_3N_4 and SiO_2-Ce_2O_3-Si_3N_4.

1 Introduction

The utility of computer based methods for coupling phase diagrams and thermochemical data for metallic systems has been well documented in many papers published in the journal *CALPHAD*. A considerable effort is being applied toward developing an extensive data base for metallic systems. Recently similar efforts have begun in order to provide a similar facility with ceramic systems. The expanded studies of SIALON composites, in which silicon and aluminum nitrides are combined with oxides of silicon, aluminum, magnesium, beryllium, cerium, yttrium, and other metals has provided additional motivation for predicting multicomponent phase diagrams of ceramic systems.

Previous work in this laboratory on the development of a data base for the calculation of quasibinary and quasiternary phase diagrams of ceramic systems (Kaufman and Nesor 1978; Kaufman 1979a, 1979b) has covered combinations of Cr_2O_3, MgO, Al_2O_3, Fe_2O_3, Fe_3O_4, 'FeO', SiO_2, CaO, Si_3N_4, and AlN. Lattice stability, solution, and compound phase parameters were derived covering the liquid, spinel, corundum, periclase, crystobalite, tridymite, quartz, hexagonal, and β' phases which appear in the binary systems composed of pairs of these compounds. Compound phases formed from specific binary combinations of these compounds (eg $MgO{\cdot}Cr_2O_3$) were also characterized from experimental observations of the binary systems of interest. Selected ternary systems have been computed from this data base for comparison with experimental sections in order to illustrate the usefulness of the data base. In this paper the data base is extended to cover Y_2O_3 and Ce_2O_3; ternary sections in the SiO_2-MgO-Si_3N_4, SiO_2-Y_2O_3-Si_3N_4, and SiO_2-Ce_2O_3-Si_3N_4 systems were also calculated between 1900 K and 2100 K for comparison with experiment.

2 Thermochemical system for characterization of phases

The method utilized for describing solution and compound phases is the same as that employed earlier (Kaufman and Nesor 1978), and has been devised to facilitate the manipulation of data. The free energy, G^L, of a liquid (solution) phase, L, in the binary system Si_3N_4-SiO_2 is given by equation (1) where T is the absolute

temperature, R is the gas constant, x is the atom fraction of SO (ie $\frac{1}{3}SiO_2$), and $(1-x)$ is the atom fraction of SN (ie $\frac{1}{4}Si_3N_4$). The amount of substance basis is thus one mole of atoms (ie a gram atom):

$$G^{L} = (1-x)^{\circ}G^{L}_{SN} + x^{\circ}G^{L}_{SO} + RT[x\ln x + (1-x)\ln(1-x)] + x(1-x)[(1-x)G^{L}_{SNSO} + xG^{L}_{SOSN}]. \quad (1)$$

Table 1. Expressions for lattice stability parameters for various phases of SiO_2, Si_3N_4, Y_2O_3, and Ce_2O_3. Sources of data: Levin et al (1964); Kaufman (1979b).

$^{\circ}G^{L}_{YO} - {}^{\circ}G^{Y}_{YO} = 22694 - 8{\cdot}368T$	$^{\circ}G^{L}_{SN} - {}^{\circ}G^{B}_{SN} = 33949 - 12{\cdot}510T$
$^{\circ}G^{L}_{YO} - {}^{\circ}G^{X}_{YO} = 0 - 2{\cdot}092T$	$^{\circ}G^{L}_{SN} - {}^{\circ}G^{Y}_{SN} = 0 - 8{\cdot}368T$
$^{\circ}G^{L}_{YO} - {}^{\circ}G^{B}_{YO} = 0 - 12{\cdot}510T$	$^{\circ}G^{L}_{SO} - {}^{\circ}G^{X}_{SO} = 3347 - 1{\cdot}674T$
$^{\circ}G^{L}_{CE} - {}^{\circ}G^{Y}_{CE} = 20334 - 8{\cdot}638T$	$^{\circ}G^{L}_{SO} - {}^{\circ}G^{R}_{SO} = 5042 - 3{\cdot}096T$
$^{\circ}G^{L}_{CE} - {}^{\circ}G^{X}_{CE} = 0 - 2{\cdot}092T$	$^{\circ}G^{L}_{SO} - {}^{\circ}G^{Y}_{SO} = 0 - 2{\cdot}092T$
$^{\circ}G^{L}_{CE} - {}^{\circ}G^{B}_{CE} = 0 - 12{\cdot}510T$	

Phases: L, liquid; Y, body-centered cubic; X, crystobalite; B, β-Si_3N_4; R, β-quartz; T, tridymite.
Atom bases: YO, $\frac{1}{2}Y_2O_3$; SN, $\frac{1}{4}Si_3N_4$; CE, $\frac{1}{2}Ce_2O_3$; SO, $\frac{1}{3}SiO_2$.
$G = G/J\ (\text{g atom})^{-1}$; $T = T/K$.

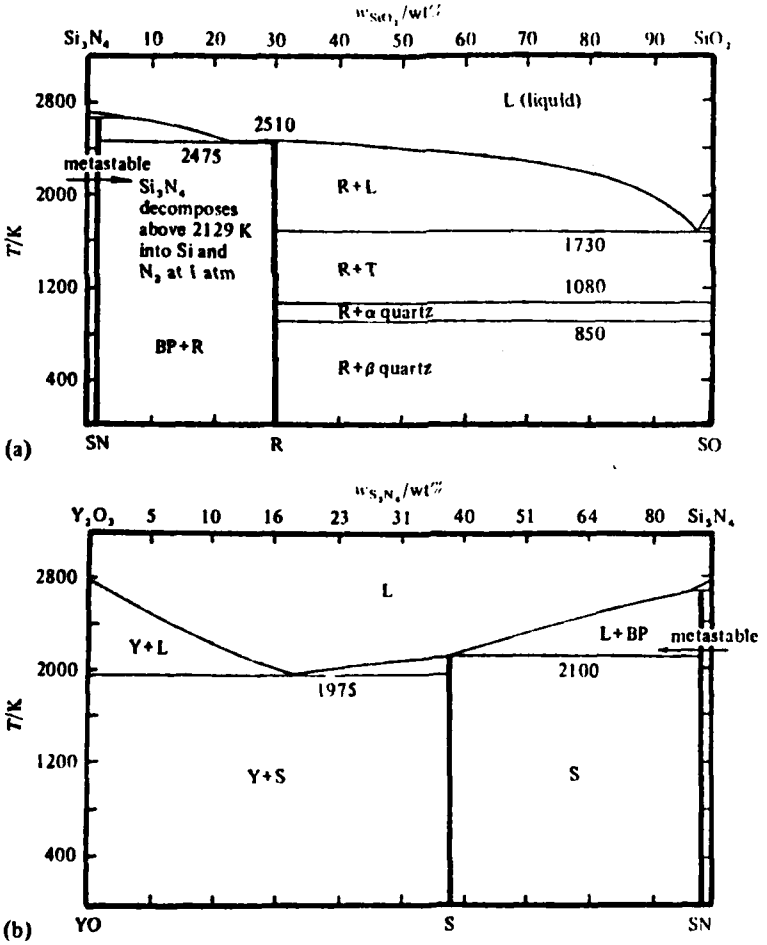

Figure 1. Calculated phase diagrams for binary systems (see tables 1-3 for explanation of symbols). (a) Si_3N_4-SiO_2; (b) Y_2O_3-Si_3N_4; (c) Y_2O_3-SiO_2; (d) Ce_2O_3-Si_3N_4; (e) Ce_2O_3-SiO_2.

Here ${}^{\circ}G^{L}_{SN}$ and ${}^{\circ}G^{L}_{SO}$ are the free energies of one gram atom of pure liquid SN and SO. Table I gives the lattice stabilities of the liquid and solid forms of SN, SO, and the other components of current interest. These data, derived from earlier studies

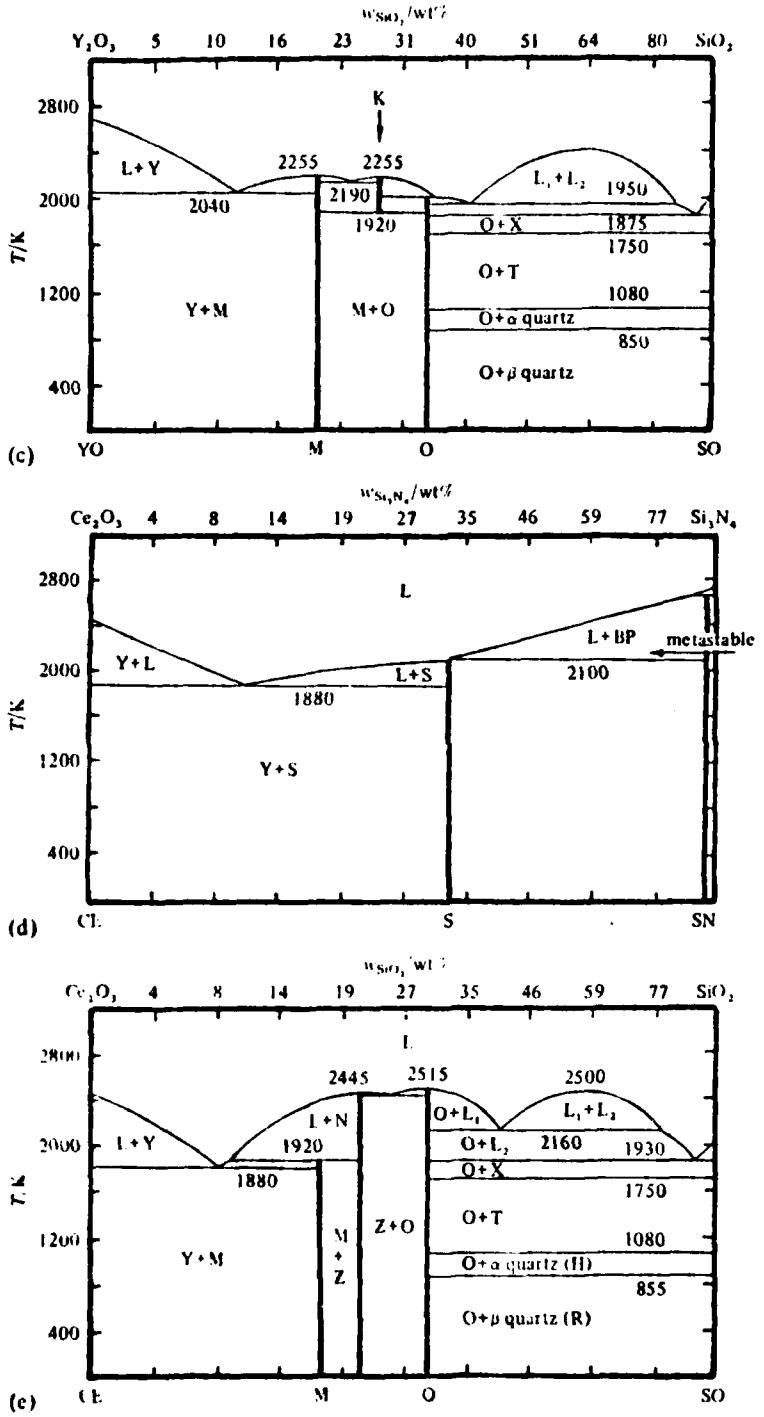

Figure 1 (continued).

and compilations of thermochemical data and phase diagrams, can be used to calculate the binary phase diagrams shown in figure 1 when combined with the parameters for solution and compound phases shown in tables 2 and 3. The solution parameters G^{L}_{SNSO} and G^{L}_{SOSN}, which describe the liquid Si_3N_4–SiO_2 solution, are listed in table 2, together with similar parameters for the liquid and solid phases. The free energy of the solid solution phases are described in a manner similar to equation (1). Thus, for example, the free energy of the body-centered cubic (Mn_2O_3) Y phase in the Y_2O_3–SiO_2 system is given by

$$G^{Y} = (1-x)^{\circ}G^{Y}_{YO} + x^{\circ}G^{Y}_{SO} + RT[x\ln x + (1-x)\ln(1-x)] + x(1-x)[(1-x)G^{Y}_{YOSO} + xG^{Y}_{SOYO}]. \quad (2)$$

The free energy differences between the L and Y forms of YO and SO, ie $^{\circ}G^{L}_{YO} - {}^{\circ}G^{Y}_{YO}$ and $^{\circ}G^{L}_{SO} - {}^{\circ}G^{Y}_{SO}$, are listed in table 1. The free energy of a compound phase such as R [ie $\frac{1}{10}(Si_3N_4 \cdot SiO_2)$ or $SN_{0.7}SN_{0.3}$] is defined from table 3 in terms of the base

Table 2. Summary of solution parameters for quasibinary systems. Sources of data: Levin et al (1964); Kaufman (1979b).

$G^{L}_{CESN} = G^{L}_{SNCE} = 4180$	$G^{L}_{YOSO} = G^{L}_{SOYO} = -92048 + 36{\cdot}82T \quad (0 \leqslant x^{a} \leqslant 0{\cdot}6)$
$G^{B}_{CESN} = G^{B}_{SNCE} = 62760$	$G^{L}_{YOSO} = -216000 + 66{\cdot}94T$
$G^{Y}_{CESN} = G^{Y}_{SNCE} = 62760$	$G^{L}_{SOYO} = -9414 + 16{\cdot}74T$ $\}$ $(0{\cdot}6 \leqslant x \leqslant 1{\cdot}0)$
$G^{L}_{SNSO} = G^{L}_{SOSN} = 29288$	$G^{Y}_{YOSO} = G^{Y}_{SOYO} = 83680$
$G^{X}_{SNSO} = G^{X}_{SOSN} = 125520$	$G^{X}_{YOSO} = G^{X}_{SOYO} = 83680$
$G^{T}_{SNSO} = G^{T}_{SOSN} = 125520$	$G^{T}_{YOSO} = G^{T}_{SOYO} = 83680$
$G^{L}_{YOSN} = G^{L}_{SNYO} = 4180$	$G^{L}_{CESO} = G^{L}_{SOCE} = -92048 + 36{\cdot}82T \quad (0 \leqslant x \leqslant 0{\cdot}6)$
$G^{B}_{YOSN} = G^{B}_{SNYO} = 83680$	$G^{L}_{CESO} = -216000 + 66{\cdot}94T$
$G^{Y}_{YOSN} = G^{Y}_{SNYO} = 83680$	$G^{L}_{SOCE} = -9414 + 16{\cdot}74T$ $\}$ $(0{\cdot}6 \leqslant x \leqslant 1{\cdot}0)$
	$G^{Y}_{CESO} = G^{Y}_{SOCE} = 83680$
	$G^{X}_{CESO} = G^{X}_{SOCE} = 83680$
	$G^{T}_{CESO} = G^{T}_{SOCE} = 83680$

[a] x is the atom fraction of SO present [see equation (2)].
For explanation of other symbols, see table 1.

Table 3. Summary of compound parameters for binary systems. (All compounds listed are stable at 298 K.) Sources of data: Jack (1977); Wills (1974, 1975); Morgan (1976); Levin et al (1964).

Compound	Name symbol	Stoichiometry	Base[a] symbol	C/J (g atom)$^{-1}$
$\frac{1}{3}(Si_2N_2O)$	R	$SN_{0.7}SO_{0.3}$	B	$62760 - 1{\cdot}255T$
$\frac{1}{12}(Y_2O_3 \cdot Si_3N_4)$	S	$YO_{0.417}SN_{0.583}$	B	$44769 + 14{\cdot}644T$
$\frac{1}{8}(Y_2O_3 \cdot SiO_2)$	M	$YO_{0.625}SO_{0.375}$	Y	$-15900 + 29{\cdot}288T$
$\frac{1}{19}(2Y_2O_3 \cdot 3SiO_2)$	K	$YO_{0.527}SO_{0.473}$	Y	$-30334 + 36{\cdot}819T$
$\frac{1}{11}(Y_2O_3 \cdot 2SiO_2)$	O	$YO_{0.455}SO_{0.545}$	Y	$-2218 + 23{\cdot}849T$
$\frac{1}{12}(Ce_2O_3 \cdot Si_3N_4)$	S	$CE_{0.417}SN_{0.583}$	B	$44769 + 14{\cdot}644T$
$\frac{1}{8}(Ce_2O_3 \cdot SiO_2)$	M	$CE_{0.625}SO_{0.375}$	Y	$418 + 24{\cdot}058T$
$\frac{1}{23}(7Ce_2O_3 \cdot 9SiO_2)$	Z	$CE_{0.565}SO_{0.435}$	Y	$6276 + 24{\cdot}434T$
$\frac{1}{11}(Ce_2O_3 \cdot 2SiO_2)$	O	$CE_{0.455}SO_{0.545}$	Y	$7531 + 25{\cdot}230T$
$\frac{1}{130}(21Si_3N_4 \cdot SiO_2)$	BP	$SN_{0.98}SO_{0.02}$	B	$71128 + 4{\cdot}184T$
$0{\cdot}0040(35Si_3N_4 \cdot Y_2O_3)$	BP	$SN_{0.98}YO_{0.02}$	B	$83680 + 4{\cdot}184T$
$0{\cdot}0040(35Si_3N_4 \cdot Ce_2O_3)$	BP	$SN_{0.98}CE_{0.02}$	B	$83680 + 4{\cdot}180T$

[a] See table 1 for explanation of these and other symbols.

phase, the compound parameter, C, and the stoichiometry, by the equation

$$G^{R} = 0{\cdot}7^{\circ}G^{B}_{SN} + 0{\cdot}3^{\circ}G^{B}_{SO} + (0{\cdot}7)(0{\cdot}3)[0{\cdot}7G^{L}_{SNSO} + 0{\cdot}3G^{L}_{SOSN} - C]\,. \quad (3)$$

Reference to table 2 shows that $G^{L}_{SNSO} = G^{L}_{SOSN} = 29\,288$ J (g atom)$^{-1}$, while table 3 shows that $C = 62\,760 - 1{\cdot}255T$ J (g atom)$^{-1}$, where $T = T/K$. Thus, we obtain

$$G^{R} = 0{\cdot}7^{\circ}G^{B}_{SN} + 0{\cdot}3^{\circ}G^{B}_{SO} - 7029 + 0{\cdot}2636T\,, \quad (4)$$

where $G = G/J$ (g atom)$^{-1}$. At 298 K reference to figure 1 shows that the stable form of quartz is the β form (designated R). Table 1 shows that

$$^{\circ}G^{B}_{SO} - {}^{\circ}G^{R}_{SO} = 5042 - 1{\cdot}006T\,. \quad (5)$$

Substitution of equation (5) into equation (4) yields an expression for the free energy of formation of $\frac{1}{10}(Si_3N_4{\cdot}SiO_2)$ at 298 K from the stable forms of its compound components as

$$\Delta G_{f,298} = G^{R} - 0{\cdot}7^{\circ}G^{B}_{SN} - 0{\cdot}3^{\circ}G^{R}_{SO} = -5516 - 0{\cdot}038T\,. \quad (6)$$

Reference to table 4 shows that the result given in equation (6) is in keeping with the experimental thermochemical data on the free energy of formation of $Si_3N_4{\cdot}SiO_2$ given by Doerner et al (1979).

Table 4 also displays the calculated free energy of formation for the remaining compounds listed in table 3 and shown in figure 1. It should be noted that the above compound parameter for $SN_{0{\cdot}7}SO_{0{\cdot}3}$ has been revised from the previously stated value $C = 115\,060 - 25{\cdot}107T$ J (g atom)$^{-1}$ (Kaufman 1979b); the current value is based on the assessment of Doerner et al (1979).

Table 4. Calculated free energies of formation of compound phases from component atom bases[a].

Compound	Name symbol	Stoichiometry	$\Delta G_{f,298}$/J (g atom)$^{-1}$
$\frac{1}{5}(Si_2N_2O)$	R	$SN_{0{\cdot}700}SO_{0{\cdot}300}$	$-5514 - 0{\cdot}038T$[b]
$\frac{1}{12}(Y_2O_3{\cdot}Si_3N_4)$	S	$YO_{0{\cdot}417}SN_{0{\cdot}583}$	$-404 - 1{\cdot}833T$
$\frac{1}{8}(Y_2O_3{\cdot}SiO_2)$	M	$YO_{0{\cdot}625}SO_{0{\cdot}375}$	$-15\,958 + 1{\cdot}389T$
$\frac{1}{19}(2Y_2O_3{\cdot}3SiO_2)$	K	$YO_{0{\cdot}527}SO_{0{\cdot}473}$	$-13\,000 - 0{\cdot}475T$
$\frac{1}{11}(Y_2O_3{\cdot}2SiO_2)$	O	$YO_{0{\cdot}455}SO_{0{\cdot}545}$	$-19\,527 - 2{\cdot}669T$
$\frac{1}{12}(Ce_2O_3{\cdot}Si_3N_4)$	S	$CE_{0{\cdot}417}SN_{0{\cdot}583}$	$-1389 - 1{\cdot}828T$
$\frac{1}{8}(Ce_2O_3{\cdot}SiO_2)$	M	$CE_{0{\cdot}625}SO_{0{\cdot}375}$	$-19\,787 + 2{\cdot}615T$
$\frac{1}{62}(7Ce_2O_3{\cdot}9SiO_2)$	Z	$CE_{0{\cdot}565}SO_{0{\cdot}435}$	$-21\,974 + 2{\cdot}606T$
$\frac{1}{11}(Ce_2O_3{\cdot}2SiO_2)$	O	$CE_{0{\cdot}455}SO_{0{\cdot}545}$	$-21\,945 + 2{\cdot}326T$
$\frac{1}{150}(21Si_3N_4{\cdot}SiO_2)$	BP	$SN_{0{\cdot}980}SO_{0{\cdot}020}$	$-720 - 0{\cdot}120T$
$0{\cdot}004(35Si_3N_4{\cdot}Y_2O_3)$	BP	$SN_{0{\cdot}980}YO_{0{\cdot}020}$	-1104
$0{\cdot}004(35Si_3N_4{\cdot}Ce_2O_3)$	BP	$SN_{0{\cdot}980}CE_{0{\cdot}020}$	-1158

[a] See table 1 for explanation of symbols.
[b] $-5781 + 0{\cdot}40T$ (Doerner et al 1979).

3 Calculation of quasiternary phase diagrams

The free energies of ternary solution phases were calculated from the binary solution phases on the basis of the Kohler equation as in previous papers (Kaufman and Nesor 1978; Kaufman 1979a, 1979b). For example, the free energy of the liquid phase in the SO–MO–SN system (MO = $\frac{1}{2}$MgO), where x is the atom fraction of MO and y

the atom fraction of SN, is given by

$$G^{L} = (1-x-y)^{\circ}G^{L}_{SO} + x^{\circ}G^{L}_{MO} + y^{\circ}G^{L}_{SN} + RT[(1-x-y)\ln(1-x-y) + x\ln x + y\ln y] + (1-x-y)x(1-y)^{-1}[(1-x-y)G^{L}_{SOMO} + xG^{L}_{MOSO}] + xy(x+y)^{-1}[xG^{L}_{MOSN} + yG^{L}_{SNMO}] + (1-x-y)y(1-x)^{-1}[(1-x-y)G^{L}_{SOSN} + yG^{L}_{SNSO}]. \quad (7)$$

The solution parameters required to specify G^{L} were given previously (Kaufman 1979a, 1979b) as $G^{L}_{SOSN} = G^{L}_{SNSO} = G^{L}_{MOSN} = G^{L}_{SNMO} = 29\,288$ J (g atom)$^{-1}$ and $G^{L}_{SOMO} = G^{L}_{MOSO} = -106\,274 + 42{\cdot}01T$ for $0{\cdot}4 \leqslant x \leqslant 1{\cdot}0$ and $G^{L}_{SOMO} = -24\,267 + 24{\cdot}27T$, $G^{L}_{MOSO} = -220\,283 + 68{\cdot}62T$ for $0{\cdot}0 \leqslant x \leqslant 0{\cdot}40$. These parameters permit explicit definition of G^{L} in composition ranges where $[x/(1-x-y)] \geqslant 0{\cdot}667$, and ranges where $[x/(1-x-y)] < 0{\cdot}667$. In the latter range, the miscibility gap present in the SO–MO binary system propagates into the ternary SO–MO–SN as shown in figure 2a. Here, the ternary miscibility gap shows the tie lines connecting the coexisting liquid compositions L_1 and L_2.

The remaining solution phases in this system, ie P, X, B, etc, are defined in similar fashion to that illustrated by equation (7). The resulting equilibria between the L and P solutions are depicted by the tie lines traversing the two-phase L+P field shown in figure 2b. The compound phases F, R, and BP which appear in the SO–MO, SO–SN, and MO–SN binary systems are defined along the lines previously

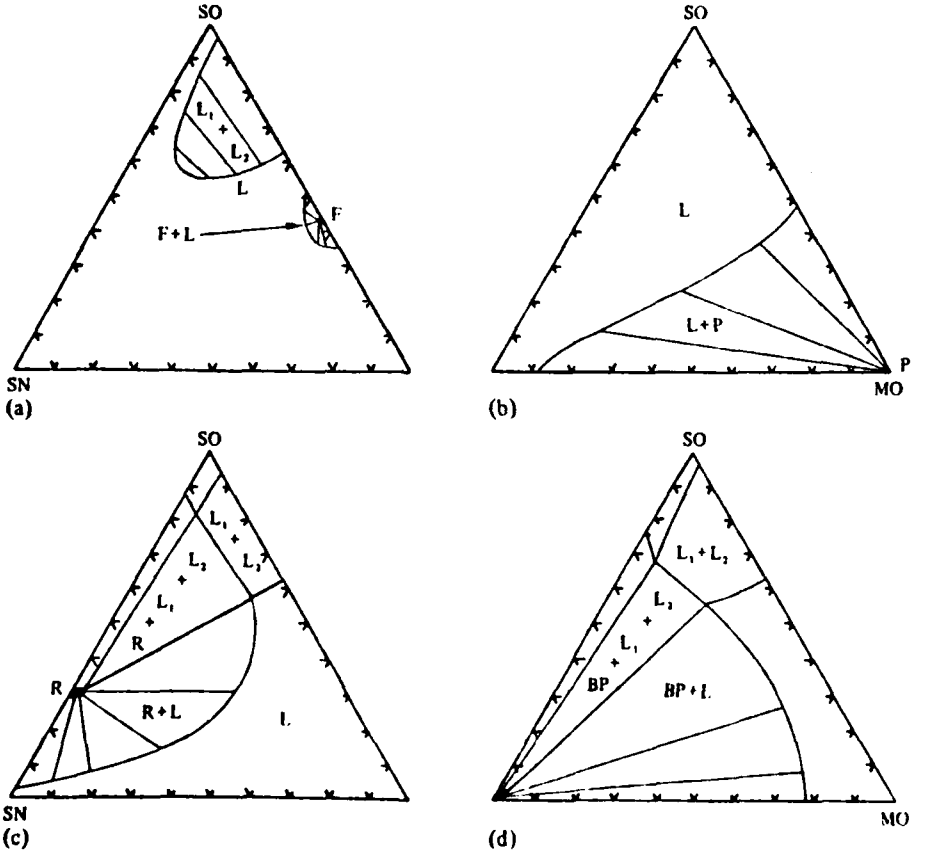

Figure 2. Calculated pairwise equilibria in the SiO_2-MgO-Si_3N_4 system at 2100 K (see tables 1-5 for explanation of symbols). (a) F-L; (b) L-P (P, periclase); (c) L-R; (d) BP-L.

established (Kaufman and Nesor 1978; Kaufman 1979a, 1979b) and are specified in table 3. Thus, for example, the free energy of the $SN_{0\cdot7}SO_{0\cdot3}$ phase (R) in the SO-MO-SN system is defined as:

$$G^{R} = z^{\circ}G^{B}_{SN} + x^{\circ}G^{B}_{SO} + y^{\circ}G^{B}_{MO} + \left(1 - \frac{y}{1-x}\right)\Delta G_{A} + \frac{y}{1-x}\Delta G_{B}$$

$$+ RT[y\ln y + z\ln z - (1-x)\ln(1-x)] + \Delta G_{E}\ , \qquad (8)$$

where x, y, and z are the atom fractions of SO, MO, and SN, respectively. Since the compound phase runs from $SN_{0\cdot70}SO_{0\cdot30}$ to $MO_{0\cdot70}SO_{0\cdot30}$, $x = 0\cdot3$, and $z = 0\cdot7 - y$. Also,

$$\Delta G_{A} = (0\cdot3)(0\cdot7)(0\cdot7G^{L}_{SNSO} + 0\cdot3G^{L}_{SOSN} - C) = -7029 + 0\cdot263T\ , \qquad (9)$$

and

$$\Delta G_{B} = (0\cdot3)(0\cdot7)(0\cdot7G^{L}_{MOSO} + 0\cdot3G^{L}_{SOMO} - C) = -22318 + 8\cdot822T\ ,$$

from tables 3 and 5 and the previous values of G^{L}_{SNSO}, G^{L}_{SOSN}, G^{L}_{MOSO}, and G^{L}_{SOMO} given in the above text. The excess free energy of mixing, ΔG_{E}, for the compound is given by

$$\Delta G_{E} = \frac{C_{AB}yz}{1-x}\ .$$

However, the parameter C_{AB} is taken as zero in all the cases treated here; thus equation (8) can be written explicitly as follows:

$$G^{R} = (0\cdot70 - y)^{\circ}G^{B}_{SN} + 0\cdot3^{\circ}G^{B}_{SO} + y^{\circ}G^{B}_{MO} - \left(1 - \frac{y}{0\cdot7}\right)(7029 - 0\cdot263T) \qquad (10)$$

$$- \frac{y}{0\cdot7}(22318 - 8\cdot822T) + 8\cdot314T[y\ln y + (0\cdot7 - y)\ln(0\cdot7 - y) - 0\cdot7\ln 0\cdot7]\ .$$

Table 5. Summary of counterphase stoichiometry and parameters employed in ternary calculations. The counterphase parameter is taken to be zero in all cases[a].

System	Stable phase (symbol)	Base	Counterphase	Base
SO-MO-SN	$SO_{0\cdot429}MO_{0\cdot571}$(F)	P	$SN_{0\cdot429}MO_{0\cdot571}$	P
	$SO_{0\cdot300}SN_{0\cdot700}$(R)	B	$SO_{0\cdot300}MO_{0\cdot700}$	B
	$SN_{0\cdot980}SO_{0\cdot020}$(BP)	B	$SO_{0\cdot500}MO_{0\cdot500}$	B
	$SN_{0\cdot980}MO_{0\cdot020}$(BP)	B	$MO_{0\cdot500}SO_{0\cdot500}$	B
SO-YO-SN	$YO_{0\cdot625}SO_{0\cdot375}$(M)	Y	$YO_{0\cdot625}SN_{0\cdot375}$	Y
	$YO_{0\cdot527}SO_{0\cdot473}$(K)	Y	$YO_{0\cdot527}SN_{0\cdot473}$	Y
	$YO_{0\cdot455}SO_{0\cdot545}$(O)	Y	$YO_{0\cdot455}SN_{0\cdot545}$	Y
	$SO_{0\cdot300}SN_{0\cdot700}$(R)	B	$SO_{0\cdot300}YO_{0\cdot700}$	B
	$SN_{0\cdot980}SO_{0\cdot020}$(BP)	B	$SO_{0\cdot500}YO_{0\cdot500}$	B
	$SN_{0\cdot980}YO_{0\cdot020}$(BP)	B	$YO_{0\cdot500}SO_{0\cdot500}$	B
SO-CE-SN	$CE_{0\cdot625}SO_{0\cdot375}$(M)	Y	$CE_{0\cdot625}SN_{0\cdot375}$	Y
	$CE_{0\cdot565}SO_{0\cdot435}$(Z)	Y	$CE_{0\cdot565}SN_{0\cdot435}$	Y
	$CE_{0\cdot455}SO_{0\cdot545}$(O)	Y	$CE_{0\cdot455}SN_{0\cdot545}$	Y
	$SO_{0\cdot300}SN_{0\cdot700}$(R)	B	$SO_{0\cdot300}CE_{0\cdot700}$	B
	$SN_{0\cdot980}SO_{0\cdot020}$(BP)	B	$SO_{0\cdot500}CE_{0\cdot500}$	B
	$SN_{0\cdot980}CE_{0\cdot020}$(BP)	B	$CE_{0\cdot500}SO_{0\cdot500}$	B

[a] See table 1 for explanation of symbols.

Since the lattice stabilities of SN, SO, and MO (ie ${}^{\circ}G^{L}_{SN} - {}^{\circ}G^{B}_{SN}$, ${}^{\circ}G^{L}_{SO} - G^{B}_{SO}$, and $G^{L}_{MO} - {}^{\circ}G^{B}_{MO}$) have already been specified the R–L equilibria (figure 2c) can be computed. Figures 2a–2d illustrate the steps which are taken in synthesizing the ternary system SO–MO–SN, (ie $\frac{1}{3}SiO_2$–$\frac{1}{2}MgO$–$\frac{1}{6}Si_3N_4$) from the component binary systems. Initially each of the equilibria between pairs of solution and/or compound phases are calculated individually. In the present case, these pairs consist first of the liquid miscibility gap (L_1–L_2 in figure 2a), followed by L–P in figure 2b. Next, the L–F and L–R equilibria which are shown in figures 2a and 2c are calculated. Superimposition of the L_1–L_2, L–F, L–P, and L–R equilibria shows that there are no interactions between any of the phase pairs except in the case of L–R and L_1–L_2. The latter, which is shown in figure 2c results in a three-phase field between R, L_1, and L_2. The boundaries of this three-phase field are the lines traversing the $L_1 + L_2$ miscibility gap illustrated in figure 2a and the tie lines which define the R–L equilibria shown in figure 2c.

The calculation of the isothermal section at 2100 K can be concluded by adding the L–BP equilibria as shown in figure 2d. In this case, as in the R–L case, there are interactions with phase pairs which have been considered previously. First there is an interaction between L–BP and the liquid gap, L_1–L_2, as illustrated in figure 2d, then there is a second interaction between the L–BP and L–P pairs. Comparison of figures 2b and 2c with 2d shows that while the L–R/L–BP and the L–BP/L–P interaction pairs form stable three-phase fields, the L–BP/L_1–L_2 interaction pair which is shown in figure 2d is metastable. This can be seen by comparing figures 2c and 2d and noting that the three-phase BP + L_1 + L_2 field is 'covered' by the R + L_1 + L_2 and R + L fields. Detailed calculation of the L–BP equilibria can be performed by defining the free energy of the BP phase on the bases of tables 1–4.

For the case of the SO–MO–SN (BP) phase, where the compound runs from $SN_{0\cdot980}SO_{0\cdot020}$ to $SO_{0\cdot50}M_{0\cdot50}$ and from $SN_{0\cdot98}MO_{0\cdot02}$ to $MO_{0\cdot50}SO_{0\cdot50}$, similar procedures are followed. For the former case,

$$G^{BP} = z^{\circ}G^{B}_{SN} + x^{\circ}G^{B}_{SO} + y^{\circ}G^{B}_{MO} + \left(1 - \frac{y}{1-x}\right)\Delta G_A + \frac{y}{1-x}\Delta G_B + \Delta G_E + RT[y\ln y + z\ln z - (1-x)\ln(1-x)]. \quad (11)$$

Here $x_{\bullet} = 0{\cdot}50$ and $x'_{\bullet} = 0{\cdot}02$, so that $p = 0{\cdot}96$, $x = x'_{\bullet} + yp = 0{\cdot}02 + 0{\cdot}96y = x_{SO}$, $y = y_{MO}$, and $z = 1 - x - y = 0{\cdot}98 - 1{\cdot}96y = z_{SN}$. Moreover, $\Delta G_E = 0$ and ΔG_A and ΔG_B can be explicitly defined:

$$\Delta G_A = (0{\cdot}02)(0{\cdot}98)(0{\cdot}98G^{L}_{SNSO} + 0{\cdot}02G^{L}_{SOSN} - C) = -820 - 0{\cdot}082T, \quad (12)$$

$$\Delta G_B = (0{\cdot}50)(0{\cdot}50)(0{\cdot}50G^{L}_{SOMO} + 0{\cdot}50G^{L}_{MOSO} - C) = -26568 + 10{\cdot}503T; \quad (13)$$

$$G^{BP} = (0{\cdot}98 - 1{\cdot}96y)^{\circ}G^{B}_{SN} + (0{\cdot}02 + 0{\cdot}96y)^{\circ}G^{B}_{SO} + y^{\circ}G^{B}_{MO} - \left(1 - \frac{y}{1-x}\right)(820 + 0{\cdot}0828T) - \frac{y}{1-x}(26568 - 10{\cdot}503T) + 8{\cdot}314T[y\ln y + (0{\cdot}98 - 1{\cdot}96y)\ln(0{\cdot}98 - 1{\cdot}96y) - (0{\cdot}98 - 0{\cdot}96y)\ln(0{\cdot}98 - 0{\cdot}96y)]. \quad (14)$$

Thus the equilibrium between the liquid and BP phase can be computed as in figure 2d. Combination of the pairwise equilibria in figure 2 yields the computed isothermal section at 2100 K shown in figure 3. Isothermal sections similarly derived at 2000 and 1900 K are shown in figure 3, along with an observed section at 1500 K due to Müller (1981). The latter is in keeping with the calculations shown at 1900 K.

Similar calculations were performed in the SO-YO-SN and SO-CE-SN systems. The results, which are complicated by the existence of stable quasiternary compounds (listed in table 6), are displayed in figures 4-7. The SO-YO-SN and SO-CE-SN sections were computed in a manner similar to that in the case of SO-MO-SN, in that the systems were first computed as if the ternary phases were absent.

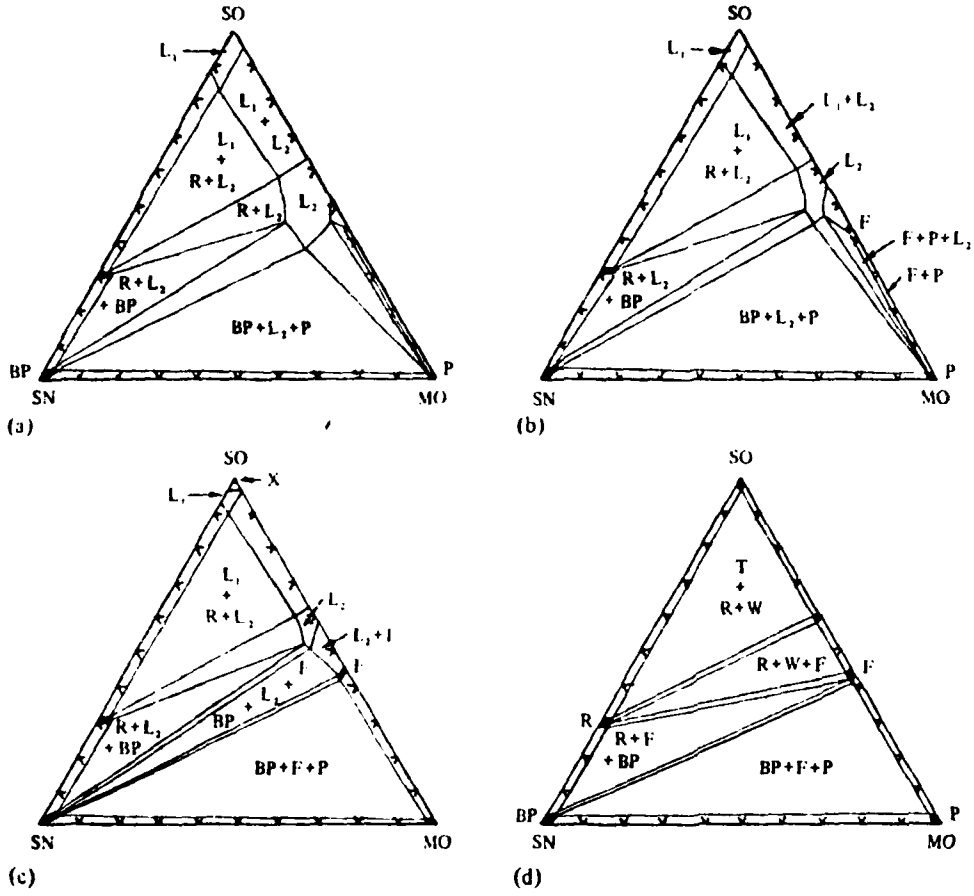

Figure 3. Calculated and observed isothermal sections in the SiO_2-MgO-Si_3N_4 system (see tables 1-5 for explanation of symbols). (a) 2100 K; (b) 2000 K; (c) 1900 K; (d) observed, 1500 K. $W = SiO_2 \cdot MgO$ ($SO_{0.6}MO_{0.4}$) (Müller 1981).

Table 6. Description of quasiternary compounds in the SiO_2-Y_2O_3-Si_3N_4 and SiO_2-Ce_2O_3-Si_3N_4 systems[a]. Sources of data: Gaukler et al (1980); Lange (1980).

Compound	Base	Stoichiometry	C/J (g atom)$^{-1}$	T_m/K	$\Delta G_{f,298}$/J (g atom)$^{-1}$
C $\frac{1}{5}(YSiO_2N)$	Y	$SO_{0.150}YO_{0.500}SN_{0.350}$	29096 + 8·368T	1953	−4393 − 2·410T
D $\frac{1}{13}(Y_4Si_2O_7N_2)$	Y	$SO_{0.100}YO_{0.667}SN_{0.233}$	13004 + 16·736T	2110	−678 − 4·127T
E $\frac{1}{21}[Y_5(SiO_4)_3N]$	Y	$SO_{0.322}YO_{0.595}SN_{0.083}$	−2155 + 20·92T	1996	−11456 − 0·883T
C $\frac{1}{5}(CeSiO_2N)$	Y	$SO_{0.150}CE_{0.500}SN_{0.350}$	31505 + 8·368T	1914	−5422 − 2·410T
D $\frac{1}{13}(Ce_4Si_2O_7N_2)$	Y	$SO_{0.100}CE_{0.667}SN_{0.233}$	14769 + 16·736T	2020	−1259 − 4·127T
F $\frac{1}{21}[Ce_5(SiO_4)_3N]$	Y	$SO_{0.322}CE_{0.595}SN_{0.083}$	3975 + 20·92T	2109[b]	−13585 − 0·883T

[a] T_m, melting point; see tables 1, 3, 4, and 5 for explanation of other symbols.
[b] Decomposes peritectically into Z and liquid above 2100 K.

Subsequently the ternary phases, designated as C, D, and E, were inserted. In keeping with previous practice, the free energy of the ternary phases C, D, and E were defined by choosing a base phase and then defining a compound parameter in conformity with experimental observation. In the present case the Y structure was chosen as the base phase, since this ternary phase composition occurs near the YO and CE corners of the SO-YO-SN and SO-CE-YO systems, as is seen in figures 5 and 6.

The free energy of the ternary compound D in the SO-YO-SN system ($D = \frac{1}{15}Y_4Si_2O_7N_2 = SO_{0.100}YO_{0.667}SN_{0.223}$) is defined as

$$G^D = 0.10\,{}^\circ G^Y_{SO} + 0.667\,{}^\circ G^Y_{YO} + 0.233\,{}^\circ G^Y_{SN} + (0.10)(0.667)^{-1}(0.1G^L_{SOYO} + 0.667G^L_{YOSO} - C) + (0.10)(0.233)(0.333)^{-1}(0.1G^L_{SOSN} + 0.233G^L_{SNSO} - C) + (0.667)(0.233)(0.90)^{-1}(0.667G^L_{YOSN} + 0.223G^L_{SNYO} - C). \quad (15)$$

Since $C = 13004 + 16.736T$, for this phase,

$$G^D = 0.10\,{}^\circ G^Y_{SO} + 0.667\,{}^\circ G^Y_{YO} + 0.233\,{}^\circ G^Y_{SN} - 9094 - 3.062T. \quad (16)$$

Thus the free energy of formation of D from the Y form of SO, YO, and SN is given by $-9094 - 3.062T$. The free energy of formation of D from the stable forms of SO, YO, and SN (ie R, Y, and B, respectively) can be computed by using the lattice

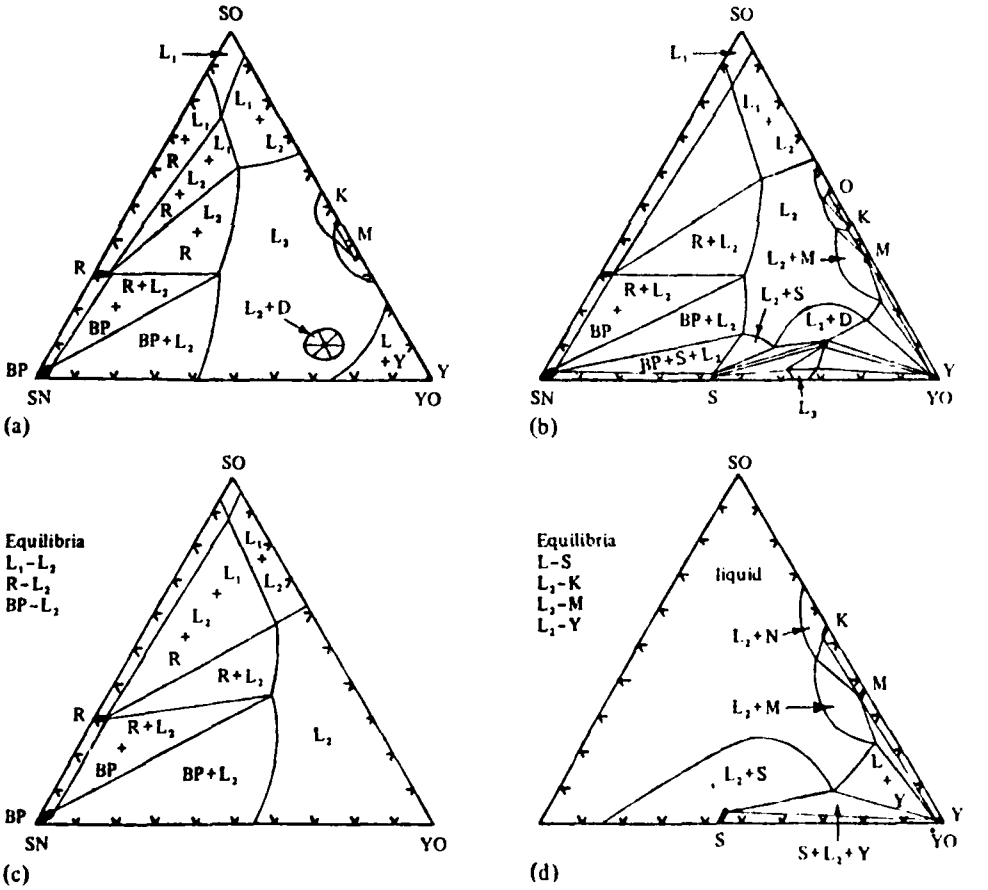

Figure 4. Calculated isothermal sections and pairwise component equilibria in the SiO_2-Y_2O_3-Si_3N_4 system (see tables 1-6 for explanation of symbols). (a) 2100 K; (b) 2000 K; (c), (d) pairwise equilibria at 1900 K.

Appendix A: Summary of Parameters for the Fe-Al System

The lattice stabilities from Ref. 9.

$$E_{G_m}^{bcc,dis} = X_{Fe}X_{Al}\,(-32345-37.92T)X_{Fe} + (-150252+51.42T)X_{Al} \quad \text{J/mol}$$

$W^1 = 1588$, $W^2 = 794$ (k units $k=13.8\cdot10^{-24}$ J/atom), $K=0.68$

$$E_{G_m}^{fcc} = X_{Fe}X_{Al}\,(-25022-38.01T)X_{Fe} + (-106841+66.70T)X_{Al} \quad \text{J/mol}$$

$$E_{G_m}^{L} = X_{Fe}X_{Al}\,(-62760-14.63T)X_{Fe} + (-96232+32.72T)X_{Al} \quad \text{J/mol}$$

$$^{\circ}G^{\theta}_{Fe_{0.25}Al_{0.75}} - 0.25\,{}^{\circ}G_{Fe}^{bcc} - 0.75\,{}^{\circ}G_{Al}^{bcc} = -35275+8.28T \quad \text{J/mol}$$

$$^{\circ}G^{\eta}_{Fe_{0.286}Al_{0.714}} - 0.286\,{}^{\circ}G_{Fe}^{bcc} - 0.714\,{}^{\circ}G_{Al}^{bcc} = -41169+11.40T \quad \text{J/mol}$$

$$^{\circ}G^{\xi}_{Fe_{0.333}Al_{0.667}} - 0.333\,{}^{\circ}G_{Fe}^{bcc} - 0.667\,{}^{\circ}G_{Al}^{bcc} = -37872+4.73T \quad \text{J/mol}$$

$$^{\circ}G^{\varepsilon}_{Fe_{0.40}Al_{0.60}} - 0.4\,{}^{\circ}G_{Al}^{bcc} - 0.6\,{}^{\circ}G_{Fe}^{bcc} = -23863-2.77T \quad \text{J/mol}$$

VI A THERMODYNAMIC EVALUATION OF THE TITANIUM-CARBON-NITROGEN PHASE DIAGRAM.

John Agren

1.0 Introduction

The use of vapor deposited TiC, TiN and Ti(C,N) coatings for improving the performance of cutting tools and wear resistant surfaces enhances the value of information on the thermochemistry and phase diagram of the Ti-C-N system.

Since the crystal structures of the compounds TiC and TiN are the same, it is likely that these compounds form a solid solution. However, the experimental Ti-C and Ti-N phase diagrams reported to date are not very well established and very little thermodynamic data is available for the binary cases or the Ti-C-N ternary. The purpose of the present work is to evaluate all the information available in terms of thermodynamic models for the individual phases and synthesize the binary and ternary phase diagrams.

2.0 Thermodynamic Models

2.1 Liquid

The simplest models that cover the whole concentration range are the regular or subregular solution models. The formation of the solid compounds TiC and TiN in the binaries suggests that some ordering or formation of molecular species might take place in the liquid around the stoichiometric compositions. However, a high degree of association is not observed in the gas phase and vaporization of titanium carbide yields titanium and carbon polymers. The Fe-S system has recently been treated by assuming the presence of molecular species (1) and by assuming ordering (2). Both treatments yield a satisfactory agreement with experimental data, and predict a very rapid change in activity close to the stoichiometric composition. This rapid change is difficult to describe with a regular or subregular solution model, and generally many terms will be needed in the series expansion of the excess energy.

F (SiO_2·MgO) and ($MgSiN_2$) above 446 K. Thus the sections shown in figure 3 represent metastable equilibria.

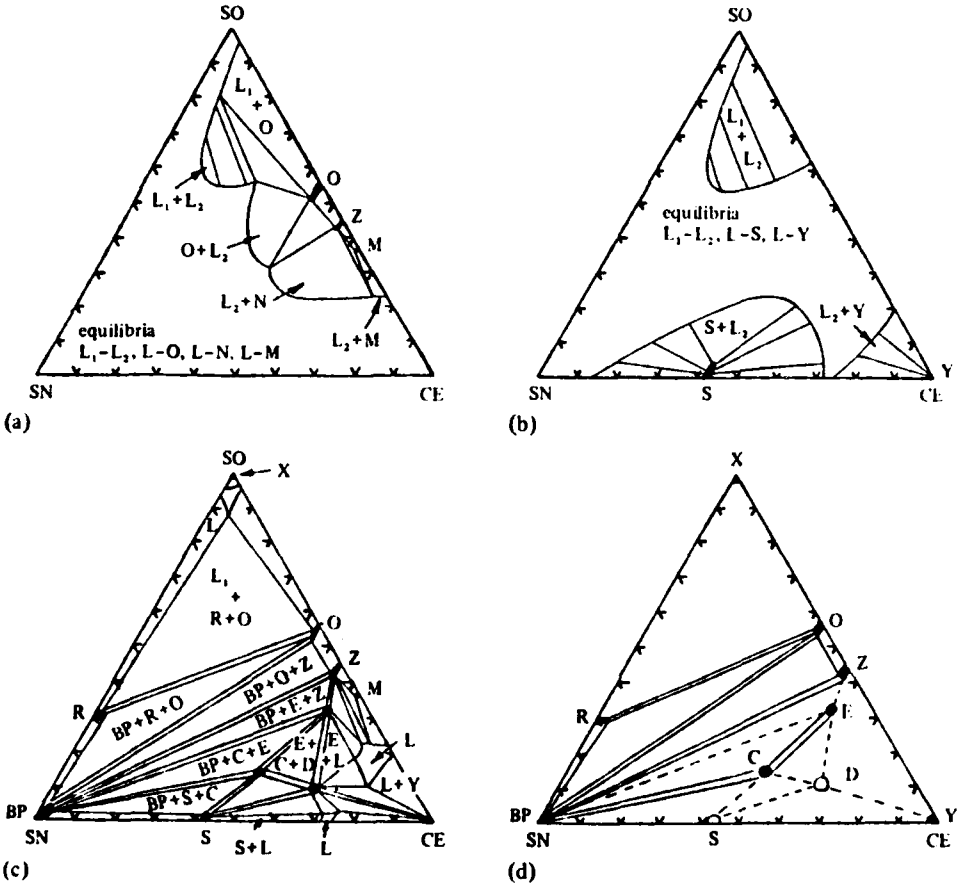

Figure 7. SiO_2-Ce_2O_3-Si_3N_4 system: (a), (b) calculated pairwise equilibria at 1900 K; (c) calculated isothermal section at 1900 K; (d) observed (Lange 1980) subsolidus equilibria at 1923-2023 K (S and D phases were expected but not observed).

References

Doerner P, Gaukler L J, Krieg H, Lukas H L, Petzow G, Weiss J, 1979 *CALPHAD* **3** 241-257

Gauckler L J, Hohnke H, Tien T Y, 1980 *J. Am. Ceram. Soc.* **63** 35-37

Jack K H, 1977 Final Technical Report, DAERO-76-G-067, European Research Office, Edison House, 223 Old Marylebone Road, London NW1 5TH, England

Kaufman L, 1979a *CALPHAD* **3** 27-44

Kaufman L, 1979b *CALPHAD* **3** 279-291

Kaufman L, Nesor H, 1978 *CALPHAD* **2** 35-53

Lange F F, 1980 *Ceram. Bull.* **59** 239-249

Levin E M, Robbins C R, McMurdie H F, 1964 *Phase Diagrams for Ceramists* (Columbus, OH: American Ceramic Society) and Supplements 1969 and 1975

Lukas H L, 1981 private communication

Morgan P E D, 1976 *J. Am. Ceram. Soc.* **59** 86

Müller R, 1981 Thesis, University of Stuttgart, Stuttgart, FRG

Wills R R, 1974 *J. Am. Ceram. Soc.* **57** 459

Wills R R, 1975 *J. Am. Ceram. Soc.* **58** 335

IV CALCULATION OF TERNARY III - V and II-IV SYSTEMS

L. Kaufman, J. Nell, K. Taylor and F. Hayes, CALPHAD (1981) 5 185-215

(This paper was presented at Calphad X, Vienna, Austria July 1981)

ABSTRACT. A data base covering the binary systems composed of Aluminum, Gallium, Indium, Phosphorus, Arsenic and Antimony has been constructed by analyzing the fifteen combinations of these elements in terms of lattice stability, solution phase and compound parameters. Partial isothermal sections in the P-In-As, As-In-Sb, P-Ga-As, Ga-Sb-In and Al-Sb-Ga systems were then calculated using the foregoing data base for comparison with experimental isothermal sections and quasi-binary III-V phase diagrams. It was found that ternary liquid and III-V compound interaction parameters were required to attain good agreement in some cases. Similar calculations were performed for the Te-Cd, Hg-Cd and Te-Hg binary systems and the Cd-Te-Hg ternary systems at pressures up to 74 atmospheres. Comparison of the calculated results with experimental data on tie-line compositions between Cd-Te-Hg liquid and quasi-binary CdTe-HgTe alloys is important in the liquid phase epitaxial growth of controlled band gap electro-optical materials.

1. Introduction

Alloy semiconductors are important for a wide range of electro-optical applications because their properties can be tailored by controlling the composition of the solid, which is grown from the liquid or deposited from the vapor. Although crystal growers have become very adept at controlling the temperature (and pressure) of the parent phase in order to obtain the desired characteristics of the crystalline alloy semiconductors, phase diagram data is indispensable in order to deal with the increasingly complex systems. Stringfellow and co-workers (1-6) have pioneered in developing simple, useful models for calculating quasi-binary systems based on III-V compounds. Stringfellow's pioneering work has been extended and expanded by Ansara and co-workers (7), Osamura and Murakami and co-workers (8-10), and Brebrick (11) who have used more extensive experimental thermochemical data and less restrictive models than the regular solution (and quasichemical) model employed by Stringfellow. The current paper attempts to assemble a data base for III-V compounds which can be employed to compute multicomponent phase diagrams over a wide range of temperatures (and pressures) both outside and within the quasi-binary plane. In addition, the Cd-Hg, Cd-Te and Hg-Te binary systems are analyzed and combined to calculate the Cd-Te-Hg ternary system over a range of temperatures (and pressures) in order to compute tie-line compositions between quasi-binary CdTe-HgTe alloys and the Cd-Te-Hg liquid. The former alloys are of current interest in synthesizing controlled band gap electro-optical materials. In the analyses of both the III-V and II-VI (Cd-Te-Hg) systems, the methods and formalism which are applied are those employed in dealing with metals and metallic alloys (12,13), silicides (14), and oxynitride systems (15).

2. Thermochemical System Employed to Characterize Binary III-V Phase Diagrams

The method employed for describing solution and compound phases is the same as that employed to describe a variety of metal, metalloid, and oxide systems (13-15) incorporating some sybolic usage which facilitates data handling as indicated below. The free energy of the liquid phase, G^L, in the binary system Al-In is given by equation (1), where T is in Kelvins, R=8.314 J/g.at°K, and x is the atomic fraction of Indium:

$$G^L = (1-x)\,{}^\circ G^L_{Al} + x\,{}^\circ G^L_{In} + RT(x\ell nx + (1-x)\ell n(1-x)) + x(1-x)[(1-x)\mathrm{LALIN} + x\mathrm{LINAL}]. \quad (1)$$

Similarly, the free energy of the fcc phase in the Al-In is defined by Equation (2) as

$$G^{fcc} = (1-x)\,{}^\circ G^{fcc}_{Al} + x\,{}^\circ G^{fcc}_{In} + RT(x\ell nx + (1-x)\,\ell n(1-x)) + x(1-x)[(1-x)\mathrm{AALIN} + x\mathrm{AINAL}] \quad (2)$$

where the difference in free energy between fcc and liquid aluminum, ALALLA, and the difference in free energy between fcc and liquid indium, ININLA, are listed in Table 1, while the solution parameters LALIN, LINAL, AALIN, and AINAL are given in Table 2. The liquid parameters for the In-As and Ga-As systems were taken directly from Brebrick's analysis (11). Brebrick also provides parameters for the In-Sb and Ga-Sb systems, namely LINSB=-3431-19.782T, LSBIN=-27698+19.581T, LGASB=21652-32.108T and LSBGA=-30020+28.259T J./g.at. While these parameters provide a good description of the In-Sb and Ga-Sb phase diagrams and the excess free energy of mixing for the liquid phases in these systems, they do not describe the enthalpy of mixing for the liquid phase in the In-Sb and Ga-Sb systems as measured by Ansara et al. (7). Thus in the case of the In-Sb system, the enthalpy of mixing defined by Brebrick's LINSB and LSBIN parameters is given by Equation (3) as

$$E_H^L = -x(1-x)[(1-x)3431+27698x] \quad J/g.at. \tag{3}$$

where $x=x_{Sb}$. By contrast, the equation for E_H^L provided by Ansara et al. (7) for In-Sb, which is based upon experimental measurements of the heat of mixing, is given by

$$E_H^L = -x(1-x)(11689+19774x-46661x^2+24980x^3) \quad J/g.at. \tag{4}$$

Ansara et al. also provide the following equation for the excess entropy of mixing of the liquid as

$$E_S^L = x(1-x)[4.602-7.799x+12.104x^2-6.782x^3] \quad J./g.at.°K \tag{5}$$

Although the excess free energy provided by Brebrick's parameters and those generated by Eqs. (4) and (5) in the temperature range of interest (near 700°K) are in relatively good agreement, the enthalpy of mixing described by Equations (3) and (4) differ by 800-1600 J/g.at. Consequently, Equations (4) and (5) were employed to derive LINSB=-15380-3.607T and LSBIN=-10293-2.393T shown in Table 2. These expressions provide a closer fit to Equations (4) and (5) than Brebrick's parameters and still yield a satisfactory agreement in the calculated and observed In-Sb phase diagram. A similar comparison can be made for the Ga-Sb system. In the latter case Brebrick's analysis yielded LGASB=21652-32.108T and LSBGA=-30020+28.259T J./g.at. By contrast, Ansara et al. (7) suggest that

$$E_H^L = x(1-x)[531-21599x+32175x^2-15788x^3] \quad J/g.at. \tag{6}$$

where $x=x_{Sb}$ and

$$E_S^L = x(1-x)[4.849-14.456x+24.527x^2-15.786x^3] \quad J/g.at.°K \tag{7}$$

The present parameters, LGASB=4962-3.209T and LSBGA=-9715-0.456T provide a better description of the experimental heat of mixing for Ga-Sb alloys embodied (12) by Equation (5) than do the parameters suggested by Brebrick. The parametric descriptions of the In-Al, Ga-Al, and In-Ga systems shown in Tables 1 and 2 were derived from the earlier description provided by Ansara et al. (12). The remaining III-V systems were characterized as shown in Tables 1-3 based on the available thermochemical and phase diagram data employing the standard compilations of such information (16-20) and available lattice stability data. Table 4 compares the calculated and observed thermochemical properties of III-V compounds based on this description while Figures 1-14 display the partial phase diagrams computed with the current description. The heat of mixing of liquid $Al_{0.5}Sb_{0.5}$ at 1400°K is given as -2477 J./g.at. based on experimental data (17) and -1126 J./g.at. on the basis of Table 2.

The free energy of the ternary liquid phase in the P-In-As system is defined on the basis of Kohler's equation as

$$\begin{aligned} G^L = {} & (1-x-y)\,{}^oG_P^L + x\,{}^oG_{In}^L + y\,{}^oG_{As}^L + RT[(1-x-y)\ln(1-x-y) + x\ln x + y\ln y) \\ & + (1-x-y)x(1-y)^{-1}[(1-x-y)LPPIN + xLINPP] + (1-x-y)y(1-x)^{-1}[(1-x-y)LPPAS + yLASPP] \\ & + xy(x+y)^{-1}[xLINAS + yLASIN] + xy(1-x-y)\,TRNL \quad J./g.at. \end{aligned} \tag{8}$$

where x is the atom fraction of In, y is the atom fraction of As and TRNL is the ternary interaction parameter. Values of TRNL for five ternary systems which have been investigated here are listed in Table 5. The specific value for the P-In-As system is 12552 J/g.at. This is a rather small value since the maximum value of the ternary term occurs at $x=y=(1-x-y)=1/3$. Thus the maximum contribution of this term is only 465 J/g.at. If attention were restricted to the quasi-binary join (i.e., where $x=0.5$) between $In_{0.5}P_{0.5}$ and $In_{0.5}As_{0.5}$ the maximum contribution is 390 J/g.at. when $x=0.5$, $y=0.25$ and $(1-x-y)=0.25$.

The free energy of the $In_{0.5}P_{0.5}$-$In_{0.5}As_{0.5}$ zinc-blende phase (S) is defined by Equation (9) as follows

TABLE 1

SUMMARY OF LATTICE STABILITY PARAMETERS
(All units in Joules per gram-atom (mole of atoms), T in Kelvins)

L=liquid*, A=fcc*, T=tetragonal, O=orthorhombic,
R=rhombohedral, X=red phosphorus structure, W=white phosphorus structure

ALALLA = 10711 - 11.506T*
ALALLO = 0 - 18.451T

GAGALO = 5590 - 18.451T
GAGALA = -5021 - 8.368T
GAGALT = -1674 - 8.368T

ININLT = 3264 - 7.594T
ININLA = 2908 - 7.113T
ININLO = 0 - 18.451T

PPPPLX = 17991 - 21.506T
PPPPWX = 18171 - 19.539T
PPPPLA = -18828 - 8.368T
PPPPLR = 4184 - 23.012T

SBSBLR = 19874 - 21.966T
SBSBLA = -18828 - 8.368T

ASASLR = 24874 - 23.012T
ASASLA = -18828 - 8.368T
ASASLX = 21631 - 21.631T

*ALALLA = $G_{Al}^{liquid} - G_{Al}^{fcc}$ = 10711 - 11.506 T J./g.at.

TABLE 2

SUMMARY OF SOLUTION PHASE PARAMETERS*
(All units in Joules per gram-atom (mole of atoms), T in Kelvins)

*for Aℓ-In system, L=liquid, A=fcc, $x=x_{In}$

$G^{L}=(1-x)G_{A\ell}^{L} + xG_{In}^{L} + RT(x\ell nx + (1-x)\ell n(1-x)) + x(1-x)[(1-x)LALIN + xLINAL]$

$G^{fcc}=(1-x)G_{A\ell}^{fcc} + xG_{In}^{fcc} + RT(x\ell nx + (1-x)\ell n(1-x)) + x(1-x)[(1-x)AALIN + xAINAL]$

LALAS = -16317 - 41.338T
LASAL = -16317 - 41.338T

LALPP = -38911 - 26.275T
LPPAL = -38911 - 26.275T

LINPP = -29288 + 5.188T
LPPIN = -79496 + 5.188T
RINPP = 8368
RPPIN = 8368

LGAPP = -90374 + 34.225T
LPPGA = -58576 - 49.036T
XGAPP = 8368
XPPGA = 8368

LGASB = 4962 - 3.209T
LSBGA = -9715 - 0.456T
RSBGA = RGASB = 8368

LALGA = 3280 - 2.021T
LGAAL = 2071 - 0.745T
AALGA = -1046 + 5.439T
AGAAL = -20962 + 26.778T
OGAAL = OALGA = 8368

LALIN = 25522 - 3.347T
LINAL = 20502 - 2.510T
AALIN = 60250 - 3.347T
AINAL = 55229 - 2.510T

LALSB = 8050 - 9.706T
LSBAL = -17054 - 9.706T

LSBAS = LASSB = 0
RSBAS = RASSB = 8368

LSBPP = LPPSB = -15899
RSBPP = RPPSB = -20920-4.184T
XSBPP = XPPSB = -15899

LASPP = LPPAS = -15899
RASPP = RPPAS = -20920-4.184T
XASPP = XPPAS = -15899

LGAAS = -1845 - 21.209T
LASGA = -41551 + 7.192T
RGAAS = RASGA = 8368

LINAS = -243 - 29.522T
LASIN = -48124 + 17.472T
TASIN = TINAS = 8368
RASIN = RINAS = 8368

TABLE 2 (CONTINUED)

SUMMARY OF SOLUTION PHASE PARAMETERS
(All units in Joules per gram-atom (mole of atoms) T in Kelvins)

LINSB = -15380 - 3.607T
LSBIN = -10293 - 2.393T
TSBIN = TINSB = 8368
RSBIN = RINSB = 8368

LGAIN = 4435 + 2.268T
LINGA = 4435 + 0.954T
TGAIN = -3431 + 21.907T
TINGA = -3376 + 24.393T
OGAIN = OINGA = 12552

TABLE 3

COMPOUND PARAMETERS FOR III-V ZINC-BLENDE COMPOUNDS

$G^S = 0.5\ G_i^{fcc} + 0.5\ G_j^{fcc} + 0.25\ [0.5\ LIIJJ + 0.5\ LJJII - C]$ Joules/g.at.

Compound	Compound Parameter (C) (Joules/g.at. °K)	Compound	Compound Parameter (C) (Joules/g.at. °K)
$Al_{0.5}P_{0.5}$	364,443 - 60.517T	$Ga_{0.5}Sb_{0.5}$	179,343 - 77.571T
$Al_{0.5}As_{0.5}$	305,348 - 78.994T	$In_{0.5}P_{0.5}$	188,749 - 64.099T
$Al_{0.5}Sb_{0.5}$	174,992 - 55.815T	$In_{0.5}As_{0.5}$	187,217 - 73.806T
$Ga_{0.5}P_{0.5}$	280,328 - 75.647T	$In_{0.5}Sb_{0.5}$	125,227 - 63.011T
$Ga_{0.5}As_{0.5}$	259,525 - 83.496T		

TABLE 4

COMPARISON OF CALCULATED AND EXPERIMENTAL THERMOCHEMICAL PROPERTIES OF III-V COMPOUNDS
(J./mol., J./mol.°K)

Compound	ΔH_f[298°K]		ΔS_f[298°K]		ΔS [fusion]	
	calculated	exptl.	calculated	exptl.(16)	calculated	exptl.
AlP	-164,849	-164,431±2929(16)	-3.97	-3.85±5.0	61.66	61.50±1.6(16)
AlAs	-117,127	-122,591±5021(16)	-4.18	-3.76±4.8	70.91	70.42(43)
AlSb	-51,045	-50,208±418(16)	-9.46	-8.86±0.8	59.32	61.67(43)
GaP	-129,971	-122,173±8368(16)	-10.92	-11.51± 1.9	66.10	66.53(43)
GaAs	-86,291	-88,575(11)	-13.51	-12.47±1.3	70.015	69.63(11)
GaSb	-41,547	-41,840±1255(16)	-14.19	-9.20±1.9	67.061	67.31(11)
InP	-84,391	-75,312±8368(16)	-21.02	-20.88±1.9	59.07	59.08(43)
InAs	-61,647	-61,923(11)	-18.74	-18.83±2.5	63.92	63.36±6.89(16)
InSb	-29,974	-30,962(11)	-15.93	-15.69±1.1	58.53	59.82(11)

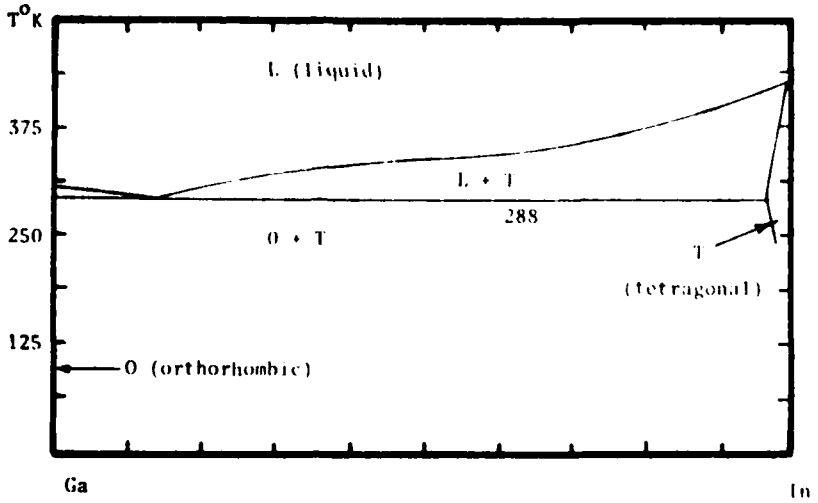

Figure 1. Calculated Ga-In Phase Diagram

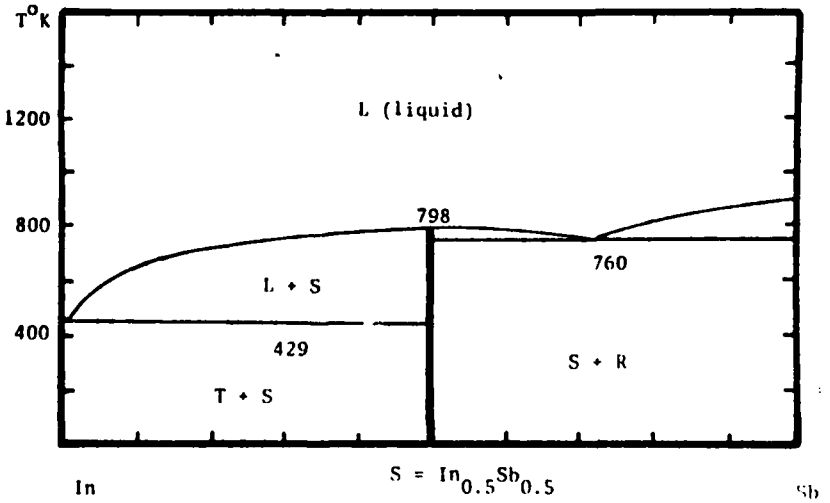

Figure 2. Calculated In - Sb Phase Diagram

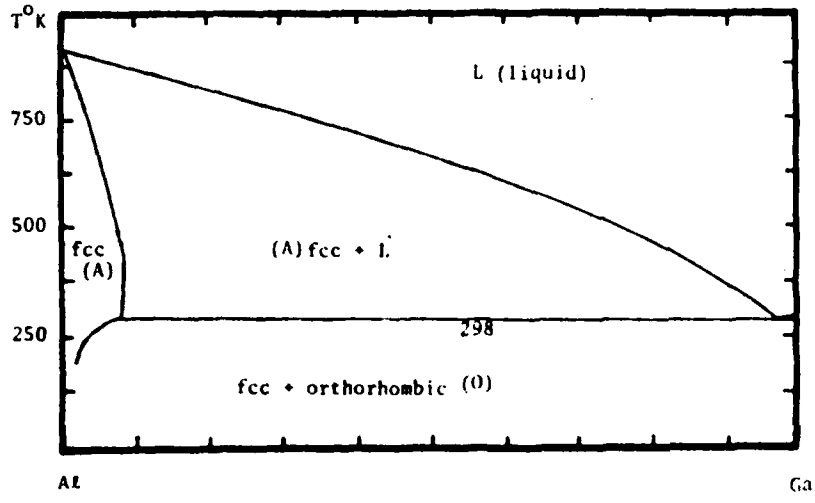

Figure 3. Calculated At-Ga Phase Diagram

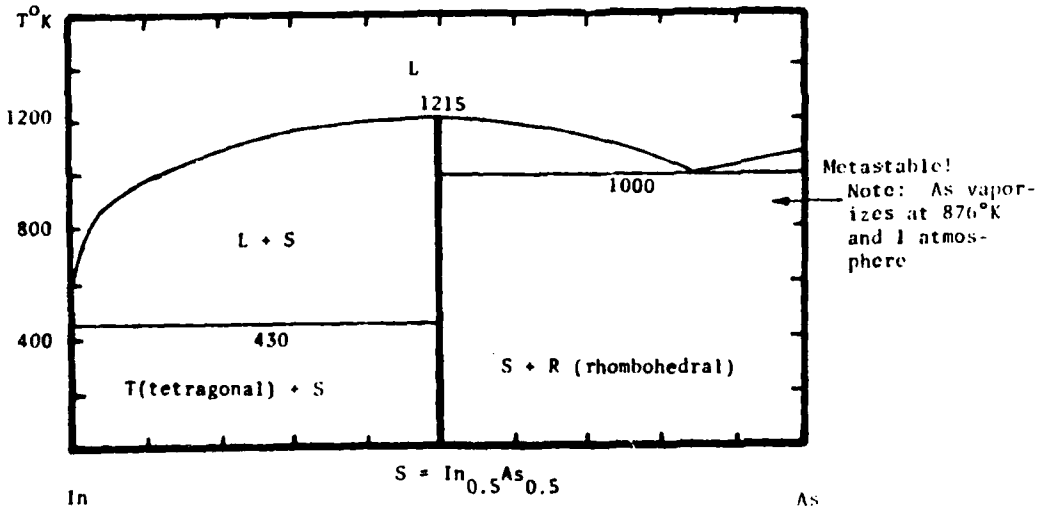

Figure 4. Calculated In - As Phase Diagram

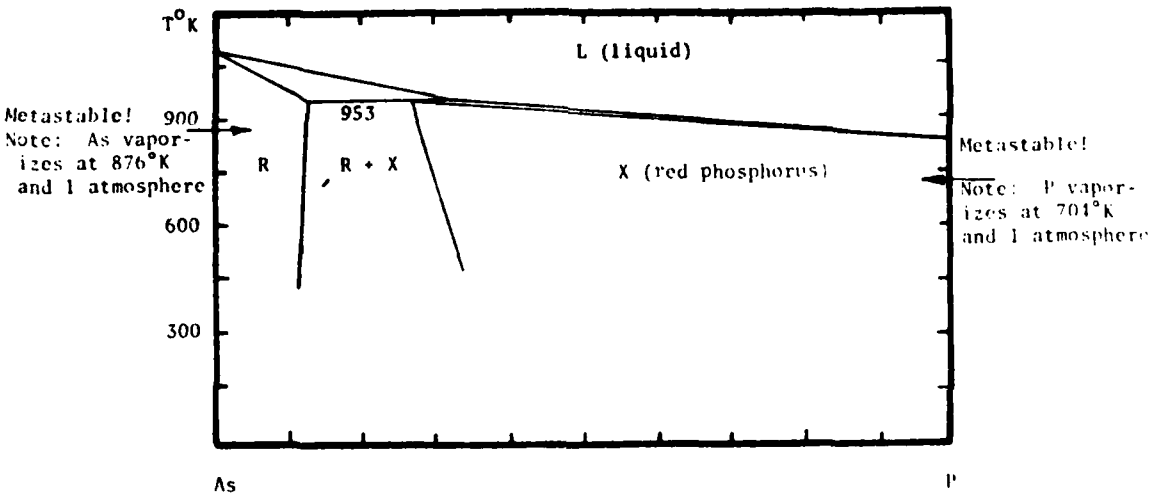

Figure 5. Calculated As-P Phase Diagram

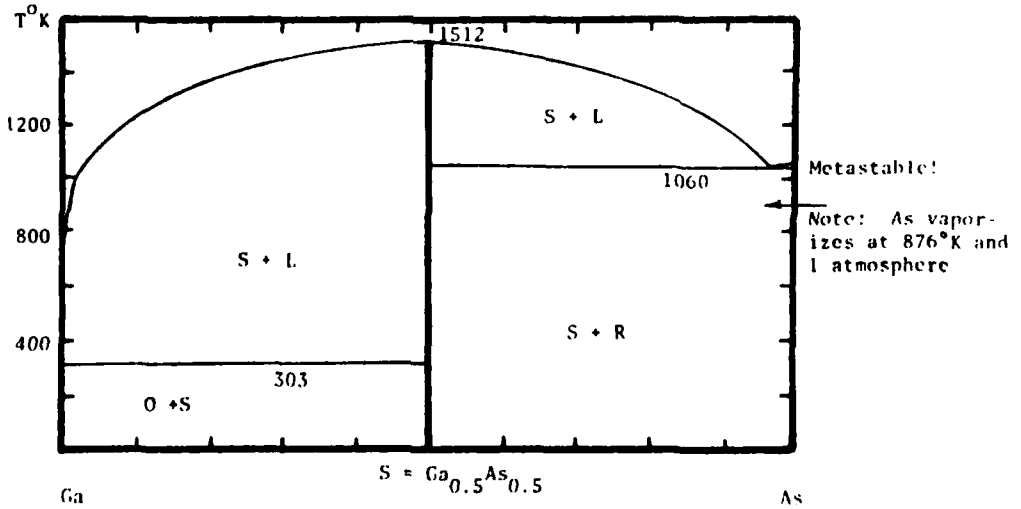

Figure 6. Calculated Ga-As Phase Diagram

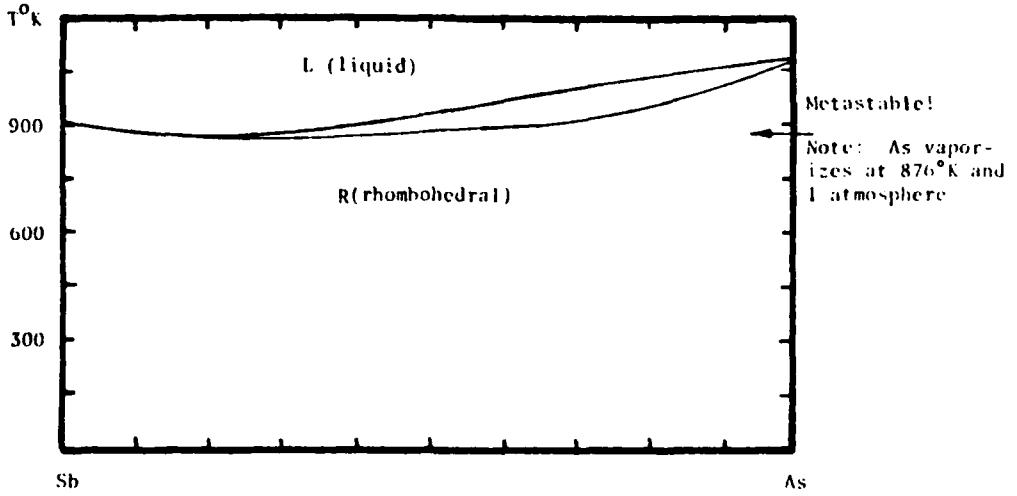

Figure 7. Calculated Sb-As Phase Diagram

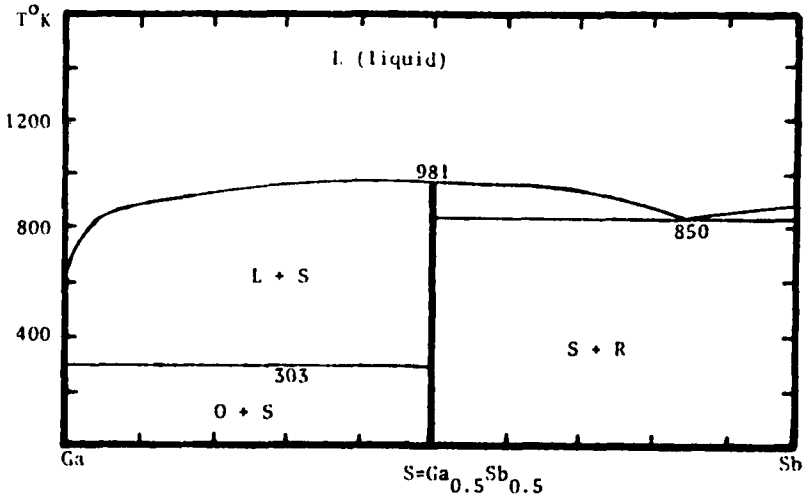

Figure 8. Calculated Ga-Sb Phase Diagram

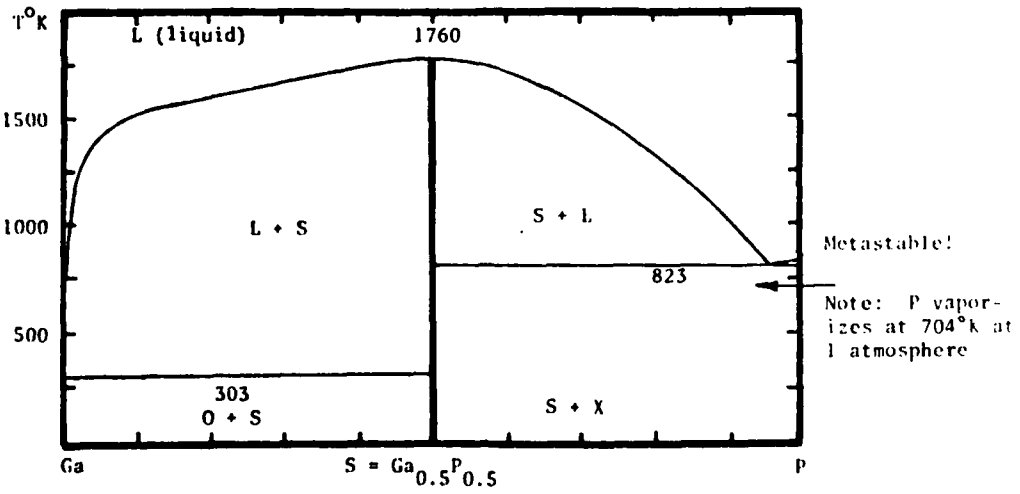

Figure 9. Calculated Ga-P Phase Diagram

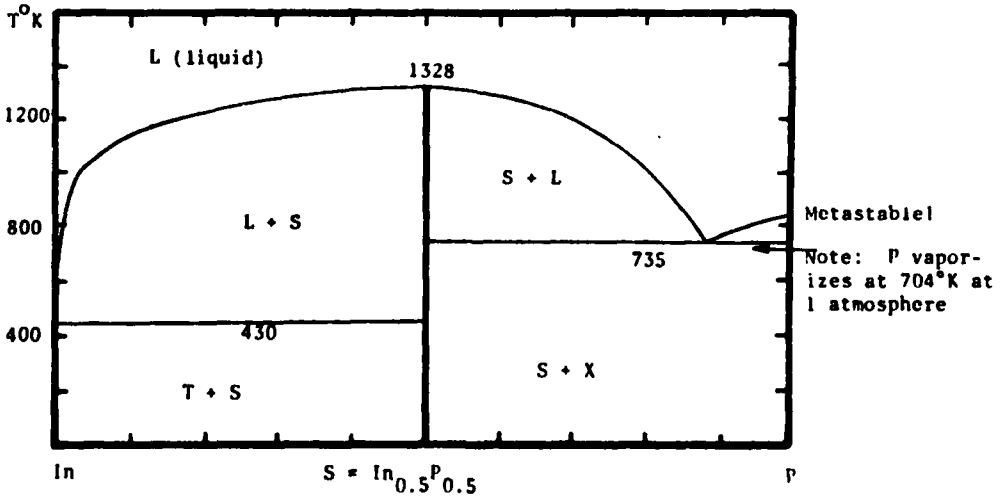

Figure 10. Calculated In-P Phase Diagram

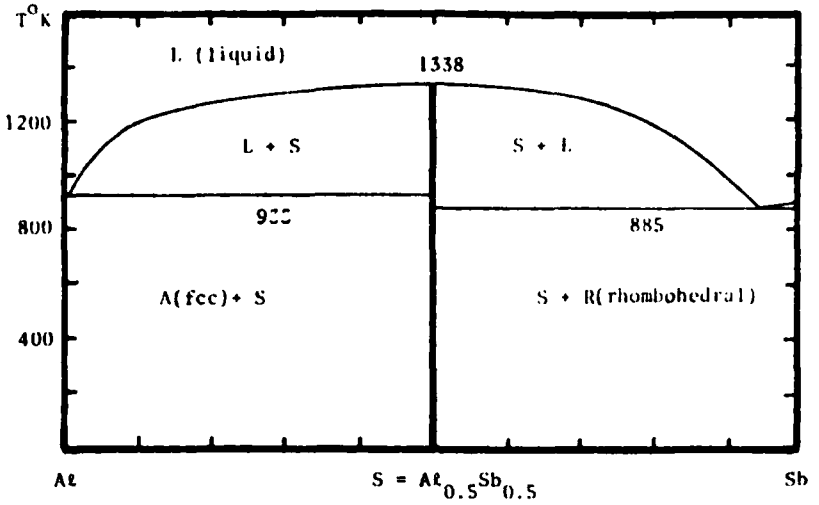

Figure 11. Calculated Al-Sb Phase Diagram

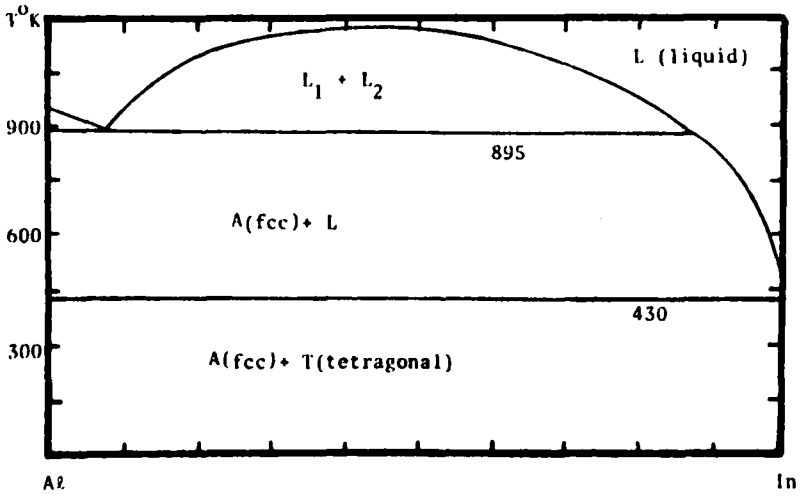

Figure 12. Calculated Al-In Phase Diagram

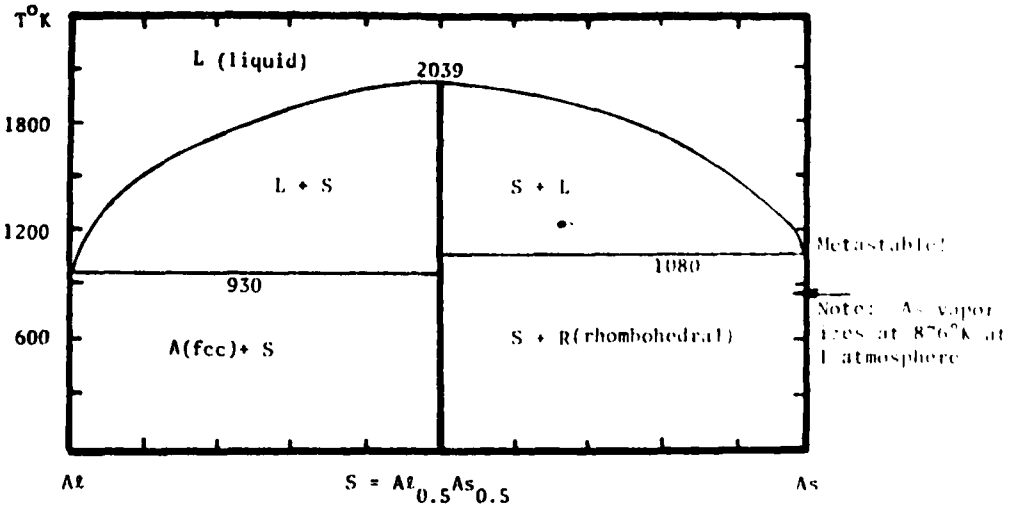

Figure 13. Calculated Aℓ-As Phase Diagram

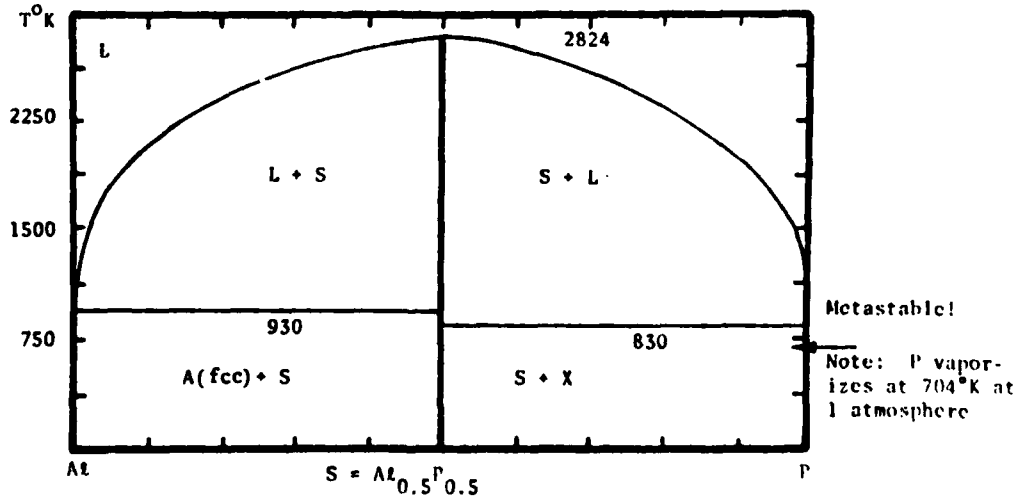

Figure 14. Calculated Aℓ-P Phase Diagram

$$G^S = (0.5-y)\,{}^oG_P^{fcc} + 0.5\,{}^oG_{In}^{fcc} + y\,{}^oG_{As}^{fcc} + (1-2y)(0.25)(0.5\ LPPIN + 0.5LINPP - C_1)$$

$$+2y(0.25)(0.5LINAS + 0.5LASIN - C_2) + CAB\ y(1-2y)$$

$$+RT(y\ln y + (0.5-y)\ln(0.5-y) - 0.5\ln 0.5) \qquad J./g.at. \qquad (9)$$

where C_1, the compound parameter for $In_{0.5}P_{0.5}$ = 188,749-64.099T J/g.at. and C_2, the compound parameter for $In_{0.5}As_{0.5}$ = 187,217 - 73.806T J./g.at., as given in Table 3. The interaction parameter for mixing $In_{0.5}P_{0.5}$ and $In_{0.5}As_{0.5}$, CAB, is equal to zero in this case, as shown in Table 5. Thus this compound is defined as an ideal solution of its components. Since the free energies of the liquid and zinc-blende phases can be defined explicitly, the partial ternary phase diagrams covering the L-S equilibria can be computed as a function of temperature. This procedure has been carried out for the ternary systems listed in Table 5. The results, displayed as isothermal sections or as quasi-binary joins, are compared with experimental findings and Stringfellow's calculations (1) in Figures 15-25. A calculated isothermal section due to Ansara et al. (7) for the Sb-Ga-In case at 823°K is included for comparison in Figure 21. The latter results are in good agreement with the current findings shown in Figure 23. Although it is not possible to make an exact comparison of the interaction parameters employed by Stringfellow in his quasi-binary calculations (1,6) and those employed here, an approximate comparison can be made in the following way. In Stringfellow's study, the quasi-binary system InP-InAs was treated as if the liquid and solid phases were both regular solutions. The interaction parameter for the liquid was taken to be 5238 J./mol. Since the heat of mixing is the product of the mol. fraction and the interaction parameter, the maximum value of the heat of mixing is (0.25)(5238)=1309 J/mol=655 J/g.at. for liquid $0.5In_{0.5}P_{0.5}$-$0.5In_{0.5}As_{0.5}$. This value is listed in Table 6 along with comparable parameters for the other systems of current interest cited by Stringfellow. The latter results are compared with those derived from the current study on the basis of Equations (8) and (9) and Table 5. As indicated above, the maximum contribution along the quasi-binary join is equal to TRNL/32 and CAB/8. Table 6 lists these values for comparison with Stringfellow's results in Table 6. While there is no obvious correlation between the current results and Stringfellow's values, all of the values listed are small! The analysis of the Ga-Sb-In system carried out by Ansara et al. (7) utilized a ternary heat of mixing equal to

$$E_H^L = x_{In}x_{Ga}x_{Sb}\,[23234x_{In} - 24066x_{Ga} + 582x_{Sb}]. \qquad (10)$$

The present analysis sets

$$E_H^L = -x_{In}x_{Ga}x_{Sb}\ 8368\ . \qquad (11)$$

At $x_{In}=x_{Ga}=x_{Sb}=0.333$, Equation (10) yields -3.1 J/g.at., while Equation (11) yields -309 J./g.at. At compositions near the edges of the ternary (0.1,0.4,0.5) Eq. (11) yields -167 J/g.at., while Eq. (10) yields results between +188 and -188 J.g./at. All of these contributions are small.

TABLE 5

COMPILATION OF TERNARY PARAMETERS FOR III-V LIQUID AND ZINC-BLENDE COMPOUND PHASES

(All Units in Joules per gram-atom (mole of atoms) T in Kelvins)

System	TRNL (Joules/g.at)	Zinc-blende Phase	CAB (Joules/g. at.)
P-In-As	12552	$In_{0.5}(P,As)_{0.5}$	0
As-In-Sb	0	$In_{0.5}(As,Sb)_{0.5}$	9623
P-Ga-As	-31380	$Ga_{0.5}(P,As)_{0.5}$	2092
Ga-Sb-In	-8368	$(Ga,In)_{0.5}Sb_{0.5}$	4602
Al-Ga-Sb	-8368	$(Al,Ga)_{0.5}Sb_{0.5}$	-4184

TABLE 6

COMPARISON OF THE MAXIMUM QUASI-BINARY HEAT OF MIXING FOR THE LIQUID AND SOLID COMPOSITIONS FROM STRINGFELLOW (1,6) AND THE CURRENT ANALYSIS (Joules/g.at.)

	LIQUID		SOLID	
System	Stringfellow(1)	Current	Stringfellow	Current
$In_{0.5}P_{0.5}$-$In_{0.5}As_{0.5}$	655	392	306	0
$In_{0.5}As_{0.5}$-$In_{0.5}Sb_{0.5}$	244	0	1197	1202
$Ga_{0.5}P_{0.5}$-$Ga_{0.5}As_{0.5}$	655	-980	515	260
$Ga_{0.5}Sb_{0.5}$-$In_{0.5}Sb_{0.5}$	1409	-260	965	571
$Al_{0.5}Sb_{0.5}$-$Ga_{0.5}Sb_{0.5}$	664	-260	12	-521

Thus the current analysis suggests a simple method for calculating isothermal sections for III-IV ternary systems. In particular, if a given section is required, the data base contained in Tables 1-3 can be employed to calculate the section of interest with TRNL= CAB=0. The process can then be repeated employing a range of TRNL and CAB similar to those shown in Table 5 to predict the spread of expected results. If a few experimental data are available at a given temperature, they can be readily employed to fix TRNL and CAB, which in turn can be employed to predict the behavior at other temperatures. It is hoped that future studies will permit improvement of the current data base.

3. Thermochemical System Employed to Characterize Binary II-VI Phase Diagrams

The II-IV compounds of $Cd_{0.5}Te_{0.5}$ and $Hg_{0.5}Te_{0.5}$ form a series of cubic zinc-blende solid solutions which offer the attractive property of a variable band gap that is a function of composition. The $(Cd,Hg)_{0.5}Te_{0.5}$ solid solution displays band gaps which run in a nearly linear fashion between the wide gap semiconductor $Cd_{0.5}Te_{0.5}$ (E_g=1.6 eV) and the semimetallic compound $Hg_{0.5}Te_{0.5}$, which can be considered to be a semiconductor with a negative band gap (37). Alloys of $Cd_{0.1}Hg_{0.4}Te_{0.5}$ and $Cd_{0.2}Hg_{0.3}Te_{0.5}$, exhibiting band gaps ranging from 0.1 to 0.5 eV, respectively, are of particular interest for detection of infrared radiation in the 2 to 20 micron range. The growth of such alloy compositions from the melt presents some difficulties due to the "width" of the two phase liquid plus solid field along the $Cd_{0.5}Te_{0.5}$-$Hg_{0.5}Te_{0.5}$ quasi-binary join. Liquid phase epitaxial (LPE) growth methods have been employed to circumvent this problem (37), but controlled growth requires a knowledge of the tie-lines between the alloy compound and the liquid. Such information can be generated experimentally with considerable effort. Alternatively, it is possible to use the CALPHAD method, which has been applied to a very wide range of systems, for calculating the ternary Cd-Te-Hg system from a knowledge of the component binary systems in order to provide the required information on tie-line composition. The description provided below provides an account of such calculations.

4. Description of the Vapor, Liquid and Zinc-blende Phases

Table 7 summarizes the current descriptions of the liquid(L), vapor(V) and zinc-blende(ζ) phases in the cadmium-tellurium-mercury system as a function of temperature (T, °K), pressure (P, atmospheres), atomic fraction tellurium(x), and atomic fraction of mercury(y). These equations, along with the associated lattice stability values relating the free energy of the vapor, liquid, fcc, and stable forms of cadmium, tellurium and mercury, have been assembled by employing existing (38,14-17) thermochemical and phase diagram data for the pure elements and binary systems. Figures 26-31 show the partial binary phase diagrams computed for the Te-Cd, Hg-Cd and Te-Hg systems at P=1 atmosphere and P=16 atmospheres. These phase diagrams follow directly from the ternary equations listed in Table 7 when they are reduced to binary systems for each of the edge binary systems in question. The small ternary terms assigned to the liquid phase (-33472xy(1-x-y)) and the zinc-blende phase (-4180y (1-2y)) Joules/g.at. were chosen in conformity with the experimental results along the $Cd_{0.5}Te_{0.5}$-$Hg_{0.5}Te_{0.5}$ quasi-binary join shown in Figures 32 and 33. Since the maximum value of these terms is attained at x=0.5 and y=0.25, it is apparent that the ternary correction term is at most about -1000 Joules/g.at. for the liquid phase and -500 Joules/g.at. for the zinc-blende phase at the x=0.5, y=0.25 composition. Table 8 compares calculated and observed thermochemical values for $Cd_{0.5}Te_{0.5}$ and $Hg_{0.5}Te_{0.5}$ at 298°K.

Figures 34-36 display calculated isothermal sections in the Cd-Te-Hg systems between 1 and 74 atmospheres at temperatures ranging from 773°K to 1213°K. These calculated isothermal sections show the tie-lines between the zinc-blende and liquid phases in addition to the three phase vapor/liquid/zinc-blende fields which are especially important in crystal

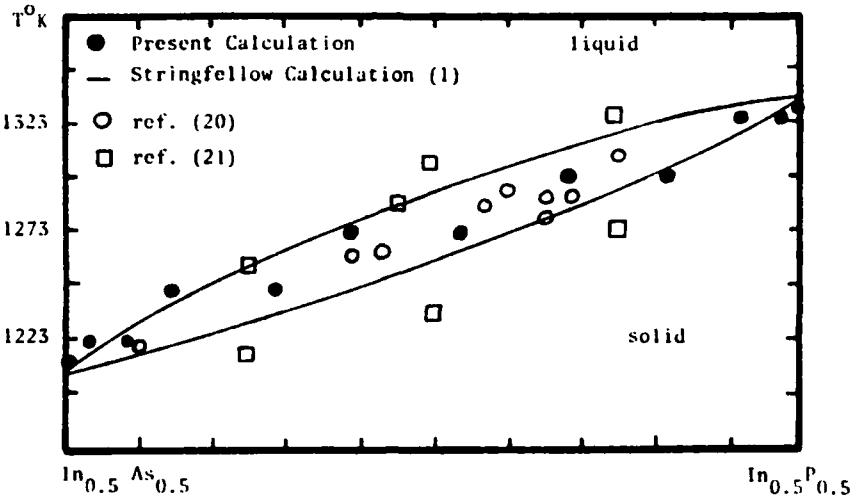

Figure 15. Calculated and Observed Equilibria Along the $In_{0.5}As_{0.5}$ - $In_{0.5}P_{0.5}$ Quasi-binary Join

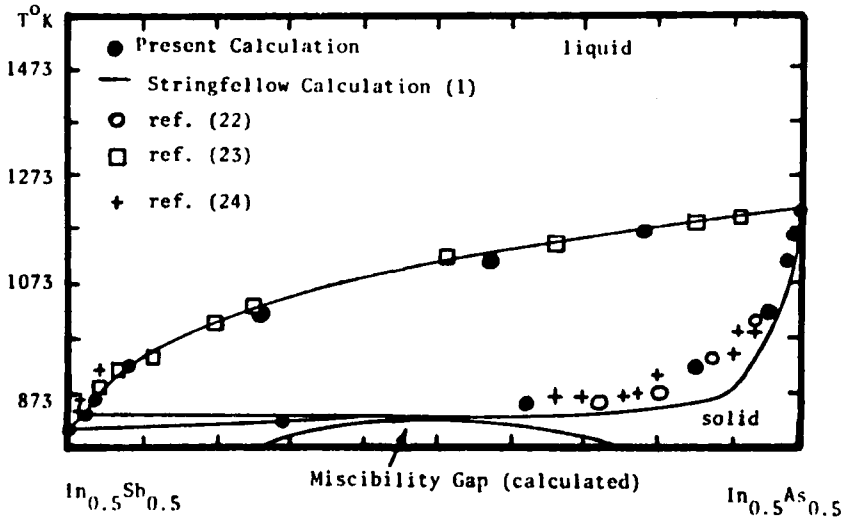

Figure 16. Calculated and Observed Equilibria Along the $In_{0.5}Sb_{0.5}$ - $In_{0.5}As_{0.5}$ Quasi-binary Join

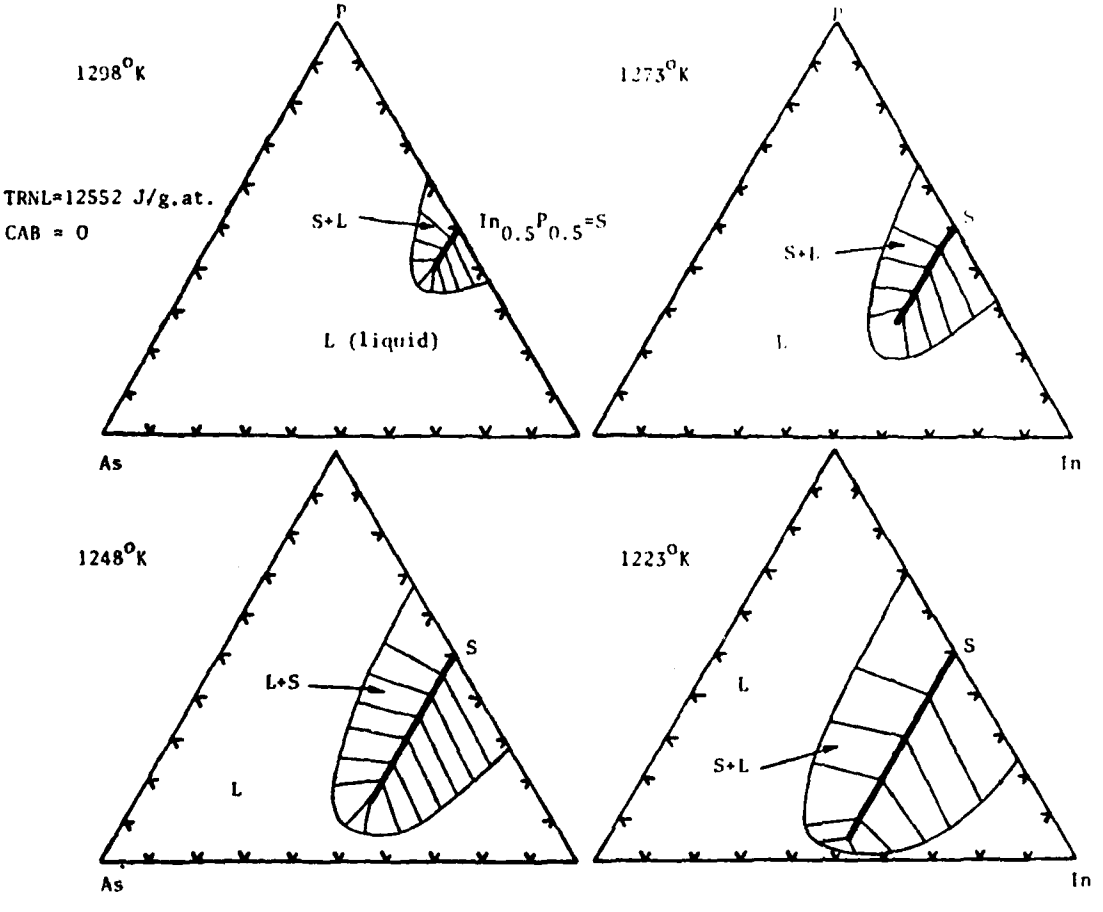

Figure 17. Calculated Partial Isothermal Sections in the Phosphorus-Indium-Arsenic System

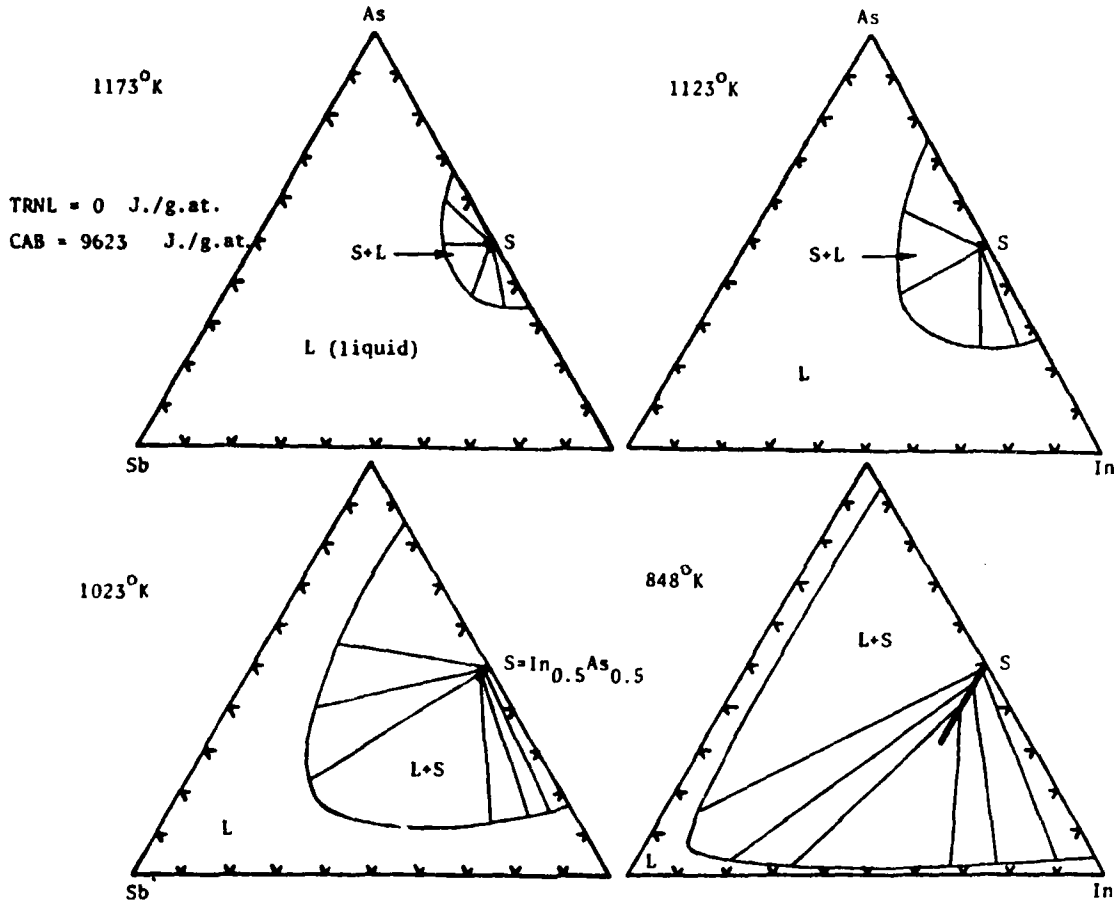

Figure 18. Calculated Partial Isothermal Sections in the Arsenic-Indium-Antimony System

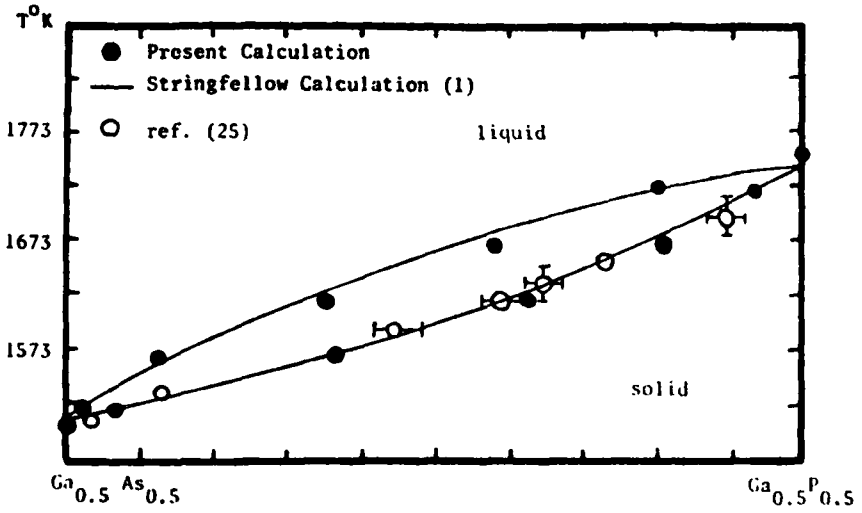

Figure 19. Calculated and Observed Equilibria Along the $Ga_{0.5}As_{0.5}$ - $Ga_{0.5}P_{0.5}$ Quasi-binary Join

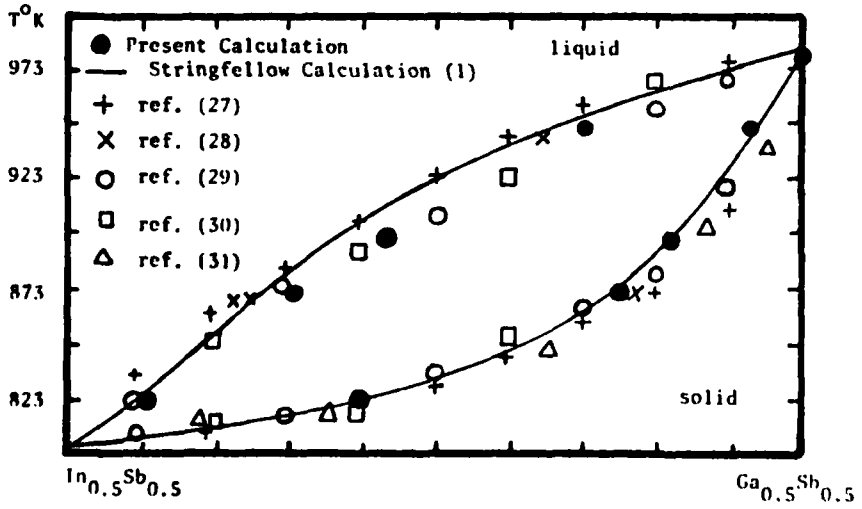

Figure 20. Calculated and Observed Equilibria Along the $In_{0.5}Sb_{0.5}$ - $Ga_{0.5}Sb_{0.5}$ Quasi-binary Join

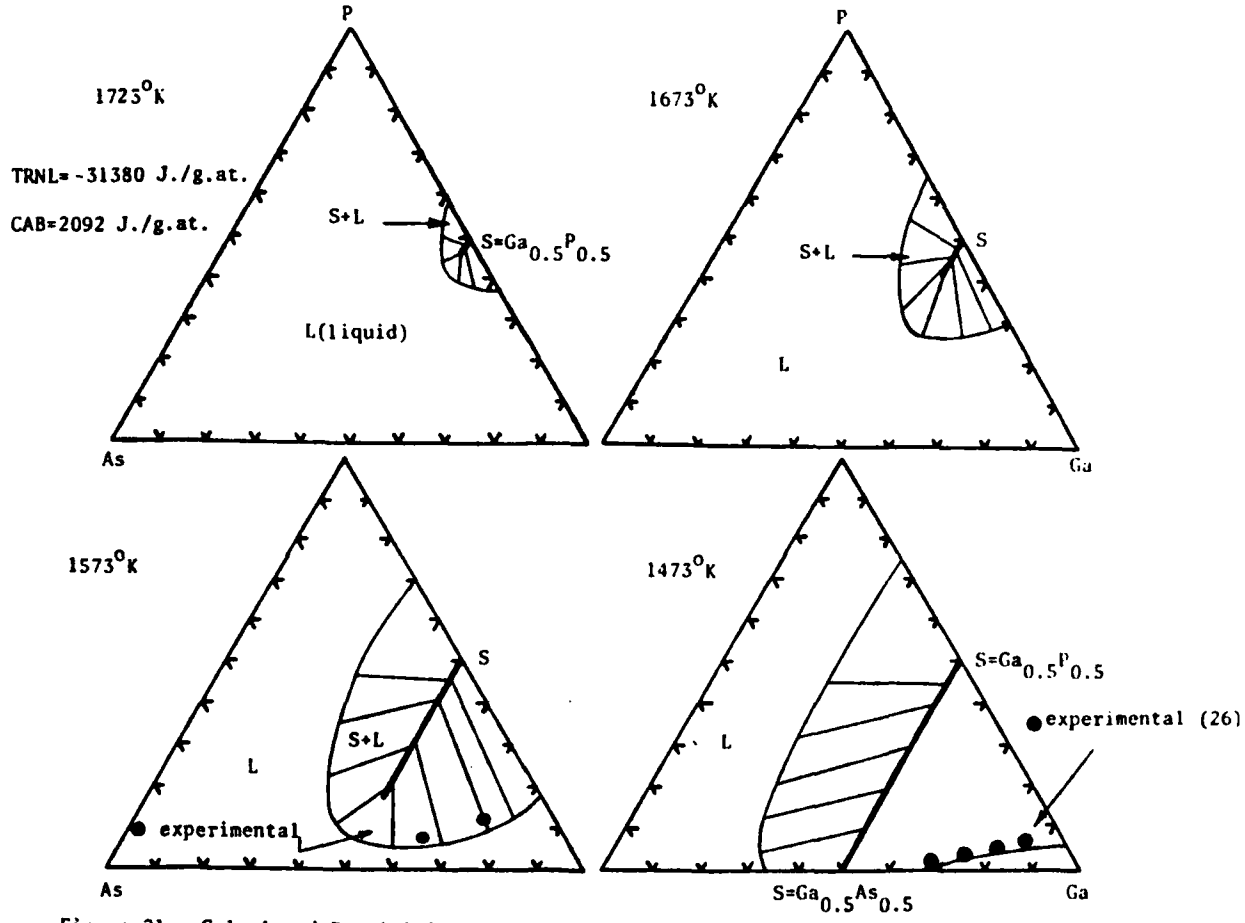

Figure 21. Calculated Partial Isothermal Sections in the Phosphorus-Gallium-Arsenic System. Experimental Values: ref. (26)

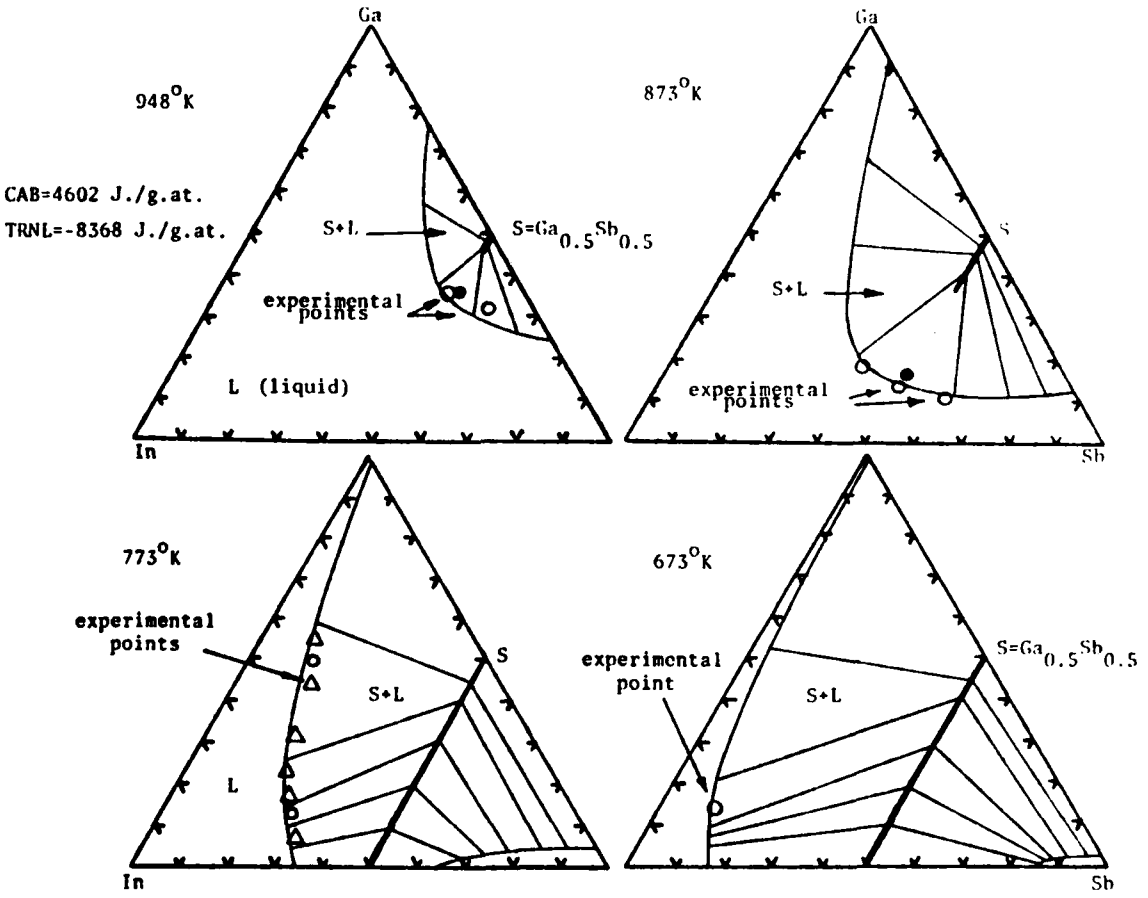

Figure 22. Calculated Partial Isothermal Sections in the Gallium-Antimony-Indium System. Experimental Values: ref. (28,30,32)

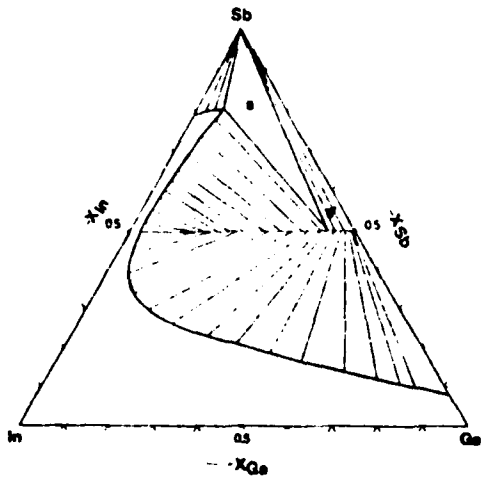

Figure 23. Calculated Partial Isothermal Section in the Sb-Ga-In System at 823°K [after ref. (7)]

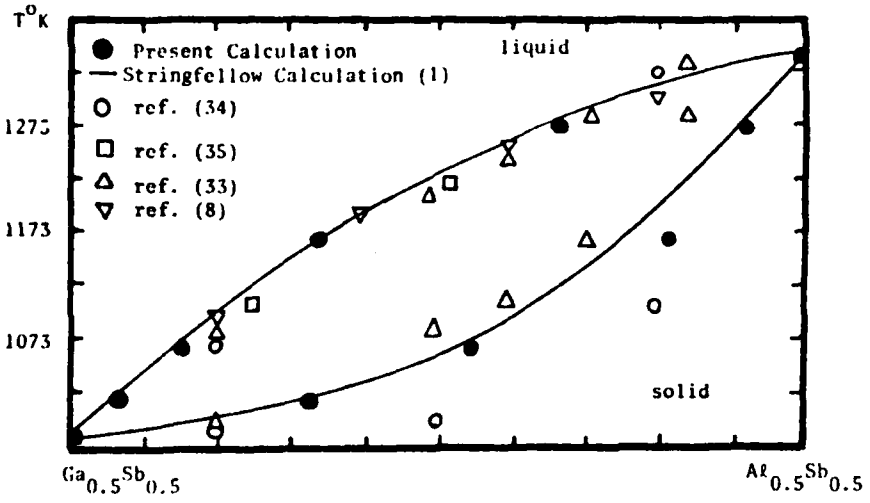

Figure 24. Calculated and Observed Equilibria Along the $Ga_{0.5}Sb_{0.5}$ - $Al_{0.5}Sb_{0.5}$ Quasi-binary Join

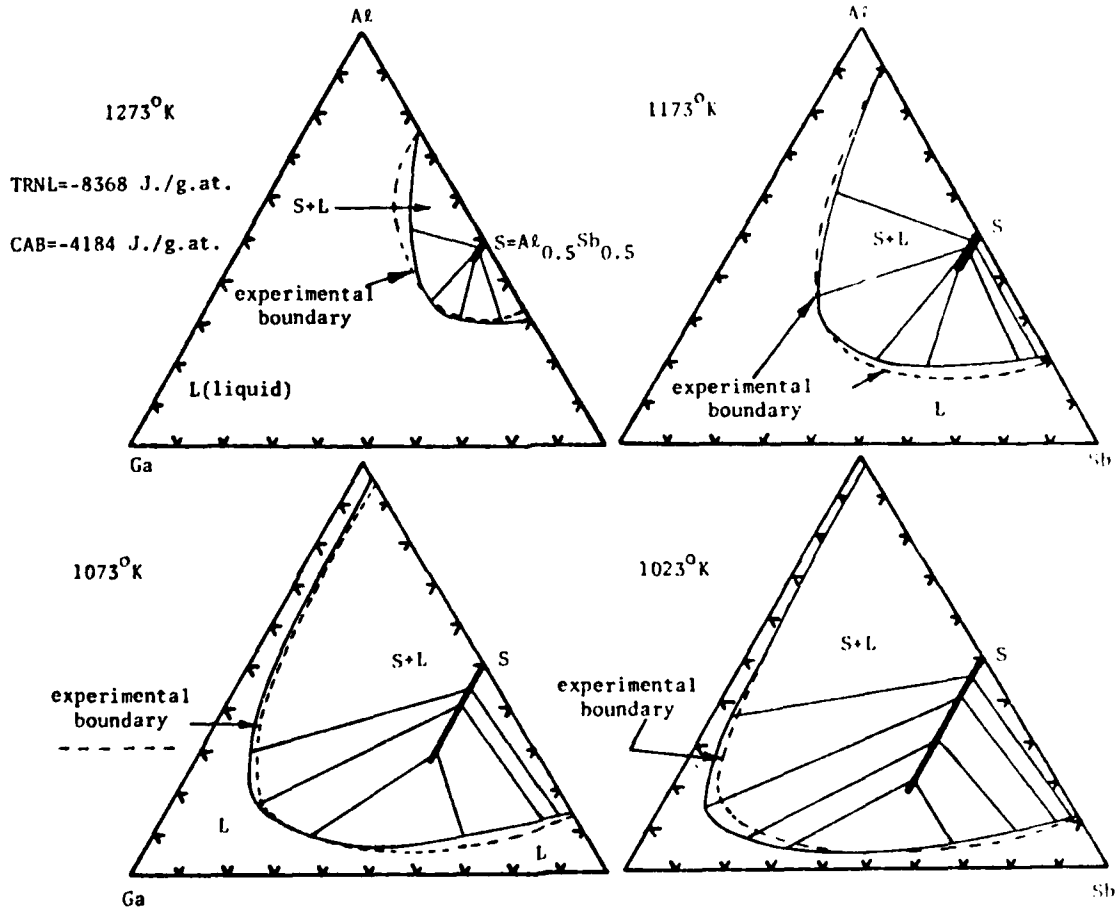

Figure 25. Calculated Partial Isothermal Sections in the Aluminum-Antimony-Gallium System. Experimental Results: ----- ref. (36)

growth operations. The calculations of tie-lines can be compared directly with the recent experimental results of Mroczkowski and Vydyanath, who determined tie-line compositions by means of "closed tube tipping experiments". In these experiments, crystals of the zinc-blende phase of fixed composition are equilibrated with the liquid phase in a graphite boat. After equilibration, the temperature was decreased by 5 to 7°C and the liquid was decanted. Subsequent electron microprobe analysis of the concentration profiles along the length of the crystal (from the zinc-blende single crystal phase into the polycrystalline phase, which forms when the contact liquid freezes) permits determination of the tie-line compositions (37). At 818°K, the following comparison can be made between the calculated and observed tie lines.

	Zinc-blende		Liquid	
Atomic Percent	Hg	Cd	Hg	Cd
Observed (37)	32.5	17.5	20.3	2.3
Calculated	32.5	17.5	19.5	2.0

This excellent comparison provides an independent check of the description of the liquid and zinc-blende free energies shown in Table 7. These equations can be used to compute the liquid/vapor/zinc-blende equilibria over a wide range of temperatures and pressures, which, in turn, can be used to define the conditions for stable conventional and LPE growth of Te-rich and Te-poor $(Cd,Hg)_{0.5}Te_{0.5}$ compositions.

5. Conclusions

The examples of calculated III-V and II-VI multi-component systems presented here illustrates the scope and utility of the method presented. The range of systems to which such computations can be applied will expand as additional binary systems are added to the data base.

References

1. G.B. Stringfellow, J. Phys. Chem. Solids 33 665 (1972).
2. G.B. Stringfellow, Materials Res. Bulletin 6 371 (1971).
3. G.B. Stringfellow and P.E. Greene, J. Electrochemical Soc. 117 1075 (1970).
4. G.B. Stringfellow (Ibid.)117 1301 (1970).
5. G.B. Stringfellow, J. Phys. Chem. Solids 35 775 (1974).
6. G.B. Stringfellow, J. Crystal Growth 27 21 (1974).
7. I. Ansara, M. Gambino and J.P. Bros, J. Crystal Growth 32 101 (1976); CALPHAD 1 27, 40 (1977).
8. K. Osamura, K. Nakajima and Y. Murakami, J. Electrochem. Soc. 126 1992 (1979).
9. K. Osamura, J. Inoue and Y. Murakami, J. Electrochem. Soc. 119 102 (1972).
10. K. Nakajima, K. Osamura and Y. Murakami, J. Electrochem. Soc. 122 1245 (1975).
11. R.F. Brebrick, Met. Tr. 8A 403 (1977). Supplemented by CALPHAD 2 17 (1978).
12. I. Ansara, J.P. Bros and C. Girard, CALPHAD 2 187 (1978).
13. L. Kaufman, CALPHAD 1 7 (1977).
14. L. Kaufman, CALPHAD 3 45 (1979).
15. L. Kaufman, CALPHAD 3 275 (1979).
16. O. Kubaschewski and C.B. Alcock, Metallurgical Thermochemistry, Fifth Edition, Pergamon Press, Oxford (1979).
17. R. Hultgren, P.D. Desai, D.T. Hawkins, M. Gleiser and K.K. Kelley, Selected Values of the Thermodynamic Properties of Metals (and Binary Alloys), (2 volumes) ASM, Metals Park, Ohio (1973).
18. M. Hansen and K. Anderko, Constitution of Binary Alloys, McGraw-Hill, N.Y. (1958).
19. R.P. Elliott and F. Shunk, First and Second Supplements, Ibid. (1965).
20. J.W. Wagner and A.G. Thompson, J. Electrochem. Soc., Spring Meeting (1970).
21. W. Koster and W. Ulrich, Z. Metallkunde 49 365 (1958).
22. J.C. Woolley and B.A. Smith, Proc. Phys. Soc. 72 214 (1950).
23. C. Shih and E.A. Peretti, Tr. ASM 48 709 (1956).
24. G.B. Stringfellow and P.E. Greene J. Electrochem. Soc. 118 805 (1971).
25. K. Osamura and Y. Murakami, Japan J. of App. Phys. 8 967 (1969).
26. M.B. Panish, J. Phys. Chem. Solids 30 1083 (1969).
27. V.B. Usimtsev, A.S. Timoshin and G.V. Kostin, Neorg. Mat. 7 2090 (1971).
28. G.M. Blom and T.S. Plaskett, J. Electrochem. Soc. 118 1831 (1971).
29. J.C. Woolley and D.G. Lees, J. Less-Common Metals 1 192 (1959).
30. J.C. Woolley B.A. Smith and D.G. Lees, Proc. Phys. Soc. London, 69B 1339 (1956).
31. J.C. Woolley and B.A. Smith, Proc. Phys. Soc. London 72 214 (1958).
32. G.A. Antypas, J. Cryst. Growth 16 181 (1972).
33. A.S. Borschevskii, I.I. Burdiyan, E.Yu. Lubenskaya and E.V. Sokolova, Zh. Nauch. Khim 4 2824 (1959).
34. I.I. Burdiyan and A.S. Borschevskii, Sov. Phys. Tech. Phys. 3 2451 (1958).
35. J.F. Miller, H.L. Goering and R.C. Himes, J. Electrochem. Soc. 107 527 (1960).
36. K.Y. Cheng and G.L. Pearson, J. Electrochem. Soc. 124 753 (1977).
37. J.A. Mroczkowski and H.R. Vydyanath, "Liquid Phase Epitaxial Growth of $(Hg_{(1-x)}Cd_x)Te$ from Tellurium Rich Solutions Using a Closed Tube Tipping Technique", J. Electrochem. Soc. 128 655 (1981).
38. R.F. Brebrick and A.J. Strauss, J. Phys. Chem. Solids, 26 989 (1965).
39. J. Steininger, J. Elect. Materials, 5 299 (1976).
40. J. Blair and R.Newnham, Metallurgy of Elemental and Compound Semiconductors, Interscience Publishers Inc., New York (1961)vol. 12.
41. T.C. Harman and A.J. Strauss, J. Appl. Phys. (Suppl.) 32 2265 (1961).
42. J.L. Schmit and C.J. Speerschneider, Infrared Physics 8 247 (1968).
43. K. Osamura and Y. Murakami, J. Phys. Chem. Solids, 36 931 (1975).

TABLE 7

SUMMARY OF FREE ENERGY EQUATIONS DESCRIBING THE VAPOR LIQUID,AND ZINC-BLENDE PHASES IN THE CADMIUM-TELLURIUM-MERCURY SYSTEM
(All units in Joules per gram-atom (mole of atoms), °K)

L=liquid phase, V=vapor phase, S=zinc-blende phase, A=fcc
R=rhombohedral (stable Hg), T=trigonal (stable Te), E=hcp (stable Cd)
x=atom fraction Te, y=atom fraction Hg, P=pressure (atmospheres)
R=8.314 J/g.at.°K

Lattice Stability Values

$G^L_{Hg} - G^R_{Hg} = 2292-9.832T$; $\bar{T}=234°K$

$G^A_{Hg} - G^R_{Hg} = 2297-1.464T$

$G^V_{Hg} - G^L_{Hg} = 59174-93.303T+RT\ell nP$

$G^L_{Te} - G^T_{Te} = 17489-24.184T$; $\bar{T}= 723°K$

$G^A_{Te} - G^T_{Te} = 17489-15.816T$

$\frac{1}{2}G^V_{Te_2} - G^L_{Te} = 58409-45.982T+0.5RT\ell nP$

$G^L_{Cd} - G^E_{Cd} = 6192-10.418T$; $\bar{T}=594K$

$G^A_{Cd} - G^E_{Cd} = 1924-2.050T$

$G^V_{Cd} - G^L_{Cd} = 102,520-98.659T+RT\ell nP$

Ternary Phases

$$G^L = (1-x-y)G^L_{Cd} + xG^L_{Te} + yG^L_{Hg} + RT\,[(1-x-y)\ell n(1-x-y)+x\ell nx+y\ell ny]$$
$$-xy(x+y)^{-1}\,[(30962+5.02T)x+(3514+16.74T)y] + y(1-x-y)[-10878+4.184T]$$
$$+x(1-x-y)(1-y)^{-1}[(1-x-y)(112968-159T) -x(75312+20.92T)]- 33472\ xy(1-x-y)$$

$$G^V = (1-x-y)G^V_{Cd} + 0.5x\ G^V_{Te_2} + y\ G^V_{Hg}$$
$$+ RT((1-x-y)\ell n(1-x-y)+x\ell nx+y\ell ny)$$

$$G^S = (0.5-y)\ G^A_{Cd} + 0.5\ G^A_{Te} + y\ G^A_{Hg} + (1-2y)[-61191+13.075T]+2y[-26798+7.11T]$$
$$+ RT[y\ell ny + (0.5-y)\ell n(0.5-y)-0.5\ell n0.5] -4180y(1-2y)$$
$$0 \leq y \leq 0.5$$

TABLE 8

COMPARISON OF CALCULATED AND OBSERVED (16) FREE ENERGY OF FORMATION AT 298°K

Compound	ΔH [298] (J./g.at.)	ΔS [298] (J./g.at.°K)
$Cd_{0.5}Te_{0.5}$	-50900 ± 400 (obs.)	-4.18 ± 1.25 (obs.)
	-51500 (calc.)	-4.14 (calc.)
$Hg_{0.5}Te_{0.5}$	-15900 ± 2100 (obs.)	-6.28 ± 1.26 (obs.)
	-18050 (calc.)	-3.39 (calc.)

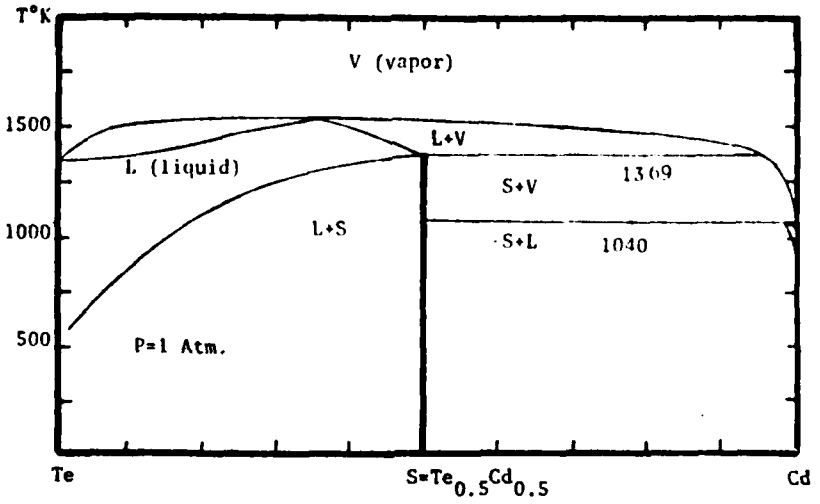

Figure 26. Calculated Partial Te-Cd Phase Diagram at 1 Atmosphere.

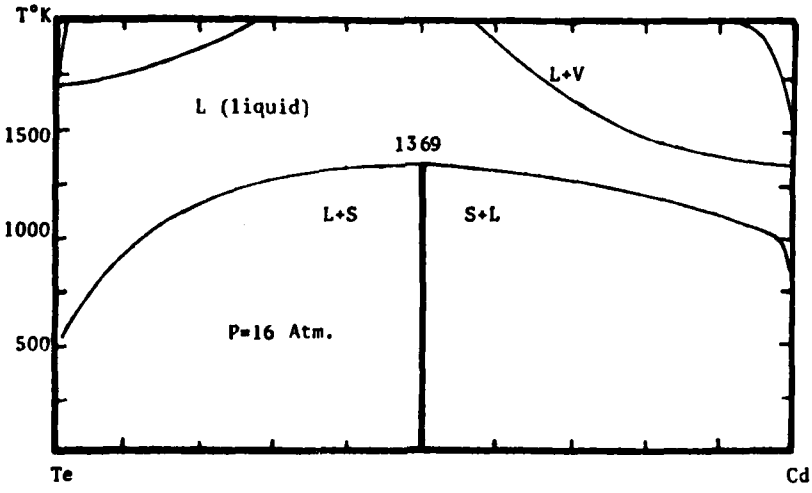

Figure 27. Calculated Partial Te-Cd Phase Diagram at 16 Atmospheres.

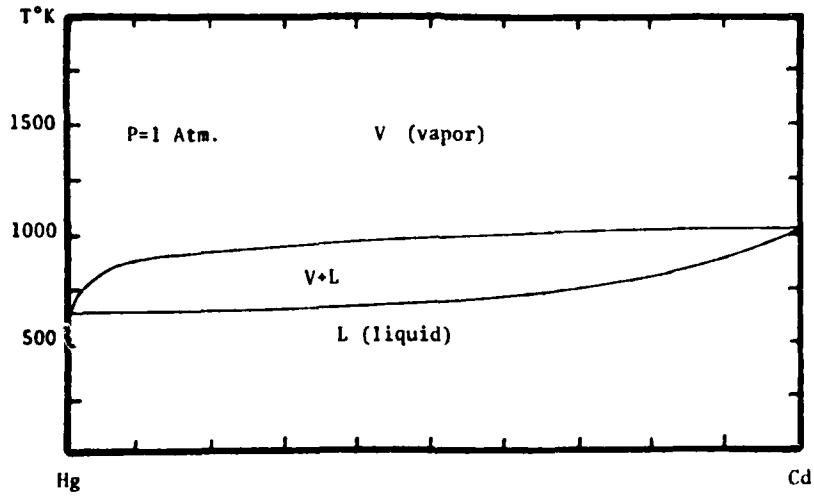

Figure 28. Calculated Partial Hg-Cd Phase Diagram at 1 Atmosphere.

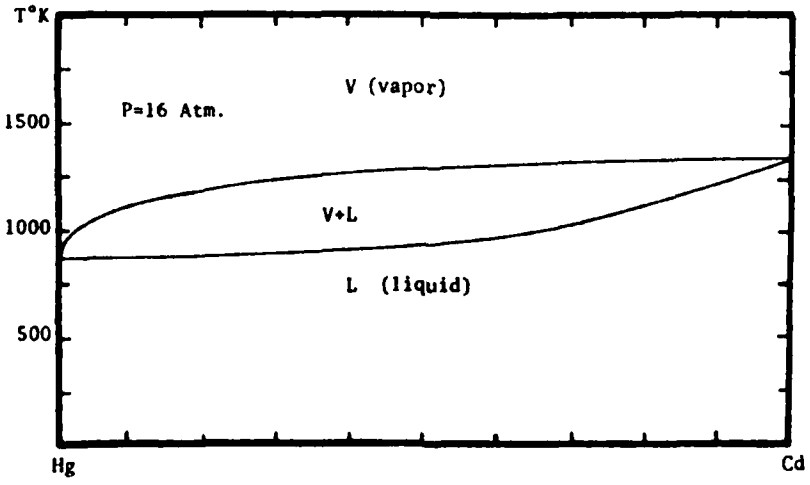

Figure 29. Calculated Partial Hg-Cd Phase Diagram at 16 Atmospheres.

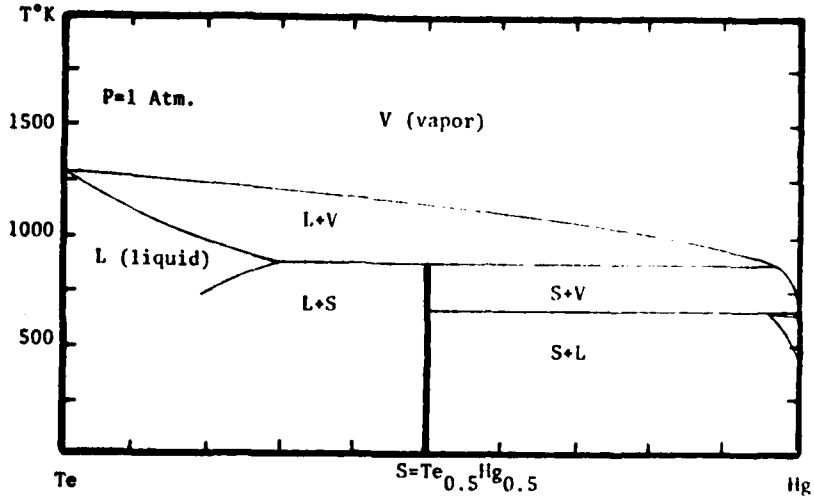

Figure 30. Calculated Partial Te-Hg Phase Diagram at 1 Atmosphere.

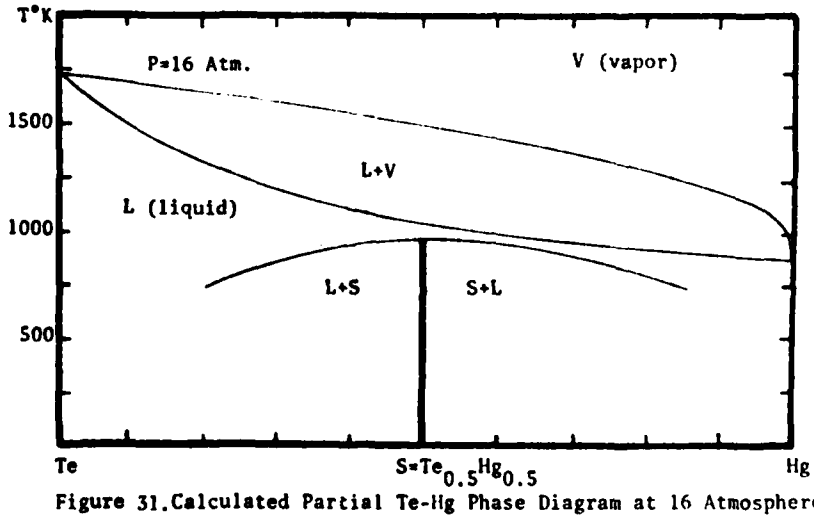

Figure 31. Calculated Partial Te-Hg Phase Diagram at 16 Atmospheres.

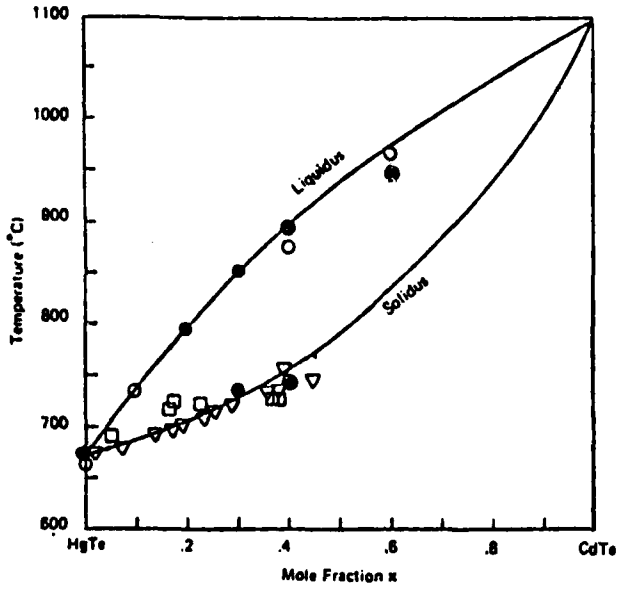

● - Steininger (39)
○ Liquidus Data - Blair and Newnham (40)
▽ Solidus Data - Harman and Strauss (41)
□ Solidus Data - Schmit and Speerschneider (42)

Figure 32. Liquidus and Solidus Curves for Pseudo-binary $Hg_{(1-x)}Cd_xTe$ Compositions (39)

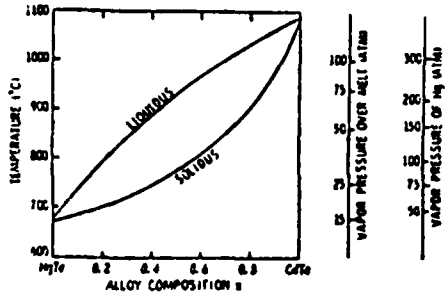

Figure 33. Composite P-T-x Diagram for the Pseudo-binary HgTe-CdTe System (39)

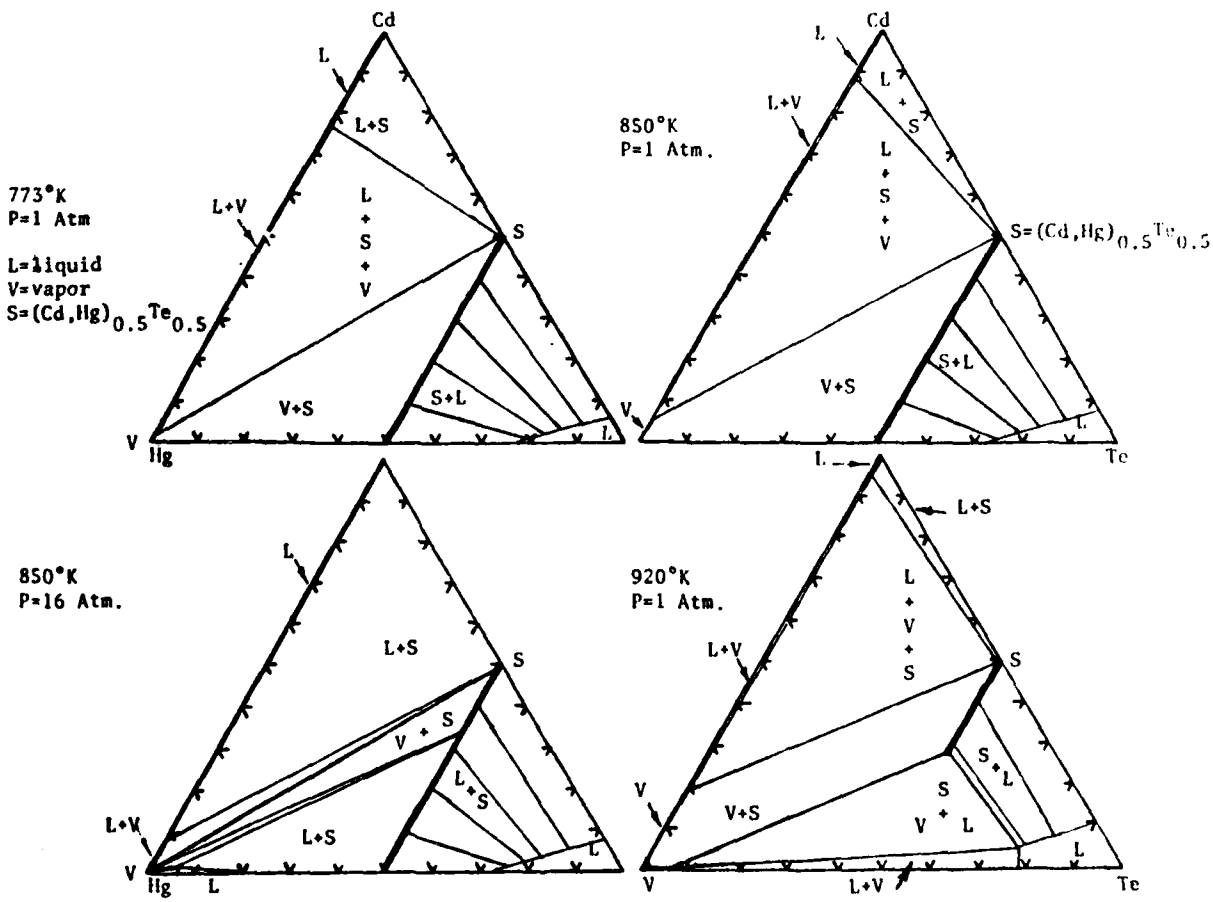

Figure 34. Calculated Isothermal Sections in the Cd-Te-Hg System

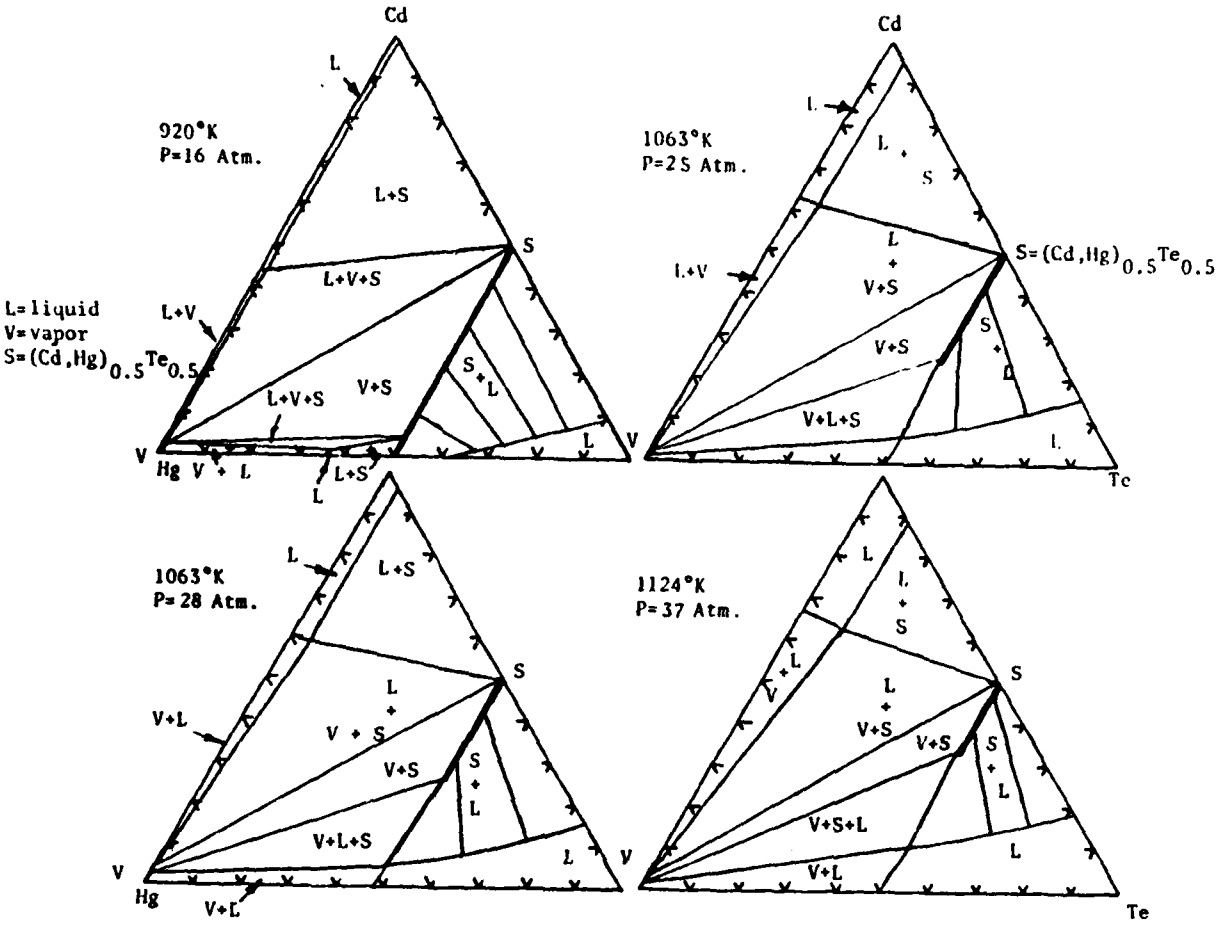

Figure 35. Calculated Isothermal Sections in the Cd-Te-Hg System

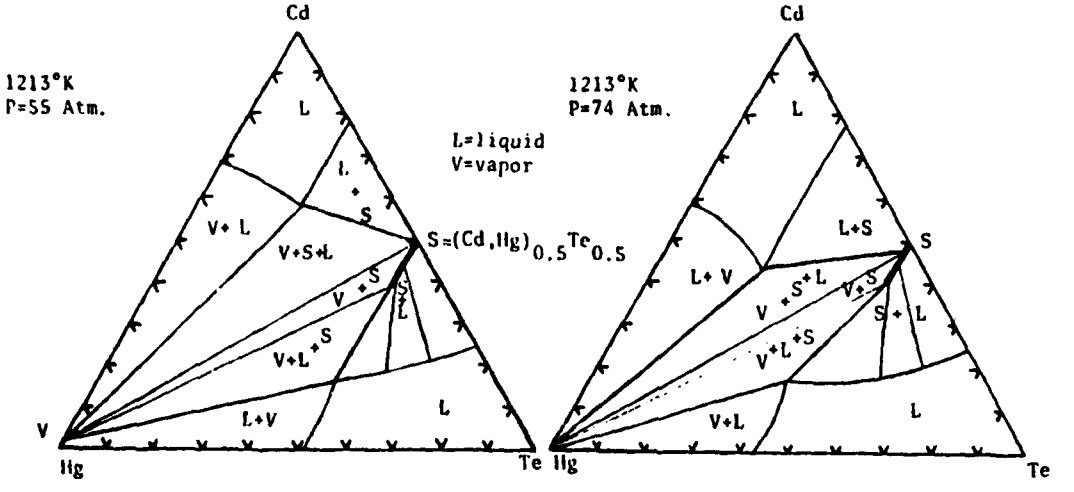

Figure 36. Calculated Isothermal Sections in the Cd-Te-Hg System at 1213°K

V CALCULATION OF TERNARY FLUORIDE GLASS COMPOSITIONS

L. Kaufman, J. Agren, J. Nell and F. Hayes, CALPHAD (1983) 7 71-83

(This paper was presented at CALPHAD XI, Argonne, Illinois May 1982

ABSTRACT. The recent discovery of a new family of non-oxide glasses based on mixtures of ZrF_4 or HfF_4 with other metallic fluorides by M. Poulain and coworkers offers great potential in optical fiber, window and source/detector application. Due to the limited phase diagram data available for the binary, ternary and multicomponent fluoride systems currently employed to synthesize these glasses most of the progress in identifying new compositions has proceeded along empirical lines. In order to remedy this situation, the CALPHAD method for coupling phase diagram and thermochemical data has been applied to develop a data base covering metallic fluorides. The objective is to permit computation of multicomponent phase diagrams which can be used to identify the composition range where the liquid is most stable. The latter offers opportunities for glass formation as demonstrated by predictions of new metallic glasses. Currently the data base covers combinations of 0.2 ZrF_4(ZF), 0.25 LaF_3(LF), 0.333 BaF_2(BF), 0.333 PbF_2(PF), 0.5 NaF(NF), 0.5RbF(RF), 0.5CsF(CF) and 0.5 KF(KF) which have been developed along the lines described earlier for III-V, II-VI and SIALON systems. These results were used to generate computed liquidus contours in LF-ZF-BF and BF-ZF-NF to disclose the range of composition in which the liquid has the greatest stability. These compositions agree well with those in which Poulain and coworkers have discovered glass formation.

1. Introduction

The utility of computer based methods for coupling phase diagrams and thermochemical data for metallic systems has been well documented in many papers published in this journal. A considerable effort is being applied toward developing an extensive base for metallic systems. Recently similar efforts have begun in order to provide a similar facility with ceramic systems (1) and semiconducting III-V compound systems (2). The prediction of compositions of high liquid stability in the titanium-beryllium-zirconium in 1973 (3) was followed by development of commercial metallic glasses in 1975 at Allied Chemical (4). In view of the recent discoveries by M. Poulain and coworkers (5,6) that zirconium fluoride glasses offer potential as optical materials it seems appropriate to consider development of a data base capable of computing composition regions of liquid stability where glass formation could be facilitated.

2. Description of the Thermochemical System Employed to Characterize Solution and Compound Phases

The method utilized for describing solution and compound phases is the same as that employed earlier (1,2) comprising some symbolic usage which facilitates data handling as indicated below. The free energy, G^L, of a liquid (solution) phase, L, in the binary system ZrF_4-RbF is given by Equation (1) where T is in Kelvins, R=8.314 J/g. at ^oK, while ^4x is the atomic fraction of RF(i.e.RF=½RbF) and (1-x) is the fraction of ZF (i.e. $1/5ZrF_4$). The mass basis is thus one mole of atoms (i.e. a gram-atom)

$$G^L=(1-x)\,{}^oG^L_{ZF}+x\,{}^oG^L_{RF}+RT(x\ell nx+(1-x)\ell n(1-x))+x(1-x)[LZFRF(1-x)+xLRFZF]\ J/g.at \qquad (1)$$

where ${}^{o}G^{L}_{ZF}$ and ${}^{o}G^{L}_{RF}$ are the free energies of one gram atom of pure liquid ZF and RF. Table 1 defines the lattice stabilities of the liquid and solid forms of ZF, RF and the other components of current interest. These data derived from various compilations of thermochemical and phase diagram data, (7-15), when combined with the solution and compound phase parameters shown in Tables 2 and 3 permit calculation of the binary phase diagrams shown in Figures 1-10. The solution parameters LZFRF and LRFZF, which describe the liquid ZrF_4-RbF solution are listed in Table 2 (LZFRF=-70710+29.288T J/g.at, LRFZF=-31380+29.288T Joules/g.at). Similar parameters for the liquid and solid phases are listed in Table 2. The free energy of the solid phases are described in a manner similar to equation (1). Thus, for example, the free energy of the soldium chloride type solid S phase in the ZF-RF system is given by

$$G^{S}=(1-x){}^{o}G^{S}_{ZF}+x{}^{o}G^{S}_{RF}+RT(x\ell nx+(1-x)\ell n(1-x))+x(1-x)[SZFRF(1-x)+xSRFZF] \text{ J/g. at.} \quad (2)$$

The solution parameters for the S phase (SZFRF=SRFZF=16736 J/g.at) are listed in Table 2. The free energy difference between the L and S forms of ZF and RF, i.e. $ZFZFLS={}^{o}G^{L}_{ZF}-{}^{o}G^{S}_{ZF}$ and ${}^{o}G^{L}_{RF}-{}^{o}G^{S}_{RF}=RFRFLS$ are listed in Table 1. The free energy of a compound phase such as $X=(1/7)(ZrF_4\cdot RbF)=ZF_{0.714}RF_{0.286}$ is defined on the basis of Table 3 in terms of the base phase, the compound parameter, C, and the stoichiometry by equation (3)

$$G^{X}=0.714{}^{o}G^{M}_{ZF}+0.286{}^{o}G^{M}_{RF}+(0.714)(0.286)[0.714LZFRF+0.286\ LRFZF-C] \text{ J/g.at.} \quad (3)$$

Reference to Table 2 shows that LZFRF=-70710+29.288T J/g.at and LRFZF= -31380+29.288T J/g.at. while Table 3 shows that C=-20669+41.84T J/g.at. Thus

$$G^{X}=0.714{}^{o}G^{M}_{ZF}+0.286{}^{o}G^{M}_{RF}-7912-2.56T \text{ J/g.at.} \quad (4)$$

At 298K reference to Figure 1 shows that the stable form of RbF is the sodium chloride S form. Table 1 shows that

$${}^{o}G^{M}_{RF}-{}^{o}G^{S}_{RF}=RFRFLS-RFRFLM=12866-1.381T \text{ J/g.at.} \quad (5)$$

Substitution of equation (5) into equation (4) yields an expression for the free energy of formation of $(1/7)(ZrF_4\cdot RbF)$ at 298K from the stable forms of its compound components as,

$$\Delta G_f[298K]=G^{X}-0.714\ G^{M}_{ZF}-0.286\ G^{S}_{RF}=-4234+2.95T \text{ J/g.at.} \quad (6)$$

The latter value is shown in Table 3.

Experimental information concerning the thermochemical properties of fluoride solutions and mixed fluoride compounds is scarce. The only experimental data located (15) is shown in Table 3 where experimental measurements of the heat of formation of liquid ZrF_4-NaF solutions at 1303K are compared with calculated values on the basis of Equation (1) and Table 2. The table lists the measured molar heat of formation (15) for specific molar concentrations along with the calculated values. The latter are obtained by converting the molar composition into appropriate fractions of NF (i.e. 1/2NaF) and ZF (i.e. $(1/5)ZrF_4$). Thus $0.75NaF-0.25\ ZrF_4$ is equal to 1.5NF-1.25ZF which is in turn equal to 2.75 gram atoms of $ZF_{0.455}NF_{0.545}$. The calculated heat of mixing of the liquid at this composition from Equation (1) and Table 2 at a composition $x_{NF}=0.545$ is -10090 Joules/g.at. Hence the calculated heat of formation of a 0.75NaF-0.25 ZrF_4 molar liquid is 2.75x(-10090)=-27760 Joules/mole. The calculated values in Table 4 are in agreement with the measured results.

3. Calculation of Quasi-Ternary Phase Diagrams

The free energy of ternary solution phases was synthesized from the binary solution phases on the basis of Kohler's equation as in the previous papers (1,2). On this basis the free energy of the liquid phase in the LF-ZF-BF system in Figure 11 where x is the atom fraction ZF, y is the atom fraction BF and 1-x-y is the atom fraction LF is given by Equation (7)

TABLE 1
SUMMARY OF LATTICE STABILITY PARAMETERS
(All Units in Joules per gram atom (mole of atoms), T in Kelvins)

ZF=(1/5)ZrF_4, RF=(1/2)RbF, NF=(1/2)NaF, CF=(1/2)CsF, KF=(1/2)KF, BF=(1/3)BaF_2

LF=(1/4)LaF_3, PF=(1/3)PbF_2

S=Sodium Chloride Structure, Stable form of NF, KF, RF and CF
L=Liquid, M=Stable form of ZF, K=Stable form of BF, J=Stable form of LF,
C=Stable form of PF

$NFNFLS^*$=(1/2)NaF(Liquid)-(1/2)NaF(S, sodium chloride)

ZFZFLM=12845-10.669T
ZFZFLS= 0-11.966T
ZFZFLK= 0- 6.069T
ZFZFLJ= 0- 7.113T
ZFZFLC= 0- 5.314T

RFRFLS=12866-12.050T
RFRFLM= 0-10.669T

NFNFLS=16799-13.263T
NFNFLM= 0-10.669T
NFNFLK= 0- 6.067T

CFCFLS=10857-11.129T
CFCFLM= 0-10.669T

KFKFLS=14121-12.468T
KFKFLM= 0-10.669T

BFBFLK= 9481- 6.067T
BFBFLM= 0-10.669T
BFBFLS= 0-13.263T
BFBFLJ= 8786- 7.113T

LFLFLJ=12560- 7.113T
LFLFLM= 0-10.669T
LFLFLK- 8673- 6.069T

PFPFLC= 5803- 5.314T
PFPFLM= 0-10.669T

*These differences specify the free energy of one phase(i.e. liquid) minus the free energy of the second phase (i.e. sodium chloride) for a given compound.

TABLE 2
SUMMARY OF SOLUTION PHASE PARAMETERS
(All Units in Joules per gram atom (mole of atoms), T in Kelvins)

LZFRF=-70710+29.288T, LZFCF=-75312+29.288T, LZFBF=-10154 ,LPFZF=LZFPF=12552
LRFZF=-31380+29.288T, LCFZF=-33472+29.288T, LBFZF= 18272 ,CPFZF=CZFPF=41840
MZFRF=MRFZF=16736 , MZFCF=MCFZF=16736, MZFBF=MBFZF=41840,MPFZF=MZFPF=41840
SZFRF=SRFZF=16736 , SZFCF=SCFZF=16736, KZFBF=KBFZF=41840,
LZFNF=-54392+29.288T, LZFKF=-75312+29.288T, LZFLF=-11088 ,LRFNF=12552
LNFZF=-29288+29.288T, LKFZF=-33472+29.288T, LLFZF= 22595 ,LNFRF=11.0T
MZFNF=MNFZF=16736 , MZFKF=MKFZF=16736, MZFLF=MLFZF=41840,SRFNF=37656
SZFNF=SNFZF=16736 , SZFKF=SKFZF=16736, JZFLF=JLFZF=41840,SNFRF=40584

LNFBF=12552, LBFNF=16736, SNFBF=SBFNF=KNFBF=KBFNF=41840
LBFLF=LLFBF=21757-6.82T, JBFLF=JLFBF=33137-12.552T, KBFLF=KLFBF=2 5104-12.552T

TABLE 3
SUMMARY OF COMPOUND PARAMETERS FOR BINARY SYSTEMS
(All units in Joules per gram atom (mole of atoms), T in Kelvins)

Compound	Name	Stoichiometry	Base	Compound Parameter	Free Energy of Formation (from stable components)
				C (Joules/g.at)	ΔG_f (Joules/g.at)
(1/7)(ZrF_4·RbF)	X	$ZF_{0.714}{}^{RF}{}_{0.286}$	M	-20669+41.84T	-4234-2.95T
(1/30)(4ZrF_4·5RbF)	R	$ZF_{0.667}{}^{RF}{}_{0.333}$	M	-19644+45.52T	-4142-4.07T
(1/9)(ZrF_4·2RbF)	Q	$ZF_{0.556}{}^{RF}{}_{0.444}$	M	-15297+51.09T	-3661-6.00T
(1/11)(ZrF_4·3RbF)	P	$ZF_{0.455}{}^{RF}{}_{0.545}$	S	-13389+58.58T	-3054-6.67T
(1/7)(ZrF_4·NaF)	X	$ZF_{0.714}{}^{NF}{}_{0.286}$	M	-17575+41.21T	-1251-3.18T
(1/11)(ZrF_4·3NaF)	P	$ZF_{0.455}{}^{NF}{}_{0.545}$	S	-11456+51.09T	-1406-4.82T
(1/7)(ZrF_4· CsF)	X	$ZF_{0.714}{}^{CF}{}_{0.286}$	M	-17322+41.84T	-6293-2.68T
(1/9)(ZrF_4·2CsF)	Q	$ZF_{0.556}{}^{CF}{}_{0.444}$	M	-16928+51.97T	-5012-5.79T
(1/11)(ZrF_4·3CsF)	P	$ZF_{0.455}{}^{CF}{}_{0.545}$	S	-12259+58.58T	-4134-6.67T
(1/7)(ZrF_4 ·KF)	X	$ZF_{0.714}{}^{KF}{}_{0.286}$	M	-19874+41.84T	-4828-3.08T
(1/9)(ZrF_4·2KF)	Q	$ZF_{0.556}{}^{KF}{}_{0.444}$	M	-13974+49.62T	-4289-5.82T
(1/11)(ZrF_4·3KF)	P	$ZF_{0.455}{}^{KF}{}_{0.545}$	S	-14351+58.58T	-3619-6.67T

TABLE 4
COMPARISON OF CALCULATED AND OBSERVED(15) HEATS OF FORMATION OF ZrF_4-NaF LIQUID SOLUTIONS (T=1303°K)

Molar Composition	ΔH_f(Observed)(15) Joules/mol	ΔH_f(Calculated)* Joules/mole	x_{NF}
0.95NaF-0.05ZrF_4	-6485±2510	-7095	0.884
0.90NaF-0.10ZrF_4	-12135±2510	-13570	0.783
0.85NaF-0.15ZrF_4	-17990±2510	-19230	0.694
0.80NaF-0.20ZrF_4	-24895±2510	-23970	0.615
0.75NaF-0.25ZrF_4	-29290±2510	-27780	0.545

x_{NF}	gram atoms / mole	E_H^L (Joules/g.at.) Heat of Mixing of Liquid
0.884	2.15 $ZF_{0.116}{}^{NF}{}_{0.884}$=1.9 NF-0.25ZF	-3300
0.783	2.30 $ZF_{0.217}{}^{NF}{}_{0.783}$=1.8 NF-0.50ZF	-5900
0.694	2.45 $ZF_{0.306}{}^{NF}{}_{0.694}$=1.7 NF-0.75ZF	-7850
0.615	2.60 $ZF_{0.385}{}^{NF}{}_{0.615}$=1.6 NF-1.00ZF	-9220
0.545	2.75 $ZF_{0.455}{}^{NF}{}_{0.545}$=1.5 NF-1.25ZF	-10100

*ΔH_f=(number of gram atoms/mole) times E_H^L

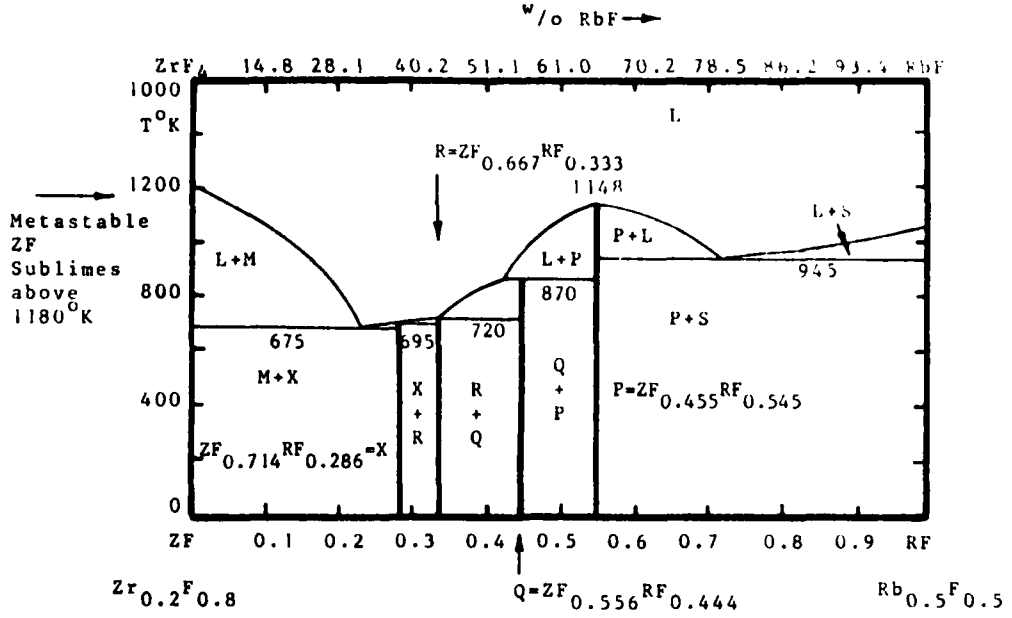

Figure 1. Calculated Zirconium Fluoride - Rubidium Fluoride Phase Diagram

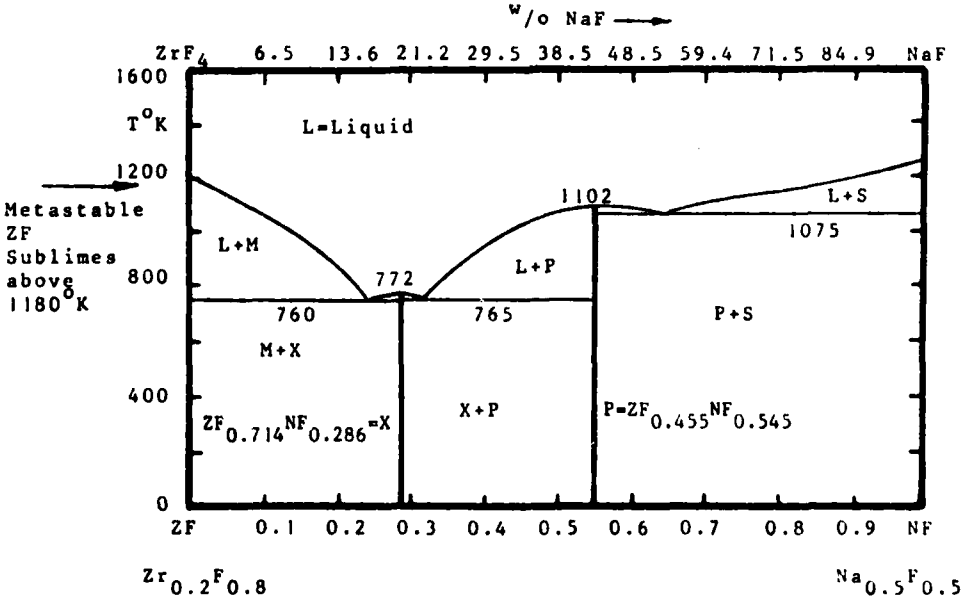

Figure 2. Calculated Zirconium Fluoride - Rubidium Fluoride Phase Diagram

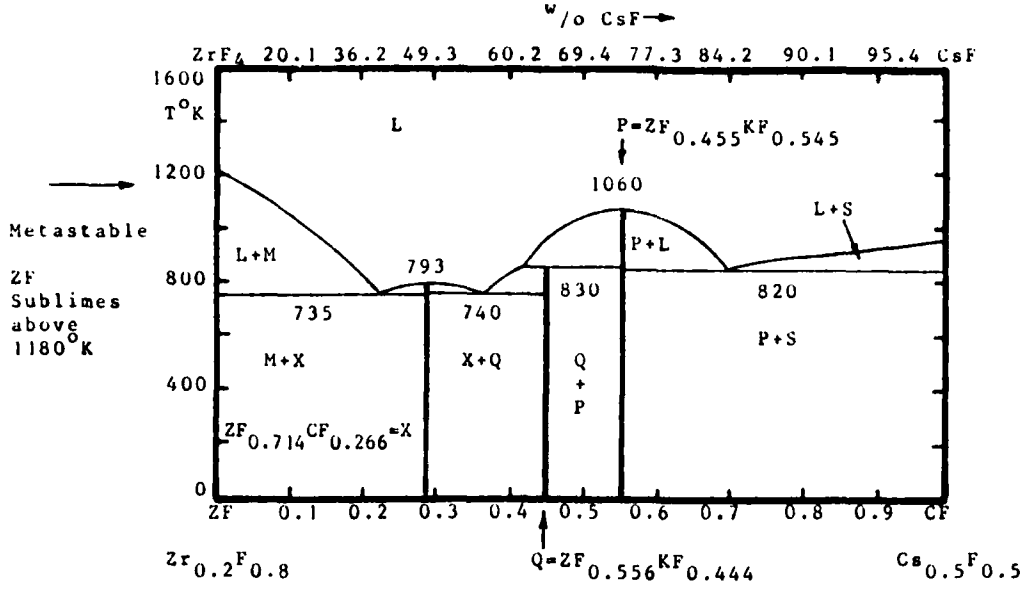

Figure 3. Calculated Zirconium Fluoride-Cesium Fluoride Phase Diagram

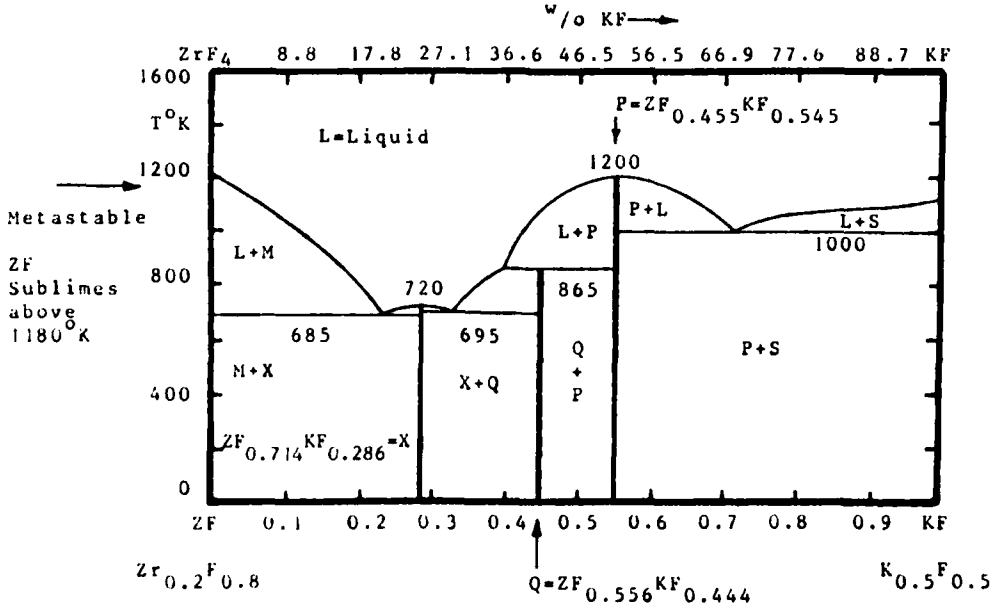

Figure 4. Calculated Zirconium Fluoride - Potassium Fluoride Phase Diagram

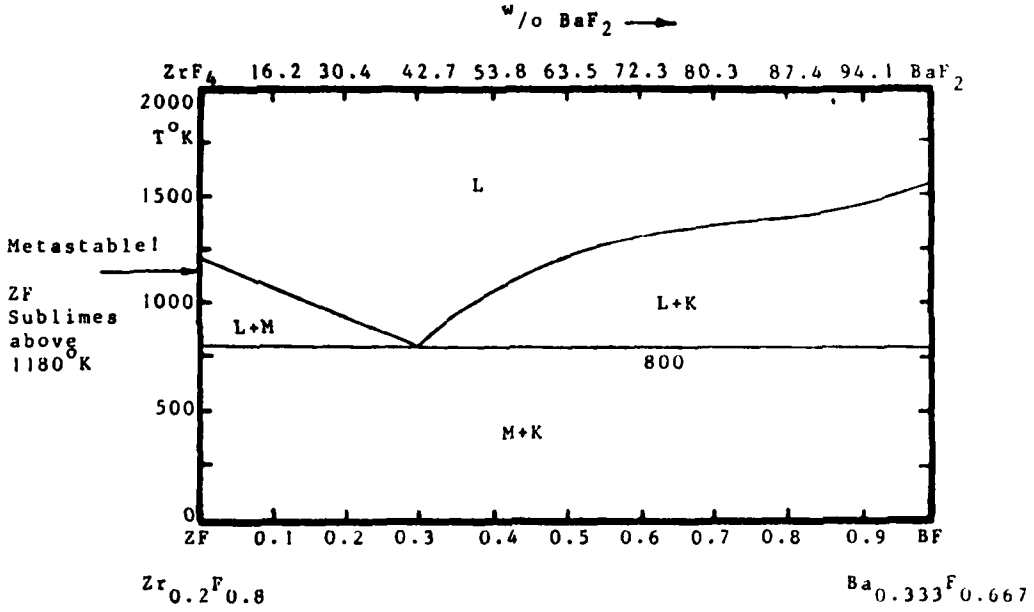

Figure 5. Calculated Zirconium Fluoride - Barium Fluoride Phase Diagram

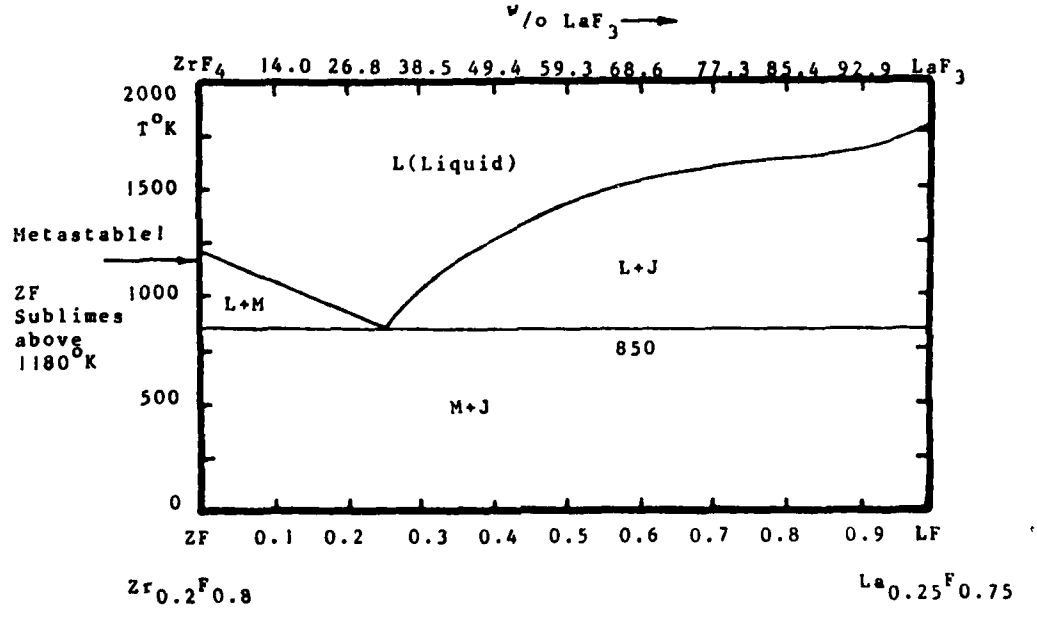

Figure 6. Calculated Zirconium Fluoride - Lanthanum Fluoride Phase Diagram

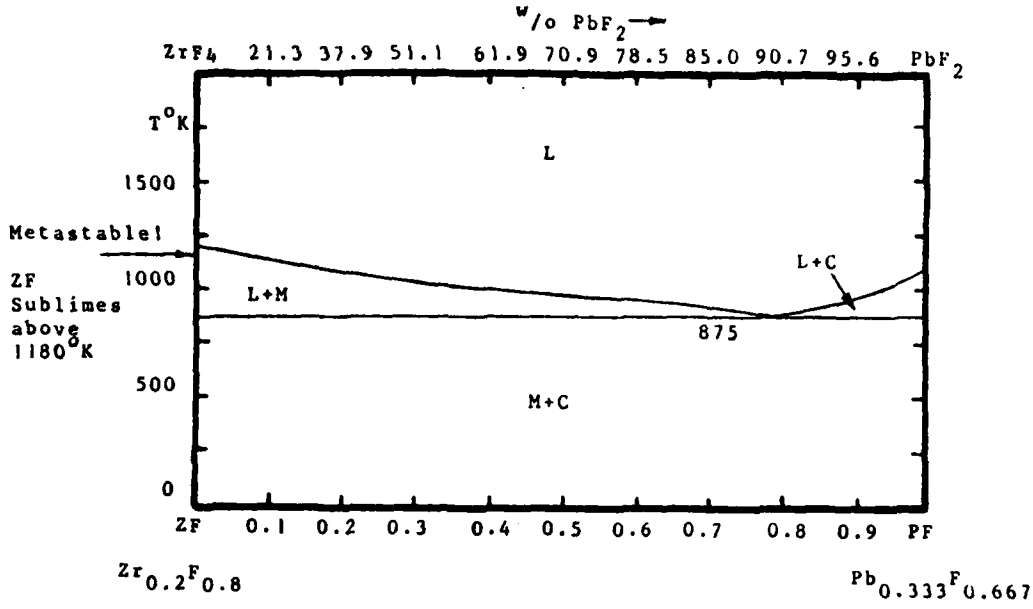

Figure 7. Calculated Zirconium Fluoride-Lead Fluoride Phase Diagram

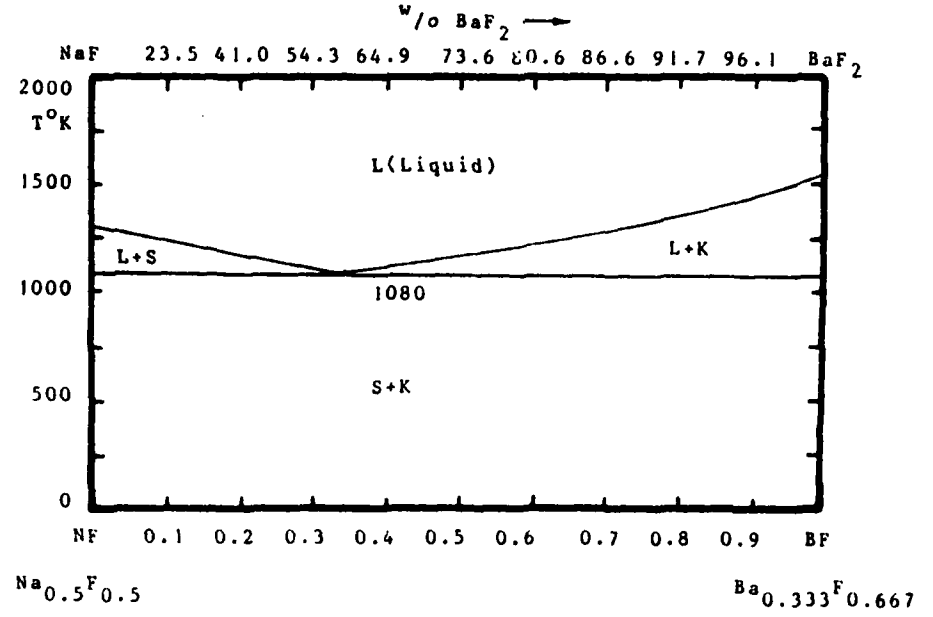

Figure 8. Calculated Sodium Fluoride - Barium Fluoride Phase Diagram

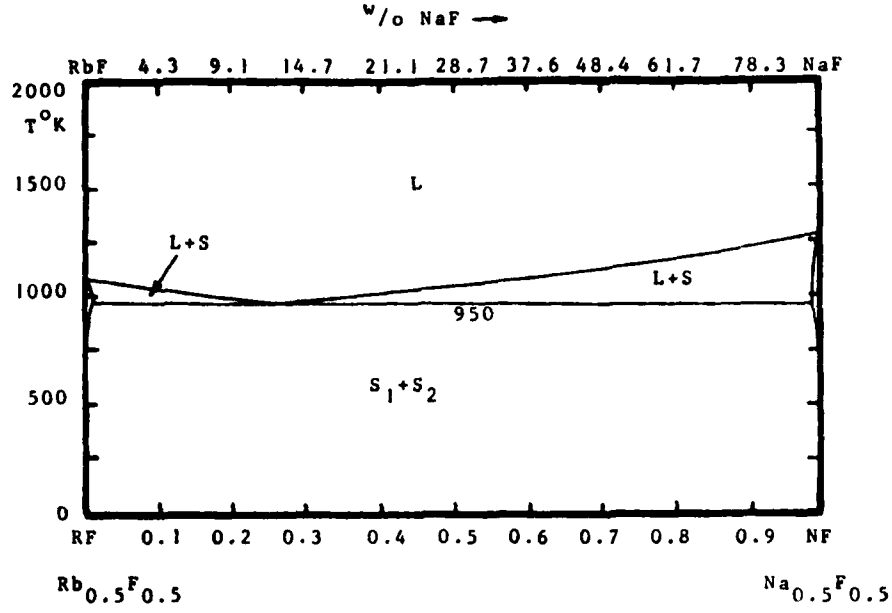

Figure 9. Calculated Rubidium Fluoride - Sodium Fluoride Phase Diagram

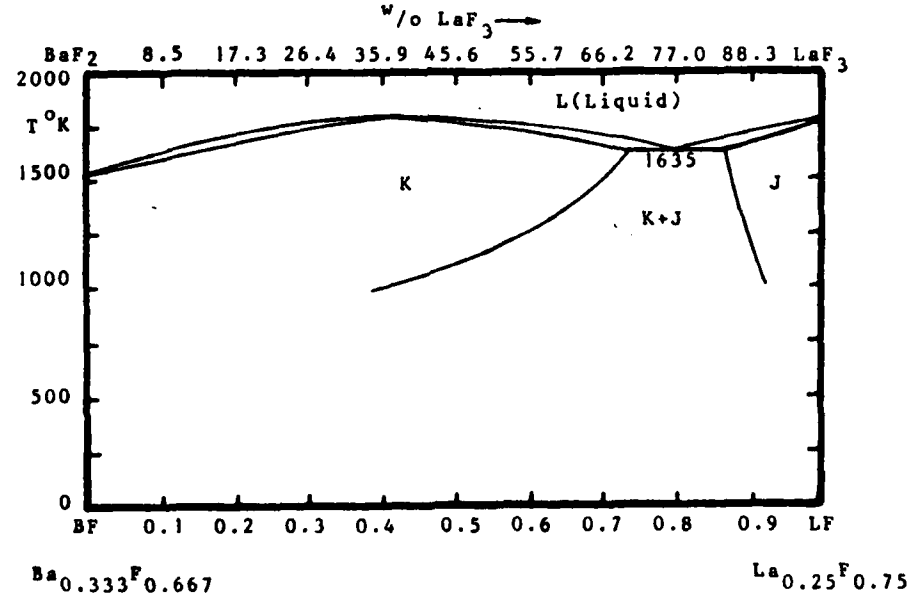

Figure 10. Calculated Barium Fluoride - Lanthanum Fluoride Phase Diagram

$$G^L=(1-x-y)\,{}^oG^L_{LF}+x\,{}^oG^L_{ZF}+y\,{}^oG^L_{BF}+RT[(1-x-y)\ell n(1-x-y)+x\ell nx+y\ell ny]$$

$$+(1-x-y)x(1-y)^{-1}[(1-x-y)LLFZF+xLZFLF]+xy(x+y)^{-1}[xLZFBF+yLBFZF]$$

$$+(1-x-y)y(1-x)^{-1}[(1-x-y)LLFBF+yLBFLF] \quad J/g.at \qquad (7)$$

All of the solution parameters required to specify Equation (7) are given in Table 2. The remaining solution phases in the ternary system i.e. S,M,J,K etc. are defined in similar fashion. Such definition permits calculation of the LF-ZF-BF ternary shown in Figure 11. The liquidus boundaries calculated between 1473K and 773K define the compositions of maximum liquid stability. Reference to Figure 11 shows that these results agree well with the glass forming range established by Lecoq and Poulain (5).

In order to consider a case like BF-ZF-NF in Figure 12 where compound phases (like X and P) are present the usual definition (1) is employed in order to define the free energy of the compound phase $NF_{0.545}{}^{ZF}{}_{0.455}$ in the ternary system BF-ZF-NF where x is the fraction of ZF, y is the fraction of BF and z is the fraction of NF. In this case the free energy of P is

$$G^P = z\,{}^oG^S_{NF}+x\,{}^oG^S_{ZF}+y\,{}^oG^S_{BF}+(1-(y/(1-x)))\Delta G_A+(y/(1-x))\Delta G_B$$

$$+RT(y\ell ny+z\ell nz-(1-x)\ell n(1-x)) \qquad J/g.at. \qquad (8)$$

Comparison of Equations (8) and (3) show that with the compound running from the stable $NF_{0.545}{}^{ZF}{}_{0.455}$ to the unstable $BF_{0.545}{}^{ZF}{}_{0.455}$, x=0.455 and z is equal to 0.545-y where y runs from zero to 0.545. Thus

$$\Delta G_A=(0.545)(0.455)[0.545LNFZF+0.455LZFNF+11456-51.09T] \quad J/g.at \qquad (9)$$

The free energy of the unstable compound $BF_{0.545}{}^{ZF}{}_{0.455}$ was defined by Equation 10 as

$$\Delta G_B=(0.545)(0.455)[0.545LBFZF+0.455LZFBF-30543] \quad J/g.at. \qquad (10)$$

in order to complete the calculation of the liquidus contours to define the range of liquid stability in Figure 12.

These results illustrate how the development of a data base for fluoride systems can be employed to usefully predict the most appropriate compositions to investigate in the search for zirconium fluoride base glasses. Needless to say the method has even greater value for multi-component systems containing more than three compounds.

4. References

1. L. Kaufman, F. Hayes and D. Birnie CALPHAD 5 163 (1981).
2. L. Kaufman, J. Nell, K. Taylor and F. Hayes CALPHAD 5 185 (1981).
3. L. Kaufman and H. Nesor, Titanium Science and Technology R.I. Jaffee and H. Burte Editors, Plenum Press, New York 2 773 (1973).
4. L. Tanner and R. Ray, Scientific American 233 15 (1975).
5. A. Lecoq and M. Poulain, J. Non-Crystalline Solids 34 101 (1979).
6. M. Poulain, M. Poulain, and J. Lucas, Rev. de Chem. Mineral 16 267 (1979).
7. J. Lumsden, Thermodynamics of Molten Salt Mixtures Academic Press, London (1966).
8. O. Kubaschewski and C.B. Alcock, Metallurgical Thermochemistry, Pergamon Press, Oxford (Fifth Edition)(1979).
9. JANAF Thermochemical Tables, Dow Chemical Co., Midland, Michigan.
10. R.E. Thoma, Advances in Molten Salt Chemistry, J. Braunstein, G. Manatov and G.P. Smith, eds. Plenum Press, N.Y. (1975) p. 302.
11. E. Levin, C.R. Robbins, and H. McMurdie, Phase Diagrams for Ceramists, American Ceramics Society, Columbus, Ohio (1964).
12. Ibid., First Supplement (1969).
13. E. Levin and H. McMurdie, Second Supplement (1975).
14. R.S. Roth, T. Negas and L.P. Cook, Ibid., Third Supplement (1981).
15. A. Fontana and R. Winand, J. Nuclear Materials 44 305 (1972).

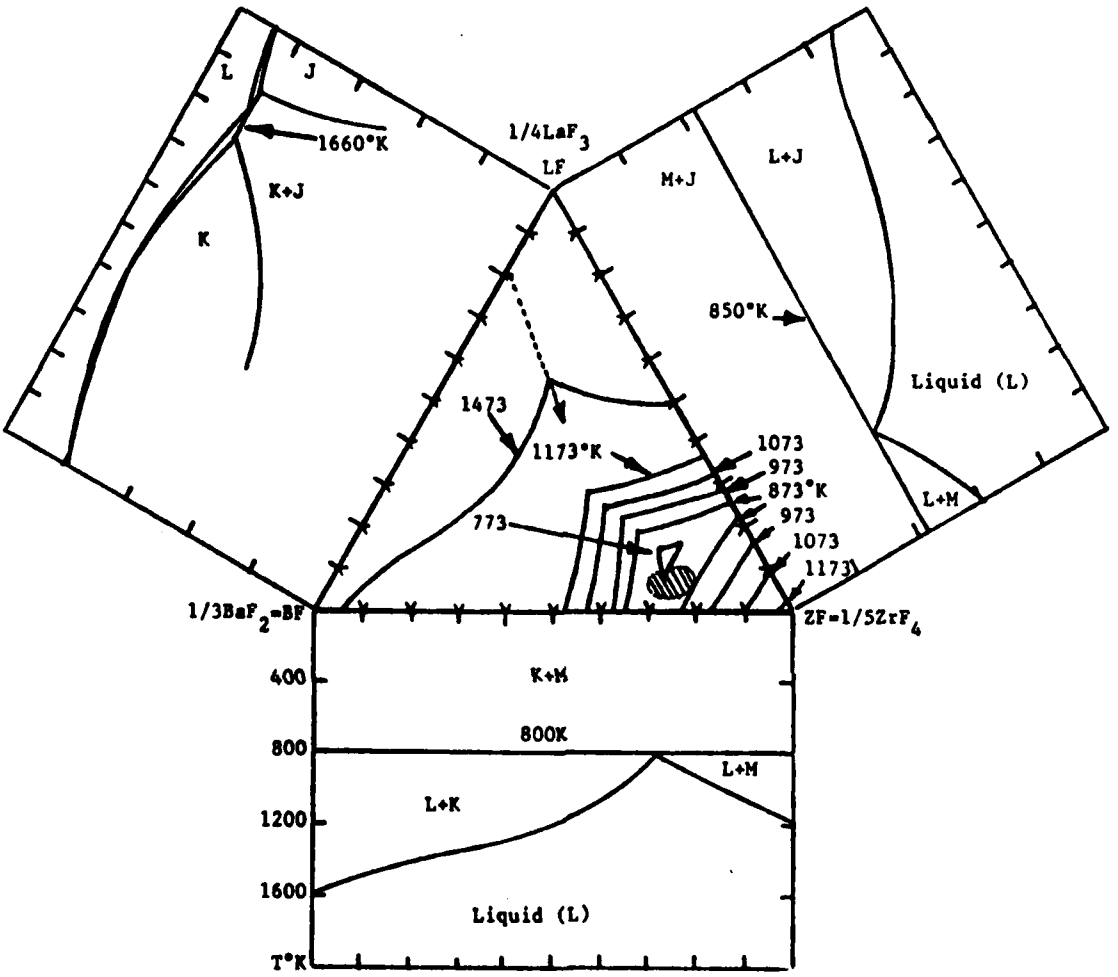

Figure 11. Calculated Edge Binary Systems and Liquidus Projections in the LF-ZF-BF System. The hatched region in the ternary denotes the glass forming composition range established experimentally by Lecoq and Poulaine (5).

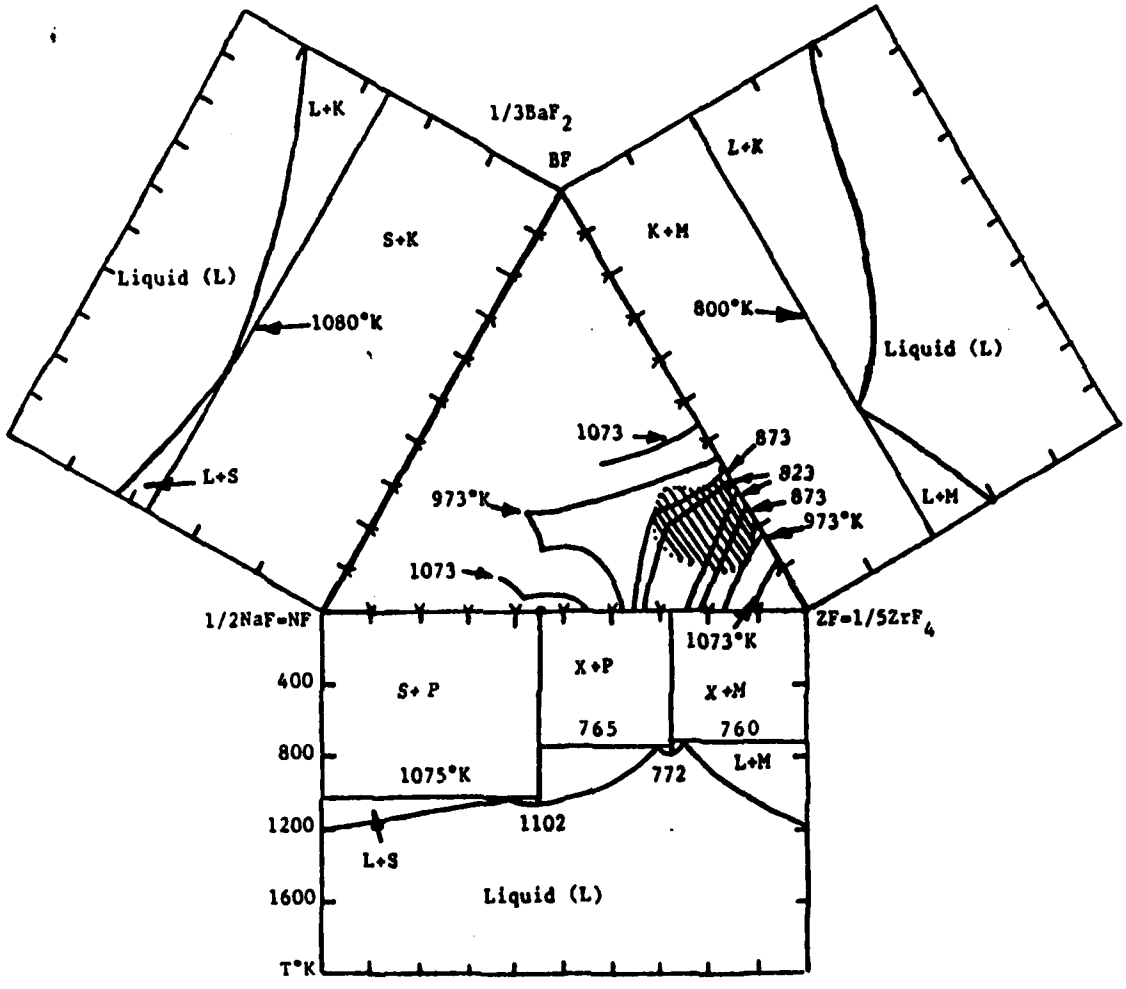

Figure 12. Calculated Edge Binary Systems and Liquidus Projections in the BF-ZF-NF System. The hatched region in the ternary denotes the glass forming composition range established experimentally by M. Poulain, M. Poulain and J. Lucas (6).

VI CALCULATION OF ORDERING TEMPERATURES FOR THE QUASI-BINARY SECTION Fe_3Al-Fe_3Si

1. Introduction

Where limited experimental data is available, the method adopted by Inden (1-7) is attractive because it requires only two ordering parameters for each of the three component binary systems, provided the temperatures of interest are above any magnetic transition temperatures. Those ordering parameters are the first and second nearest neighbor (chemical) interaction parameters denoted $W^{(1)}$ and $W^{(2)}$. These can be related to heats of formation as well as critical ordering temperatures, as will be shown in the following section. The Fe-Si binary system (Fig. 1) has already been characterized in some detail (3,4) and the previously determined values of $W^{(1)}_{Fe\text{-}Si}$ and $W^{(2)}_{Fe\text{-}Si}$ have been used unaltered in the present work Table I). Their validity has been confirmed by the successful prediction of ordering equilibria in ternary Fe-Si-Co alloys (8). The Fe-Al system is inherently more complicated (9,10) (Fig. 2) and several additional effects have been recently added by Köster et al (11). Nonetheless the major features have been reproduced by the simplified Inden model(12). Only a minor change has been made in the value of $W^{(1)}_{Fe\text{-}Al}$ used previously by Inden (6) in the light of the available experimental data for Fe-Si-Al alloys (Table II). The derivation of suitable values of suitable $W^{(1)}_{Si\text{-}Al}$ and $W^{(2)}_{Si\text{-}Al}$ values poses a problem in so far that all experimentally accessible properties for these alloys refer to either FCC Aluminum or diamond cubic Silicon. One has therefore to extract the relevant values of $W^{(1)}_{Si\text{-}Al}$ and $W^{(2)}_{Si\text{-}Al}$ from whatever data is available for BCC ternary alloys.

2. Experimental Information on Fe-Al-Si Alloys

Lihl, Burger, Sturm and Ebel (14) have given a general indication of the location of the ordering region in Fe-Al-Si alloys (Fig. 3). However there is considerable divergence between this estimate and the investigation of Katsnel'son and Polishchuk (13). More weight has been given to the latter work as it utilized relative intensities of superlattice lines (Fig. 4) whereas the work by Ebel et al merely interpreted changes in d-spacing as ordering effects. An NMR study of $Fe_3Si_{(1-x)}Al_x$ alloys (15) suggests that Aluminum and Silicon substitute interchangeably on one specific sublattice, which confirms that the interaction energy between Silicon and Aluminum is relatively low.

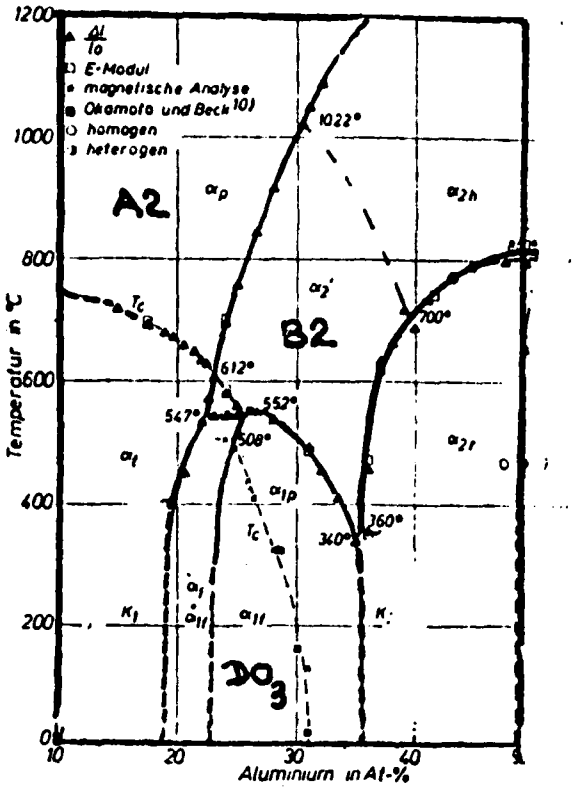

Fig. 1 Iron-Aluminum Diagram

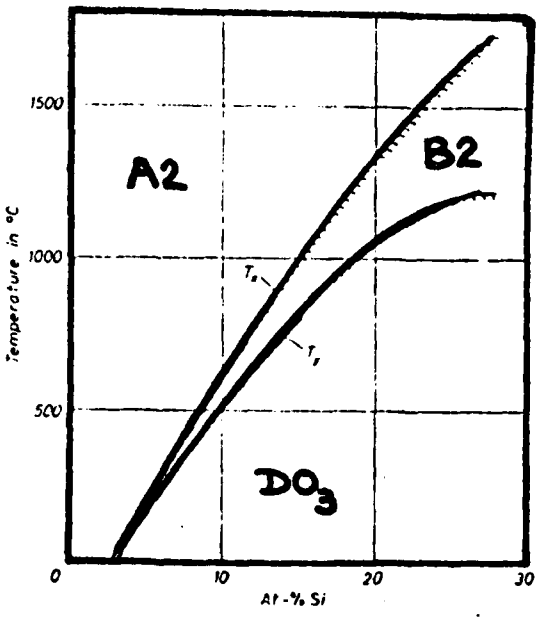

Fig. 1. Configuration diagram of bcc, paramagnetic iron-silicon solid solutions

Fig. 2 Iron-Silicon Diagram

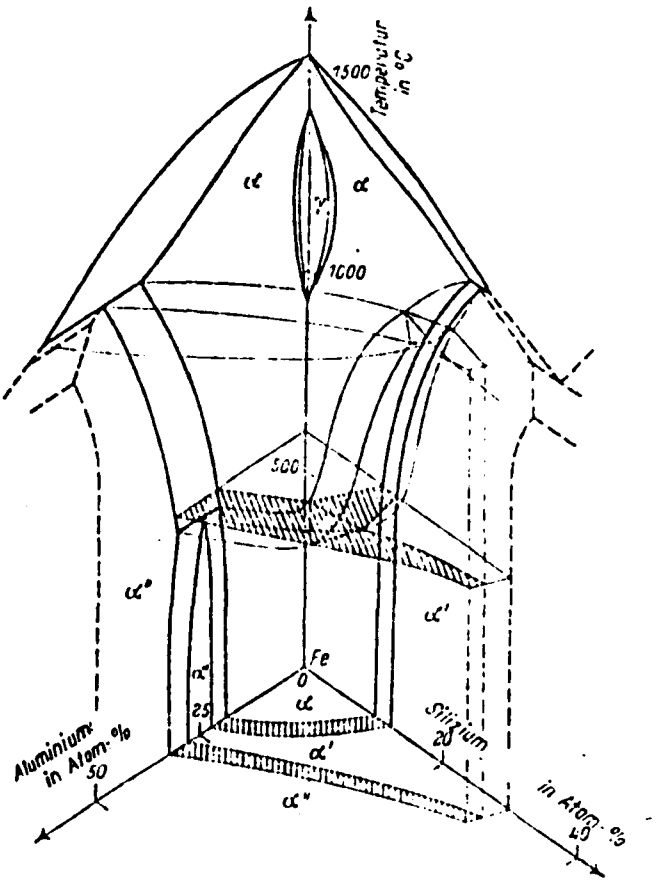

Fig. 3 Suggested Ternary Phase Boundaries for Fe-Al-Si alloys from F. Lihl et al (14)

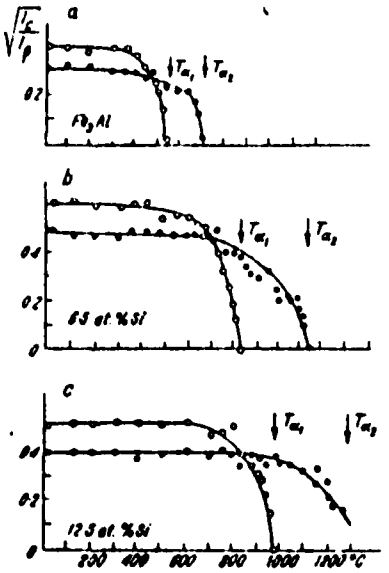

Fig. 4 Critical Temperatures suggested by the temperature dependence of superstructure lines from Katsnel'son (13)

3. Ordering Model

(a) Definition of order parameters

The main feature of the BWG model is the description of atomic distributions inside specifically defined sublattices. The choice follows from the kind of interaction between atoms. Any BCC lattice may be divided into four FCC sublattices, I, II, III, and IV, with the atomic configurations described by occupation probabilities 'p_i^L' of sublattice site 'L' by the component 'i'. (Fig. 5)

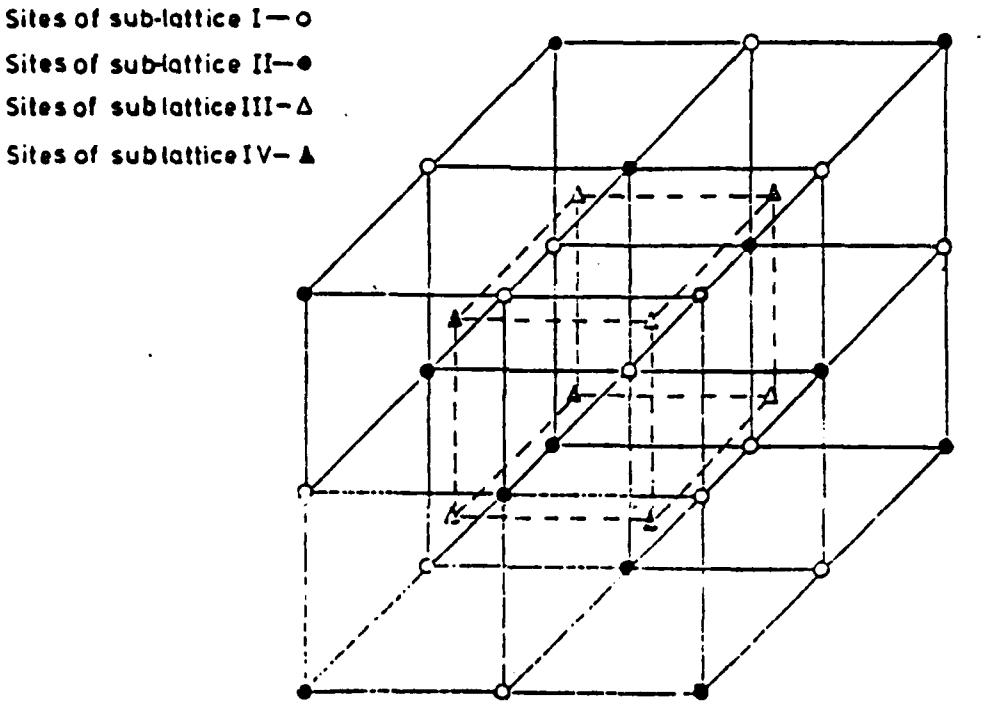

Fig. 5 Relative position of sublattices in the DO_3 structure.

The atomic configuration in a binary alloy A_CB_{1-C} can then be described with the aid of the following three parameters, which are a combination of the independent occupation probabiliti p_i^L.

$$x = \frac{1}{4}\left(p_A^{I} + p_A^{II} - p_A^{III} - p_A^{IV}\right) \qquad (1a)$$

$$y = \frac{1}{2}\left(p_A^{III} - p_A^{IV}\right) \qquad (1b)$$

$$z = \frac{1}{2}\left(p_A^{I} - p_A^{II}\right) \qquad (1c)$$

The greatest value of these parameters corresponds to the highest degree of order, and the concentrations of A and B, (C_A and C_B) set limits on the values of x, y and z. For the binary case these are given by:

(a) $0 \leq x \leq C_B$ for $0 \leq C_B \leq 0.5$ (2a)

(b) $0 \leq y \leq \min (C_A - x, C_B + x)$ (2b)

(c) $0 \leq z \leq \min (C_A + x, C_B - x)$ (2c)

Case 1

The random BCC lattice (A2) has an equal distribution of the atoms on the four sublattices and corresponds to $x = y = z = 0$.

Case 2

The state $x \neq 0$, $y = z = 0$ indicates 'A' preferentially occupying sublattices I and II ($x > 0$), or III and IV ($x < 0$). It follows that the number of AB neighbors in nearest neighbor (n.n) positions is increased, i.e. this corresponds to the B2 structure.

Case 3

It follows that $y \neq 0$, describes a surplus of A atoms in next nearest neighbor (n.n.n) positions, which corresponds to the DO_3 structure. As far as the present problem is concerned we need not consider z. (See Refs. 1,2)

(b) Free Energy Expressions and Interaction Parameters

The most stable atomic configuration then follows from the minimum value of the configurational free energy/mole ΔG^{BCC} which is given by:

$$\Delta G^{BCC}_{BINARY} = U^o - NC_AC_B\,(4W^{(1)} + 3W^{(2)}) - \frac{N}{2}\left[(8\,W^{(1)} - 6W^{(2)})\,x^2 + 3W^{(2)}\,(y^2 + z^2)\right] + \frac{NkT}{4}\sum_L \left[p_A{}^L \ln p_A{}^L + p_B{}^L \ln p_B{}^L\right] \quad (3)$$

U^o is the internal energy of pure components; the second term is the energy of mixing; the third term gives the energy contribution due to ordering, and the fourth term is the entropy contribution of the configuration which is also expressed in terms of x, y, z. N is Avagadro' number, and k the Boltzmann constant. $W^{(1)}$ and $W^{(2)}$ are defined below and for eqn (3) to be valid, these must be expressed in k units where 1 k unit = 3.3×10^{-24} cal or 13.8×10^{-24} J. The values of $W^{(1)}$ and $W^{(2)}$ are related to the nearest and next nearest neighbor bond energies $V_{ij}{}^{(k)}$ as follows:

$$W^{(1)} = -2V_{AB}{}^{(1)} + V_{AA}{}^{(1)} + V_{BB}{}^{(1)} \quad (4a)$$

$$W^{(2)} = -2V_{AB}{}^{(2)} + V_{AA}{}^{(2)} + V_{BB}{}^{(2)} \quad (4b)$$

According to this definition, positive values for $W^{(1)}$ and $W^{(2)}$ correspond to greater affinity between unlike atoms. All interchange energies are presumed to be independent of temperature and of environment of other atom sites where the interchange process is considered

If the values of $W^{(1)}$ and $W^{(2)}$ are known, ΔG^{BCC} can be calculated with respect to the ordering parameters x, y, z using the necessary equilibrium conditions including particularly:

$$\frac{\partial G}{\partial x} = \frac{\partial G}{\partial y} = \frac{\partial G}{\partial z} = 0 \; ; \quad (T, C) \qquad (5)$$

and other subsidiary conditions.

(c) Expressions for critical ordering temperatures in binary alloys

The critical temperatures $T_x(A2/B2)$, $T_y(B2/DO_3)$, define the regions in which minimum free energy is obtained by the A2, B2 and DO_3 configurations respectively. For the binary case these are given by:

$$kT_x = kT^{A2/B2}_{(BWG)} = (8W^{(1)}_{BWG} - 6W^{(2)}_{BWG}) \cdot C_A C_B \qquad (6a)$$

$$kT_y = kT^{B2/DO_3}_{(BWG)} = 6W^{(2)}_{BWG} \cdot (C_A - x)\,(C_B + x) \qquad (6b)$$

where x is the appropriate value of the ordering coefficient at the temperature T_y.

Since $W^{(K)}$ are energy parameters, they are most easily determined from energy measurements like enthalpies of mixing of random alloys, or enthalpies of formation ΔH (C,T) of alloys with given atomic configurations. These entities can immediately be expressed by means of $W^{(K)}$ for a binary alloy $A_{1-C}B_C$ with reference to the pure components in the same crystal structure as the alloy formed. For BCC alloys:

$$\Delta H^{A2} = -N\,C(1-C)\left[4W^{(1)} + 3W^{(2)}\right] \qquad \ldots\ (7)$$

$$\Delta H^{B2} = -N\left[C(4W^{(1)} + 3W^{(2)}) - 6C^2\,W^{(2)}\right] \quad \text{for } C < 0.5$$

$$\Delta H^{DO_3} = -N\,C\,(4W^{(1)} + 3W^{(2)}) \quad \text{for } 0 < C < 0.25$$

$$\text{OR} \quad = -N\left[1.5W^{(2)} + C(4W^{(1)} - 3W^{(2)})\right] \quad \text{for } 0.25 < C < 0.5$$

$$\Delta H^{B32} = -N\left[C\,(4W^{(1)} + 3W^{(2)}) - 4C^2\,W^{(1)}\right] \quad \text{for } C < 0.5$$

$W^{(K)}_{BWG}$ values obtained from an analysis of critical temperatures (e.g. via equations 6a, 6b), can be related to the $W^{(K)}$ values in thermochemical equations (e.g. equ. 7) by a scale factor x (listed in Table I). See References (182). (The differences between $W^{(K)}$ and $W^{(K)}_{BWG}$ are essentially due to the omission of short range order in the BWG model.)

4. Expressions for the Free Energy and critical ordering temperature in ternary alloys as used in the present work

In the ternary case there is a slight difference in the definition of the order parameters (5). If the total number of atoms is N, distributed over $4N_o$ lattice sites, the occupation probabilities p_i^L ($i = A,B,C,$; $L = I, II, III, IV$) are combined to give the order parameters as follows:

$$(a)\quad x_j = \tfrac{1}{4}\left(p_j^{I} + p_j^{II} - p_j^{III} - p_j^{IV}\right) \qquad (8a)$$

$$(b)\quad y_j = \tfrac{1}{4}\left(p_j^{III} - p_j^{IV}\right) \qquad (8b)$$

$$(c)\quad z_j = \tfrac{1}{4}\left(p_j^{I} - p_j^{III}\right) \qquad (8c)$$

with $j = A, B$

A similar condition to Equation (5) occurs except now there are two x parameters, two y parameters and two z parameters, corresponding to the degree of order of two solutes and not just one. For the purpose of determining T_x and T_y temperatures it is only necessary to consider x_A and x_B. The limiting values of x_A, x_B in the ternary case are:

(a) The maximum value of x_A is the smaller of a or (1-a). (9a)

(b) The maximum value of x_B is the smaller of b or $(c - x_A)$ (9b)

In the specific case of $Fe_3Al_{(1-x)}Si_x$ alloys, where a = Fe, b = Al and c = Si, this leads to a situation where (a) is always 0.75 and therefore $x_{A(max)} = 0.25$. Likewise since $c = (1-a-b)$, $x_{B(max)} = -b$. The configurational free energy/mole ΔG of the three-component solid solution is then given by:

$$\begin{aligned}\Delta G^{(BCC)} = U_o - N\Big\{ & 4\left(C_AC_BW^{(1)}_{AB} + C_AC_CW^{(1)}_{AC} + C_BC_CW^{(1)}_{BC}\right) \\ & + 3\left(C_AC_BW^{(2)}_{AB} + C_AC_CW^{(2)}_{AC} + C_BC_CW^{(2)}_{BC}\right)\Big\} \\ & - \frac{N}{2}\Big\{ E^R_{AC}\,x_A^2 + E^R_{BC}\,x_B^2 + \left(E^R_{AC} + E^R_{BC} - E^R_{AB}\right) x_A\,x_B \\ & + 3W^{(2)}_{AC}\left(y_A^2 + z_A^2\right) + 3W^{(2)}_{BC}\left(y_B^2 + z_B^2\right) + 3\left(W^{(2)}_{AC} + W^{(2)}_{BC} \right. \\ & \left. - W^{(2)}_{AB}\right)\left(y_Ay_B + z_Az_B\right)\Big\} - \frac{NkT}{4}\sum_i\sum_L p_i^{(L)} \ln p_i^{(L)}\end{aligned} \qquad \ldots (10)$$

where $E^R_{ij} = \left(8\,W^{(1)}_{ij} - 6W^{(2)}_{ij}\right)$

$$k\,T_x^{BWG}(A2/B2) = 0.5\left\{\sum_{ij} C_iC_jE_{ij} + \sqrt{\left(\sum_{ij} C_iC_jE_{ij}\right)^2 - 4C_AC_BC_C\,(E_{AC}E_{BC}) \cdots}\right.$$

$$\left. \cdots - \tfrac{1}{4}\left[E_{AC} + E_{BC} - E_{AB}\right]^2\right)\Big\} \qquad \ldots (11)$$

where $ij = AB, AC, BC$ and $E_{ij} = \left\{8W^{(1)}_{ij} - 6W^{(2)}_{ij}\right\}_{BWG}$

$$k\,T_y^{BWG}(B2/L2_1) = 3\left\{\Omega + \sqrt{\Omega^2 - 4W^{(2)}_{AC}\,W^{(2)}_{BC} - \left[W^{(2)}_{AC} + W^{(2)}_{BC} \cdots\right.\right.}$$

$$\left.\left. \cdots - W^{(2)}_{AB}\right]^2\right\}_{BWG}(C_A - x_A)\,(C_B - x_B)\,(C_C + x_A + x_B)\Big\} \quad \ldots (12)$$

where $\Omega = (W^{(2)}_{AC})_{BWG}\,(C_B + C_C + x_A)\,(C_A - x_A)$

$$+ (W^{(2)}_{BC})_{BWG}\,(C_A + C_C + x_B)\,(C_B - x_B)$$

$$- \left[W^{(2)}_{AC} + W^{(2)}_{BC} - W^{(2)}_{AB}\right]_{BWG}(C_B - x_B)\,(C_A - x_A);$$

and x_A and x_B are the values of the order parameter in nearest neighbour positions at $T = T_y$.

5. Calculation of T_x and T_y for the Fe-Al-Si System

The following procedure was adopted to obtain optimum values of $W^{(1)}$ and $W^{(2)}$ (BCC Al-Si). Examination of various pairs of solutes shows that for BCC alloys $W^{(2)}/W^{(1)}=0.5$, as is indeed the case for the other pairs concerned in the present case (Table I). It was therefore assumed that $W^{(2)}/W^{(1)}$ BCC (Al-Si) = 0.5. Inspection of the superlattice intensities Fig. (5) show that a considerable degree of order exists in the B2 lattice prior to DO_3 formation; the maximum theoretical values of x_A and x_B can therefore be used in preliminary calculations.

Trial values of $W^{(1)}_{Al\text{-}Si}$(BCC) were then inserted into equations until a reasonable fit was obtained for both T_x and T_y for a selected alloy composition.

As shown in (Fig. 6) there is a limit beyond which further changes in $W^{(1)}$(and $W^{(2)}$] are counterproductive, which reflects the assumption that the real values of x_A and x_B are lower than the maximum values assumed in this preliminary calculation. Varying x_A and x_B in an iterative fashion can then be used to establish more realistic values of x_A and x_B as shown in (Table III). This result can be cross-checked for other trial compositions and a pattern established for the variation of x_A and x_B with composition. This appears to be a very simple variation, with x_A constant at 0.18 (compared to the initially assumed maximum value of 0.25), and x_B equal to a constant fraction of C_{Al} (the constant being the ratio $(x_A/x_A(max))$ or 0.72). These values of $W^{(1)}$, $W^{(2)}$, x_A and x_B when inserted into equations (11 & 12) yield the results shown in (Table IV), and a more direct comparison with experimental results is given in (Table V), and (Fig. 7).

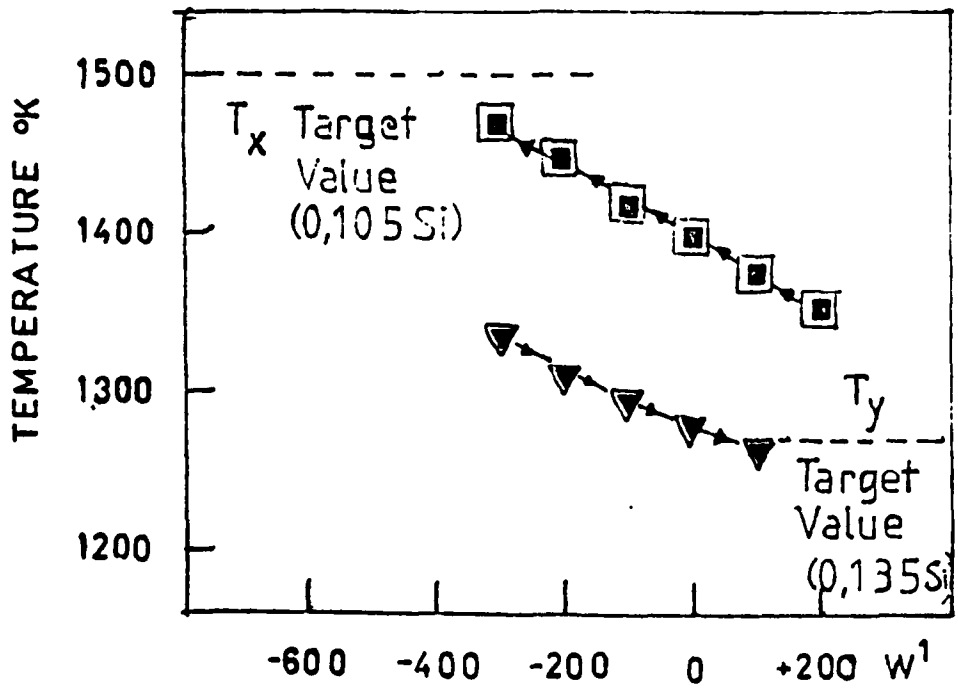

Trial Values of $W^{(1)}$ Al-Si

Fig. 6 Effect of varying $W^{(1)}$ Al-Si on calculated T_x and T_y temperatures using the assumption of full A2/B2 ordering at T_y.

6. Discussion

The degree of agreement obtained is very satisfactory, and further calculations in this system based on these interaction parameters should yield equally reliable results. There is some indication that the equilibrium values of x_A and x_B for the binary alloys Fe_3Al and Fe_3Si are in fact slightly higher than would be indicated by the simplifying assumptions just outlined (see Table II). Whether it is necessary to calculate equilibrium values of x_A and x_B vigorously for every composition instead of using the simplifying formula depends on the accuracy with which the ordering temperatures need to be known and also to some extent on the cooling rates required to attain equilibrium under practical conditions. Table VI gives some idea of the effect of small variations in ordering parameters. Additionally, the values of T_x and T_y shown in (Fig. 7) refer to the so-called constitutive phase boundaries and, analogous to the T_o lines of more common phase diagram calculations, assume no two phase regions exist. To establish the full phase diagram a more complex minimization program must be utilized (1, 2, 8) which is rather lengthy but requires no further new input data. It should also be noted that all calculations have been made on the basis that the temperatures of interest are above the magnetic transition temperatures in the system; if it is intended to investigate ordering below the Curie Temperature, additional terms have to be introduced into equations (10-12). In either circumstance the quoted values of $W^{(1)}$ and $W^{(2)}$ can be used to derive heats of formation for solid Al-Si BCC alloys which can be used to refine the calculation of the liquidus and solidus line in these systems, (17,18).

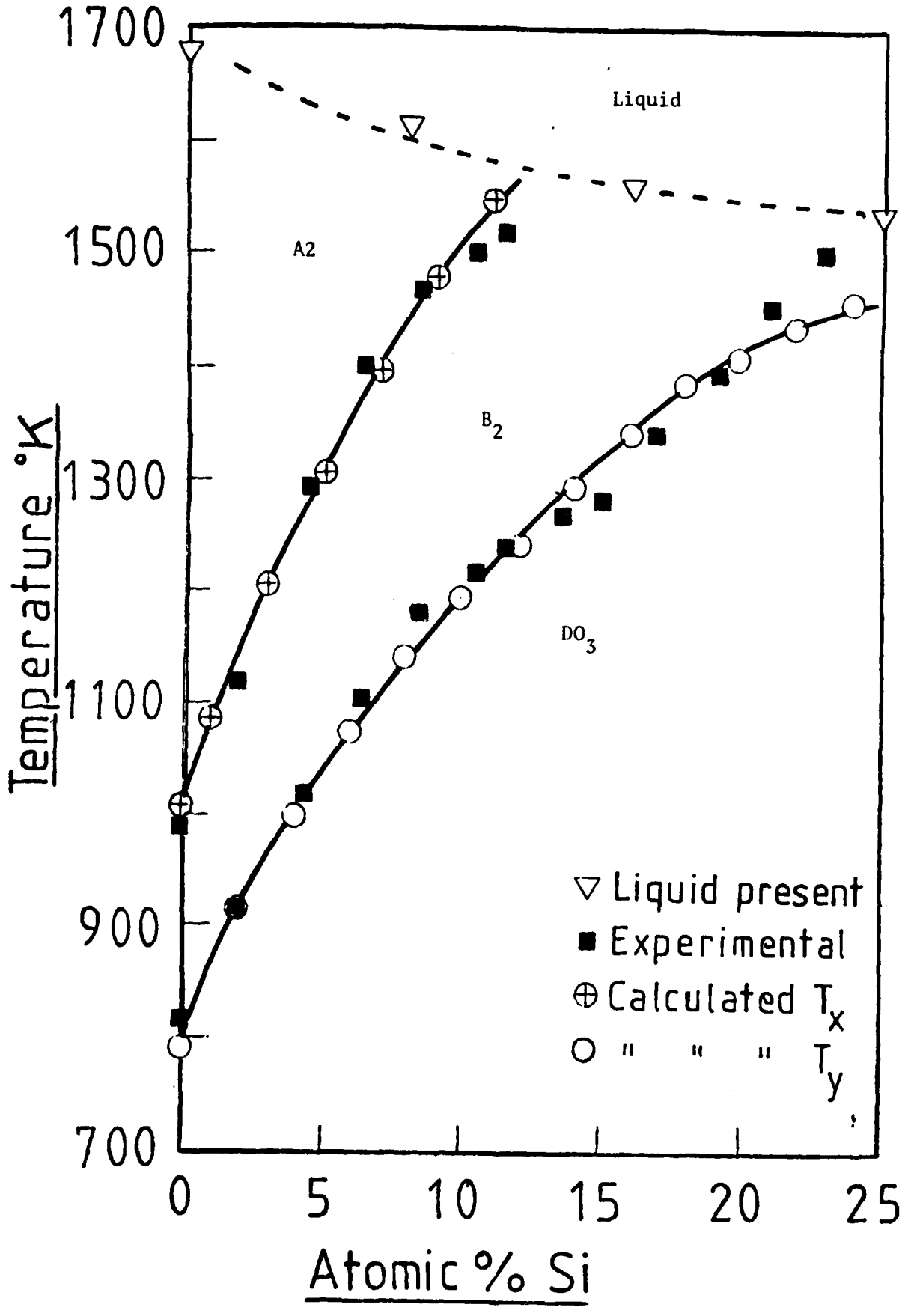

Fig. 7 Comparison of calculated and experimental ordering temperatures in the section Fe_3Al-Fe_3Si

TABLE I

OPTIMIZED VALUES OF W_1 AND W_2 (k units)

X	SYSTEM	W	INDEN (6)	KATSNEL'SON (13)	USED IN THIS WORK	RATIO W_2/W_1
.68	FeAl	W_1	1005	1090 1063	1080	
	FeAl	W_2	539	583 547		
		(W_2/W_1)	0.54	0.52		0.50
	Al-Si	W_1			-480	
	Al-Si	W_2			-250	
		(W_2/W_1)				0.52
.71	Fe-Si	W_1	2010	-	2010	
	Fe-Si	W_2	1000	1067	1000	
		(W_2/W_1)	0.50	1000		0.50

TABLE II

DERIVATION OF A2/B2 ORDERING PARAMETERS FOR Fe_3Al

SHOWING THE EFFECT OF CHANGING $W^{(1)}$(Fe-Al)

$W^{(1)} = 1080$ $W^{(2)} = 540$ $T_x = 1012K$

x_A	T_y	$(\delta \Delta G/\delta x_A)$
.17	789	-326
.18	794	-227
.19	798	-95
.20	801	+80
.21	804	+321
.22	807	+665

$W^{(1)} = 1005$ $W^{(2)} = 540$ calc $T_x = 900K$

x_A	T_y	$(\delta \Delta G/\delta x_A)$
.15	777	-93
.16	783	-15
.17	789	+81
.18	794	+204
.19	798	+360
.20	801	+560

TABLE III

TYPICAL TRIAL CALCULATION OF ORDER PARAMETERS AND T_y FOR A TERNARY ALLOY CONTAINING 75Fe, 13.5Al and 11.5Si

x_A	x_B	T_y	$\Delta G/\alpha x$	$\delta\Delta G/\delta x$
+.169	-.080	1243	+42	-41
+.171	-.081	1244	+25	-23
+.171	-.081	1244	+39	+13
+.172	-.081	1245	- 4	-41
+.172	-.082	1245	+ 8	- 4
+.173	-.082	1245	+21	+32
+.173	-.082	1246	-23	-23

Input Energy Parameters BWG Values in K Units

1005*, 540, -480, -250, 2010, 1000

Calculated T_x = 1516

* Note $W^{(1)}$ FeAl here is not the value finally adopted (1080)

TABLE IV

CALCULATED VALUES OF T_x AND T_y (°K)

Si%	T_x	Si%	T_y	(x_B)
.25	1890			
		.24	1458	-.007
.23	1855			
		.22	1433	-.022
.21	1816			
		.20	1403	-.036
.19	1773			
		.18	1370	-.050
.17	1724			
		.16	1334	-.065
.15	1671			
		.14	1293	-.079
.13	1613			
		.12	1247	-.094
.11	1548			
		.10	1196	-.108
.09	1477			
		.08	1139	-.123
.07	1397			
		.06	1074	-.137
.05	1307			
		.04	998	-.151
.03	1204			
		.02	908	-.166
.01	1083			
		0	794	-.180

W^1_{FeAl} 1080 W^1_{AlSi} - 480 W^1_{FeSi} 2010 x_A = .18 (at T_y)

W^2_{FeAl} 540 W^2_{FeAl} - 250 W^2_{FeAl} 1000 $x_B = C_B(-0.72)$

TABLE V

COMPARISON OF CALCULATED AND EXPERIMENTAL VALUES

Si(at%)	T_y(OK)		T_x(OK)	
	Exptl	Calcd	Exptl	Calcd
0.23%	1500	1446	-	1855
0.21	1450	1418	-	1816
0.195	1390	1392	-	1773
0.17	1340	1353	-	1724
0.15	1280	1314	-	1671
0.135	1270	1282	-	1613
0.115	1240	1235	1520	1565
0.105	1220	1259	1500	1531
0.085	1180	1154	1470	1458
0.065	1100	1091	1400	1376
0.045	102L	1018	1290	1283
0.02	910	908	1120	1147
0	820	794	980	1012

$x_A = .18 \qquad x_B = -.72x\ C_B$

(Calculated value for T_x Fe_3Si is 1890°K)

TABLE VI

(a) The Effect of Arbitrarily Reducing the Order Parameters on the Calculated T_y Temperature for Fe75, Al 13.5, Si 11.5

x_A	x_B	calc T_y (°K)
.25	-.135	1264
.125	-.065	1182
.08	-.04	1115
.04	-.02	1035

(b) The Effect of varying the order parameters within the limits found for other compositions

x_A	x_B	calc T_y (°K)
.175	-.082	1245
.18	-.097	1235
.16	-.11	1181
.19	-.13	1202
.18	-.12	1201

7. References

1. G. Inden, Z. Metallk, 66 577 (1975)
2. G. Inden, Z. Metallk. 63 253 (1972)
3. G. Schlatte, G. Inden, W. Pitsch, Z. Metallk 65 94 (1974)
4. G. Inden, Z. Metallk. 68 529 (1977)
5. G. Inden, Thesis Techniche Hochschule Aachen (1970)
6. G. Inden, J. de Physique (C7) 38 373 (1977)
7. G. Inden, Physica 103B 82 (1981)
8. W. Meyer & G. Inden Phys. Stat. Solidi (a) 56 481 (1979) (see also ibid 177)
9. P.R. Swann, W.R. Duff, R.M. Fisher Trans. Met Soc AIME 245 851 (1975).
10. S.M. Allen, J.W. Cahn, Acta Met 24 425 (1975)
11. W. Köster, T. Gödecke, Z. Metallk. 71 (12) 765 (1980)
12. G. Inden, Private Communication (1981)
13. A.A. Katsnel'son, V.Ye Polishchuk, Phys. Met. Metallog. 36 86 (1973) or (Fiz. Met. Metallog. 36 (2) 321)
14. F. Lihl, R. Burger, F. Sturn, H. Ebel, Arch. Eisenhutten W. 39 877 (1968)
15. V. Niculescu, K. Raj, T. Burch, J.I. Budnick, J. Phys, F. 7 (3) L73 (1977)
16. L. Chandrasekaran, Ph.D. Thesis, Univ. of Surrey (1980)
17. L. Kaufman, H. Nesor, CALPHAD 2 (4) 332 (1978)
18. P. Dörner, E.T. Henig, H. Krieg, H.L. Lukas, G. Petzow, CALPHAD 4 (4) 241 (1980)

VII A SIMPLIFIED TREATMENT OF THE THERMODYNAMICS OF THE ORDER-DISORDER REACTIONS IN THE Fe-Al, Fe-Al-Mn and Fe-Al-Ni Systems

The Gibbs energy difference between ordered and disordered bcc phase in the Fe - Al system is presented as an explicit expression of composition. A power series expansion based on the shape of the Cp-curve is used. The thermodynamics of the Fe - Al phase diagram is evaluated and the diagram is calculated with the new model for the bcc phase. The Fe - Al - Mn and Fe - Al - Ni ternaries are calculated applying a subregular approximation of the new series-expansion. The deviations from previous calculations where no distinction between ordered and disordered bcc was made, are found to be very small.

1. Introduction

It is well known that different types of ordering (i.e. magnetic or chemical) contribute considerably to the thermodynamic properties of a solid solution. Consequently the corresponding phase diagram might be strongly affected by the occurance of ordering. Inden (1) has presented extensive theoretical analyses of the order/disorder reactions in binary alloys. In a disordered, random solution the Bragg-Williams approximation and different regular solution models yield the Gibbs energy as a simple algebraic function of the composition of the solution. In a partially ordered phase the simple models also predict a dependence of the degree of order on composition and temperature. The most stable state of ordering for a certain composition and temperature is then the one that yields the lowest Gibbs energy. Thus it is not possible to write the Gibbs energy simply as an explicit function of the composition. In many applications it is desirable to express the Gibbs energy as a explicit function of composition. Inden (2) has presented a method where the ordering contribution to Gibbs energy is expanded in a power series of the temperature. The coefficients are functions of composition and adjusted to fulfill certain criteria. In the present work a slightly different method will be applied to the Fe-Al system. The method is based on the work by Inden (3) and has recently been applied to the magnetic ordering in alloys (4). The purpose of the present work is to show how the order/disorder reactions can be incorporated in a Calphad framework without an undue increase in complexity.

2. The Model

The integral molar Gibbs energy, G_m, of a phase can be separated into two parts.

$$G_m = G_m^{dis} + (G_m - G_m^{dis}) \tag{1}$$

The first term G_m^{dis} is the Gibbs energy for the completely disordered state and is obtained from a regular solution type of model, i.e. --

$$G_m^{dis} = X_{Fe}\,{}^{o}G_{Fe} + X_{Al}\,{}^{o}G_{Al} + RT\left(X_{Fe}\ln X_{Fe} + X_{Al}\ln X_{Al}\right) + X_{Fe}X_{Al}\,L_{FeAl} \tag{2}$$

where L_{FeAl} is a constant for a regular solution and exhibits a linear concentration dependency in the subregular case. ${}^{o}G_{Fe}$ and ${}^{o}G_{Al}$ are the Gibbs energies for the pure elements for the structure considered.

The second term will now be evaluated by a method which has been applied to the magnetic ordering in bcc-Fe (4,5,6), and is a modification of a method initially proposed by Inden(3). Inden found that the following expressions gave an adequate description of the contribution from order/disorder reactions to the specific heat c_p,

$$\Delta c_p^{\alpha} = k^{\alpha} R \ln \frac{(1+\tau^3)}{(1-\tau^3)} \qquad \tau < 1 \tag{3a}$$

$$\Delta c_p^{\beta} = k^{\beta} R \ln \frac{(\tau^5+1)}{(\tau^5-1)} \qquad \tau > 1 \tag{3b}$$

where $\tau = T/T_C$, T_C being the critical temperature where all long range order vanishes. The superscripts α and β denote the states with long range order and short range order respectively, and, k^{α} and k^{β} are constants. By applying the first three terms in the Mc Laurin series expansion of Eq. 3, and integrating from $T = \infty$, where $G^{\beta} = G^{dis}$, to obtain the corresponding enthalpy and entropy, we can write down the expression for the Gibbs energy. It is convenient to express k^{β} and k^{α} in terms of the enthalpy difference between the ordered and the completely disordered state at 0 K, because this quantity is easy to obtain by counting the number of different bonds. By introducing f as the fraction of total enthalpy that is absorbed above T_C (i.e., f=0 when there is no short range ordering above T_C and the total enthalpy is then due to long range ordering only). We obtain:

$$-RT_C\,k^{\beta} = \frac{140}{79}\; f\; \Delta H_{T=0}^{dis \rightarrow ord} \tag{4a}$$

$$-RT_C\,k^{\alpha} = \frac{120}{71}\; (1-f)\; \Delta H_{T=0}^{dis \rightarrow ord} \tag{4b}$$

Inden (7) suggests that f=0.4 should be used for bcc-phases in general. By inserting Eq. 4 in our expression for $G_m - G_m^{dis}$ and setting f=0.4 we obtain:

$$G_m - G_m^{dis} = \Delta H_{T=0}^{dis \rightarrow ord} \; I(\tau) \tag{5}$$

where

$$I(\tau) = \begin{cases} 0.7089 \left(\tau^{-4}/_{10} + \tau^{-14}/_{315} + \tau^{-24}/_{600}\right) & \tau > 1 \quad (6a) \\ 1 - 1.1046\tau + 1.0141 \left(\tau^{4}/_{6} + \tau^{10}/_{135} + \tau^{16}/_{600}\right) & \tau < 1 \quad (6b) \end{cases}$$

For B2 ordering Inden obtained 7a and 7b by counting the number of different bonds;

$$\Delta H_{T=0}^{dis \rightarrow ord} = \begin{cases} -RX_{Al}^2 \; (4W^1 - 3W^2) & 0 < X_{Al} \leq 0.5 \quad (7a) \\ -R(1-X_{Al})^2 (4W^1 - 3W^2) & 0.5 \leq X_{Al} < 1 \quad (7b) \end{cases}$$

and the Bragg-Williams approximation yields;

$$T_C = X_{Al}(1-X_{Al}) \; (8W^1 - 6W^2) \tag{8}$$

W^1 and W^2 are the so called"exchange energies"(expressed in k-units) for the nearest and next nearest neighbours. The Bragg-Williams approximation does not account for short range order and consequently it predicts a critical temperature T_C which is too high. Inden found that one could introduce a correction factor κ to the value calculated by means of Eq. 8 and obtain good agreement with calculations based on the cluster-variation method which do account for short range order.

3. Application to the Fe-Al Phase Diagram

For Fe-Al Inden (2) reports W^1=1478 and W^2=794 (k-units, k=13.8.10^{-24} J/atom) and κ=0.68. By applying these values it is possible to calculate the critical temperatures for B2 and DO_3 ordering. This was done by Miodownik (8) who also made a comparison with experimental information and

found the calculated temperatures too low. To obtain agreement with the experimental temperatures at X_{Al}=0.25 he chose W^1=1588 but kept the other values unchanged. A further investigation reveals that there are still large discrepancies when $X_{Al}<0.25$ or $X_{Al}>0.25$. To obtain a better agreement over the whole composition range W^1 and W^2 must be allowed to vary with composition. This can be done with a reasonable increase in effort and good agreement with the low-temeprature data is then obtained. However, it is found that this procedure overestimates the stability of the bcc-phase relative to the liquid at high Al-content ($X_{Al}\gtrsim 0.4$) where no information on the critical temperatures is available. To overcome this problem it is necessary also to introduce temperature-dependencies in W^1 and W^2. It is a substantial increase in complexity to evaluate both a concentration and temperature dependency and it was thus decided to accept Miodownik's parameters to avoid these difficulties.

Eqs. 5-10 completely determine the term $G_m-G_m^{dis}$ in Eq. 1. The remaining thermodynamic quantities are now to be determined to comply with the available information.

Kaufman and Nesor (9) analyzed the Fe-Al phase diagram without distinguishing between the ordered and disordered bcc-phase. The present analysis follows their evaluation except that the ordering has been accounted for. The total Gibbs energy of the bcc-phase was obtained by adding the ordering contribution given by Eq. 5 to the Gibbs energy of the disordered solution given by Eq. 2. It was then necessary to adjust all parameters given by Kaufman and Nesor and the new parameters are summarized in Appendix A.

4. Calculated Quantities

The recalculated phase-diagram is shown in Figs. 1-3. Fig. 2 shows a magnified view of the compound equilibria and Figs. 3a and 3b show the equilibria with the fcc-phase. In Figs. 4a and 4b comparisons are made with thermochemical data from Hultgren (10) the calculations according to Kaufman and Nesor (9) and the present analysis. While the agreement between the enthalpy of formation as reported by the different sources is satisfactory, there are larger discrepancies for the excess free energy of Al. However, the experimental scatter was large in the latter quantity and the new values fall within the error limits given by Hultgren.

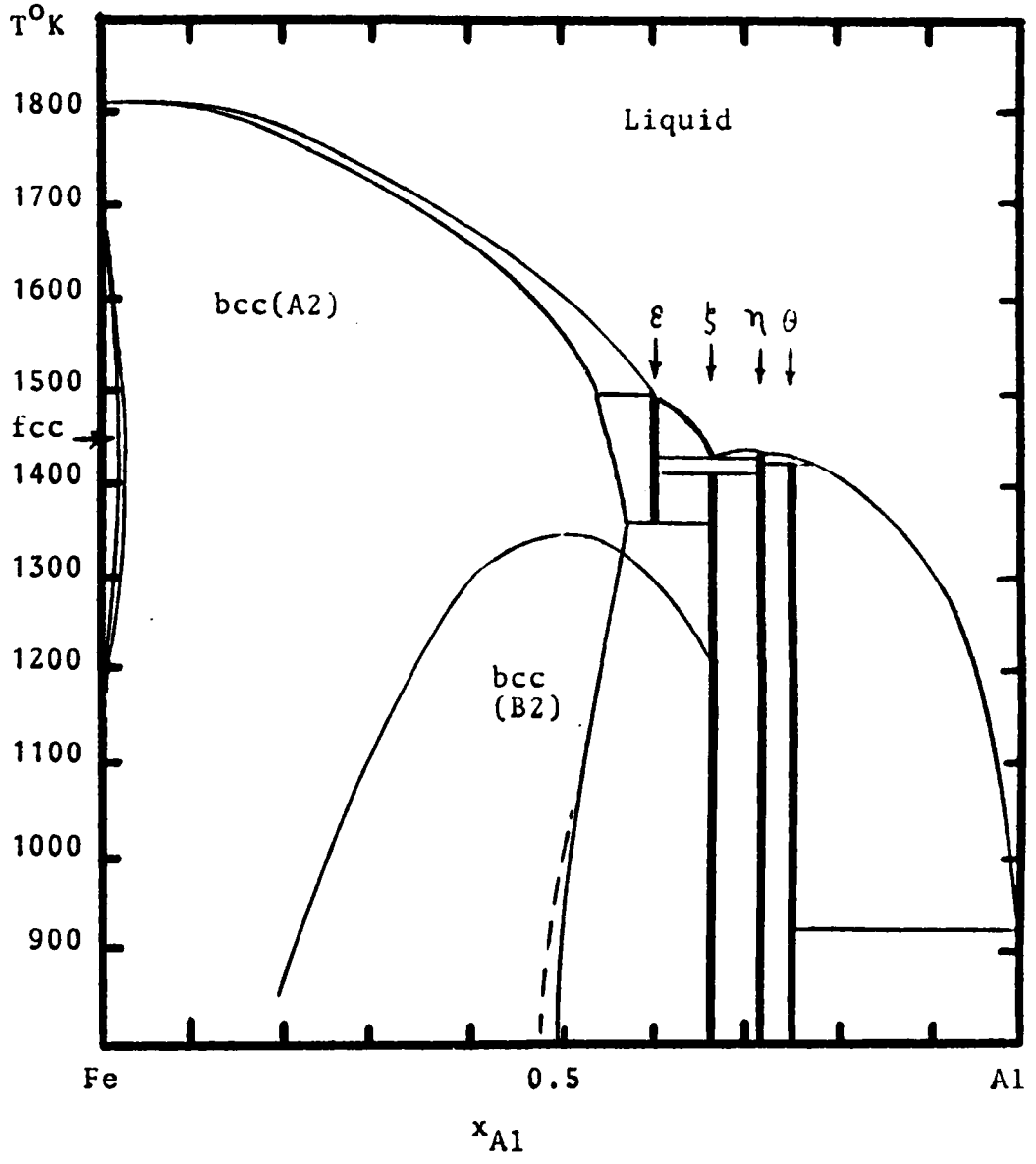

Figure 1. Calculated Iron-Aluminum Phase Diagram (see Figure 3a for the fcc/bcc detailed equilibria)

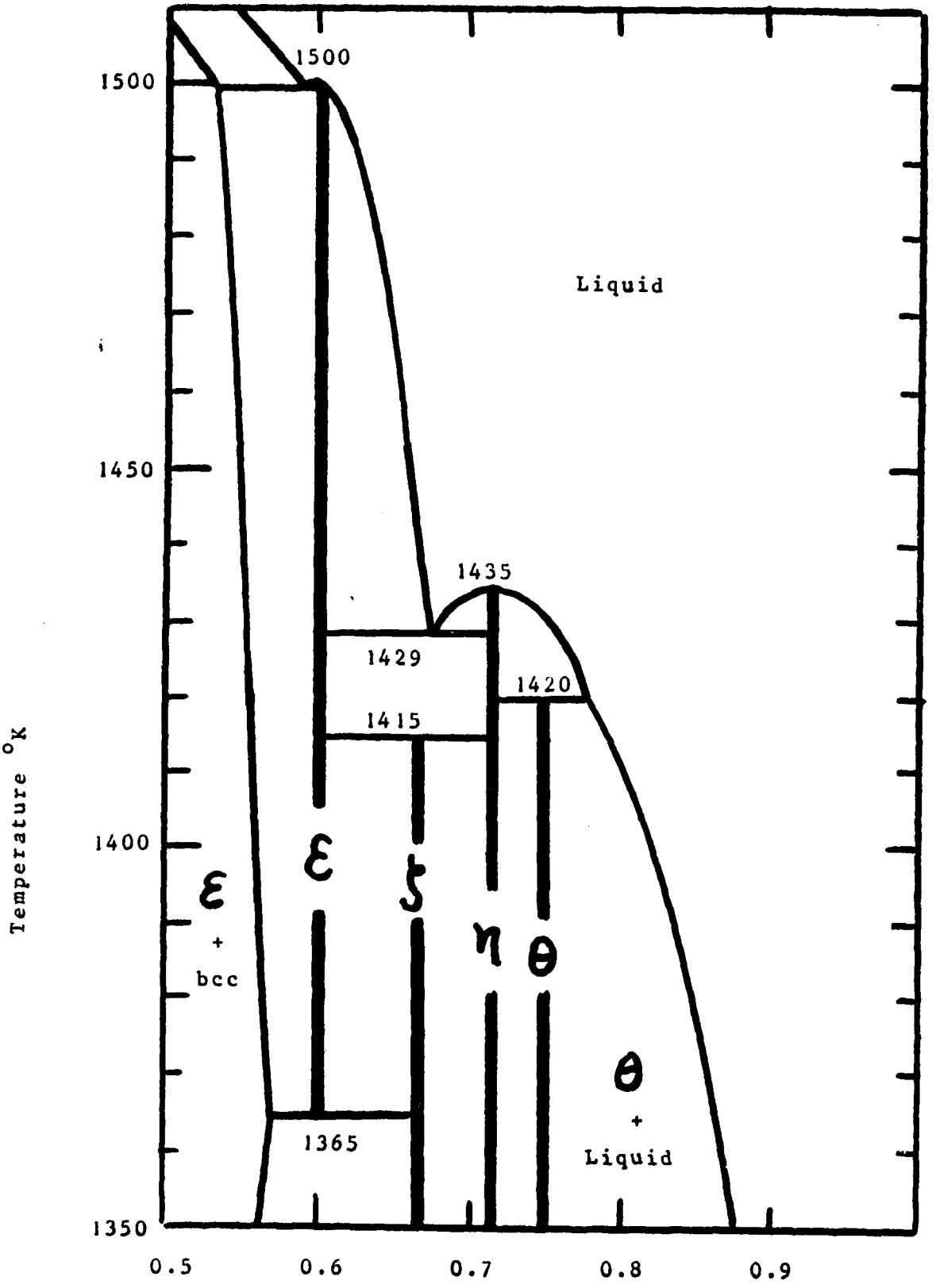

Figure 2. Calculated Compound Equilibria in the Iron-Aluminum System

AD-A136 085 COMPUTER-BASED METHODS FOR THERMODYNAMIC ANALYSIS OF MATERIALS PROCESSING(U) MANLABS INC CAMBRIDGE MASS L KAUFMAN 30 NOV 83 AFOSR-TR-83-1099 F49620-80-C-0020 2/2

UNCLASSIFIED F/G 9/2 NL

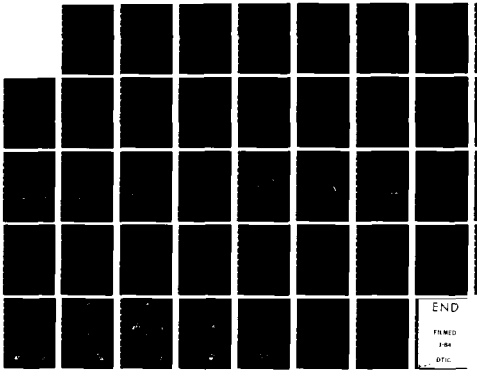

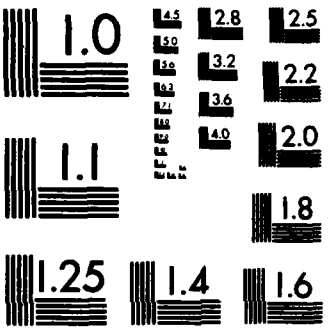

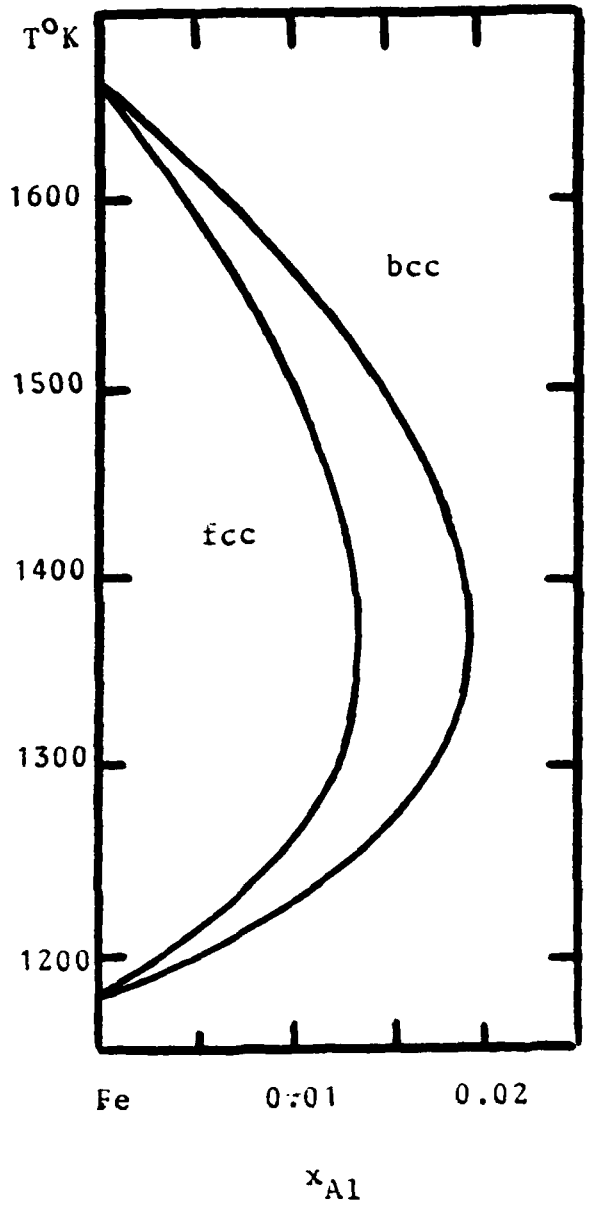

Figure 3a. Calculated bcc/fcc Equilibria in the Iron-Aluminum System.

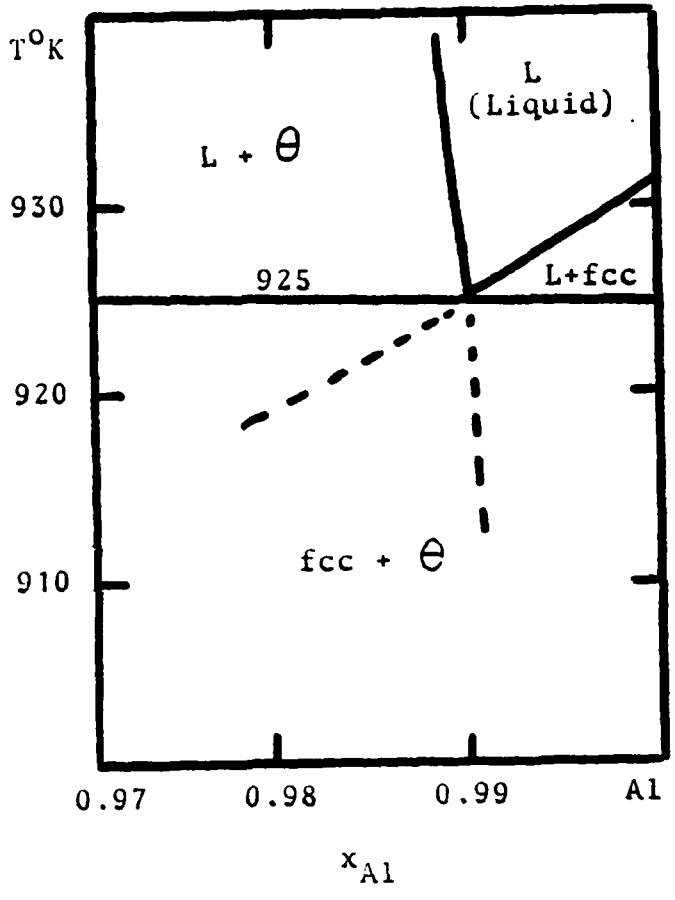

Figure 3b. Calculated Equilibria in the Aluminum-Rich Part of the Iron-Aluminum System.

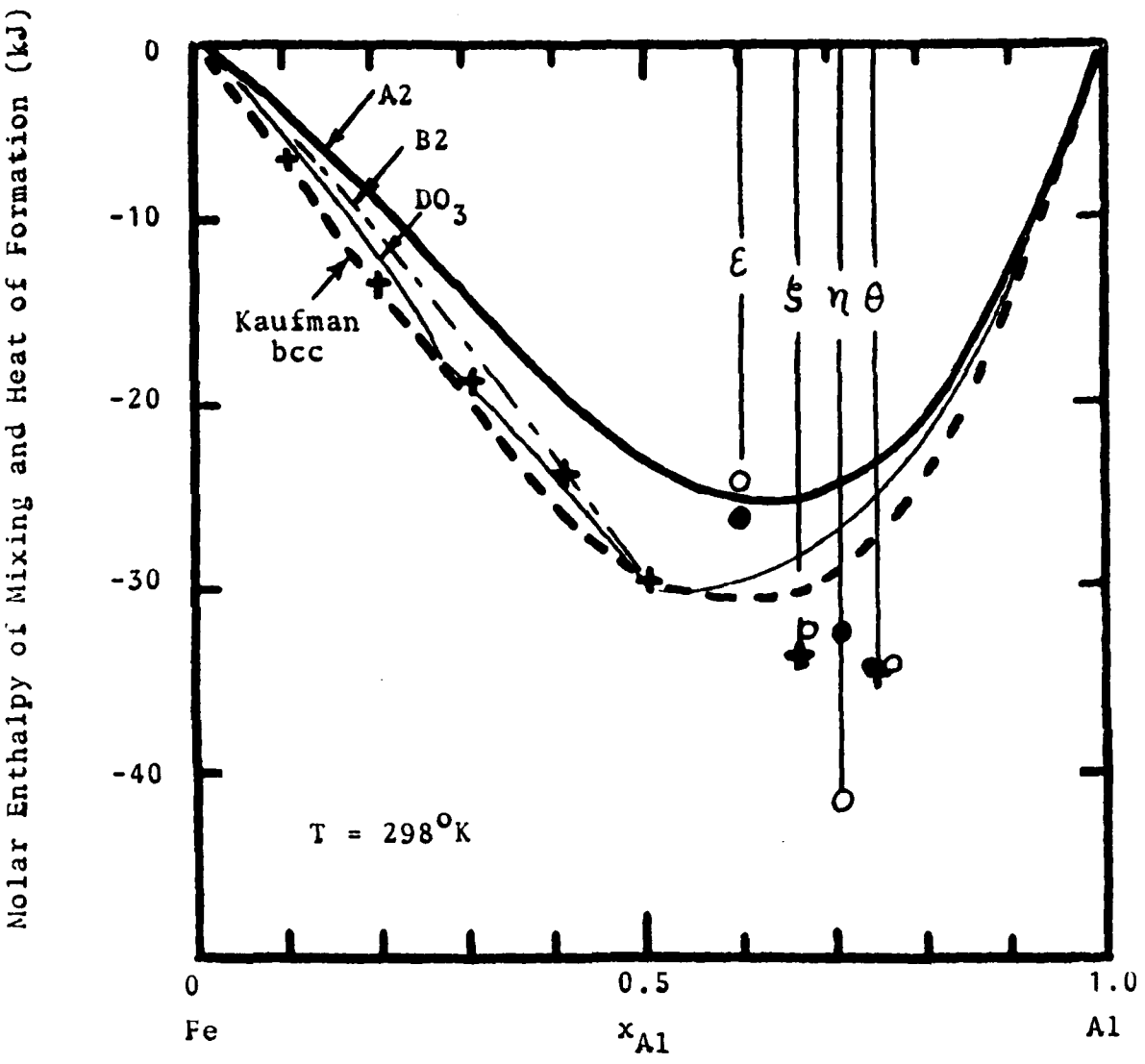

Figure 4a. Molar Enthalpy of Mixing of Iron-Aluminum Alloys and Heat of Formation of Compounds as a function of Composition at 298°K. The Crosses denote the values given by Hultgren (Reference 10), the dashed heavy curve for the bcc phase is due to Kaufman and Nesor (Reference 9) and the open circles for the compound phases is due to Kaufman and Nesor (Reference 9). The remaining curves and the closed circles are from the present analysis.

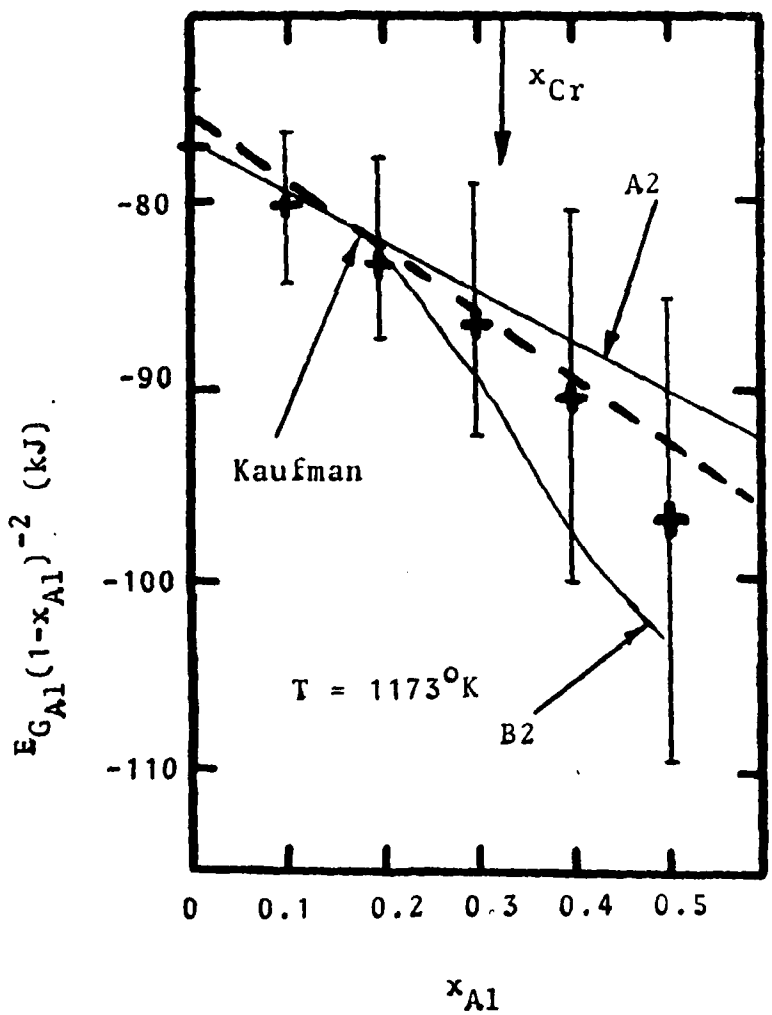

Figure 4b. The Partial Excess Gibbs Free Energy of Aluminum in bcc iron-aluminum alloys at 1173°K divided by the atomic fraction of iron squared shown as a function of the aluminum concentration. The heavy line is due to Kaufman and Nesor (Reference 9) while the crosses (and error bars) are from Hultgren (Reference 10). The remaining curves refer to the present analysis.

5. Subregular Approximation

It is interesting to see to what extent the new formalism can be approximated by a subregular model. The following approximations were obtained for $X_{Al}<0.5$ by plotting the quantity $\Delta G/X_{Al}X_{Fe}$ and fitting a suitable straight line to the resulting curve. The following results were obtained

for $T > T_{cr}$ and $X_{Al}>0.2$

$$\Delta G/X_{Al}X_{Fe} = 2.016.10^{-3}\left(4W^1-3W^2\right)^5 T^{-4}\left(3.75X_{Fe}-11.49X_{Al}\right) \quad (9a)$$

$$X_{Al}<0.2,\ \Delta G = 0 \quad (9b)$$

For $T < T_{cr}$

$$\Delta G/X_{Fe}X_{Al} = R(4W^1-3W^2)\left(0.4444X_{Fe} - 2.4126X_{Al}\right)$$

$$-R\,\frac{1.1046}{2\kappa}\,T\left(0.9789X_{Fe} - 8.8171X_{Al}\right)$$

$$-T^4/\left(4W^1-3W^2\right)^3\left(68.19X_{Fe} + 142X_{Al}\right)$$

where $\Delta G = {}^{E}G^{bcc} - {}^{E}G^{bcc}_{(dis)}$ (10)

with the actual values for Fe-Al inserted we obtain (with A2=disordered bcc)

$T > T_{cr}$, $X_{Al}> 0.2$:

$$G_m^{ord}-G_m^{A2} = X_{Fe}X_{Al}\left(7.455\ 10^{15}\ X_{Fe} - 22.844\ 10^{15}X_{Al}\right)T^{-4} \quad (11)$$

$T < T_{cr}$:

$$G_m^{ord} - G_m^{A2} = X_{Fe}X_{Al}\left[\left(14669-6.61T-1.09\ 10^{-9}\ T^4\right)X_{Fe} + \left(-79635 + 59.54T - 2.27\ 10^{-9}\ T^4\right)X_{Al}\right] \quad (12)$$

Both above and below the critical temperature a strong asymmetric term is obtained. The temperature dependencies T^{-4} and T^{4} are also strong.

In Figs. 5a, b, c and d these approximation formulas have been compared with Eqs. 5-8. The agreement is quite good except in the transition region between disordered and ordered state.

6. Calculation of Isothermal Sections in Fe-Al-X, X=Mn,Ni

Once the thermodynamics of the binary solutions have been established the properties of a ternary phase can be evaluated directly, assuming that there are no specific ternary effects. In a rigorous treatment the order disorder contribution is still given by eqs. 5-6, but ΔH and T_c are now to be evaluated for the actual ternary composition. It is a straight forward procedure to derive expressions for ΔH and T_c in the ternary case but the final expressions are rather complicated. In the present case a simpler approach will be taken. The Kohler method has been applied frequently to synthesize the properties of a ternary solution when the binaries are known, see for example ref.11 . Admittedly there is no physical justification for this method in the present case and its general features have recently been questioned(12). However, the use of the method is widespread and, for the sake of simplicity, it was applied here as follows: First a ternary calculation was made using the subregular model assuming a completely disordered bcc-phase described by the Kohler method. Thereafter a new calculation was performed with the order-disorder contribution added. When $X_{Al}/(X_{Fe}+X_{Al}) < 0.20$ the latter contribution is approximately zero, as can be seen from Fig. 5, and the phase boundaries follow the first set of curves. When $_{Al}/(X_{Fe}+X_{Al}) > 0.30$ the subregular solution approximation is a good approximation of the order-disorder contribution and the phase boundaries thus follow the second set of curves. The curves in the transition region were drawn by hand assuming a gradual shift from one set of curves to the other set.

All parameters, except those for Al-Fe, were taken from the ManLabs data bank (14). The results are presented in Figs. 6-7

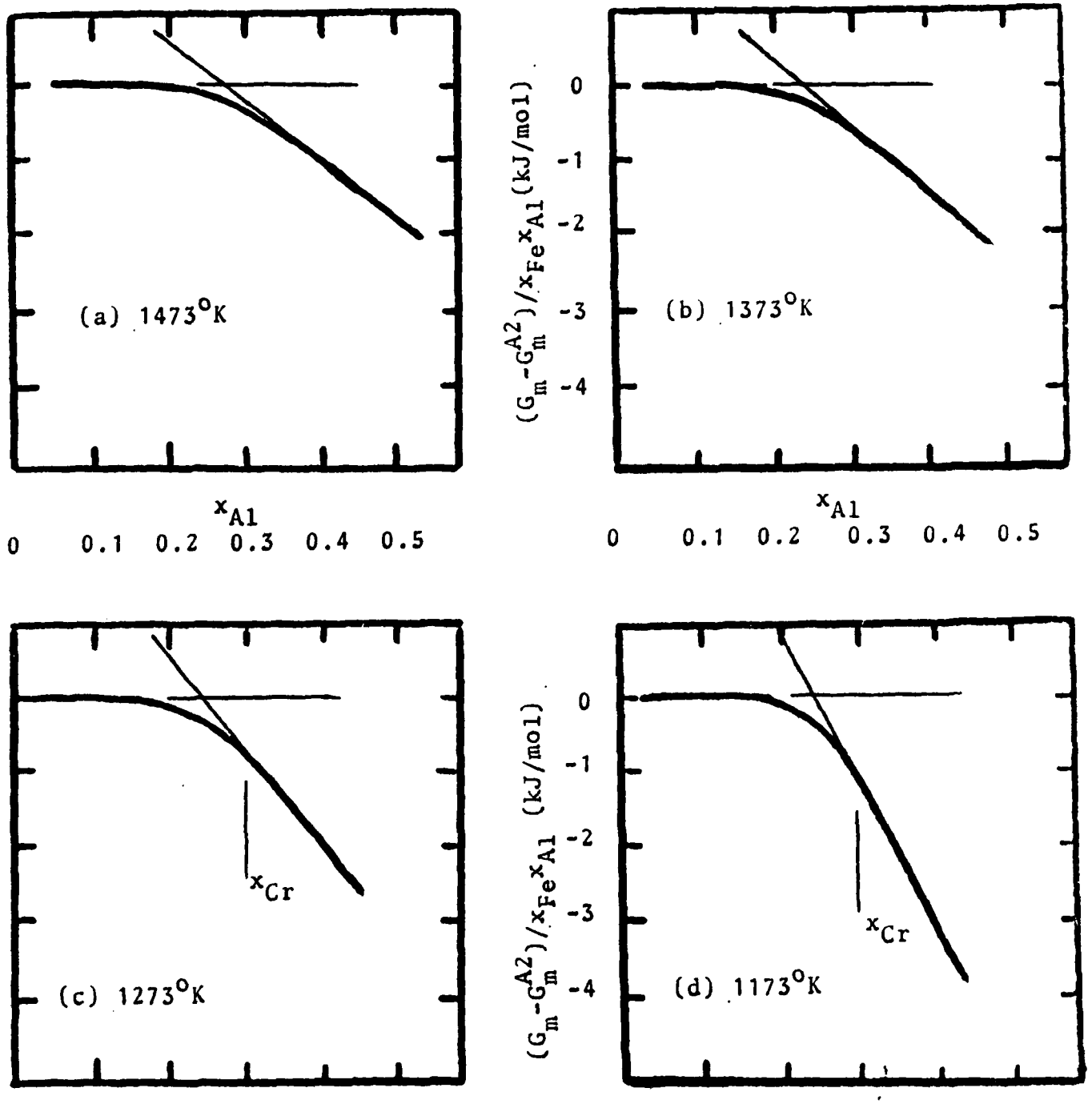

Figure 5. Calculated regular solution parameter for bcc Iron-Aluminum alloys as a function of composition at various temperatures. The thick curve represents the present analysis while the thin segments represent the subregular approximation.

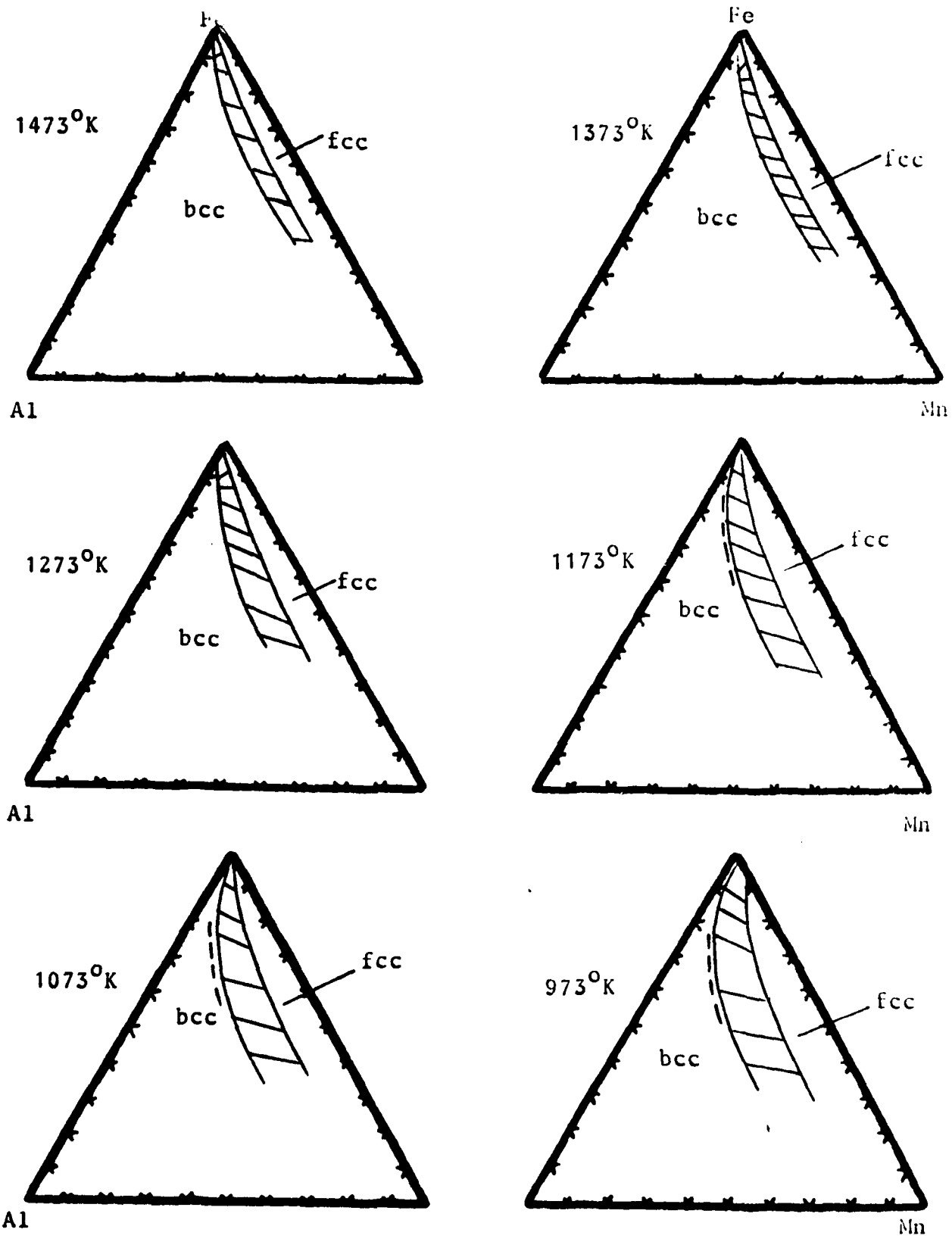

Figure 6. Calculated fcc/bcc Equilibria in the Iron-Manganese Aluminum System as a function of temperature between ordered bcc and fcc solid solutions. The dashed curve shows the phase boundary for the disordered bcc phase. No difference was noted above 1173°K.

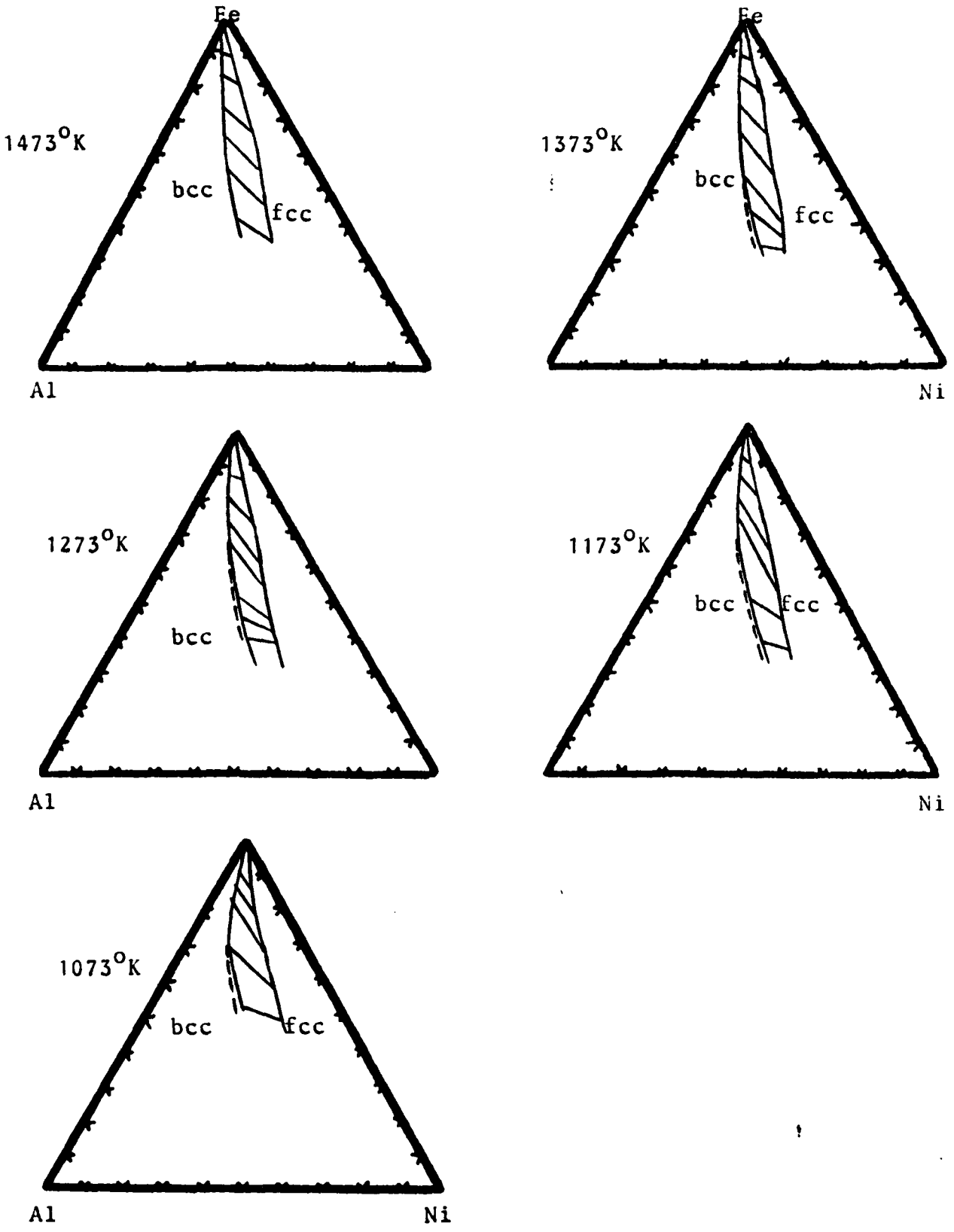

Figure 7. Calculated fcc/bcc Equilibria in the Iron-Nickel-Aluminum System as a function of temperature between ordered bcc and fcc solid solutions. The dashed curve shows the phase boundary for the disordered phase.

It can be seen that the order-disorder contribution to the Gibbs energy generally yields a very small shift of the calculated phase boundaries. Furthermore, a comparison with the calculations by Kaufman, (13) who did not distinguish between ordered and disordered state, shows that there are no significant discrepancies. The curves fall very close to each other.

It will now be argued that the present procedure probably over-estimates the effect of ordering on the bcc/fcc equilibrium. For a given temperature the composition range within which ordering occurs is approximately given by the parabola: $X_{Al}\ X_{Fe}$ = constant which starts from the binary Al-Fe-side and loops into the ternary. The exact relation is complicated (8) and requires detailed knowledge about the order-disordering reactions in the other two binaries. The parabola is a reasonable approximation when the maximum ordering temperatures are low (but still above $0^{o}K$) in the other systems. In Fig. 8 the parabola has been plotted at different $X_{Al}\ X_{Fe}$ values. When these plots are superimposed on the calculated bcc/fcc equilibria it is found that all temperatures the bcc/fcc phase boundary falls well outside the field of ordered bcc. It is thus concluded that the true phase boundaries must follow the ones calculated with a disordered bcc phase.

As a final conclusion, it would be worthwhile to examine the degree of order at each composition in the bcc phase at the two phase bcc + fcc boundary. For consistency this degree of order should coincide with the degree of order in the iron-aluminum binary at the same X_{Al}/X_{Fe} ratio which characterizes the ternary composition. If this is <u>not the case</u>, then the ternary free energy synthesized from the binary components incorrectly reflects the wrong degree of order. In the present case the errors introduced by such an inconsistency do not appear to be very large. However, it is possible that such errors could be substantial in other cases and should be guarded against.

Note in Proof

The prior discussion of Section 3 drew attention to the discrepancy between the experimental ordering temperature and the calculated value for $0.25 \leq X_{Al} \leq 0.50$. It was noted that compositionally dependent values of

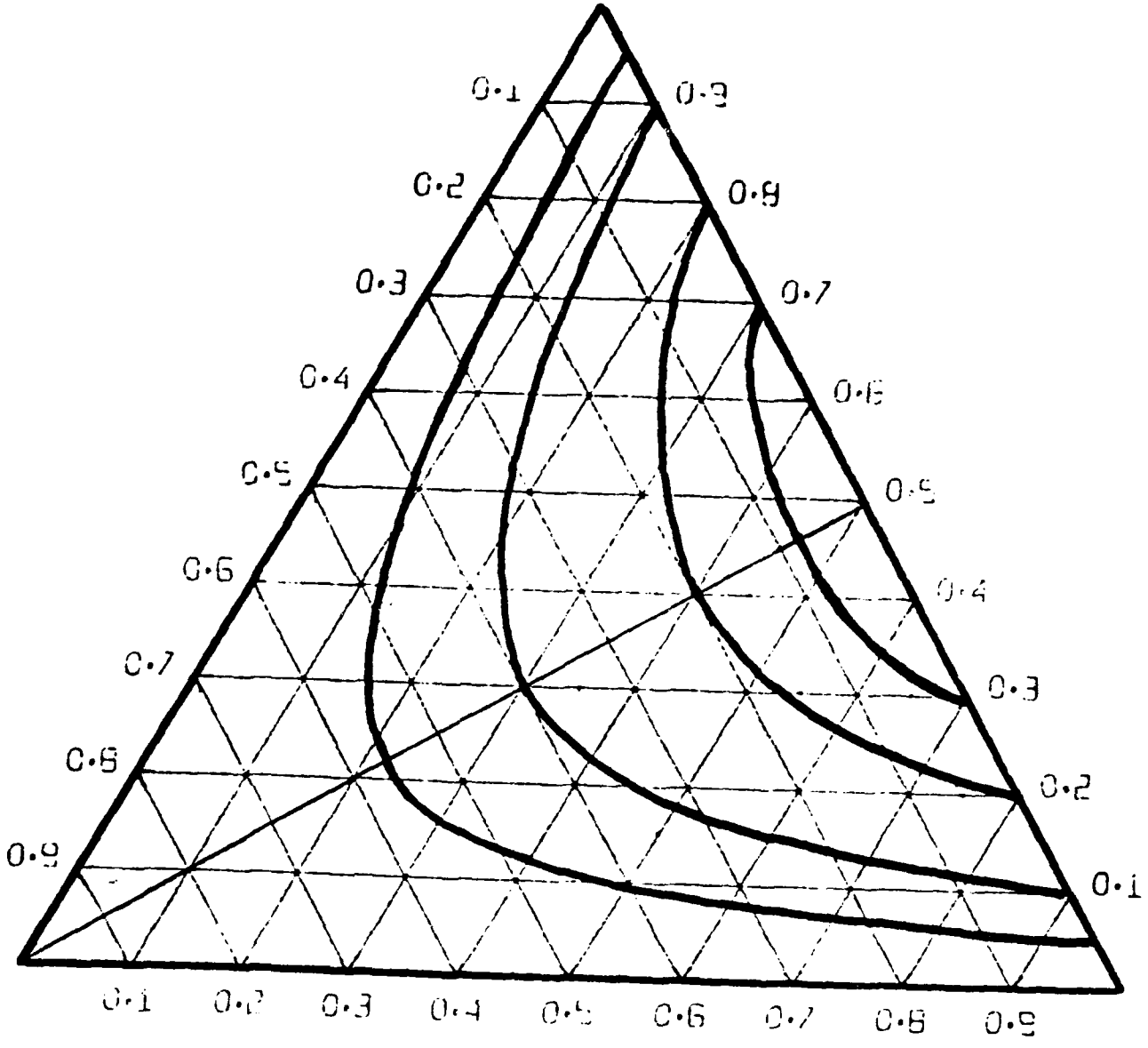

Figure 8. Parabola $X_A X_B$ = constant at different values of the constant.

W^1 and W^2 would be required to eliminate this discrepancy. It was also noted that such an alteration would lead to a stabilization of the bcc phase at high temperature and a resulting excessive elevation of the melting points. Notwithstanding these difficulties an attempt was made to evaluate W^1 and W^2 as a function of composition in order to produce an ordering temperature vs. composition curve for $0.25 \leq X_{Al} \leq 0.50$ (8) corresponding to 1260K at X_{Al} = 0.30 and 1570K at X_{Al}= 0.40. The resulting expression for W^1 is given by Equations 13 and 14 as:

$$W^1 = 1480 + 625\ X_{Al} \qquad (13)$$

and

$$W^2 = 846 - 372\ X_{Al} \qquad (14)$$

These new values compare with the previous values of W^1 = 1478 and W^2 = 794 listed in Section 3. These expressions for W^1 and W^2 as provided by Equations (13) and (14) were substituted directly into Equations (5) through (8) to reformulate the thermochemical properties of the iron-aluminum system. No further changes in the remaining parameters for the iron-aluminum system were made at this stage. This procedure did indeed produce an excessive stabilization of the bcc phase with respect to the liquid. Nevertheless, this new formulation of the bcc phase was employed directly to derive an effective subregular description as in Section 5. The latter step was accomplished by evaluating W^1 and W^2 at X_{Al} = 0.5 from Equation 13 and 14 since at X_{Al} = 0.5 the largest difference between this approximation and the former calculation exists. Thus for this case W^1 = 1793 and W^2 = 660. Employing these values in Equations (9) and (10) permits redefinition of the excess free energy of iron-aluminum alloys in the subregular approximation. Subsequent recalculation of the Fe-Ni-Al fcc/bcc equilibrium at 1273 with the modified results did not yield results significantly different from those shown in 7c. It is therefore concluded that the results described in Section 6 would not be materially altered by introducing compositionally dependent values of W^1 and W^2 for the purpose of obtaining a better description of the ordering temperature at compositions containing more than 25 atoms percent aluminum.

Appendix A: Summary of Parameters for the Fe-Al System

The lattice stabilities from Ref. 9.

$$E_{G_m}^{bcc,dis} = X_{Fe}X_{Al}\,(-32345-37.92T)X_{Fe} + (-150252+51.42T)X_{Al} \quad \text{J/mol}$$

$W^1 = 1588$, $W^2 = 794$ (k units $k=13.8\cdot10^{-24}$ J/atom), K=0.68

$$E_{G_m}^{fcc} = X_{Fe}X_{Al}\,(-25022-38.01T)X_{Fe} + (-106841+66.70T)X_{Al} \quad \text{J/mol}$$

$$E_{G_m}^{L} = X_{Fe}X_{Al}\,(-62760-14.63T)X_{Fe} + (-96232+32.72T)X_{Al} \quad \text{J/mol}$$

$$^{\circ}G^{\theta}_{Fe_{0.25}Al_{0.75}} - 0.25\,{}^{\circ}G^{bcc}_{Fe} - 0.75\,{}^{\circ}G^{bcc}_{Al} = -35275+8.28T \quad \text{J/mol}$$

$$^{\circ}G^{\eta}_{Fe_{0.286}Al_{0.714}} - 0.286\,{}^{\circ}G^{bcc}_{Fe} - 0.714\,{}^{\circ}G^{bcc}_{Al} = -41169+11.40T \quad \text{J/mol}$$

$$^{\circ}G^{\xi}_{Fe_{0.333}Al_{0.667}} - 0.333\,{}^{\circ}G^{bcc}_{Fe} - 0.667\,{}^{\circ}G^{bcc}_{Al} = -37872+4.73T \quad \text{J/mol}$$

$$^{\circ}G^{\varepsilon}_{Fe_{0.40}Al_{0.60}} - 0.4\,{}^{\circ}G^{bcc}_{Al} - 0.6\,{}^{\circ}G^{bcc}_{Fe} = -23863-2.77T \quad \text{J/mol}$$

References

1. G. Inden: Acta Met. 22 (1974) p 945.

2. G. Inden: Project Meeting CALPHAD V 21-25 June 1976, Max-Planck-Institut fur Eisenforschung G.m.b. H, Dusseldorf/W. Germany, p 4-1.

3. G. Inden: Ibid, p 111. 4-1.

4. S. Hertzman and B. Sundman: CALPHAD (in print)

5. M. Hillert and M. Jarl: CALPHAD, 2 (1978) p 227.

6. J. Agren: Met Trans A, 10A (1979) p 1847.

7. G. Inden: personal communication

8. A.P. Miodownik: Computer Based Methods for Thermodynamic Analysis of Materials Processing, ManLabs, Inc., Cambridge, Mass. 02139 November 1981, Contract F49620-80-C-0020 AFOSR Bolling AFB (D.C. 20332).

9. L. Kaufman and H. Nesor, CALPHAD 2 (1978) p 325.

10. R. Hultgren et. al.: Selected Values of the Thermodynamic Properties of Metals (and Binary Alloys), (2 volumes) ASM, Metals Park, Ohio (1973).

11. L. Kaufman: CALPHAD, 1 (1977) p.7

12. J. Brynestad: CALPHAD, 5 (1981) p. 103

13. L. Kaufman (in ref. 8)

14. ManLabs-NPL, Materials Data Bank, Instruction Manual, ManLabs, Inc. Cambridge, Mass. 02139

VIII A THERMODYNAMIC EVALUATION OF THE TI-C-N SYSTEM

1.0 Introduction

The use of vapor deposited TiC, TiN and Ti(C,N) coatings for improving the performance of cutting tools and wear resistant surfaces enhances the value of information on the thermochemistry and phase diagram of the Ti-C-N system.

Since the crystal structures of the compounds TiC and TiN are the same, it is likely that these compounds form a solid solution. However, the experimental Ti-C and Ti-N phase diagrams reported to date are not very well established and very little thermodynamic data is available for the binary cases or the Ti-C-N ternary. The purpose of the present work is to evaluate all the information available in terms of thermodynamic models for the individual phases and synthesize the binary and ternary phase diagrams.

2.0 Thermodynamic Models

2.1 Liquid

The simplest models that cover the whole concentration range are the regular or subregular solution models. The formation of the solid compounds TiC and TiN in the binaries suggests that some ordering or formation of molecular species might take place in the liquid around the stoichiometric compositions. However, a high degree of association is not observed in the gas phase and vaporization of titanium carbide yields titanium and carbon polymers. The Fe-S system has recently been treated by assuming the presence of molecular species (1) and by assuming ordering (2). Both treatments yield a satisfactory agreement with experimental data, and predict a very rapid change in activity close to the stoichiometric composition. This rapid change is difficult to describe with a regular or subregular solution model, and generally many terms will be needed in the series expansion of the excess energy.

The abnormal behavior of the activity, compared to what the regular solution model predicts, reveals itself in the phase-diagram by giving the compound a liquidus curve formed more like a wedge instead of a parabola.

In the present case the experimental data on the L/TiC (liquid/TiC) and L/TiN equilibia is too meager to reveal the shape of the liquidus curves accurately, and no thermodynamic data for the liquid phase is available. For the sake of simplicity the liquid was thus described with the subregular solution model. The corresponding equations are summarized in Appendix B.

2.2 Solid Phases

The TiC and TiN phases both have a Nacl-structure. However, a rather wide range of homogenuity is observed: $Ti_{(1-x)}C_x$ with $0.32 < x < 0.49$. First an attempt was made to describe TiC as a subregular solution. This attempt was not very successful and a new approach was tried. From the crystallographic point of view TiC and TiN consists of two sublattices and the variation in composition is due to a varying number of vacant carbon or nitrogen sites. (3). It was thus decided to apply the sublattice model which was developed by Hillert and Staffansson (4) and later generelized by Sundman and Agren (5) and recently applied to the Fe-S system (2). This approach was more successful and yielded a satisfactory description of all the available information.

Hexagonal titanium exhibits a rather large solubility for N and the choice of thermodynamic model might be important. Recently (6) the hexagonal solution of N in Fe was treated by means of the sublattice model. In agreement with that treatment we chose the upper limit of N-solubility in hcp-Ti as 1/3 corresponding to the compound Ti_2N. For the bcc-phase we also applied the sublattice model with 3 interstials per Ti-atom as in the Fe-C-case (see Ref.6)

The equations for the sublattice model are summarized in Appendix B.

3.0 Evaluation of Parameters for Phases in the Titanium-Carbon System

The free energy of formation of stoichiometric TiC has been tabulated by Hultgren (3). Figure 1 shows the data given by Hultgren as symbos and the solid line is a least square fit (assuming a linear temperature dependency) to the data. The dashed line is calculated according to the parameters given by Kubaschewski and Alcock (7). The result of the least square fit is:

$$ {}^{o}G^{fcc}_{TiC} - {}^{o}G^{bcc}_{Ti} - {}^{o}G^{Gr}_{C} = -45012 + 3.428T \quad \text{(cal/mol)} \quad (1) $$

and was accepted in the present study. Storms (8) has compiled data on the Ti partial pressure over TiC at equilibrium with graphite at different temperatures (See Fig. 2) Kubaschewski and Alcock (7) give the vapor-pressure of pure Ti as:

$$ \log P^{o}_{Ti} = -24400/T - 0.91 \log T + 10.299 \quad (2) $$

From Eq? we can evaluate the corresponding free energy difference;

$$ {}^{o}G^{gas,\ latm}_{Ti} - {}^{o}G^{bcc}_{Ti} = 111645 - 47.124T + 1.808\ T\ln T \quad \text{(cal/mol)} \quad (3) $$

By combining the information from Storms (8) with Eq.3 and

$$ {}^{o}G^{fcc}_{Ti} - {}^{o}G^{bcc}_{Ti} = -240 + 0.9T \quad \text{(cal/mol)} \quad (4). $$

from Kaufman (9) and take the composition of TiC in equilibrium with graphite as $x^{fcc}_{C} = 0.49$ according to Rudy's phase diagram (10) we can calculate the partial excess quantities ${}^{E}G_{Ti}$ and ${}^{E}G_{C}$ as functions of temperature for this particular composition. The phase-boundary Ti/TiC, as reported by Rudy (10), can be used to evaluate ${}^{E}G_{Ti}$ at different temperatures along the phase-boundary when the solubility of C in Ti is neglected. Assuming linear temperature-dependency it was then possible to evaluate ${}^{o}L^{Tifcc}_{CVa}$ and ${}^{1}L^{Tifcc}_{CVa}$ from the partial quantities. The following expressions were obtained:

$$ {}^{o}L^{Tifcc}_{CVa} = -16099 + 0.36T \quad \text{(cal/mol)} \quad (5a) $$

$$ {}^{1}L^{Tifcc}_{CVa} = -38801 + 11.03T \quad \text{(cal/mol)} \quad (5b) $$

The solid line in Figure 2 is calculated by the application of Eqs. 5a and 5b. The agreement with the experimental information is

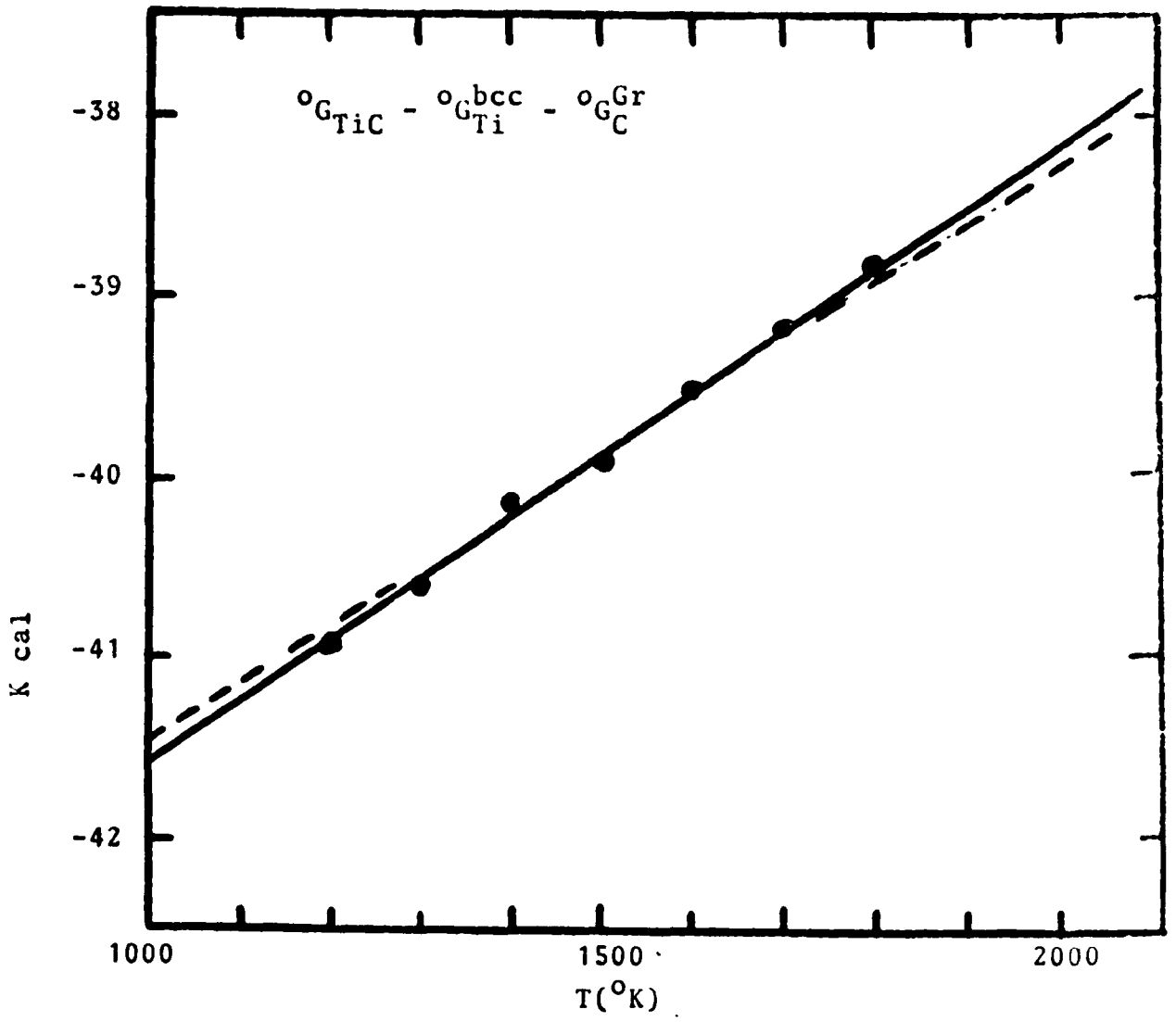

Figure 1. The Free Energy of Formation of TiC from bcc Ti and Graphite as a function of Temperature. Solid Curve designates the present analysis while the Dashed Curve is after Kubaschewski and Alcock (Ref. 6) and the points are from Hultgren (Ref. 3)

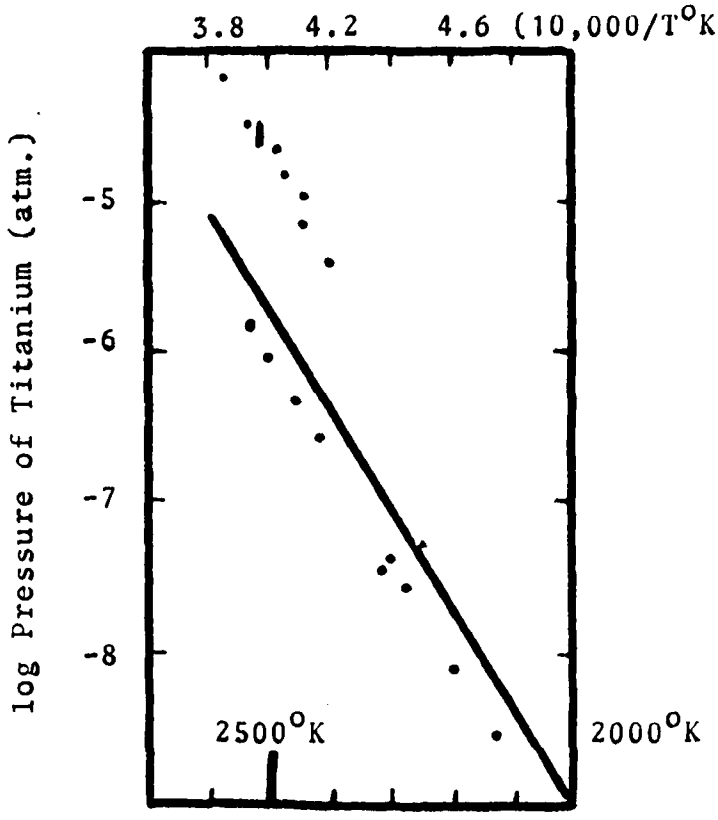

Figure 2. Pressure of Titanium over TiC + Graphite as a function of Temperature. Solid curve is from the present analysis, points are from Ref. 7.

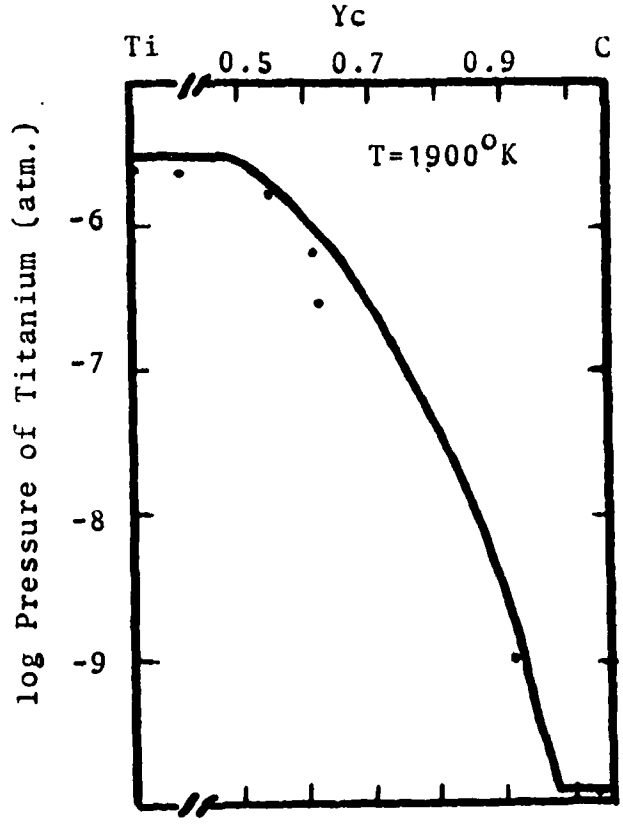

Figure 3. Pressure of Titanium over TiC at 1900°K. Solid Curve is from Present Analysis. Points are from Ref.7.

very good. In Figure 3 the Ti partial pressure as a function of composition at 1900 K has been plotted. The symbols are experiments reported by Storms (8) and the solid line is calculated from the present analysis. The agreement is satisfactory.

The position of the melting-point of TiC according to Rudy (10) is $x_C = 0.44$ and $T_m = 3340$k. By applying the new evaluation of TiC and the lattice stabilities reported by Kaufman (9) one can evaluate the subregular solution parameters that yield this melting-point. Furthermore, temperature dependencies in these parameters can be evaluated from the condition that the L/TiC/Gr eutectic occurs at 3049K and the L/TiC/Ti eutectic at 1923K (from Ref. 10.) The following values are then obtained:

$$ {}^{o}L^{L}_{CTi} = -23185 - 10.5T \quad \text{(cal/mol)} \quad (6a) $$

$$ {}^{1}L^{L}_{CTi} = 30516 - 10.5T \quad \text{-11-} \quad (6b) $$

The sublattice model for the bcc-phase yields a reasonable description with the following parameters:

$$ L^{Tibcc}_{CVa} = -50000 \quad \text{(cal/mol)} \quad (7a) $$

$$ {}^{o}G^{bcc}_{TiC_3} - {}^{o}G^{hcp}_{Ti} - 3\,{}^{o}G^{gr}_{C} = -44996 + 0.49T \quad (7b) $$

The hcp-phase has a very low solubility of carbon and it is thus difficult to evaluate the interaction parameter. Arbitrarily, this was chosen the same as in bcc i.e.

$$ L^{hcp}_{CVa} = L^{bcc}_{CVa} = -50000 \quad \text{(cal/mol)} \quad (8a) $$

Subsequently

$$ {}^{o}G^{hcp}_{Ti_2N} - 2\,{}^{o}G^{hcp}_{Ti} - 1/2\,{}^{o}G^{Gr}_{C} = 5574 \quad (8b) $$

was chosen to yield a three-phase equilibrium fcc/bcc/hcp at 1193K.

All parameters are summarized in Appendix B.

4. Evaluation of Parameters for Phases in the Titanium-Nitrogen System.

In general the data for the TiN-System is meager. The phase diagram given by Hultgren (3) is not very well established and is basically the same as the one in Hansen's compiliation (11).

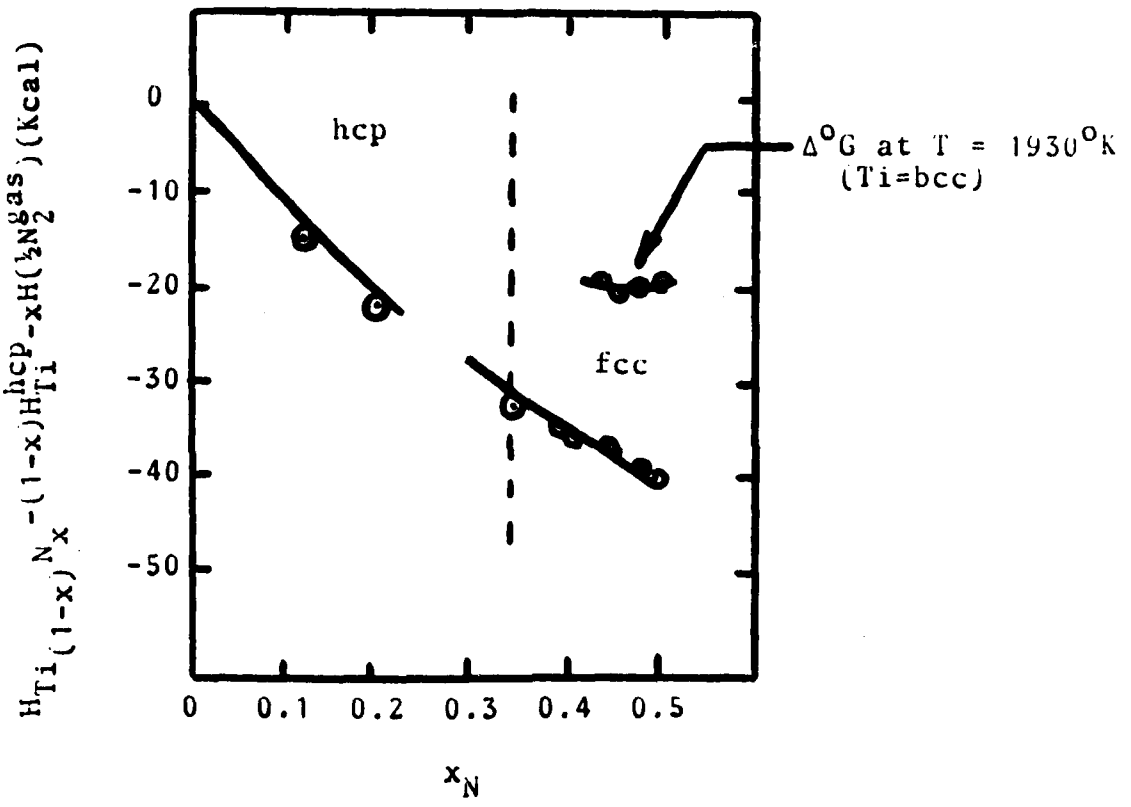

Figure 4. Enthalpy and Gibbs energy change for the reaction
$(1-x)Ti(hcp)+x(\frac{1}{2}N_2 gas,\ 1\ atm.) \rightarrow Ti_{(1-x)}N_x$

Solid curves calculated: Symbols after Hultgren Reference 4.

The free energy of formation for stoichiometric TiN however, seems well known. A least square fit to the values given by Hultgren [5] yields:

$$ {}^{o}G^{fcc}_{TiN} - {}^{o}G^{hcp}_{Ti} - 1/2\ {}^{o}G^{gas}_{N_2} = -79666 + 21.42T \quad \text{(cal/mol)} \quad (9) $$

This expression yields values in good agreement with those calculated for Kubaschewski and Alcock (7). In addition some information on the enthalpy of mixing in the solid phases is available from Hultgren. Hultgren also gives the free energy of mixing for $0.45 < x_N < 0.5$ at 1930K. A solution parameter $L^{Tifcc}_{NVa} = -25000 + 4.4T$ was found to describe the information on the fcc phase satisfactory. In Fig. 4 the calculated values have been plotted together with Hultgren's values. The parameters for the hcp-phase was subsequently evaluated from the fcc/hcp phase boundaries as reported by Hultgren. The following values were obtained.

$$ {}^{o}G^{hcp}_{Ti_2N} - 2\ {}^{o}G^{hcp}_{Ti} - 1/2\ {}^{o}G^{gas}_{N_2} = -93490 + 24.71T \quad (10a) $$

$$ L^{Tihcp}_{NVa} = -9985 - 3.44T \quad (10b) $$

The enthalpy of mixing in the hcp phase can now be calculated as a function of composition and the result is presented in Fig. 6 together with two experimental values given by Hultgren. The agreement is satisfactory.

In Hultgren's phase diagram a tetragonal phase Ti_2N with a very narrow composition range is shown at low temperatures. This phase was treated as a stoichiometric compound in the present evaluation and it's free energy of formation was evaluated from the reported phase boundary with hcp at 1310K and 1200K, yielding the following expression:

$$ {}^{o}G^{tetragonal}_{Ti_2N} - 2\ {}^{o}G^{hcp}_{Ti} - 1/2\ {}^{o}G^{gas}_{N_2} = -120692 + 43.06T \quad \text{(cal/mol)} \quad (11) $$

The highest temperature where this phase is stable is then calculated as 1321K.

It is very difficult to evaluate two parameters for the bcc-phase because the N-solubility is rather low. Quite arbitarily it was then chosen to put:

$$ L^{Tibcc}_{NVa} = 0 \quad (12) $$

The remaining parameter was then adjusted to yield a hcp/bcc equilibrium in reasonable agreement with Hultgren's phase diagram.

The following value was obtained:

$$ {}^{o}G^{bcc}_{TiN_3} - {}^{o}G^{hcp}_{Ti} - 3/2\ {}^{o}G^{gas}_{N_2} = -104155 + 31.22T \qquad (13) $$

No thermodynamic data for the liquid phase is available. The two subregular solution parameters were adjusted to yield an fcc/L equilibrium in reasonable agreement with Hultgrens phase diagram. The following parameters were found:

$$ {}^{o}L^{L}_{NTi} = -64482 - 7.5T \qquad \text{(cal/mol)} \quad (14a) $$

$$ {}^{1}L^{L}_{NTi} = -40975 + 7.5T \qquad \text{(cal/mol)} \quad (14b) $$

All parameters are now fixed and a complete phase diagram can be calculated. The parameters are summarized in Appendix B.

5.0 Calculation of Ti-C Phase Diagram

Combination of the equations in Appendix B and the parameters in Appendix C permit calculation of the phase diagram by standard methods. The result is presented in Fig 5.

Figure 6 compares the experimental points, the phase boundaries (dashed curve) suggested by Rudy (10) and the calculated results (solid lines). The agreement with the suggested solidus curve is very good whereas the agreement with the suggested liquidus curve is not so good. However, the liquidus curve has not been established experimentally to date. It should however, be mentioned that the appearence of order or molecular species in the melt will deform the liquidus curve to a shape more like the one proposed by Rudy. (10).

6.0 Calculation of the Ti-N Phase Diagram

The calculated titanium-nitrogen phase diagram is shown in Fig 7. In addition Hultgrens phase diagram is displayed using dashed lines. The solid-phase equilibria are in a very good agreement and the fcc/L-equilibrium is satisfactory. In both Hansen's and Hultgren's phase diagrams, the latter equilibria was designated by dashed lines to indicate that the shape of the curves is very uncertain. The most serious discrepancy between the reported phase diagram and the calculated one is the temperature of the three-phase equilibrium L/bcc/hcp.

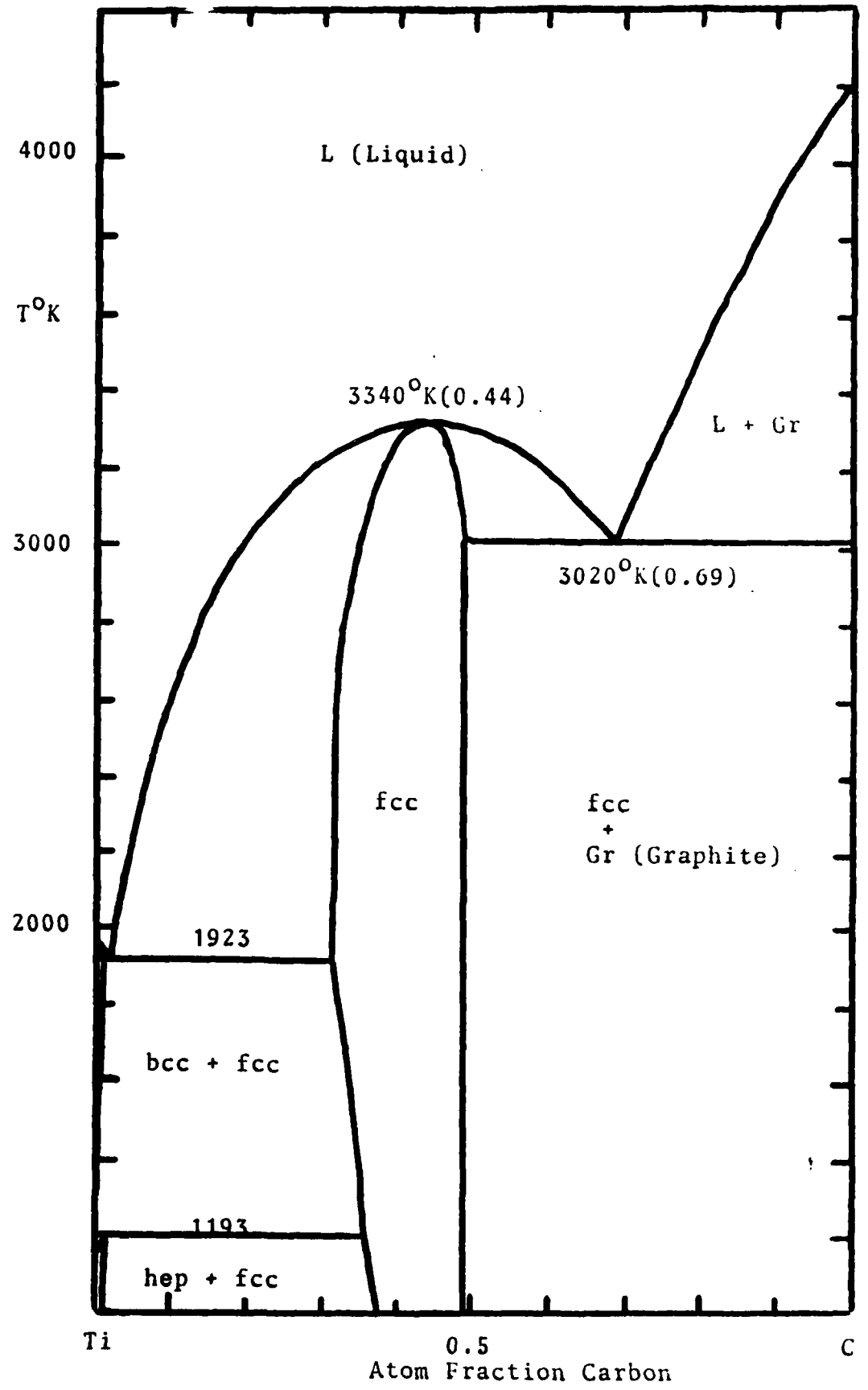

Figure 5. Calculated Titanium-Carbon Phase Diagram

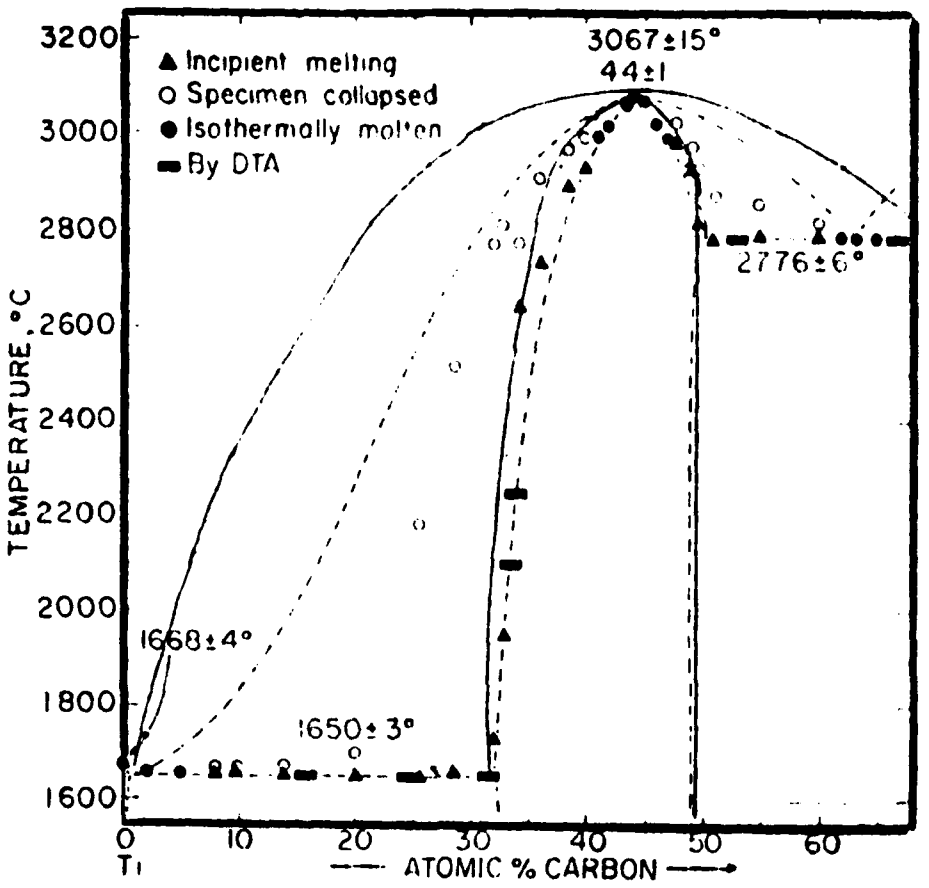

Figure 6. Liquid-Fcc Equilibrium in the Titanium-Carbon System. Solid Curves are calculated. Dashed Curves and Experimental Points are from Reference 9.

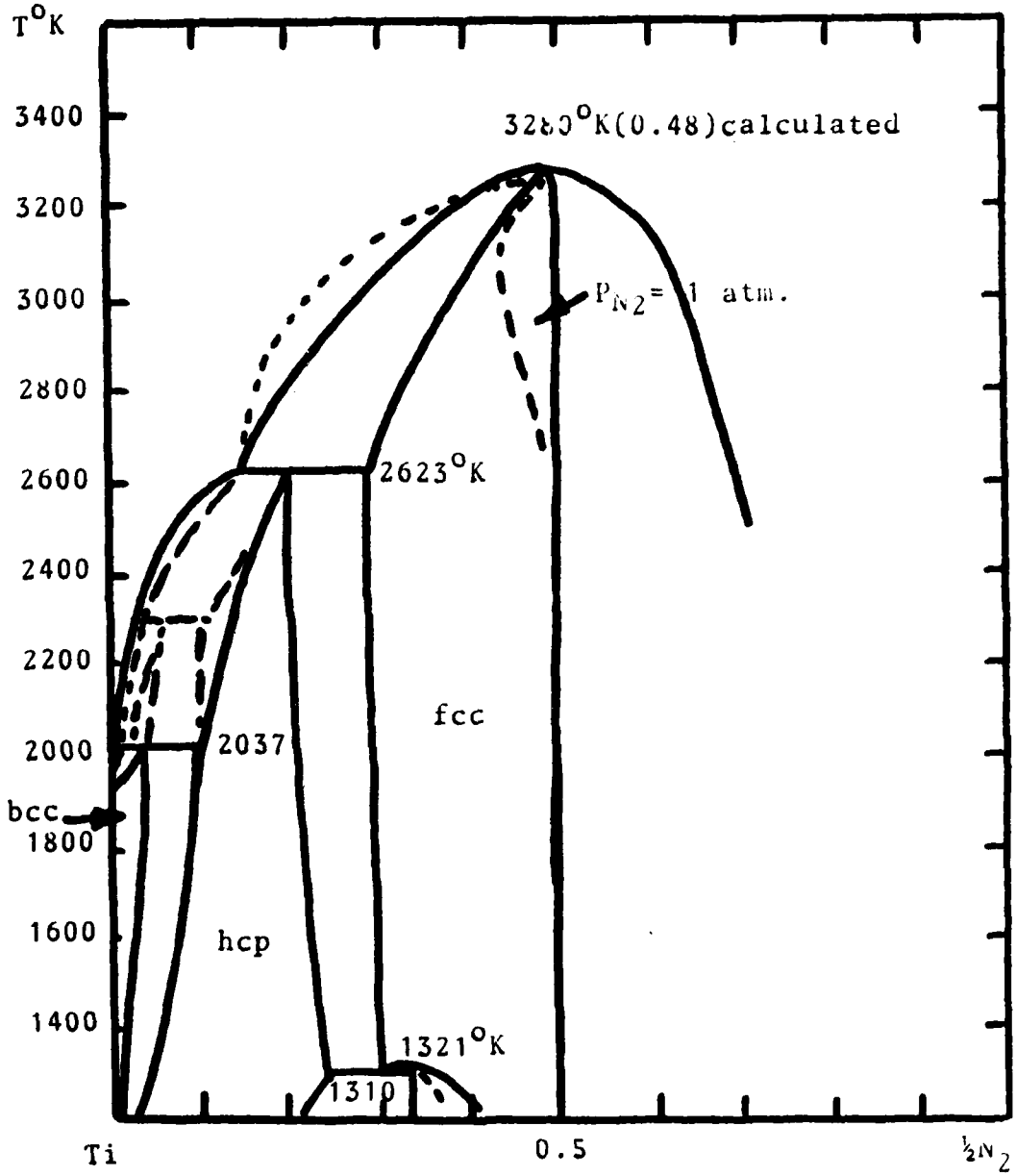

Figure 7. Titanium-Nitrogen Phase Diagram, Solid Curves are calculated, Dashed Curves are after Hultgren Reference 4.

In Hultgren's diagram it is around 2293K (2020 ^{o}C) whereas the calculation yielded 2037k (1764^{o}C). It is easily demonstrated that this part of Hultgren's diagram cannot be self consistent since close to the edges of a phase-diagram the width of a two-phase field is approximately given by $\Delta G/RT$, where ΔG is the free energy difference between the two phases for the solvent (i.e. Ti in this case). At 2293K we have for the width of the L/bcc-field,: $\Delta G/RT = 0.15$, whereas Hultgrens diagram yields about 0.02. A two-phase field which is wider than 0.02 will tend to push the three-phase equilibrium to lower temperature. Altering the width of the two-phase field by changing solution phase parameters cannot be done realistically because the nitrogen concentration in the liquid is too low. It might instead be possible to change the description of the bcc phase but the N-concentration in that is also rather low and non-realistic values are required to obtain agreement with Hultgren. In the latter case one also has to change the hcp and fcc-phases if one wants to keep the agreement with the solid-phase equilibria in the reported phase diagram.

7.0 Calculation of Ternary Sections in the Ti-C-N system

In general calculation of the Ti-C-N system requires description of the C-N binary in addition to the Ti-C and Ti-N binaries discussed above. However, since the information required to evaluate such C-N interactions is not available, they were assumed to be equal to zero as a first approximation. On this basis the ternary sections at 1600,1800 and 2500K for the N-C-Ti system shown in Figures 8,9,10 were calculated. The calculation shows that the fcc-field extends from the TiC to the TiN side and that the hcp phase disolves very little carbon.

8.0 Vapor deposition of solid $Ti_{(1-x-y)}C_xN_y$

From a practical point of view it is interesting to determine what composition an input gas must have in order to yield a specific composition x,y of the carbo-nitride. The limiting values at 1800K in the binary Ti-C system, using a mixture of $TiCl_4$, CH_4 and H_2 of P_{tot} = 1 atm, was calculated by Bernard et. al. (12). In principle their calculation could

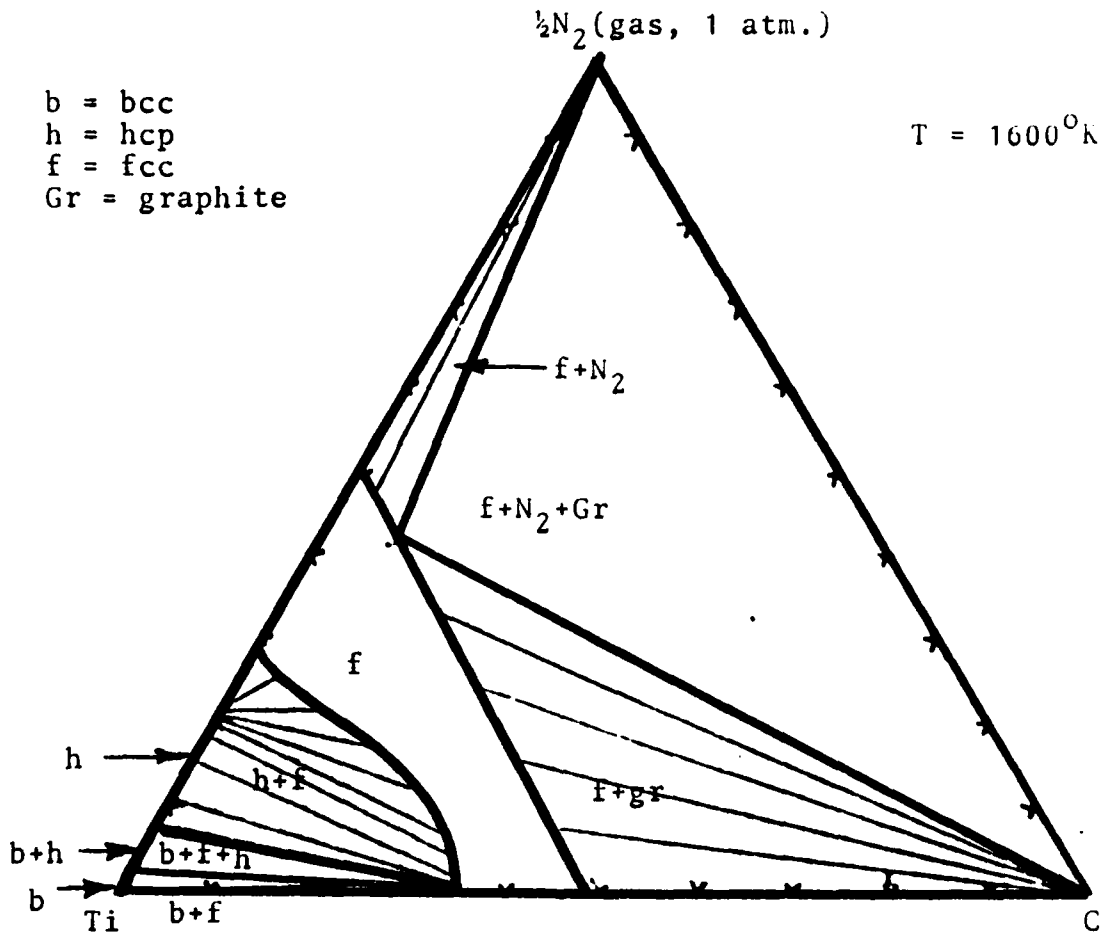

Figure 8. Calculated Isothermal Section at 1600°K in the Titanium-Carbon-Nitrogen System.

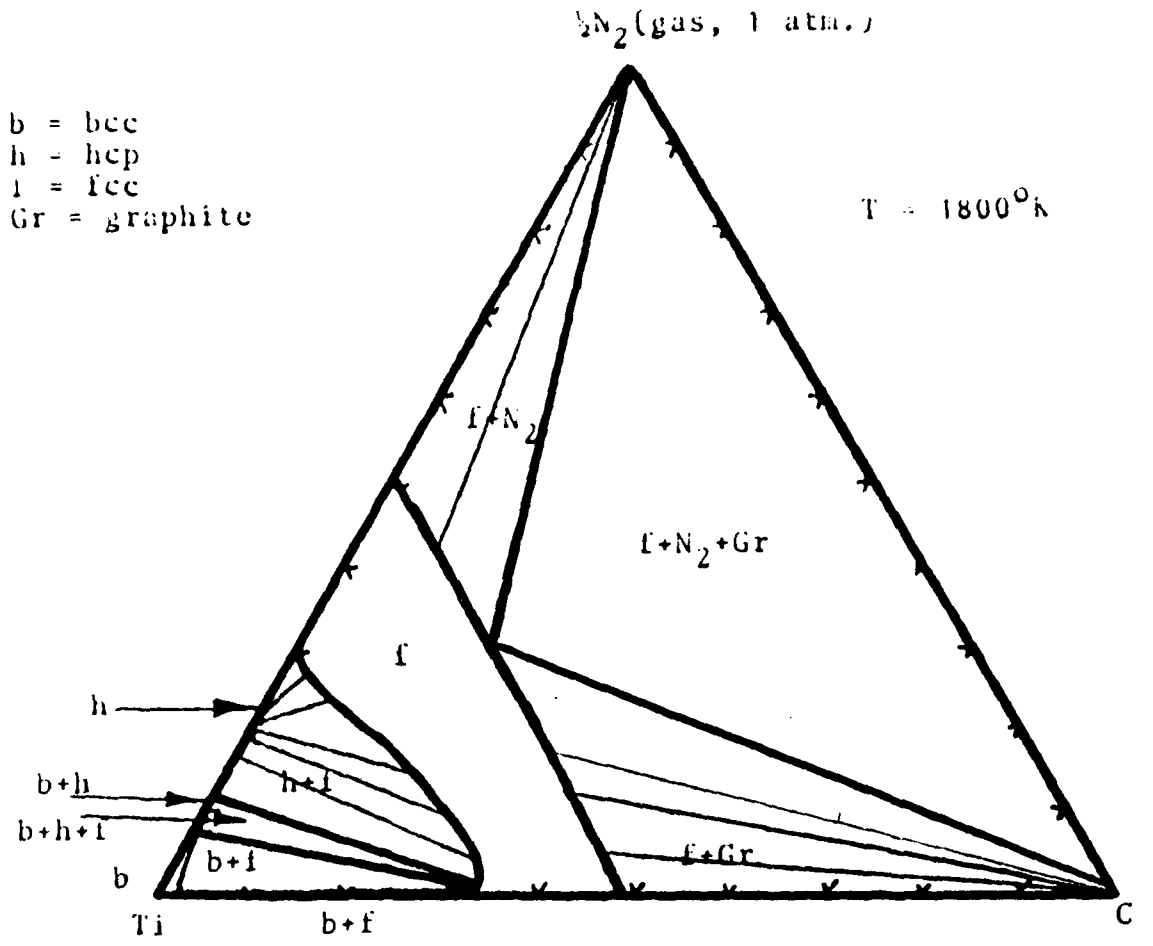

Figure 9. Calculated Isothermal Section in the Titanium-Carbon-Nitrogen System at 1800°K

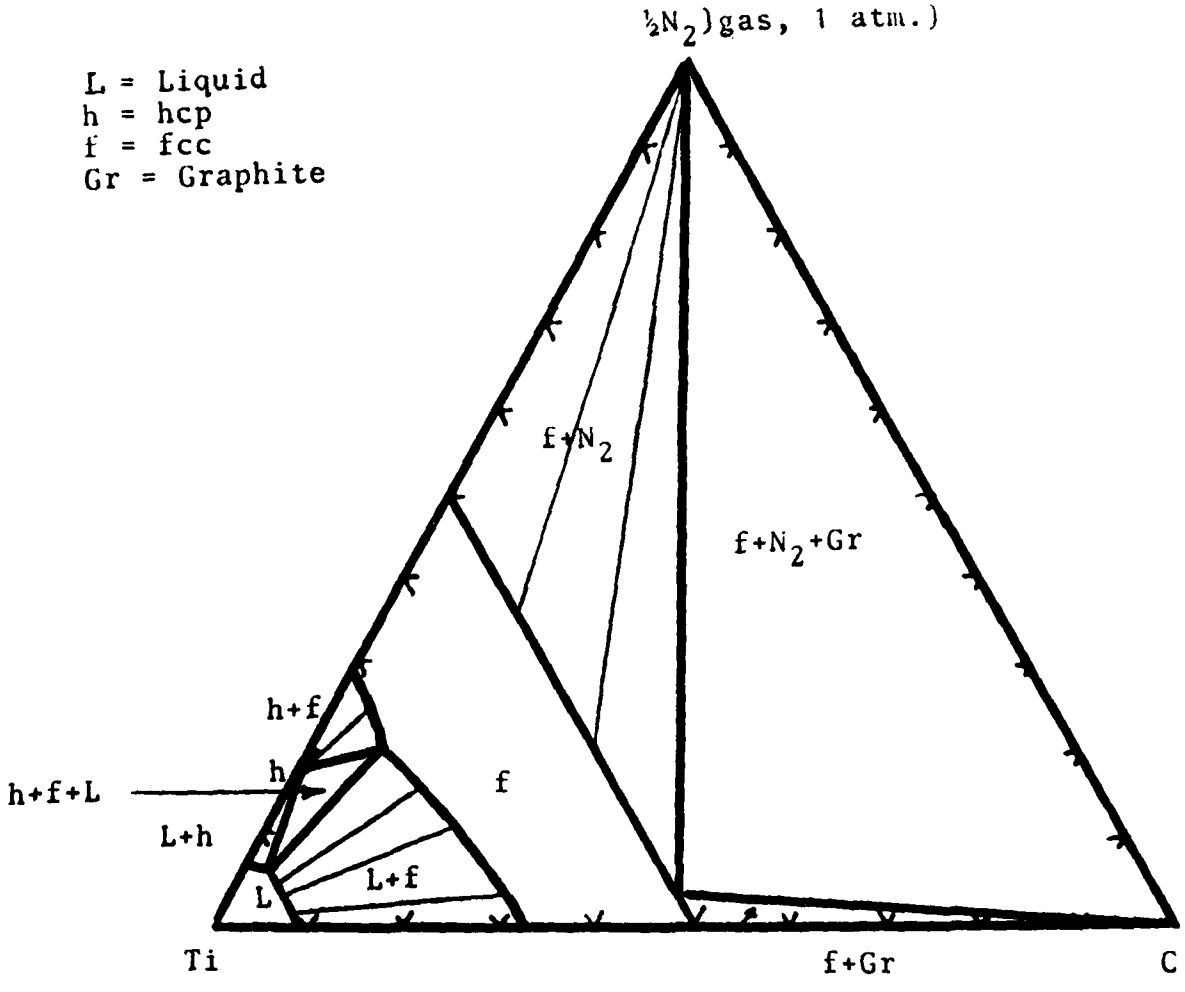

Figure 10. Calculated Isothermal Section in the Titanium-Carbon-Nitrogen System at 2500°K

be repeated not only for the extreme compositions (corresponding to equilibrium with graphite and almost a pure Ti respectively) but for a whole family of different compositions. Each composition would be represented as a curve in the $P^o_{TiCl_4}$ - $P^o_{CH_4}$ - plot. The calculation is quite straight forward. From the given solid phase composition the C- and Ti-activities can be calculated. By keeping these activities and the total gas-pressure fixed and solving the non-linear system of equations formed by equilibrium and stoichiometric conditions for the gas-mixture one obtains $P^o_{TiCl_4}$ when $P^o_{CH_4}$ is specified or vice versa. If a nitrogen-bearing component, e.g. NH_3, is added to the input-gas the deposited phase will also contain some N. The input-gas composition required to obtain a certain solid-phase composition is calculated in the same way as in the binary case. From the solid phase compositon the C-, N- and Ti-activities are calculated and the values obtained are inserted to the equilibrium and stoichiometric conditions. In this case, however, each solid phase composition is not represented by a curve in the $P^o_{TiCl_4}$ - $P^o_{CH_4}$ - plot, but by a surface in the $P^o_{TiCl_4}$ - $P^o_{CH_4}$ - $P^o_{NH_3}$ - plot. In Figures 11-13 the calculated iso-activity lines in the fcc-phase have been ploted for each component at 1800K so that the activities can be estimated easily for a certain composition at this temperature. As expected, the nitrogen and carbon activities required to obtain a solid phase without vacancies, i.e. $x_{Ti} = 0.5$, are infinitely high.

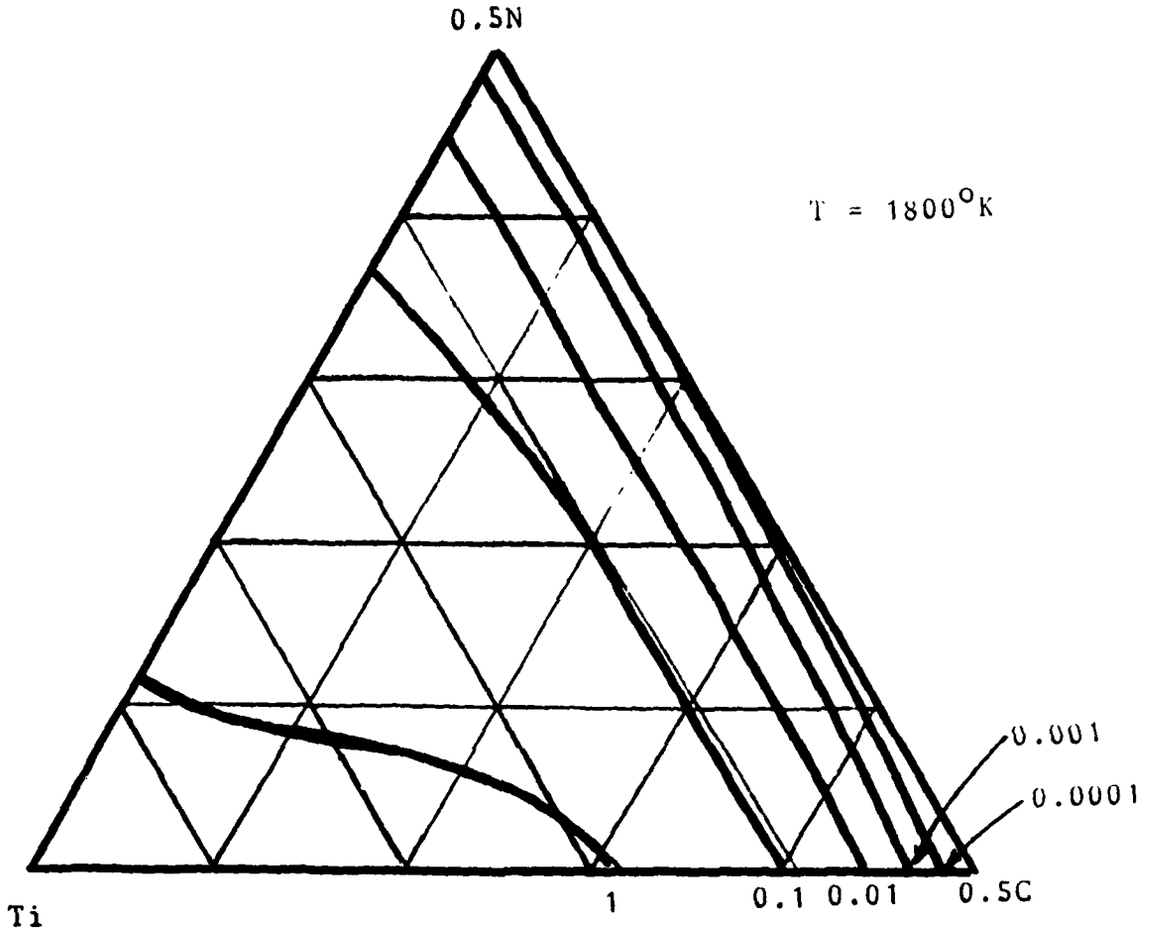

Figure 11. Calculated Iso-activity lines for Titanium in Ti(C,N) at 1800K

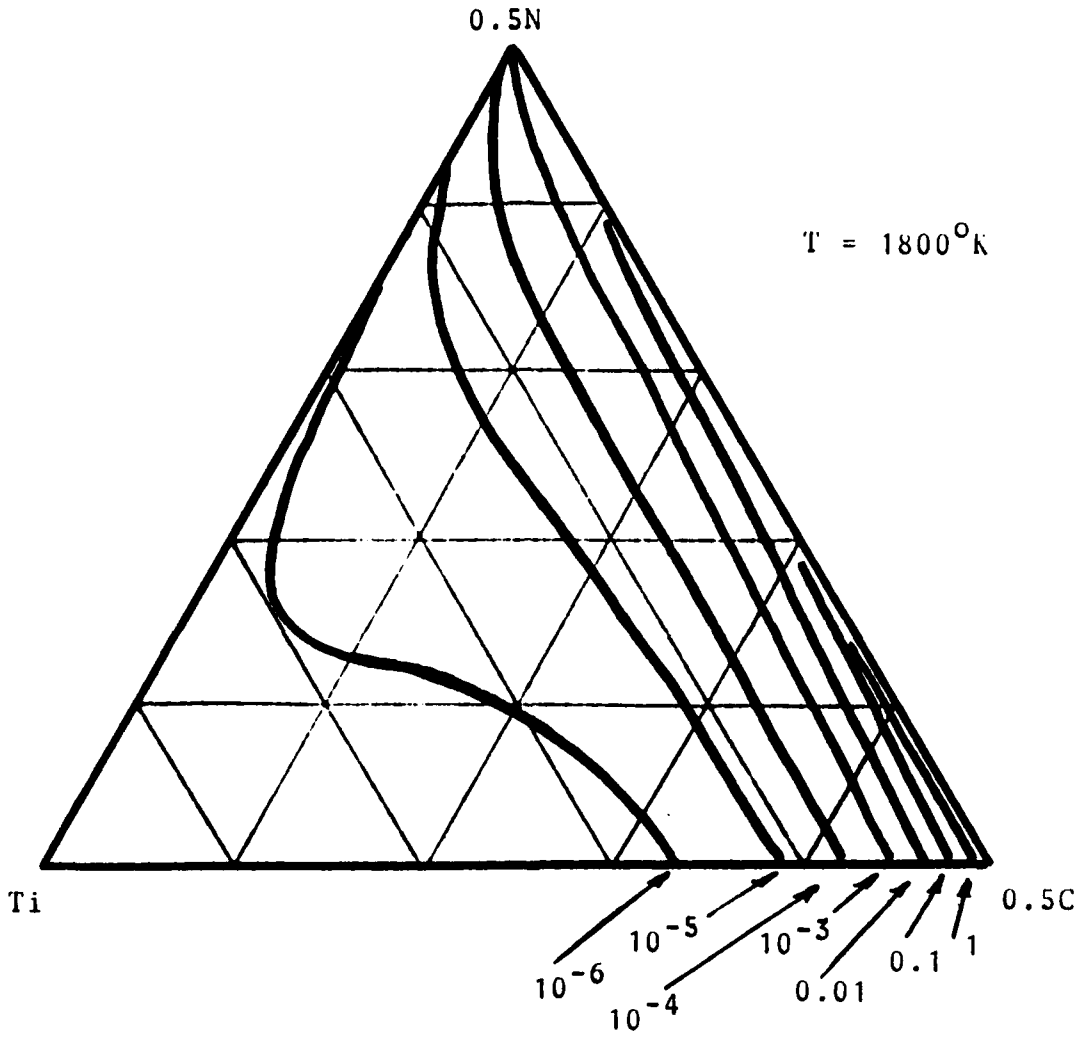

Figure 12. Calculated Iso-activity lines for carbon in Ti(N,C) at 1800°K

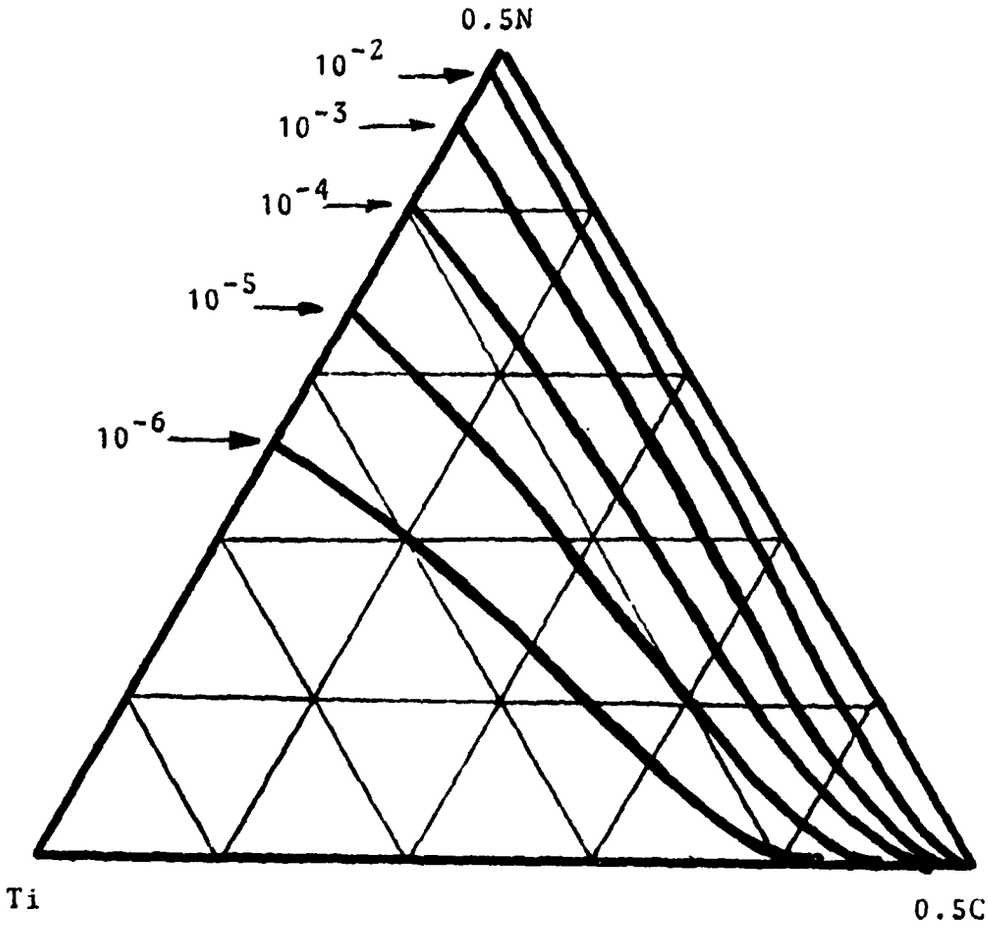

Figure 13. Calculated Iso-activity lines for N (i.e. $\frac{1}{2}N_2$) at 1800K in Ti(C,N).

Appendix B

For a ternary regular solution we apply the following equation for the integral Gibbs energy:

$$G_m = x_A {}^oG_A + x_B {}^oG_B + x_C {}^oG_C + RT\left[x_A \ln x_A + x_B \ln x_B + x_C \ln x_C\right] + x_A x_B L_{AB} + x_A x_C L_{AC} + x_B x_C L_{BC} \quad (A1)$$

where x_A, x_B, x_C are the molar fractions and subjected to the condition :

$$x_A + x_B + x_C = 1 \quad (A2)$$

${}^oG_A$, ${}^oG_B$, ${}^oG_C$ are the Gibbs energies for the pure components in the phase under consideration, and L_{AB}, L_{AC}, L_{BC} are interaction-parameters. In a subregular solution the interaction parameters exhibit a linear concentration dependence in the binary edge-systems. In this report the following representation has been applied in the binaries:

$$L_{AB} = {}^oL_{AB} + {}^1L_{AB}(x_A - x_B) \quad (A3)$$

The same representation will also be applied for a ternary solution. By standard methods the partial quantities are derived:

$$G_j = {}^oG_j + RT \ln x_j + {}^EG_j \qquad j=A,B,C \quad (A4)$$

where

$${}^EG_A = x_B(1-x_A){}^oL_{AB} + \left[x_B^2 + 2x_B(1-x_A)(x_A-x_B)\right]{}^1L_{AB} + x_C(1-x_A){}^oL_{AC} + \left[x_C^2 + 2x_C(1-x_A)(x_A-x_C)\right]{}^1L_{AC} - x_Bx_C{}^oL_{BC} - 2x_Bx_C(x_B-x_C){}^1L_{BC} \quad (A5)$$

$${}^EG_B = x_A(1-x_B){}^oL_{AB} - \left[x_A^2 - 2x_A(1-x_B)(x_A-x_B)\right]{}^1L_{AB} + x_C(1-x_B){}^oL_{BC} + \left[x_C^2 + 2x_C(1-x_B)(x_B-x_C)\right]{}^1L_{BC} - x_Ax_C{}^oL_{AC} - 2x_Ax_C(x_A-x_C){}^1L_{AC} \quad (A6)$$

$${}^EG_C = x_A(1-x_C){}^oL_{AC} - \left[x_A^2 - 2x_A(1-x_C)(x_A-x_C)\right]{}^1L_{AC} + x_B(1-x_C){}^oL_{BC} - \left[x_B^2 - 2x_B(1-x_C)(x_B-x_C)\right]L_{BC}^1 - x_Ax_B{}^oL_{AB} - 2x_Ax_B(x_A-x_B){}^1L_{AB} \quad (A7)$$

The sublattice model takes the following form for the case of Ti on one sublattice and a mixture of C, N and Va (=vacant sites) on the other sublattice (i.e. $Ti_a (C,N,Va)_c$)

$$G_m = y_C {}^oG_{Ti_aC_c} + y_N {}^oG_{Ti_aN_c} + y_{Va} a^oG_{Ti}$$
$$+ RT c\left[y_C \ln y_C + y_N \ln y_N + y_{Va} \ln y_{Va}\right]$$
$$+ y_C y_N L^{Ti}_{CN} + y_C y_{Va} L^{Ti}_{CVa}$$
$$+ y_N y_{Va} L^{Ti}_{NVa} \qquad (A8)$$

where the site fractions, y can be calculated from the ordinary mole fractions by the equations:

$$y_C = \frac{a}{c} x_C/(1-x_C - x_N) \qquad (A9)$$

$$y_N = \frac{a}{c} x_N/(1-x_C - x_N) \qquad (A10)$$

and $y_{Va} = 1-y_C - y_N$ (A11)

The subscript m in equation A8 signifies that G is counted per mole of formula unit: $Ti_a(C,N,Va)_c$. In order to compute G for a mole of atoms (or a gram atom) equation A8 must be multiplied by the factor $(a/a)\ (1-x_N-x_C)$. The following values of a and c hold:

fcc: a=1, c=1
bcc: a=1, c=3
hcp: a=2, c=1 (A12)

${}^oG_{Ti_aC_c}$ and ${}^oG_{Ti_aN_c}$ are the Gibbs energy of formation for the compounds. These compounds may or may not be stable. Moreover, experimental data may or may not be available for the compounds.

The L-parameters are interaction parameters and are defined to vary with composition as:

$$L_{ij} = {}^oL_{ij} + {}^1L_{ij}\ (y_i - y_j) \qquad (A13)$$

The partial quantities become:

$$G_C = \frac{1}{c}\left({}^{o}G_{Ti_aC_c} - a\,{}^{o}G_{Ti}\right) + RT\left(\ln y_C - \ln y_{Va}\right)$$

$$+ {}^{E}G_C$$

$$G_N = \frac{1}{c}\left({}^{o}G_{Ti_aN_c} - a\,{}^{o}G_{Ti}\right) + RT\left(\ln y - \ln y_{Va}\right)$$

$$+ {}^{E}G_N$$

$$G_{Ti} = {}^{o}G_{Ti} + RT\,\frac{c}{a}\ln Y_{Va} + {}^{E}G_{Ti}$$

Furthermore;

$${}^{E}G_C = \frac{1}{c}\left({}^{E}G_{Ti_aC_c} - {}^{E}G_{Ti_a\,Va_c}\right) \qquad (A13)$$

$${}^{E}G_N = \frac{1}{c}\left({}^{E}G_{Ti_aN_c} - {}^{E}G_{Ti_aVa_c}\right) \qquad (A14)$$

$${}^{E}G_{Ti} = \frac{1}{a}\,{}^{E}G_{Ti_aVa_c} \qquad (A15)$$

and

$${}^{E}G_{Ti_aC_c} = y_N(1-y_C)\,{}^{o}L^{Ti}_{CN} + \left[y_N^2 + 2y_N(1-y_C)(y_C-y_N)\right]{}^{1}L^{Ti}_{CN}$$
$$+ y_{Va}(1-y_C)\,{}^{o}L^{Ti}_{CVa} + \left[y_{Va}^2 + 2y_{Va}(1-y_C)(y_C-y_{Va})\right]{}^{1}L^{Ti}_{CVa}$$
$$- y_Ny_{Va}\,{}^{o}L^{Ti}_{NVa} - 2y_Ny_{Va}(y_N-y_{Va})\,{}^{1}L^{Ti}_{NVa} \qquad (A16)$$

$${}^{E}G_{Ti_aN_c} = y_C(1-y_N)\,{}^{o}L^{Ti}_{CN} - \left[y_C^2 - 2y_C(1-y_N)(y_C-y_N)\right]{}^{1}L^{Ti}_{CN}$$
$$+ y_{Va}(1-y_N)\,{}^{o}L^{Ti}_{NVa} + \left[y_{Va}^2 + 2y_{Va}(1-y_N)(y_N-y_{Va})\right]{}^{1}L^{Ti}_{NVa}$$
$$- y_Cy_{Va}\,{}^{o}L^{Ti}_{CVa} - 2y_Cy_{Va}(y_C-y_{Va})\,{}^{1}L^{Ti}_{CVa} \qquad (A17)$$

$${}^{E}G_{Ti_aVa_c} = y_C(1-y_{Va})\,{}^{o}L^{Ti}_{CVa} - \left[y_C^2 - 2y_C(1-y_{Va})(y_C-y_{Va})\right]{}^{1}L^{Ti}_{CVa}$$
$$+ y_N(1-y_{Va})\,{}^{o}L^{Ti}_{NVa} - \left[y_N^2 - 2y_N(1-y_{Va})(y_N-y_{Va})\right]{}^{1}L^{Ti}_{NVa}$$
$$- y_Cy_N\,{}^{o}L^{Va}_{CN} - 2y_Cy_N(y_C-y_N)\,{}^{1}L^{Ti}_{CN} \qquad (A18)$$

Appendix C

Summary of parameters for Ti-C-N system. (cal/mol, conversion to J/mol by multiplying by 4.184).

Liquid

$$^{o}G^{L}_{Ti} - {}^{o}G^{hcp}_{Ti} = 4920 - 2.9T \qquad \text{(Ref. 8)}$$

$$^{o}G^{L}_{C} - {}^{o}G^{gr}_{C} = 27300 - 6.5T \qquad \text{-11-}$$

$$^{o}G^{L}_{N} - \tfrac{1}{2}\,{}^{o}G^{gas}_{N_2} = -2077 + 15.98T \qquad \text{-11-}$$

Subregular solution, G_m given by Eq. A1.

$$^{o}L^{L}_{CN} = {}^{1}L^{L}_{CN} = 0$$

$$^{o}L^{L}_{CTi} = -23185 - 10.5T,\ {}^{1}L_{CTi} = 30516 - 10.5T$$

$$^{o}L^{L}_{NTi} = -68482 - 7.5T,\ {}^{1}L_{NTi} = 40975 + 7.5T$$

fcc

$$^{o}G^{fcc}_{Ti} - {}^{o}G^{hcp}_{Ti} = 800 \qquad \text{(Ref. 8)}$$

$$^{o}G^{fcc}_{TiC} - {}^{o}G^{hcp}_{Ti} - {}^{o}G^{Gr}_{C} = -43972 + 2.528T$$

$$^{o}G^{fcc}_{TiN} - {}^{o}G^{hcp}_{Ti} - \tfrac{1}{2}\,{}^{o}G^{gas}_{N_2} = -79666 + 21.42T$$

Sublattice model, Gm given by Eq. A8 a=c=1

$$^{o}L^{Tifcc}_{CN} = {}^{1}L^{Tifcc}_{CN} = 0$$

$$^{o}L^{Tifcc}_{CVa} = -16099 + 0.36T,\ {}^{1}L^{Tifcc}_{CVa} = -38801 + 11.03T$$

$$^{o}L^{Tifcc}_{NVa} = -25000 + 4.4T,\ {}^{1}L^{Tifcc}_{NVA} = 0$$

hcp

Ref state for Ti

$${}^{o}G^{hcp}_{Ti_2C} - 2\,{}^{o}G^{hcp}_{Ti} - {}^{o}G^{Gr}_{C} = 5574$$

$${}^{o}G^{hcp}_{Ti_2N} - 2\,{}^{o}G^{hcp}_{Ti} - \frac{1}{2}\,{}^{o}G^{gas}_{N_2} = -93490 + 24.71T$$

sublattice model, G_m given by Eq. A8 a = 2, c = 1

$${}^{o}L^{Tihcp}_{CN} = {}^{1}L^{Tihcp}_{CN} = 0$$

$${}^{o}L^{Tihcp}_{CVa} = -50000, \quad {}^{1}L^{Tihcp}_{CVa} = 0$$

$${}^{o}L^{Tihcp}_{NVa} = -9985 - 3.44T, \quad {}^{1}L^{Tihcp}_{NVa} = 0$$

bcc

$${}^{o}G^{bcc}_{Ti} - {}^{o}G^{hcp}_{Ti} = 1040 - 0.9T$$

$${}^{o}G^{bcc}_{TiC_3} - {}^{o}G^{hcp}_{Ti} - 3\,{}^{o}G^{gr}_{C} = -44996 + 0.49T$$

$${}^{o}G^{bcc}_{TiN_3} - {}^{o}G^{hcp}_{Ti} - 3/2\,{}^{o}G^{gas}_{N_2} = -104155 + 31.22T$$

sublattice model, G_m given by Eq. A8 a = 1, c = 3

$${}^{o}L^{Tibcc}_{CN} = {}^{1}L^{Tibcc}_{CN} = 0$$

$${}^{o}L^{Tibcc}_{CVa} = -50000, \quad {}^{1}L^{Tibcc}_{CVa} = 0$$

$${}^{o}L^{Tibcc}_{NVa} = {}^{1}L^{Tibcc}_{NVa} = 0$$

Tetragonal

$${}^{o}G^{tet}_{Ti_2N} - 2\,{}^{o}G^{hcp}_{Ti} - \frac{1}{2}\,{}^{o}G^{gas}_{N_2} = -120692 + 43.06T$$

Stoichiometric Phase

Gas $\quad {}^{o}G^{gas}_{Ti} - {}^{o}G^{hcp}_{Ti} = 112685 - 48.024T + 1.808\,T\ln T$ (Ref. 6)

REFERENCES

1. R.C. Sharma and Y.A. Chang: Metall Trans. B, 10 B (1979) pp 103-108.

2. A. Fernandez Guillermet, M. Hillert, B. Jansson and B. Sundman: Metall Trans. B, 12B (1981) pp. 745-754

3. R. Hultgren et. al: Selected Values of the Thermodynamic Properti of Metals (and Binary Alloys), (2 volumes) ASM, Metals Park, Ohio 1973.

4. M. Hillert and L. I. Staffansson: Acta Chem Scand. 24 (1970) pp 3618-26.

5. B. Sundman and J. Agren: J. Phys. Chem. Solids, 42 (1981) pp 297-301

6. J. Agren: Metall. Trans, A, 10A (1979) pp 1847-52.

7. O Kubaschewski and C.B. Alcock: Metallurgical Thermochemistry, 5th edition, Pergamon Press, Oxford 1979.

8. E.K. Storms Refractory Carbides Academic Press, New York 1967.

9. L. Kaufman: CALPHAD I (1977) P.7

10. E. Rudy, D.P. Harmon, and C.E. Brukl (1965) Wright-Patterson Air Force Base Tech. Rept. No AFML-TR-65-2, Part 1 Volume II.

11. M. Hansen and K. Anderko: Constitution of Binary Alloys 2nd Edition, McGraw Hill 1958.

12. F. Teyssandier, M. Ducarroir and C. Bernard: The Industrial Use of Thermochemical Data, pp 301-311, Edited by T.I. Barry, The chemical Society, special publication No. 34 London 1980.

IX CALCULATION OF THE Al_2O_3-ZrO_2-Y_2O_3 SYSTEM

1.0 Introduction

Zirconium Dioxide is an important technological ceramic because of its refractory nature and abrasive properties. In combination with additions of Al_2O_3, SiC, SiO , Y_2O_3, CaO and MgO its properties can be tailored for a wide variety of uses as a thermal and/or an oxidation barrier or a structural ceramic.Recent developments (1-3) have shown that by combination with Al_2O_3, Si_3N_4 and SiC enhanced fracture toughness can be developed in ZrO_2 composites. Heuer (4) has shown that tough zirconia-containing ceramics can be fabricated which derive their usefull strength from the stress-induced martensitic transformations of zirconia percipitates from the tetragonal (T) to monoclinic (M) structures. Electron diffraction and transmission electron micrographic studies have shown that in partially stabilized ZrO_2 with tetragonal (T) phase particles in a cubic (A) matrix and/or tetragonal (T) structures in a fine-grained alumina matrix microcrack formation around crack tips leads to enhanced toughness. In view of the wide range of applications for ZrO_2 and ZrO_2 composites it seems worthwhile to add this compound to the exisiting data base (5,6) described in Sections II and III. Accordingly the following analysis of the ZrO_2-Al_2O_3 and ZrO_2-Y_2O_3 were carried out and coupled with the available description of the Y_2O_3-Al_2O_3 shown on page 11 to calculate isothermal sections in the Al_2O_3-ZrO_2-Y_2O_3 system.

2.0 Analysis of the Y_2O_3-Al_2O_3, ZrO_2-Y_2O_3 and ZrO_2-Al_2O_3 System

The analysis of the binary systems was performed along the line described in Section II using available phase diagrams (7-11) and thermochemical data (12) for the compounds of interest, in the course of this study it was noted that Y_2O_3 exhibits a high temperature transition from the Mn_2O_3 structure to a high temperature form on heating above 2500K (8).

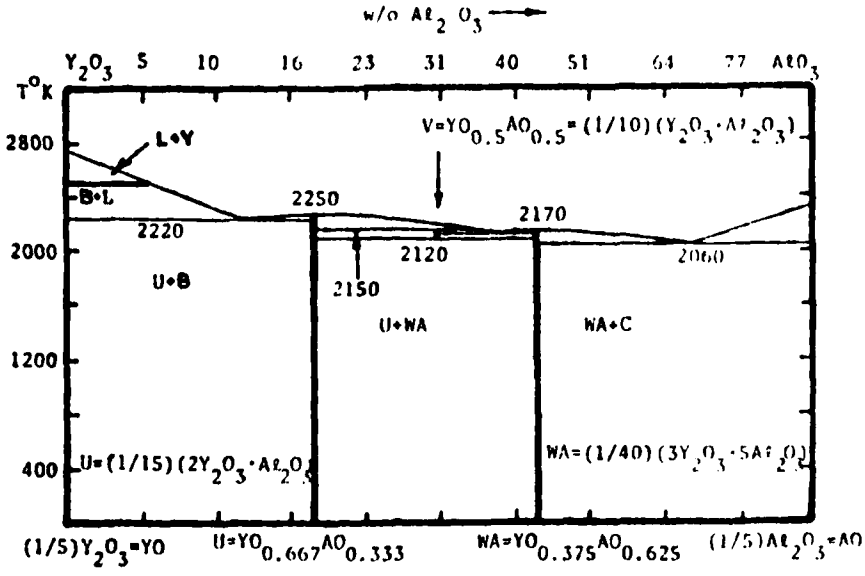

Figure 6. Calculated $1/5Y_2O_3$ - $1/5Al_2O_3$ Phase Diagram

Figure 1. Recalculated (1/5) Y_2O_3-(1/5)Al_2O_3 Phase Diagram

This fact has been reflected by recalculating the YO-AO diagram in Figure 1 above by applying the new description for YO in place of that given in Section II to reflect allotropism in YO. Although this is a small change it will be employed in future considerations.

Tables 1 and 2 provide the lattice stability, solution phase and compound phase parameters required to calculate the ZO-YO and ZO-AO phase diagrams which agree with the experimental results available (8,9). The recalulated YO-AO phase diagram is obtained by employing the revised lattice stability description for YO shown on page 132 with the previoulsy published (5) solution and compound phase parameters shown on pages 6 and 7.

3.0 Calculation of the Al_2O_3-ZrO_2-Y_2O_3 System

Figure 4 and 5 display isothermal sections in the Al_2O_3-ZrO_2-Y_2O_3 system at temperatures between 2700K and 1700K. These sections illustrate the ranges of liquid and solid solution stability and the extent of compound intrusion as a fuction of temperature. Expansion of the data base by analysis of other ZrO_2 binary systems sch as ZrO_2-Cr_2O_3, ZrO_2-CaO, ZrO_2-MgO, ZrO_2-SiO_2, ZrO_2-SiN_4 and ZrO_2-BeO would permit synthesis of many technologically important quasi-ternary systems.

TABLE 1

Summary of Lattice Stability Parameters, T in Kelvins

(All units in Joules per gram atom (mole of atoms), T in Kelvins)

AO=(1/5) Al_2O_3, ZO=(1/3) ZrO_2, YO=(1/5) Y_2O_3, L= Liquid

C= Corundum, Y=high temperature (hexagonal) Y_2O_3, B-bcc

(Mn_2O_3) Y_2O_3, A=ZrO_2 cubic, T=ZrO_2 Tetragonal, M=ZrO_2 Monoclinic

ZOZOLA=(1/3) ZrO_2 (liquid)-(1/3) ZrO_2 (CaF_2) Cubic

AOAOLC=23640-10.209T
AOAOLA= - 9.832T
AOAOLT= -10.586T

ZOZOLA=29008- 9.832T
ZOZOLC= -10.209T
ZOZOLY=17991- 8.368T
ZOZOLB=24853- 9.205T

ZOZOAT=1987-0.753T
ZOZOTM=2008-1.381T

YOYOLY=22694- 8.368T
YOYOLB=26878-10.042T
YOYOLA=22615- 9.832T
YOYOAT=-8368- 0.753T
YOYOTM=-8368- 1.381T

TABLE 2

Summary of Solution and Compound Phase Parameters

(All units in Joules per gram atom (mole of atoms), T in Kelvins)

LZOAO=17573, LAOZO=39748, TZOAO=TAOZO=AZOAO=AAOZO=62760

CAOZO=CZOAO=62760

Solution Phases

LZOYO= 14016 + 4.184T
LYOZO= 14016 + 4.184T
BZOYO= 2929 + 8.368T
BYOZO= 2929 + 8.368T
AZOYO=-12552 +11.297T
AYOZO= 837 + 4.602T

YZOYO= 2929 + 8.368T
YYOZO= 2929 + 8.368T
TZOYO=-12552 + 11.297T
TYOZO= 837 + 4.602T
MZOYO= 4184 + 11.297T
MYOZO= 837 + 4.602T

Compound Phase = P = (1/19)($3ZrO_2 \cdot 2Y_2O_3$)=(1/19) ZO_9YO_{10}= $ZO_{0.474}YO_{0.526}$, Base =A, Compound Parameter C= 31798 + 11.09T, Gibbs Energy of Formation from (1/3) ZrO_2(M) and (1/5) Y_2O_3(B), ΔG_f=-286-2.86T

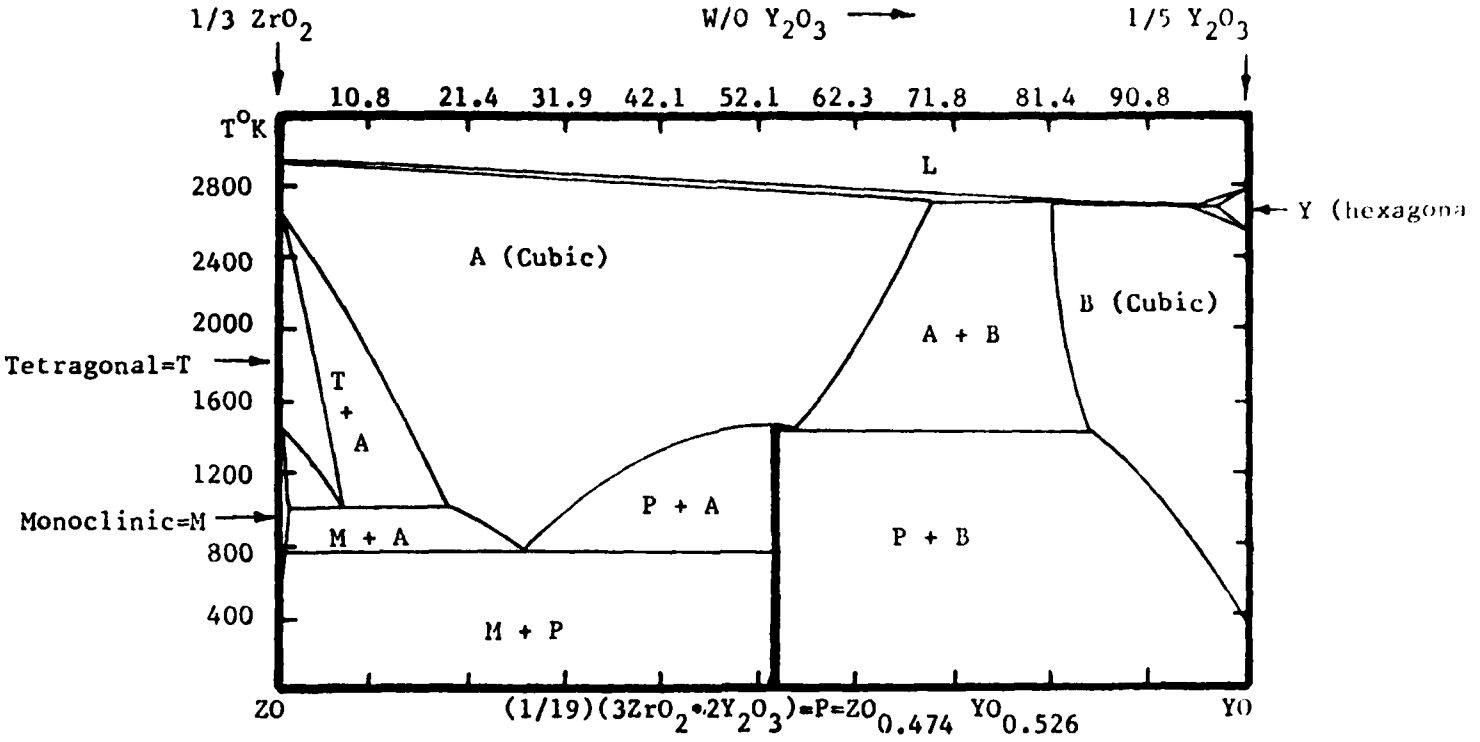

Figure 2 Calculated ZrO_2-Y_2O_3 Phase Diagram

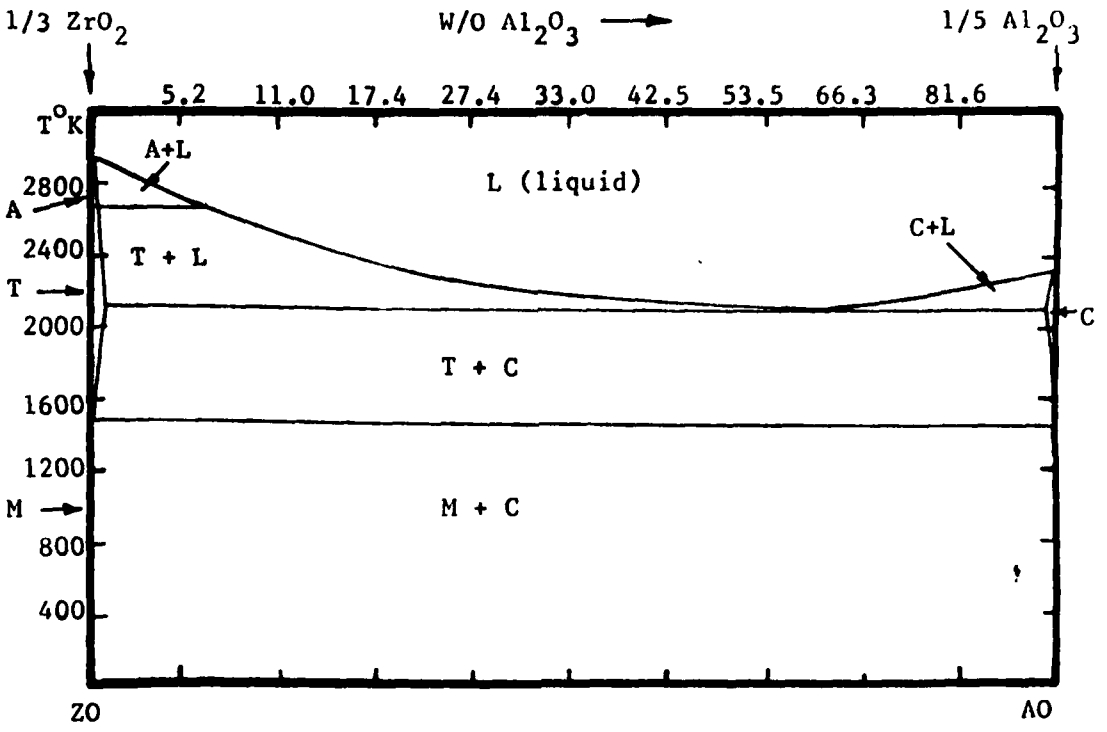

Figure 3 Claculated ZrO_2-Al_2O_3 Phase Diagram

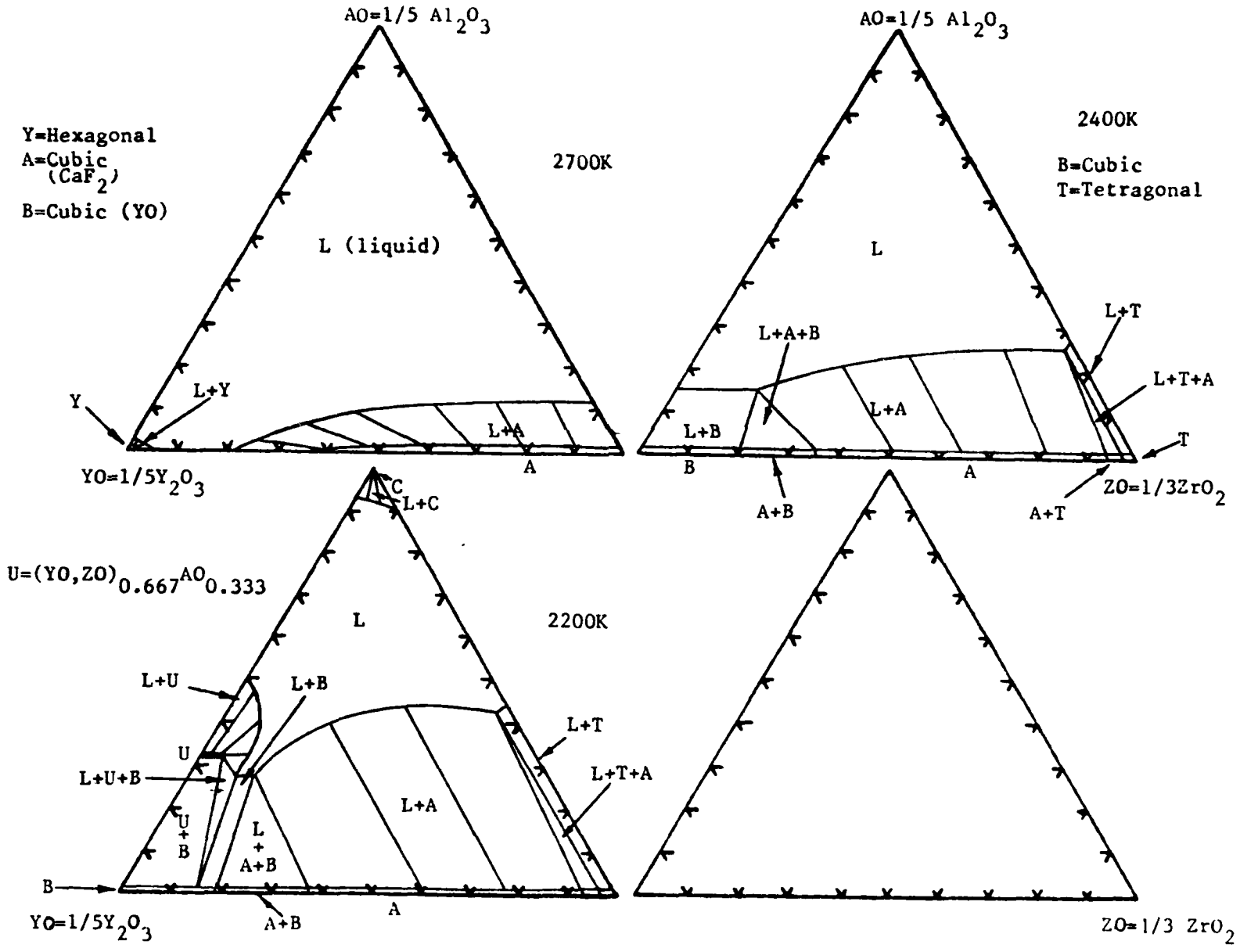

Figure 4 Calculated Isothermal Sections in the Al_2O_3-ZrO_2-Y_2O_3 System

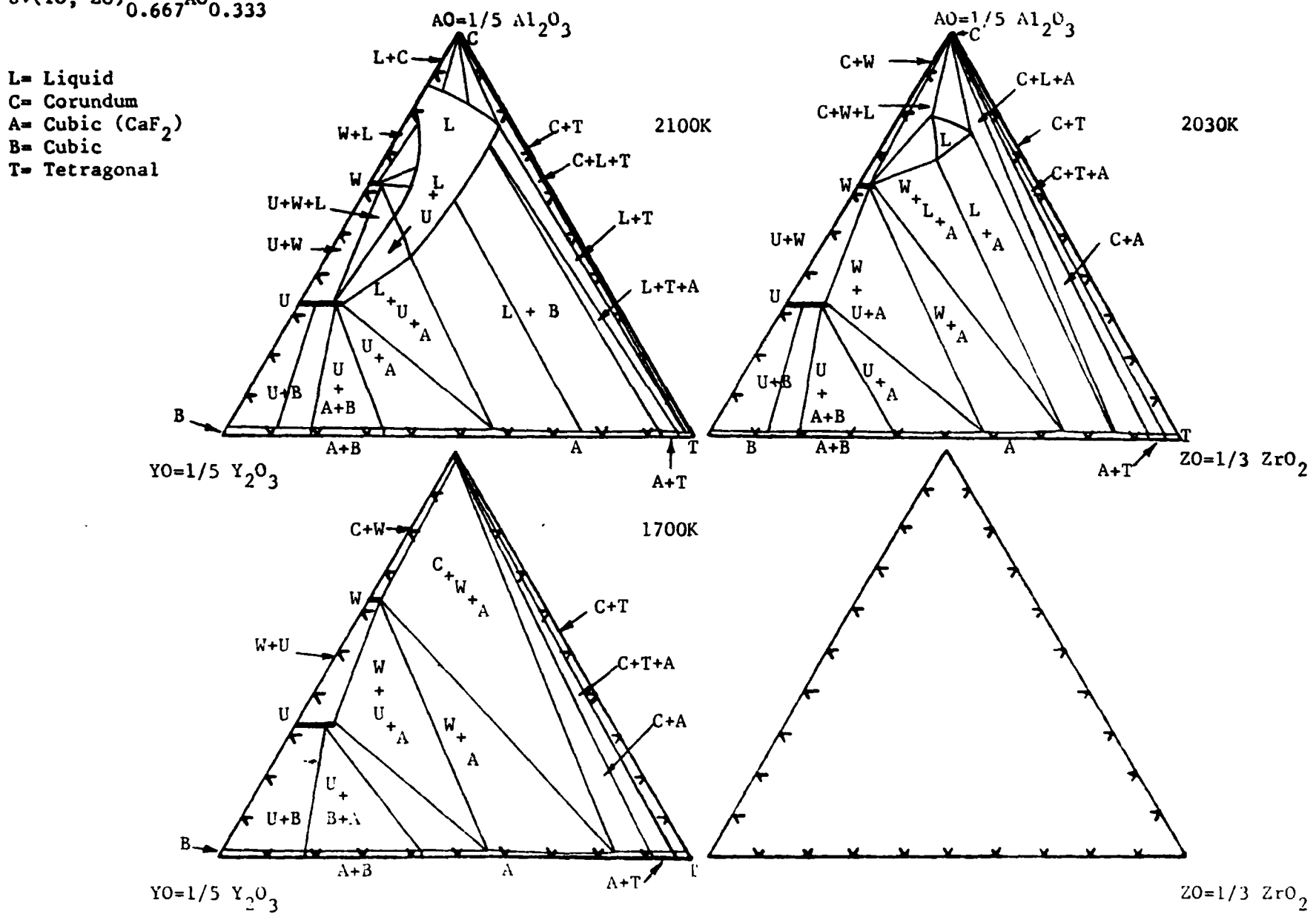

Figure 5 Calculated Isothermal Sections in the Al_2O_3-ZrO_2-Y_2O_3 System

REFERENCES

1. N. Claussen, J. Steeb, R.F. Pabst, American Ceramic Society Bulletin 56 599 (1977)
2. N. Claussen and J. John, A. American Ceramic Society 61 94 (1978)
3. L.J. Gauckler, J. Lorenz, J. Weiss and G. Petzow, Science of Ceramics 10 577 (1980)
4. A.H. Heuer, Second Conference on the Science and Technology of Zirconium Dioxide, Stuttgart June 1983
5. L. Kaufman, F. Hayes and D. Birnie, CALPHAD, 5 163 (1981)
6. L. Kaufman, F. Hayes and D. Birnie, High Temperatures-High Pressure 14 619 (1982)
7. H.G. Scott, Journal of Materials Science, 10 1527 (1975)
8. V.S. Stubican and J.R. Hellman, Advances in Ceramics 3 25 (1980), A. Heuer and L.W. Hobbs Eds. American Ceramic Society Columbus, OHIO
9. G.R. Fischer, L.J. Manfredo, R. N. McNally and R.C. Doman, Journal of Materials Science 16 3447 (1981)
10. J.M. Maider, T.E. Mitchell and A.H. Heuer, Acta Metallurgica 31 387 (1983)
11. E.M. Levin, C.R. Robbins and H.F. McMurdie, Phase Diagrams for Ceramists American Ceramics Society, Columbus, OHIO (1964) First Supplement (Ibid) (1969) Second Supplement (Ibid) (1975)
12. O. Kubaschewski and C.B. Alcock, Metallurgical Thermochemistry Fifth Edition (1979) Pergamon Press, Oxford.

X CALCULATION OF THE HEAT OF FUSION OF EUTECTIC FLUORIDE GLASSES IN THE ZrF_4-BaF_2 AND THE ZrF_4-LaF_3 SYSTEMS

1.0 Introduction

The current analysis of the ZrF_4-BaF_2 and ZrF_4-LaF_3 systems shown on page 65 is the first step in calculation of the ternary LaF_3-ZrF_4-BaF_2 system shown on page 69. Very little experimental data exist for these systems. One method of improving the level of confidence in the calculations and the current degree of knowledge concerning these systems would be to measure the heat liberated by solidification (or absorbed during fusion) of liquids of the eutectic composition at the eutectic temperature. Such measurements can readily be performed by differential scanning claorimetry. The calculations presented below provides values for the heat of fusion based on the description contained in Section V.

2.0 Calculation of Heat of Fusion

The heat of fusion, ΔH, at the eutectic temperature, T_E, and the eutectic composition, X_E, for the ZF-LF case is defined as

$$\Delta H = H^L[T_E, x_E] - (1-x_E)\, H^M_{ZF} - x_E\, H^J_{LF} \qquad (1)$$

$$\Delta H = x_E(1-x_E)\,[(1-x_E)\,LZFLF + x\,LLFZF] + (1-x_E)\,\Delta H^{M\to L}_{ZF} + x_E\,\Delta H^{J\to L}_{LF} \qquad (2)$$

where $X_E = 0.25$, $T_E = 850K$ and LZFLF=-11088 J/g.at. LLFZF= 22595 defining the enthalpy of the liquid. The last two terms are (0.75) (12845) and (0.25) (12560), from page 61, respectively so that

$$\Delta H = -500 + 9634 + 3140 = 12274 \text{ J/g.at.}$$

since $ZF_{0.75}LF_{0.25}$ corresponds to (3/20) ZrF_4-(1/16) LaF_3, then one gram atom corresponds to 25.1 grams of ZrF_4 and

12.3 grams of LaF_3 or a total of 37.4 grams. Hence a mixture containing 32.9 w/o of LaF_3 would exhibit a heat of fusion of 328 J/gm., on the basis of these calculations. Similarly a calculation of the heat of fusion for the ZF-BF case suggests that a mixture containing 42.7 w/o BaF_2 would exhibit a heat of fusion of 281 J/gm. near 800K.

Measurement of these heats of fusion by scanning calorimetry would be very valuable in improving the present calculations.

XI CALPHAD CALCULATION OF THE EFFECT OF AlF_3 ADDITIONS ON THE GLASS COMPOSITIONS OF TERNARY ZrF_4-LaF_3-BaF_2 FLUORIDES

(presented at the Second Interantional Symposium on Halide Glasses. Rensselaer Polytechnic Institute, Troy New York 12181, USA, 2-5 August 1983, Sponsored by AFOSR, ONR, Corning, GTE, and Spectran Corporation.)

1.0 Introduction

The discovery of a family of non-oxide glasses based on mixtures of ZrF_4 or HfF_4 with other metallic fluorides by Poulain and coworkers offers great potential in optical fiber, windows and source/detector applications. Due to limited phase diagram data available for binary, ternary and multicomponent fluoride systems employed to synthesize these glasses progress in identifying new compositions has proceeded along empirical lines. In order to remedy this situation, the CALPHAD method (1-3) for coupling phase diagram and thermochemical data has been applied to develop a data base covering metallic fluorides. The objective is to permit computation of multicomponent phase diagrams which can be used to identify the composition range where the liquid is most stable. The latter offers opportunities for prediction of new glasses. Currently, the data base covers combinations of 0.2 ZrF_4(ZF), 0.25 LaF_3(LF), 0.333 BaF_2(BF), 0.333 PbF_2(PF), 0.5 NaF (NF), 0.5 RbF (RF), 0.5 CsF (CF) and 0.5 KF developed along the lines described earlier for III-VI, II-VI and SIALON systems (2-3). This has been presented in Section V Figure 11 on page 69 shows calcualtion of isothermal sections in the LF-ZF-BF system illustrating the range of composition where the liquid has the greatest stability. The compositions agree with those where Poulain and coworkers found glass formation (4,5) and were presented in 1982 (6) and recently published (7). The current data base has been extended to cover AlF_3 (AF=0.25AlF_3) by employing experimental data provided by Thoma (8) to evaluate AFAFLT=13389-8.368T J/g.at. and LAFZF=25104 J/g.at.=LZFAF, LAFBF=4184 J/g. at.=LBFAF and LAFLF= 20920 J/g. at.=LLFAF. These parameters permit calcuation of the range of maxium stability of the liquid phase for ternary LF-ZF-BF glasses with additions of 4, 9 and 15 atom percent of AF.

2.0 Calculation of the Range of Liquid Stability

In line with the development in Section V the equilibrium between a liquid with x_1 atom fractions of LF, x_2 atom function of ZF and x_3 atom fractions of BF and x_4 atom fractions of AF; and solid LF having the J structure solid ZF having the M structure and solid BF having the K structure is given by equations (1) to (3), when LLFBF=LBFLF; LZFAF=LAFZF; LLFAF=LAFLF and LBFAF=LAFBF as in the case at hand!

$$\begin{aligned}\text{LFLFLJ}=&-RT\ln x_1 - x_1x_2\,(x_1+x_2)^{-1}(1-x_2+x_2(x_1+x_2)^{-1})\ \text{LLFZF}\\ &-x_2^2\,(x_2(x_1+x_2)^{-1}-x_1)(x_1+x_2)^{-1}\text{LZFLF}\\ &-x_3(1-x_1)\text{LLFBF}-x_4\,(1-x_1)\ \text{LLFAF}\\ &+x_2x_3(x_2+x_3)^{-1}\,(x_2\text{LZFBF}+x_3\text{LBFZF})\\ &+x_2x_4\ \text{LZFAF}+x_3x_4\text{LAFBF}\end{aligned}\tag{1}$$

$$\begin{aligned}\text{ZFZFLM}=&-RT\ln x_2-x_1x_2(x_1+x_2)^{-1}(1-x_2+x_1(x_1+x_2)^{-1})\ \text{LZFLF}\\ &-x_1(x_1^2(x_1x_2)^{-1}-x_1x_2)(x_1+x_2)^{-1}\text{LLFZF}-x_4(1-x_2)\text{LZFAF}\\ &-x_2x_3(x_2+x_3)^{-1}(1-x_2+x_3(x_2+x_3)^{-1})\text{LZFBF}+x_1x_3\text{LLFBF}\\ &+x_3^2(x_2+x_3)^{-1}(x_2-x_3(x_2+x_3)^{-1})\text{LBFZF}+x_1x_4\text{LLFAF}+x_3x_4\text{LAFBF}\end{aligned}\tag{2}$$

$$\begin{aligned}\text{BFBFLK}=&-RT\ln x_3-x_1(1-x_3)\ \text{LLFBF}-x_4(1-x_3)\text{LAFBF}\\ &-x_3x_2(x_3+x_2)^{-1}(1-x_3+x_2(x_2+x_3)^{-1})\ \text{LBFZF}+x_1x_4\text{LLFAF}\\ &+x_2^2(x_2+x_3)^{-1}(x_3-x_2(x_2+x_3)^{-1})\ \text{LZFBF}+x_2x_4\text{LZFAF}\\ &+x_1x_2(x_1+x_2)^{-1}(x_1\text{LLFZF}+x_2\ \text{LZFAF})\end{aligned}\tag{3}$$

Equations (1-3) are solved at 773K, 873K and 973K for x_4 0.00, 0.04, 0.09 and 0.15 respectively in Figures 1-6 which show the tie lines from the liquid phase composition to solid J (LF), solid M (ZF) and solid K (BF). Figures 7 and 8 show only the composite liquid phase boundries between 773K and 973K for AF=0.00 to 0.15 and Figure 9 shows the liquid phase boundries at 773K compared with limited AF=0.04. The present calculations for AF=0.09 and AF=0.15 suggest that at these levels glass formation will be easier and that the center of the glass forming region will shift toward lower LF concentrations

Note in Proof

At the Second International Conference on Halide Glasses, where this presentation was made, it was noted that the compounds $ZrF_4 \cdot BaF_2$ and $ZrF_4 \cdot LaF_3$ had been reported to be stable phases. Exact references were not provided but one participant suggested a congruent melting point for $ZrF_4 \cdot BaF_2$ ($ZF_{0.625}BF_{0.375}$) at 817K. Comparison with Figure 5 on page 65 shows that if such a compound were inserted and a congruent melting point would be required, the liquidus temperature, currently about 1000K would have to be lowered. Such an alteration would require small changes in the values of LZFBF and LBFZF in Table 2 on page 61. However, the eutectic temperature of 800K predicted in Figure 5 page 65 and the succeeding results of Section V and the present section would not be materially affected. A reference to differential thermal analysis studies of $ZrF_4 \cdot BaF_2$ by Y. Kowmoto and F. Sakaguchi submitted for publication to the Bulletin of the Chemical Society of Japan was reported but has not been aquired to date.

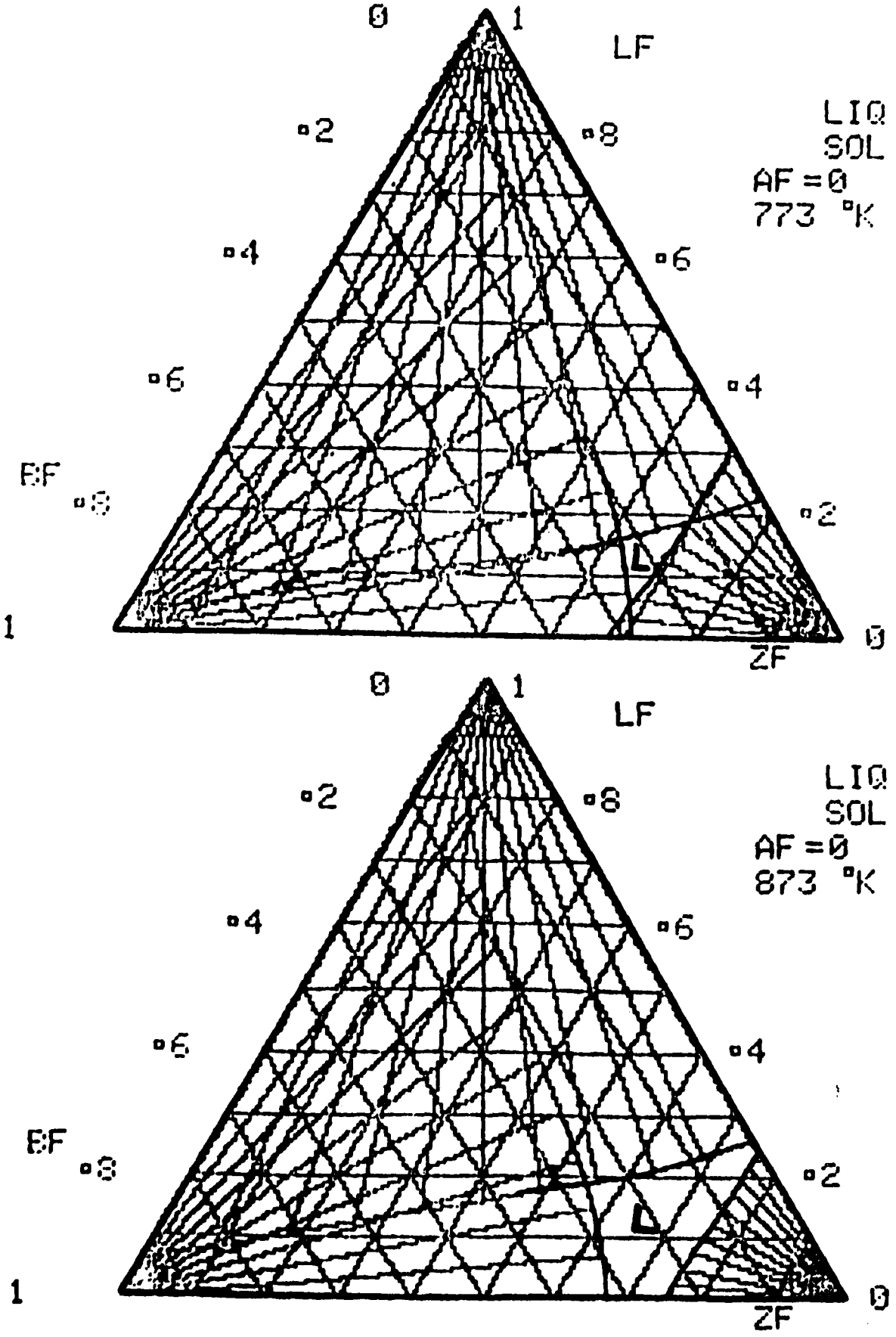

Figure 1 Calculated Solid-Liquid Equilibria in LF-ZF-BF with AF=O

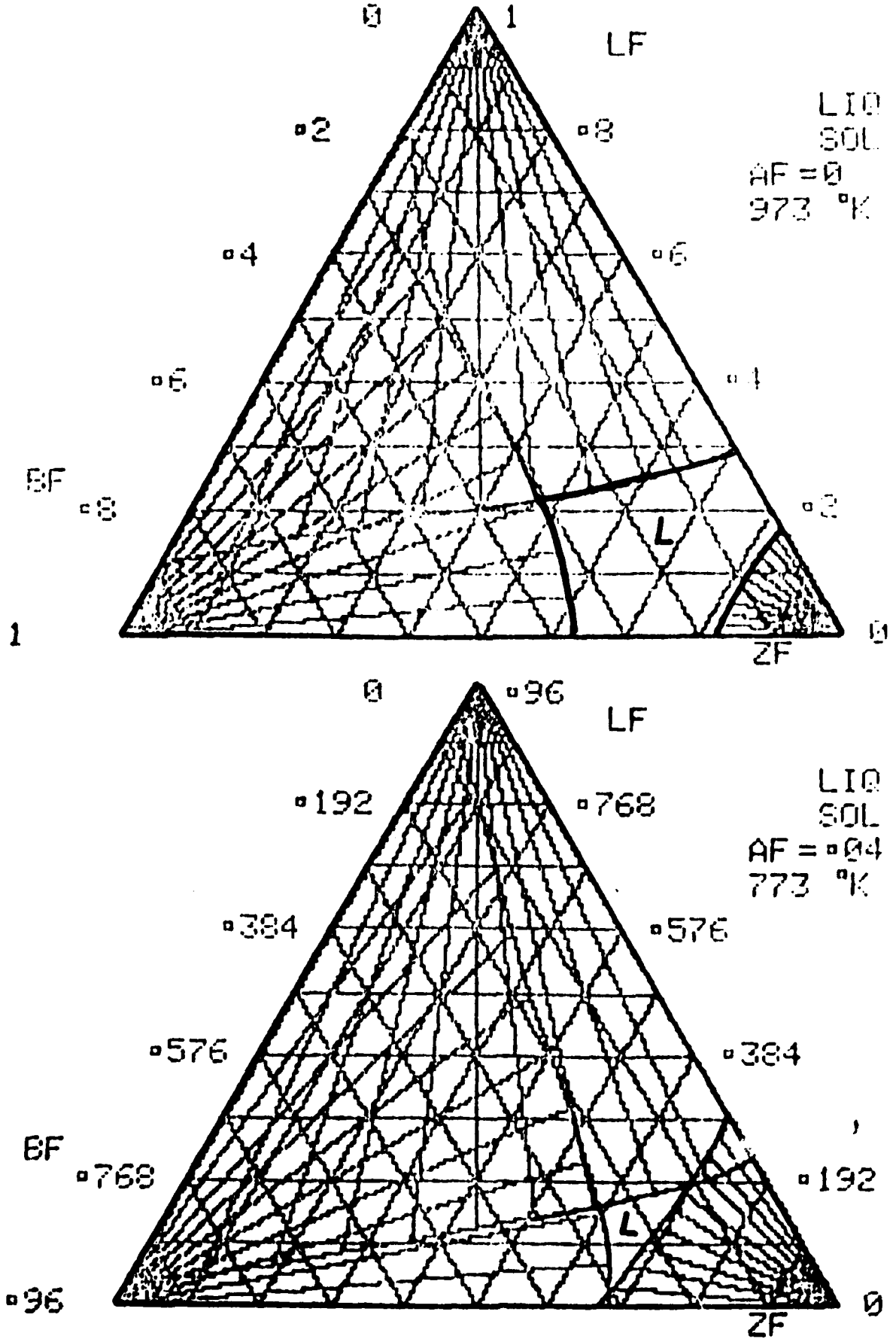

Figure 2 Calculated Solid-Liquid Equilibria in LF-ZF-BF with AF=0 (above), AF=0.04 (below)

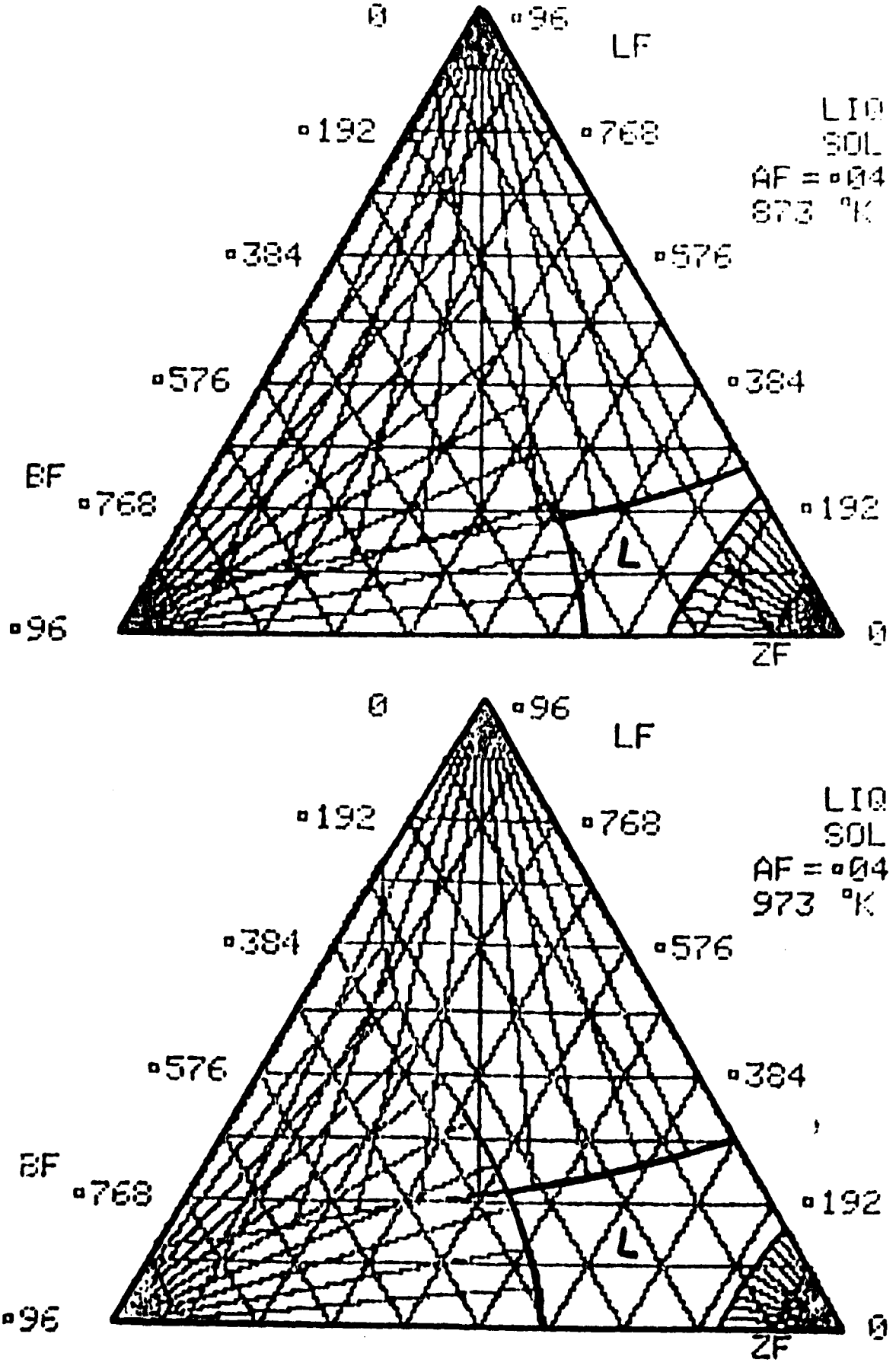

Figure 3 Calculated Solid-Liquid Equilibria in LF-ZF-BF with AF=0.04

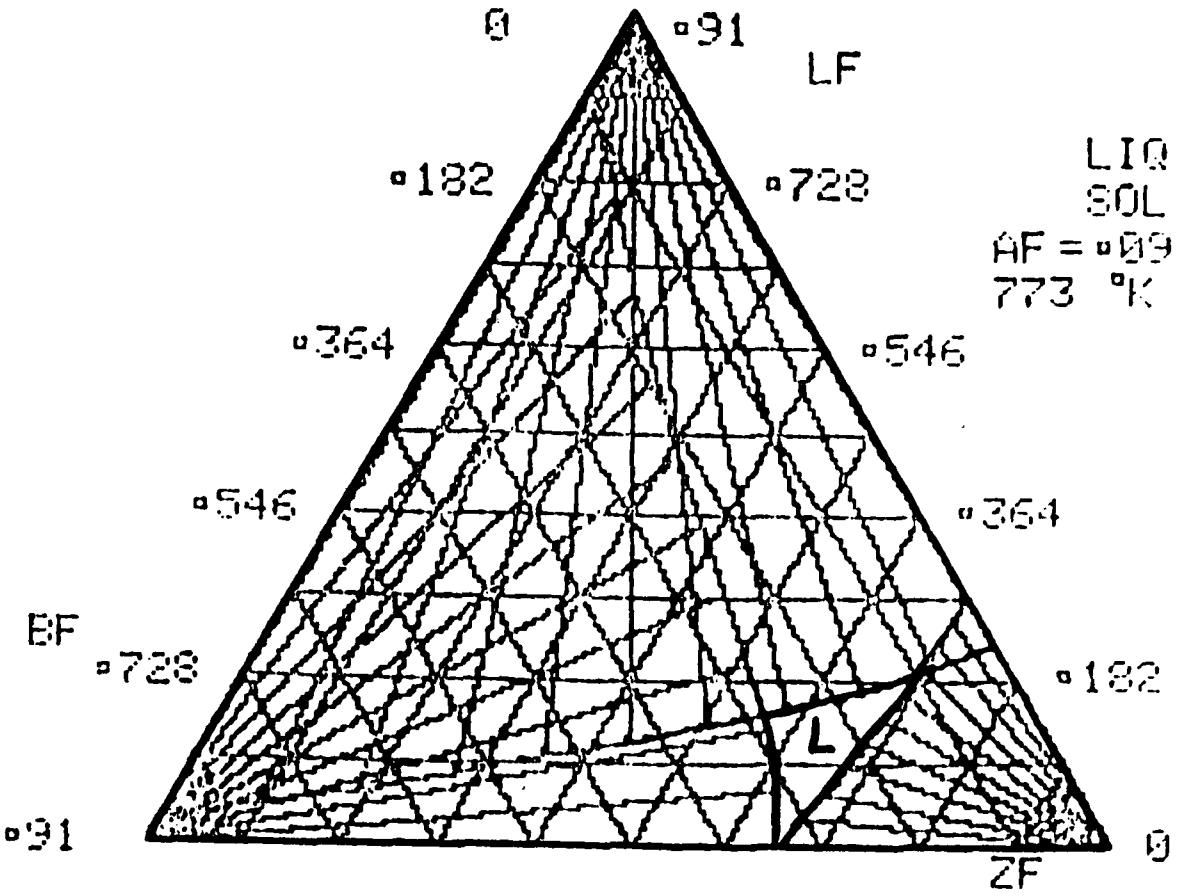

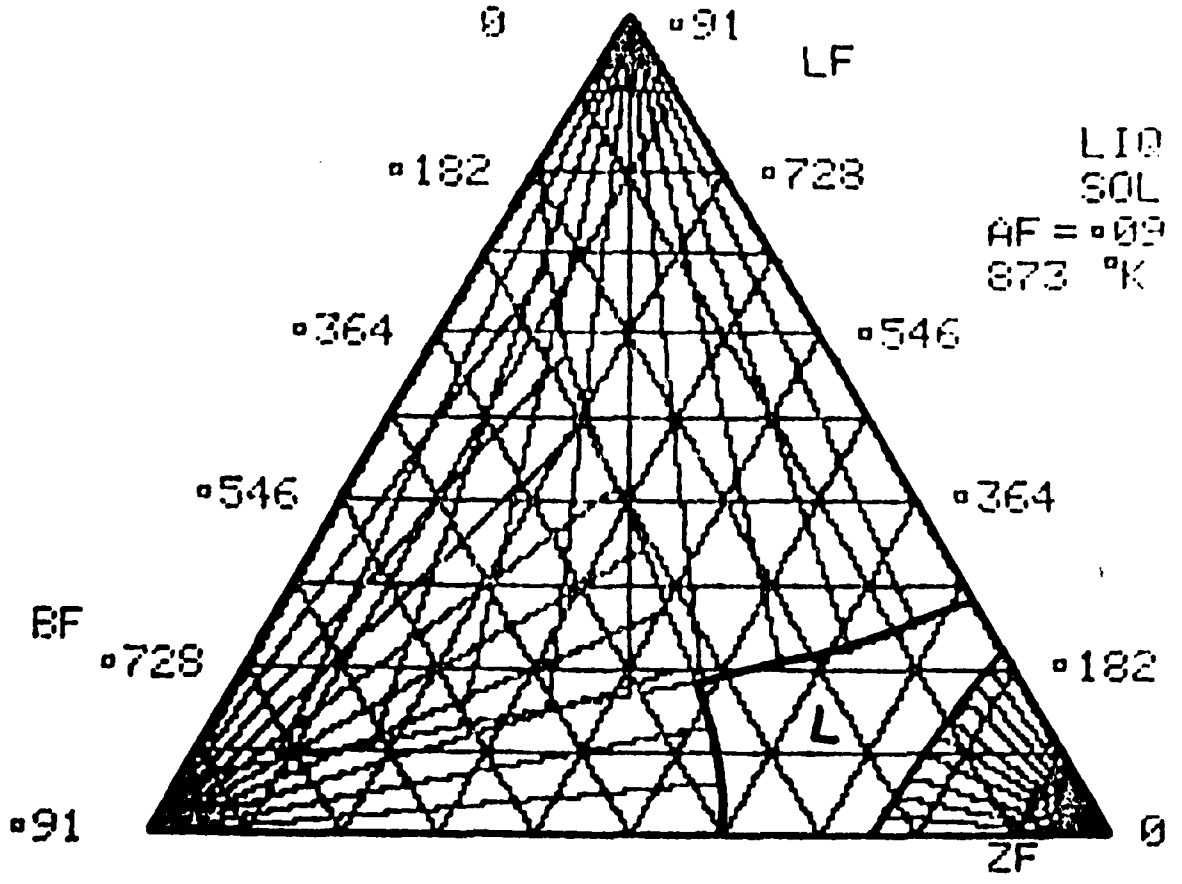

Figure 4 Calculated Solid-Liquid Equilibria in LF-ZF-BF with AF=0.09

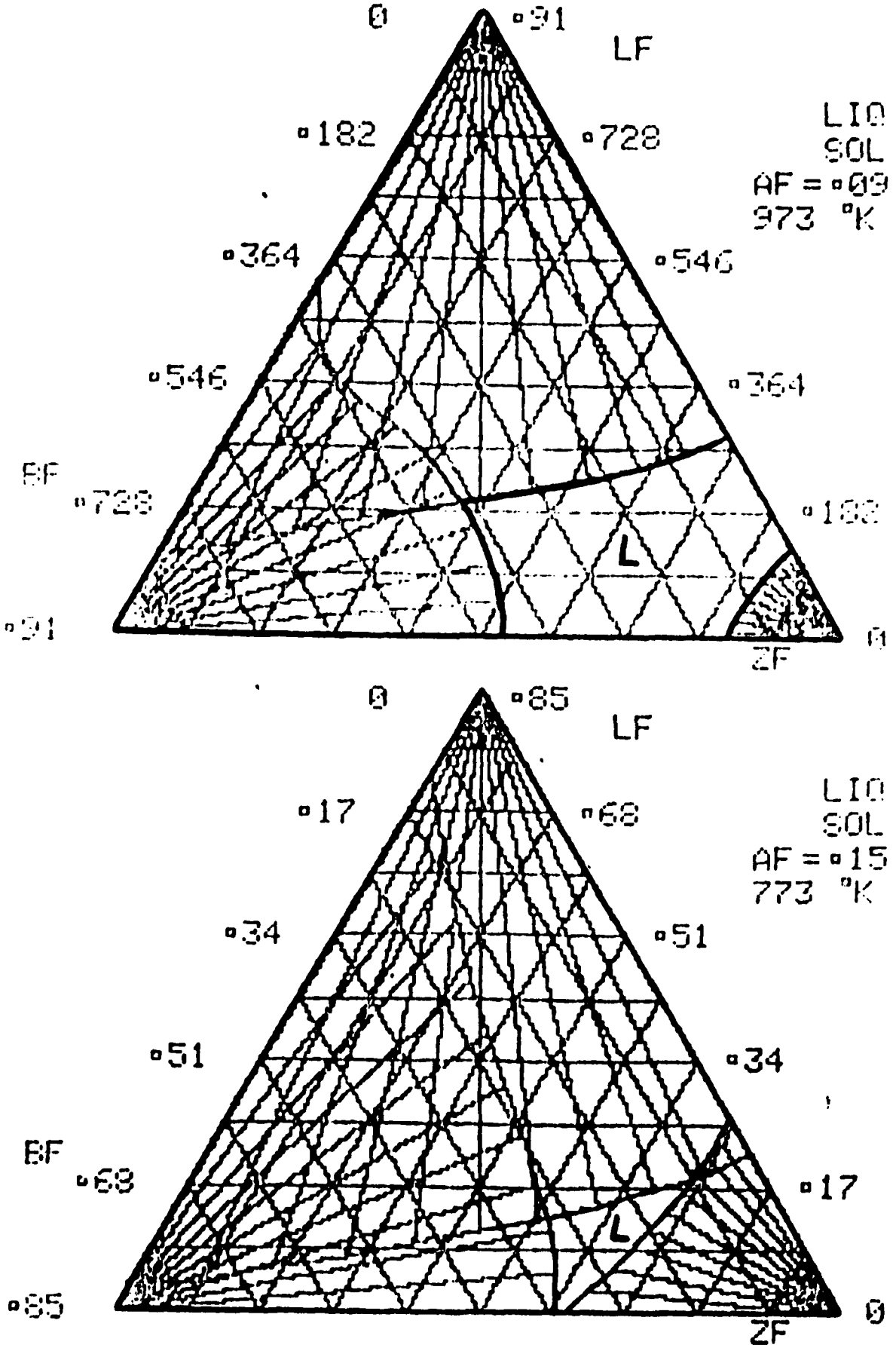

Figure 5 Calculated Solid-Liquid Equilibria in LF-ZF-BF with AF=0.09 (above) AF=0.15 (below)

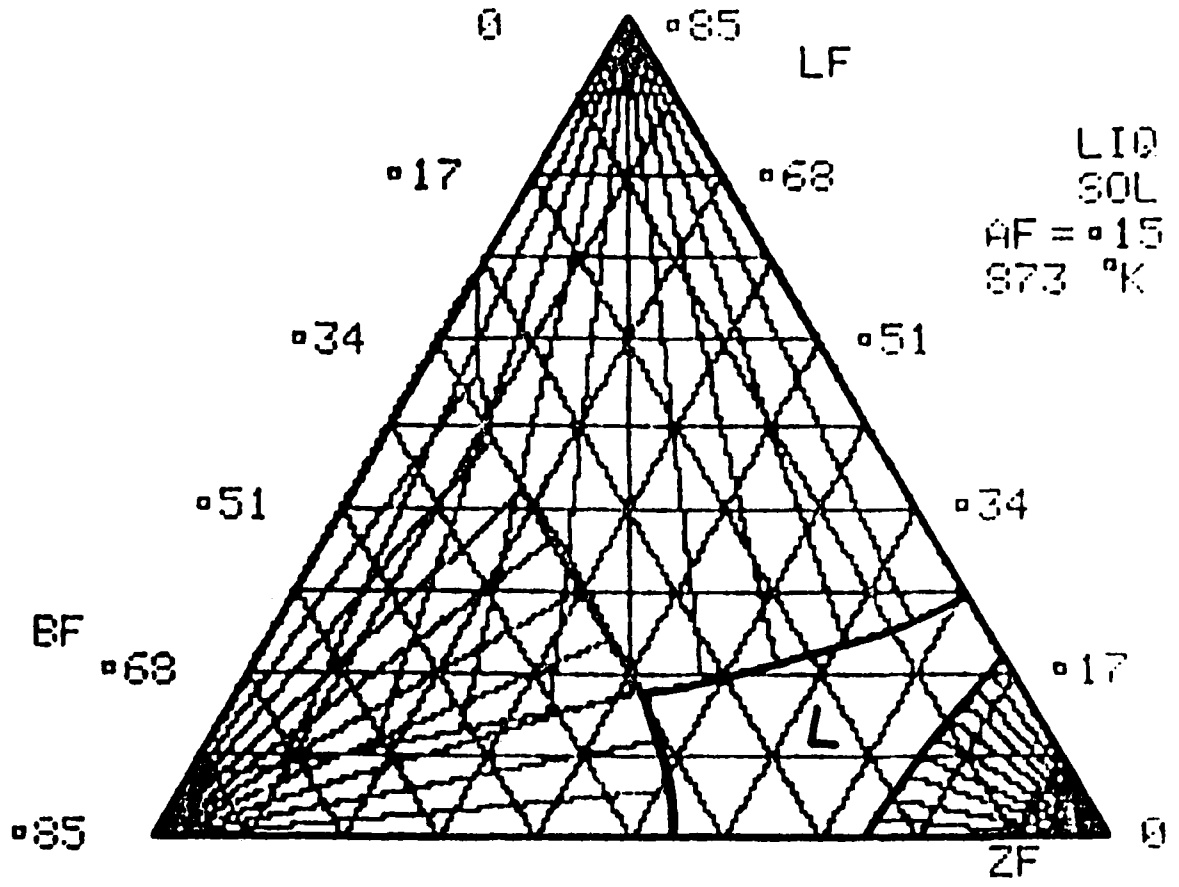

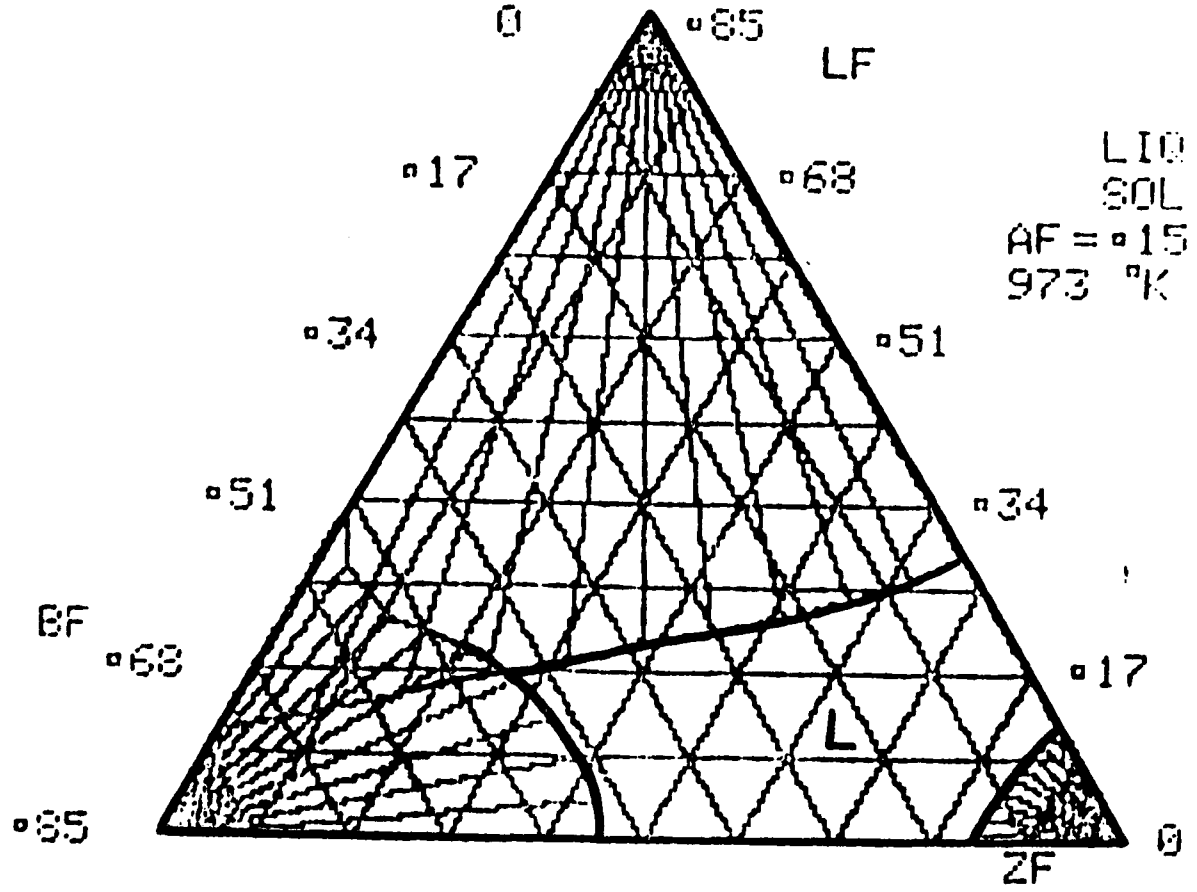

Figure 6 Calculated Solid-Liquid Equilibria in LF-ZF-BF with AF=0.15

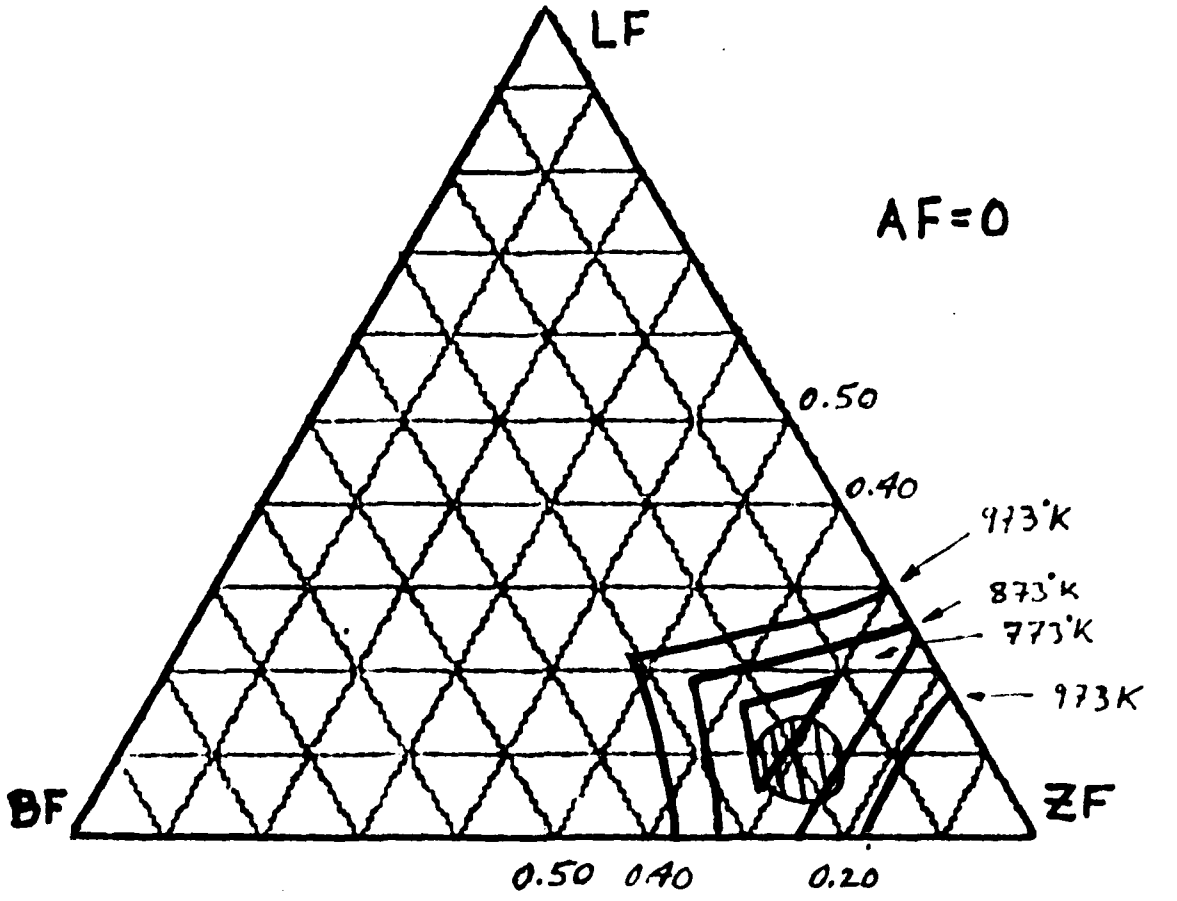

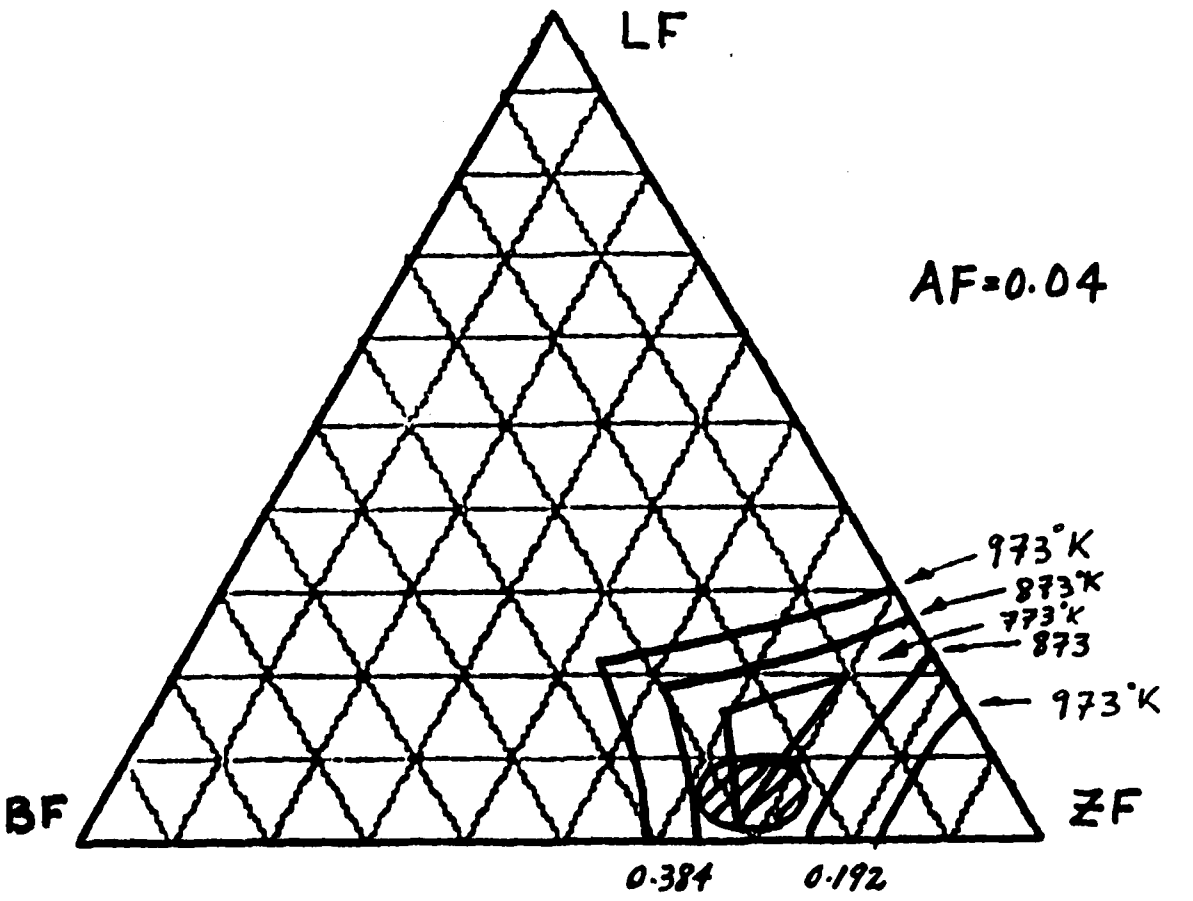

Figure 7 Composit Solid-Liquid Equilibria in LF-ZF-BF with AF=0 and AF=0.04

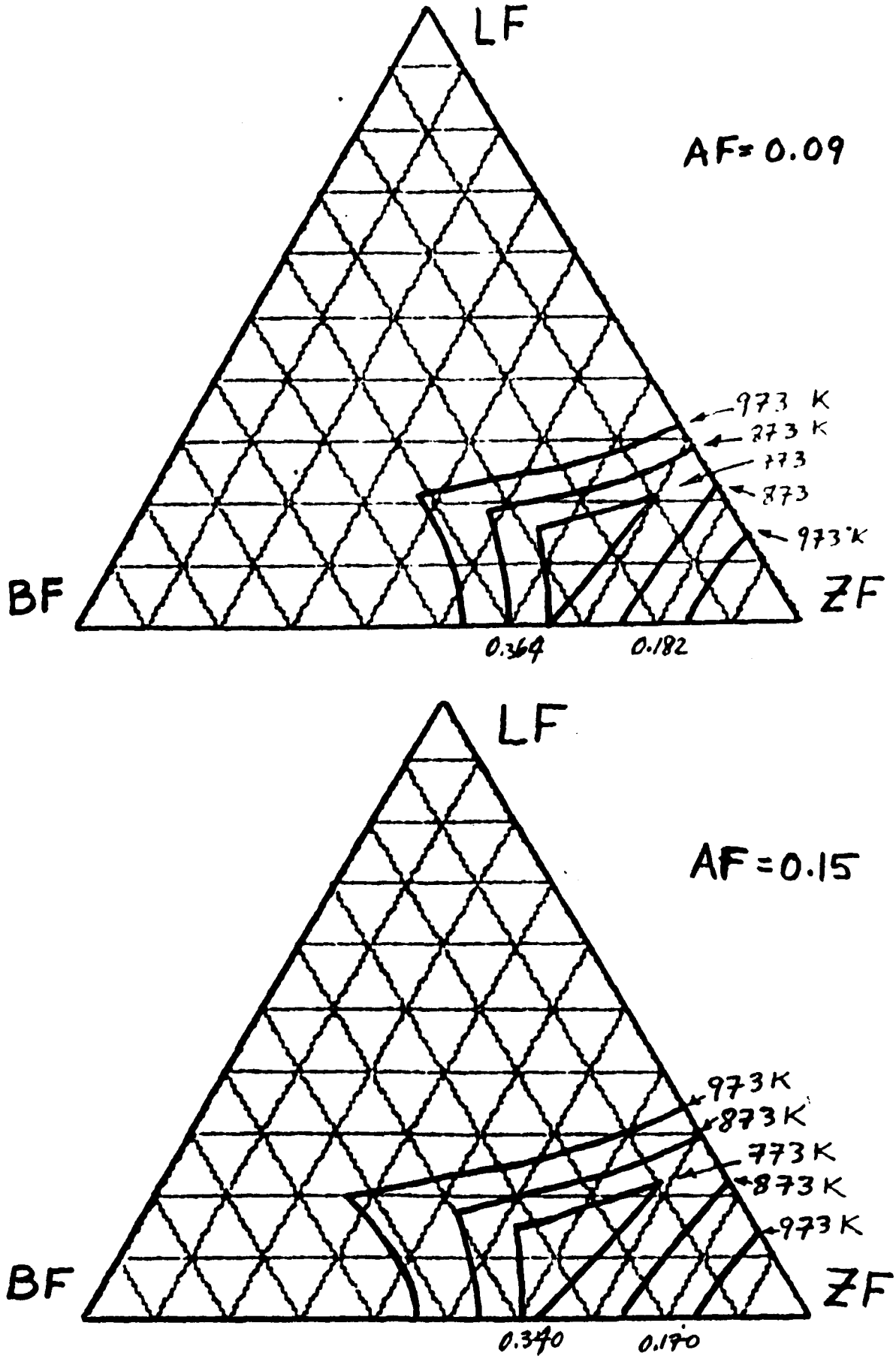

Figure 8 Composit Solid-Liquid Equilibria in LF-ZF-BF with AF=0.09 and AF=0.15

LF=0.25 LaF_3, ZF=0.20 ZrF_4, BF=0.333 BaF_2, AF=0.25 AlF_3

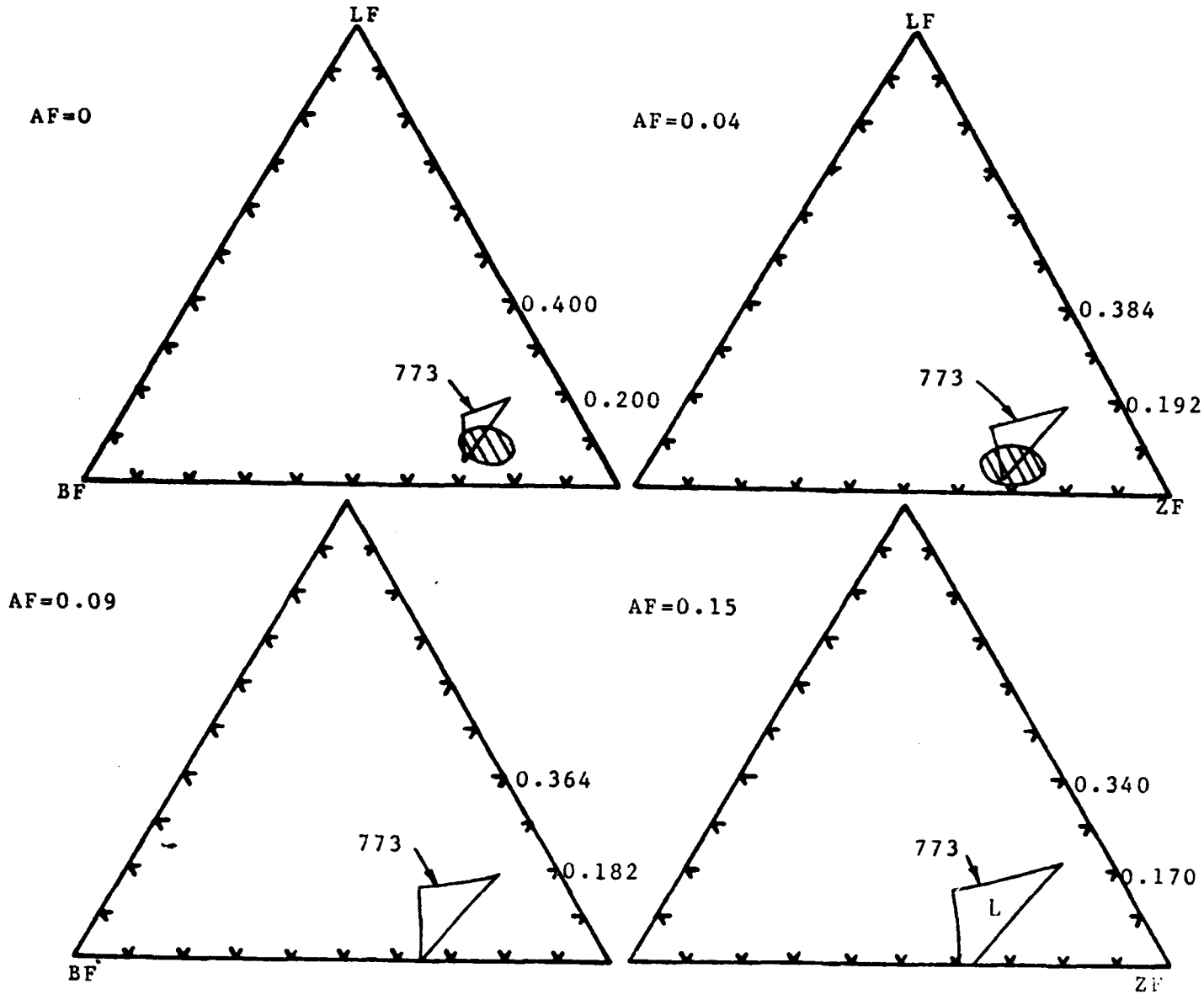

Figure 9 Calculated Range of Liquid Stability at 773°K at different Aluminum Fluoride levels compared with the observed ranges of glass formation (hatched) (9)

REFERENCES

1. L. Kaufman, CALPHAD (1977) 1 14.

2. L. Kaufman, F. Hayes and D. Birnie, CALPHAD (1981) 5 185.

3. L. Kaufman, J. Nell, K. Taylor and F. Hayes, CALPHAD (1981) 5 185.

4. A. Lecoq and M. Poulain, J. Non-Crystalline Solids (1979) 34 101.

5. M. Poulain, M. Poulain and J. Lucas, Rev. De Chem. Mineral (1979) 16 267.

6. L. Kaufman, J. Agren, J. Nell and F. Hayes "Calculation of Ternary Glass Compositions" FIRST INTERNATIONAL SYMPOSIUM OF HALIDE GLASSES, Churchill College Cambridge, England March 1982.

7. L. Kaufman, J. Agren, J. Nell and F. Hayes, CALPHAD 7 71 (1983)

8. R.E. Thoma, Advances in Molten Salt Chemistry, J. Braunstein, G. Manator and G.P. Smith Eds. Plenum Press, N.Y. (1975) page 302.

9. A. Lecoq and M. Poulain, Verres Refract. 34 333 (1980).

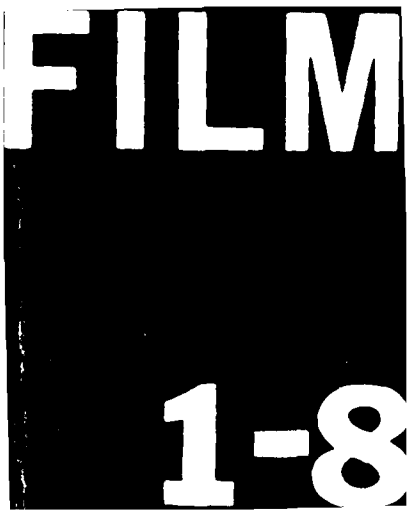
FILM
1-8